Advanced Materials for Electro-Driven Ion Separation and Selectivity

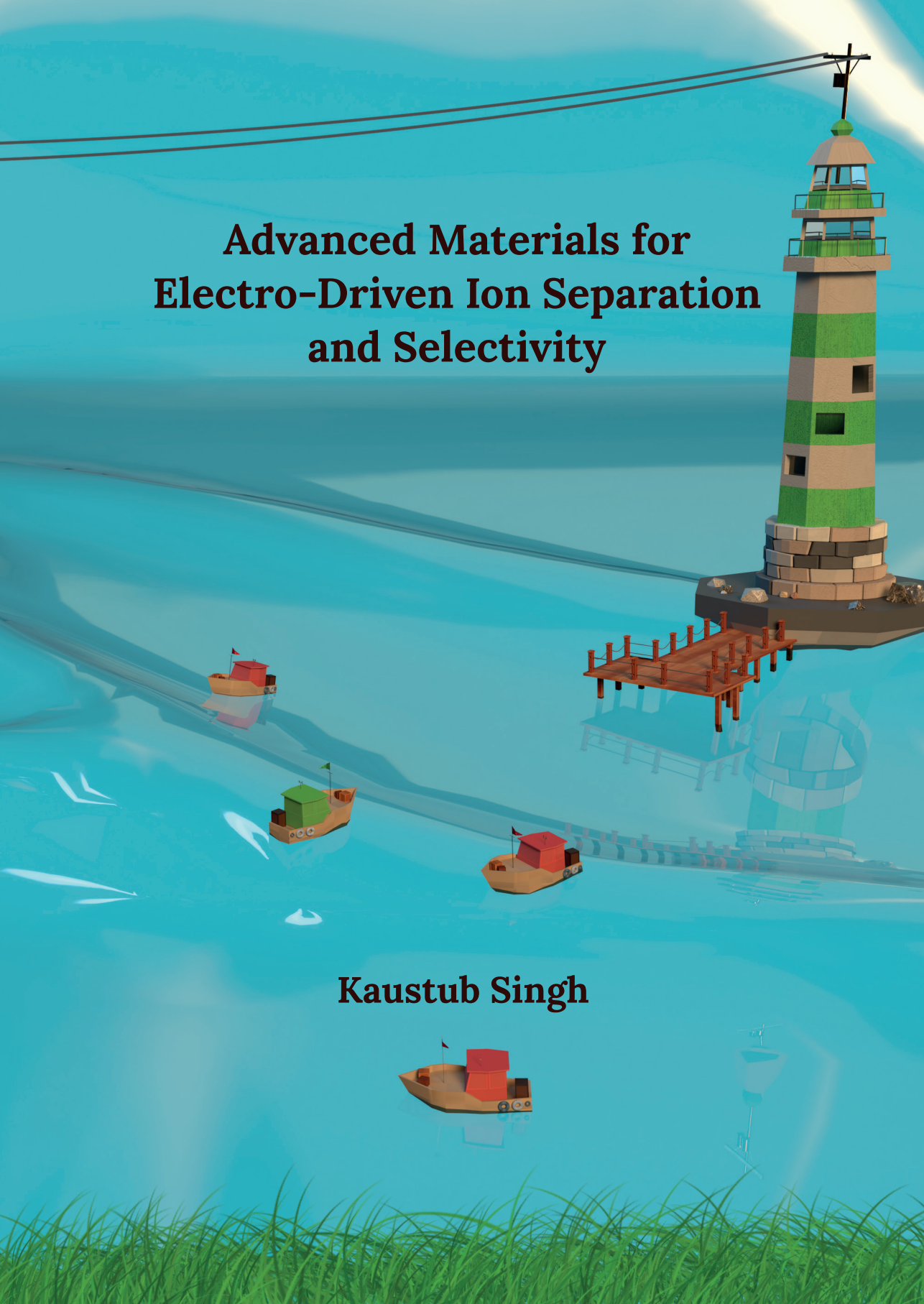

Kaustub Singh

Propositions

1. The ion preference of Prussian blue analogue lattices is altered by N-coordinated transition metals.
   (this thesis)
2. Symmetric cell designs irretrievably change the landscape of ion selectivity in capacitive deionization.
   (this thesis)
3. Research on energy storage also releases energy to power other research fields.
4. Scientific conferences with longer lunches and shorter scientific talks are the future.
5. Awards are the least scientific aspect of science.
6. Comics impart better human values than a treatise in philosophy.
7. The cloudy illustration in the work from: S. K. Patel, M. Qin, W. S. Walker, and M. Elimelech, *Environ. Sci. Technol.*, 2020, 54, 3663 – 3677, runs the risk of being cursory by neglecting the prospect of ion selectivity in electro-driven ion separation.

Propositions belonging to the thesis, entitled

Advanced materials for electro-driven ion separation and selectivity

Kaustub Singh

Wageningen, 16 March 2022

Advanced Materials for Electro-Driven Ion Separation and Selectivity

Kaustub Singh

Thesis committee

Promotors

Dr L. C. P. M. de Smet
Associate professor, Laboratory of Organic Chemistry
Wageningen University & Research

Prof. Dr H. Zuilhof
Professor of Organic Chemistry
Wageningen University & Research

Other members

Prof. Dr C. G. P. H. Schroën, Wageningen University & Research
Prof. Dr L. C. Rietveld, Delft University of Technology, The Netherlands
Dr M. Metzger, Dalhousie University, Canada
Dr X. Su, University of Illinois, at Urbana Champaign, USA

This research was conducted under the auspices of the Graduate School VLAG (Advanced studies in Food Technology, Agrobiotechnology, Nutrition and Health Sciences)

Advanced Materials for Electro-Driven Ion Separation and Selectivity

Kaustub Singh

Thesis

submitted in fulfilment of the requirements for the degree of doctor
at Wageningen University
by the authority of the Rector Magnificus,
Prof. Dr A.P.J. Mol,
in the presence of the
Thesis Committee appointed by the Academic Board
to be defended in public
on Wednesday 16 March 2022
at 4 p.m. in the Aula.

Kaustub Singh
Advanced Materials for Electro-Driven Ion Separation and Selectivity
249 pages.

PhD thesis, Wageningen University, Wageningen, The Netherlands (2022)
With references, with summary in English

ISBN 978-94-6447-090-1
DOI https://doi.org/10.18174/562259

Contents

"To begin, begin"

William Wordsworth

1 Introduction

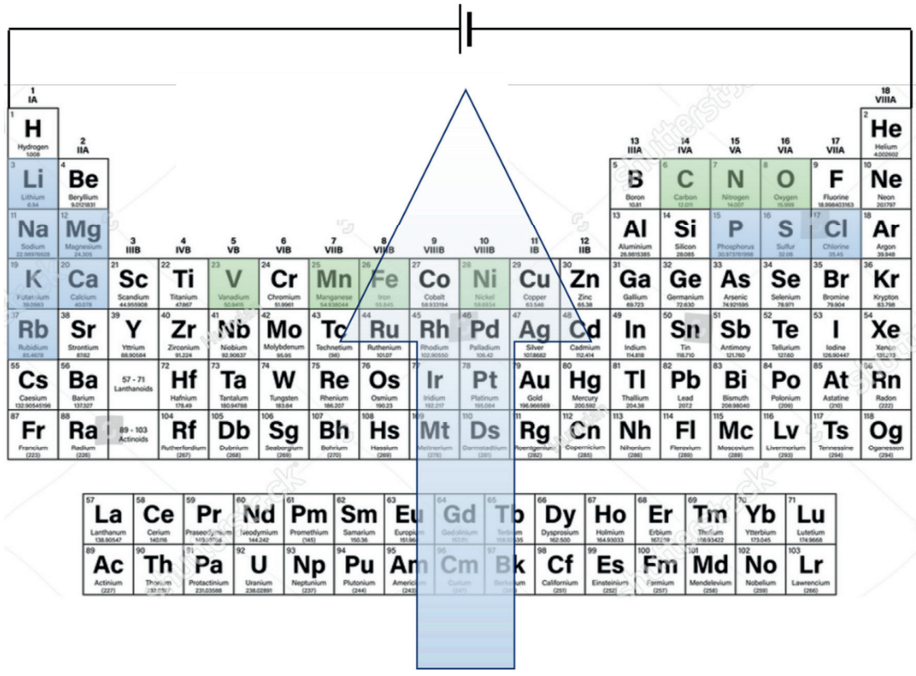

Sections of this chapter are part of the following publication:

Gamaethiralalage, J. G., Singh, K., Sahin, S., Yoon, J., Elimelech, M., Suss, M. E., Liang, P., Biesheuvel, P.M., Zornitta, R.L. & de Smet, L. C. P. M. (**2021**). Recent advances in ion selectivity with capacitive deionization. *Energy & Environmental Science*, *14*(3), 1095-1120.

Treatment of water for domestic and industrial use is an ubiquitous process today. This treatment can be physical, chemical, or biological.[1] Such treatment processes have become important since the resources of usable water are limited, and with an ever-increasing demand, the stress on these resources has risen at a commensurate rate.[2,3] Therefore, the ability to effectively treat and reuse water will determine the lifetime of its resources. The removal of salts and minerals from water is one such treatment that is of high priority. So, what is it and why is it necessary?

This removal is referred to as water desalination.[4–6] It can be performed on water originating from different sources including seas, wells, rivers, and industrial/agricultural wastewater.[7] Technological progress to remove salt efficiently and cost-effectively from water, and to make it (re)usable remains the collective goal of the research efforts within the field of water desalination.[1,8] In addition to the production of water for domestic and industrial use, removal of salts and minerals from water facilitates ion selectivity, making it possible to harvest/recover materials (salts/ions) of value by selectively separating them from water.[3] There are ample examples where removal of specific species is desirable due to their toxicity (arsenic, boron, heavy metals),[9] water hardening (calcium, magnesium),[10] effect on plant health (sodium in irrigation water [11]), value (lithium,[12] gold,[13] phosphate[14]) or for their simple identification (ion sensing).[15] Introducing selectivity in desalination systems is a challenge and demands rigorous research and development efforts.

The processes facilitating desalination are usually powered in three ways – heat,[16] pressure,[4] and electric field.[17,18] Processes powered by heat are referred to as phase change/thermal, while those relying on pressure and electric field are referred to as single-phase processes. Typical examples of the processes powered by heat include multi-stage flash and multi-effect distillation,[1,5] whereas reverse osmosis (RO), electrodialysis (ED), and capacitive deionization (CDI) are examples of the processes powered by pressure and electric field,.[19,20] The share of these technologies in global water desalination efforts is illustrated in **Figure 1.1.**

Commercially available thermal technologies are mostly used for desalination of highly saline water with concentrations of dissolved species > 20,000 ppm. Since the brackish water resources are vastly more than that of freshwater, utilizing these resources for use in daily life is an attractive proposition.[7] It is challenging to accomplish this via thermal technologies due to their high energy demands, environmental impact, water recoveries (defined as the ratio of desalinated water produce and water treated), and potential advantages offered by emerging single-phase desalination technologies, including lower energy consumption and higher water recovery.[5,19] These arguments have shifted the research focus away from thermal technologies towards the single-phase desalination technologies. One such emerging desalination technology forms the basis of exploration of this thesis.

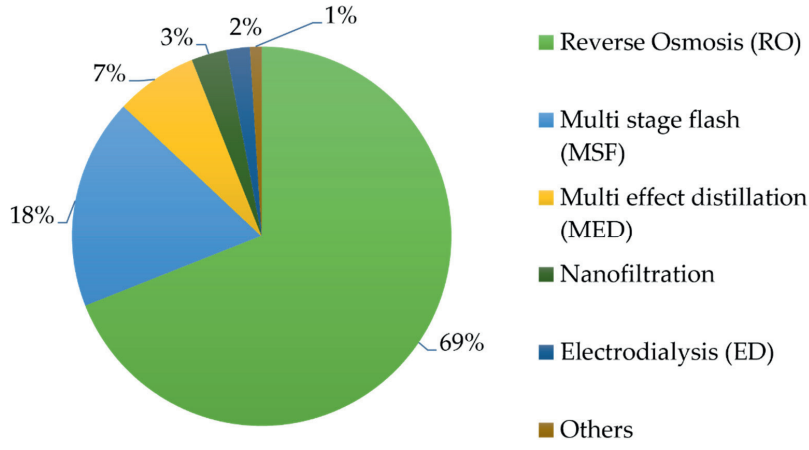

Figure 1.1: Share of different technologies in global desalination, by capacity.[21]

Among single-phase desalination methods, pressure and electro-driven processes demonstrate tremendous promise due to their easy operation, mild environmental impact, and potentially low energy consumption. As a result, they have also proved to be fertile ground for exciting research prospects. Most notable among these technologies are reverse osmosis (RO), electrodialysis (ED), and more recently, capacitive deionization (CDI). These desalination processes involve a flow system in which saline feedwater is pumped into a desalination unit (or a cell) and the output from these flow systems is (usually) a diluted effluent and a concentrated brine. What takes place within the flow unit is desalination and is either driven by applied pressure (RO) or electricity (ED, CDI). In this thesis, the focus will be on CDI. Before diving into it, RO and ED will be briefly introduced along with the need for research into their alternatives.

RO is a pressure-driven desalination technology in which feedwater (brackish with salt concentration in 5 – 50 mM range or seawater with salt concentration in the 600 mM range) is forced through a semi-permeable, hydrophilic membrane that selectively rejects solute, including the salt ions (both positively charged cations and the negatively charged anions), and allows water to pass through it.[4,19,22] As a result, RO can potentially desalinate feeds to completion by rejecting all the dissolved salts, while all water molecules have to pass through. The state-of-the-art for RO has seen a dramatic progress, making it one of most widely used water desalination technology available today, with large-scale adoption in nearly 120 countries in the world.[4,5,23,24] However, RO has its own set of challenges that include operation costs, requirement of pre- and post-treatment steps, membrane fouling, and a lack of single solute (or ionic) selectivity.[22,23,25,26] These challenges demand a two-pronged approach: increased research efforts within the field of RO,[26,27] and generating alternatives to RO for water desalination.[19] An electro-driven approach to water desalination offers this alternative and includes technologies such as ED and CDI. Below is a brief interlude on ED.

Unlike the pressure-driven technology mentioned above, where the aqueous medium dissolving the salts moves out leaving the brine behind, the electro-driven technologies target the dissolved species itself. It is made possible as the salts present in the feed dissociate into cations and anions carrying positive and negative charge, respectively. These charged species are then manipulated by an electric field that is generated by an externally applied current/voltage. ED, the second-most utilized brackish water desalination technology after RO[5] with applications in *e.g.* the bioprocessing and food industry,[17] employs an electric field via application of current/voltage to two faradaic electrodes. The presence of these faradaic electrodes in an ED cell implies that the desalination operation can seemingly continue uninterrupted, provided the reactants are available to sustain the reaction on electrode surface (usually water splitting resulting in hydrogen and oxygen evolution). These electrodes are separated by a series of ion-exchange membranes (IEMs) that can selectively reject cations (anion-exchange membranes, AEMs) and anions (cation-exchange membranes, CEMs). Therefore, an ED cell has multiple chambers that take in a feed of brackish or sea water and produce a brine and a desalinated stream. An AEM selectively allows anions to pass through and reject cations while the CEM does the opposite. This ion selectivity is referred to as permselectivity and is useful in water desalination applications where discrimination between ions carrying same charge is not required.[28,29] In addition, membranes can also deliver selectivity between ions carrying identical charges by incorporating functional groups in the membrane matrix or via surface modification, such as layer-by-layer deposited polyelectrolyte multilayers,[30,31] that alter the counter-ion – membrane interaction.[31–36] It is also claimed that ED membranes are less prone to fouling and scaling than that of RO, resulting in higher recovery rates.[17] However, studies have nevertheless indicated fouling to be present in an ED cell.[31] Furthermore, the high cost of IEMs and non-ideal perm-selectivity (resulting in leakage of co-ions) prohibit widespread adoption of ED.[37] In addition to tackling these issues, it is prudent to look for alternative electro-driven deionization strategies. This is where CDI appears on the scene.

CDI is a water desalination technology that, like ED, uses an electric field to manipulate dissolved salt ions in the feed solution.[18,20,38–40] It has gained a lot of attention for brackish water desalination and ion selective processes.[3,41] The main difference between CDI and ED lies in the nature of the cell component responsible for generation of the electric field. In place of faradaic electrodes that provide electrons via charge transfer reactions on the surface, the electric field in CDI is produced between electrodes that store ions without changing their (electro)chemical characteristics.[42,43] Thus, the electrodes in CDI are capacitive in nature and as a result, desalination via these electrodes depends on their ability to store ions and part of the energy used to facilitate this desalination can be recovered.[44] This seemingly minor change in the nature of the electrodes enables easy ion desorption and ion-selective properties in CDI cells[3,45–47] and, potentially, lower energy consumption in comparison to other technologies such as RO since the energy can be recovered from capacitive electrodes.[24,48] ED has also been

tested with capacitive electrodes, in combination with an energy-generation application where energy recovery is not involved.[49]

Several different configurations of a CDI cell are shown in **Figure 1.2.**[3] The variations in design stem from the use of different electrodes (regular porous carbon,[50,51] flow electrodes,[52,53] and (cation-selective) intercalation electrodes[54–56]), with or without membrane. The conventional design has two porous electrodes separated by a feed channel and is depicted in **Figure 1.2a**. The rest of the configurations follow the choice of electrode materials, appropriately highlighting the importance of electrode materials in CDI. Within the category of capacitive electrodes, there exist a vast library of materials that can store ions. The story of CDI starts with the materials used to prepare the electrodes. So, let us look at the type of electrode materials available for a CDI cell.

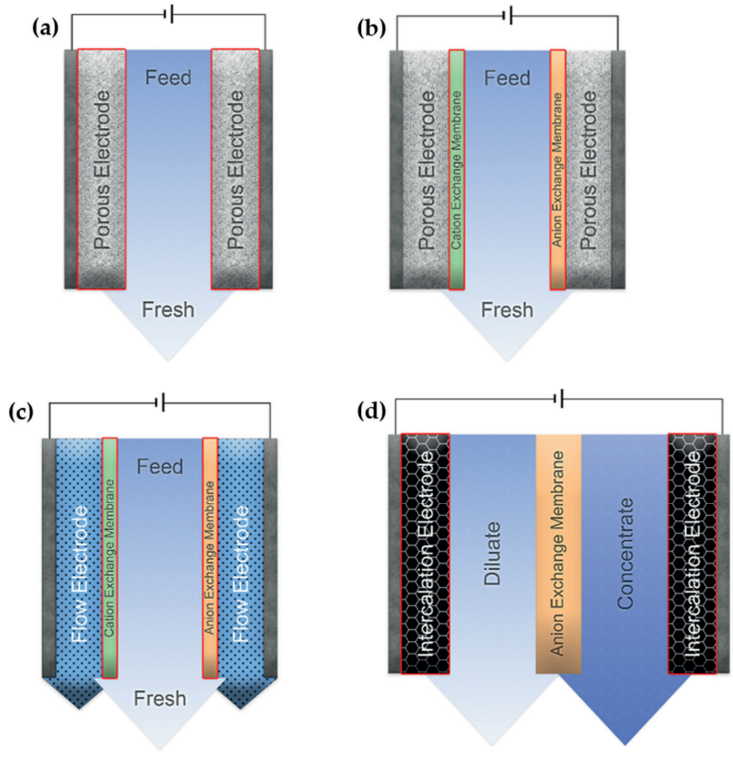

Figure 1.2: Different CDI configurations prepared by a variety of membranes and electrode material combinations. **(a)** Original CDI cell with porous, capacitive electrodes; **(b)** an MCDI cell with IEMs isolating the porous electrodes from the feed; **(c)** flow electrode CDI cell with IEMs separating the feed from the electrode suspension; **(d)** CDI cell with intercalation electrodes, containing two chambers separated by an AEM. (Figure adopted from *Gamaethiralalage et al.*[3])

1.1 Electrode materials

The library of electrode materials in CDI can be neatly divided into carbon and non-carbon-based electrodes. Since CDI began with porous carbon as an electrode material, carbon has conventionally been the go-to material for CDI electrode fabrication. The pores can accommodate ions in an electrical double layer and the theory behind this is well understood and documented.[57–59] The popularity of carbon is well-founded as it is:

1. inexpensive.[60]
2. non-toxic, environmentally friendly, and has been commonly used as an adsorbent.[61]
3. conductive, implying that the contribution of ohmic losses to the total cell voltage is well contained, which leads to a strongly reduced energy consumption for desalination.[62]
4. porous, that results in a large surface area (up to 3600 m^2/g).[63,64] Thus, it provides ample space to store both cations and anions.
5. tunable, *e.g.*, the size of the nanopores, providing a higher degree of control over the storage of ions in the electrode.

Apart from the above-mentioned properties, carbon in its different forms such as activated carbon, cloth, and graphite felt can be modified/impregnated with advanced functional groups.[65–69] Such modifications can either boost the charge storage capacity of the electrode or introduce new properties to the bare carbon such as ion selectivity. However, they may have an adverse effect on the charge efficiency of the desalination operation.[70] Furthermore, suspension of carbon in electrolytes can be used as a flow electrode, as shown in **Figure 1.2c**. In this configuration, the electrode slurry is pumped in the side chambers, while the feed flows in the middle chamber, separated from the flow electrodes by IEMs.[71] For all its benefits and versatility, carbon electrodes also have shortcomings including:

1. Co-ion repulsion.[60,72] In this unproductive phenomenon, ions with the same charge as that of the electrode are expelled from it. Consequently, the efficiency of the ion storage process is compromised because the charge injected into the electrode for storage of ions from water is used to repel co-ions from the electrode, resulting in reduced desalination. This situation can be prevented by placing membranes between the feed and the electrode, essentially isolating the electrodes. Such a system is called membrane capacitive deionization (MCDI) and is an active area of research. A schematic of an MCDI cell is depicted in **Figure 1.2b**. While placement of IEMs solves the co-ion repulsion, it increases the overall cost of the desalination unit as well.
2. Lack of inherent ion selectivity.[73] As discussed before, the selective removal of ions is a crucial application of water desalination and can be successfully achieved with CDI. However, carbon, without any modifications or membranes, shows limited selectivity towards ions, and therefore is more difficult to employ in its pristine state in

applications such as resource recovery, production of fine chemicals, agricultural wastewater treatment, and water softening.

3. Change in pH of the feed solution.[74] During desalination with carbon electrodes, the pH of the treated solution may change due to parasitic side reactions such as oxidation of carbon, reduction of water etc.,[75] at the surface of carbon electrodes.

Due to these shortcomings, need has emerged to explore either modifications[76] or entirely new alternatives to carbon as an electrode material in CDI. One elegant method in which the latter has been done is by deriving inspiration from the highly developed field of energy storage. There are neat parallels between the two applications *i.e.*, CDI and energy storage: both require reversible storage of ions from an electrolyte and rapid charging/discharging for a feasible operation. This is where the intercalation materials come into the scene of CDI.

Intercalation materials, originally studied for energy storage with organic[77,78] as well as aqueous electrolytes,[79,80] have found use as electrode materials in CDI.[41,81] Their use is of interest due to a unique combination of six key factors: a) high equilibrium charge storage capacity in the electrochemical stability window of water, b) (mostly) non-toxic nature, c) easy fabrication, d) absence of co-ion repulsion that obviates the need of an IEM and enhances the efficiency of ion electrosorption, and e) an inherent selectivity towards ions, usually on the basis of their size/hydration energy, f) high degree of customizability, as the number

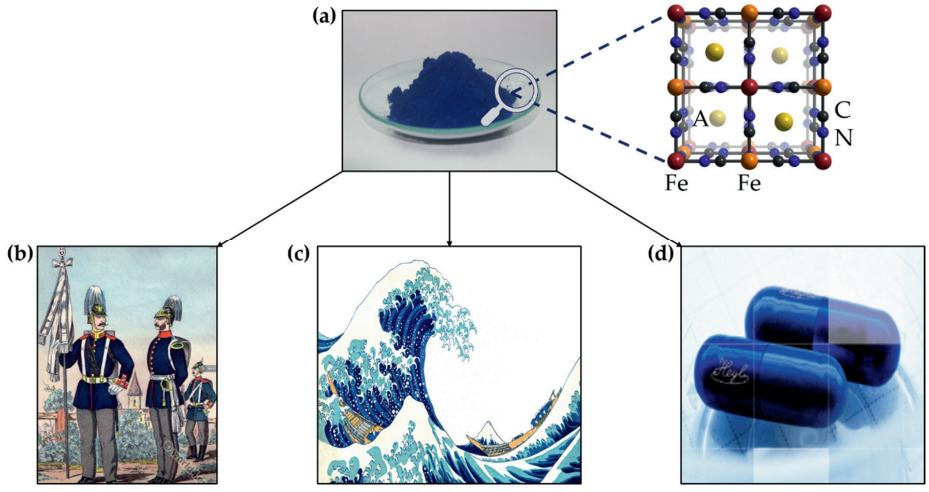

Figure 1.3: Versatile uses of **(a)** Prussian Blue (PB) powder (source – wikipedia.org) in **(b)** textile colouring (image source – pinterest.com), **(c)** pigments in artworks (image source - commons.wikimedia.org), and **(d)** medication for heavy metal poisoning (worldpress.com). The inset in **(a)** depicts the crystal lattice, characteristic of PB powders. The elements constituting the lattice are Fe, C, and N. The alkali metal ion **A**, present in the interstitial lattice site of PB, is generally K or Na.

of industrially useful intercalation materials is large and rapidly growing (largely because of battery research, showing the strong interdependency of seemingly unrelated scientific fields).[3] The mechanism of charge storage in these materials involves intercalation of cations (of multiple valences) in a lattice[82–86] or between layers.[87–89] As a result, they do not require high surface areas to achieve high storage capacity.[90,91] Furthermore, they provide a wide range of chemistries for the curious to explore.[92,93] Among all the intercalation compounds explored as a possible electrode material in CDI, including $NaMnO_2$ (NMO),[94–96] $NaFe_2P_2O_7$,[97] $NaTi_2(PO_4)_3$[98] and others,[89,99,100] Prussian blue (PB) and its analogues (PBAs) have attracted most attention.[101] These compounds also form the focal point of this thesis.

Prussian blue (PB), one of the oldest synthetic pigments, has found many different applications as shown in **Figure 1.3**, including textiles coloring, 18th-century artworks and heavy-metal poisoning medication. Its use in ion storage applications only started four decades ago with the discovery of redox activity of iron present in the PB lattice,[102] shown as an inset in **Figure 1.3a**. In general, PB in its reduced form has the chemical formula $A_2M[Fe(CN)_6]$, where A is an alkali metal (usually Na, K).[82] The elements are usually assembled in a cubic lattice structure with metals Fe and M connected by −C≡N− (cyanide) ligand. For PB, the element M, coordinated to nitrogen, is Fe. When M is anything other than Fe, such as Ni,[103] Cu,[80] and V,[104] or other transition metal, [92,105] the compound is referred to as Prussian blue analogue (PBA). The use of PBAs in CDI has attracted attention because of their open crystal structure, customizable chemical composition, higher equilibrium salt adsorption capacity compared to carbon, and an inherent selectivity among cations. [3,11,90,106,107] The ions removed from water are stored in the interstitial lattice sites of the PBAs. So far, only cations are known to intercalate into these sites, making PBAs perfectly selective towards cations. This insertion is accompanied by a simultaneous change in the oxidation state of a redox-active constituent of the PBA lattice, usually the carbon-coordinated Fe.[84,108] Upon (de)intercalation of a cation into/out of the interstitial site, the Fe undergoes a corresponding reversible redox transformation. This mechanism underlines the ion storage and ion selectivity in PBAs, and these applications will be explored in detail in the upcoming chapters.

Depending on the choice of the electrode materials, a CDI cell can be constructed in any of the four configurations depicted in **Figure 1.2.** A typical example of time-dependent and cyclic change in the concentration of an effluent stream exiting a CDI cell that is operated under a constant current is given in **Figure 1.4.**[91,109] The graph gives the salt concentration of the effluent (treated solution) taken at the outlet of the cell. The black line parallel to the x-axis depicts the inlet concentration of the feed solution, c_{feed}, and the blue curve depicts the change in c_{feed}. Desalination occurs when the blue curve for the effluent concentration dips below c_{feed}. This desalination is characterized by the reduction in concentration, Δc, over one half cycle, as shown in the figure.

Since the ions removed from the feed are electrosorbed in electrodes that have a fixed capacity, the desalination step is followed by their regeneration. In this step, the ions in the saturated electrode are expelled into a separate stream of water, making the electrosorption highly reversible. One desalination and one regeneration step together complete one cycle of operation, as depicted in **Figure 1.4.** After one cycle, a certain amount of salt is removed from the desalinated stream and deposited into the regeneration/concentrated stream. The capacitive electrodes play the role of an intermediary in this salt transfer and the amount of salt transferred from the diluted to the concentrated stream is proportional to the amount of charge injected into the electrode by the external circuit in the adsorption half cycle.

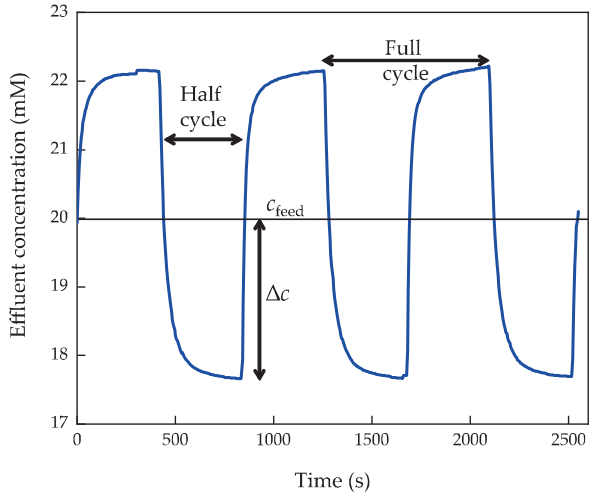

Figure 1.4: A typical plot from a desalination experiment in which the concentration of treated water (effluent) coming out of the cell, operated under constant current, is measured as a function of time. Various operation parameters such as desalination cycle, concentration reduction, Δc, and feed concentration, c_{feed}, are marked on the graph.

The salt removal is usually facilitated by two modes: constant current (CC) or constant voltage (CV).[110] In CC, a fixed current is applied to the cell. This action fixes the rate of ions (and charge) transported to/from the electrodes, per unit time. Consequently, the cell voltage rises or drops, in response to the fixed rate of ion transport, demanded by the external circuit. It is often the case that a cut-off voltage is set in this mode to prevent the cell voltage from exceeding a limiting value and to avoid faradaic side reactions of parasitic nature. On the other hand, in constant-voltage mode of operation, the cell voltage is fixed via the external circuit. This action fixes the difference between the potential of the two electrodes. Since the electrode potential depends on the concentration of ions stored in them, an application of constant voltage results in a corresponding change in the ion concentration of the electrodes. In a direct response to the applied voltage, ions and charges are transported between the electrodes and through the external circuit, respectively, until the ion concentration in the electrodes are

equilibrated at the level dictated by the applied voltage. When compared, in CC mode the cell voltage changes over time in response to a fixed ion transport rate, while in CV mode the ion transport (current) is set up to compensate for the difference in electrode potential implemented by the external circuit. The use of these modes will be demonstrated in the upcoming chapters.

Once a CDI cell is assembled and the operation has commenced under a specified mode (CC or CV), the desalination performance is assessed according to operation parameters.[40] A brief description of these is necessary to comprehend the CDI framework and the discussion in the following chapters.

1.2 CDI parameters

Parameters necessary to assess the performance of a CDI cell can be categorized into separation conditions, performance metrics, and performance indicators.[40] These are explained in the following sub-sections.

1.2.1 Separation conditions

The separation conditions define the situation under which the performance of a CDI cell should be measured. They are defined as follows.

1. Concentration reduction, Δc

The reduction in concentration of the feed solution, as depicted in **Figure 1.4**, is the first direct indication of a desalination operation and is usually calculated as the average over a half cycle:

$$\langle \Delta c \rangle = \frac{N_d}{V_d}, \tag{1.1}$$

where N_d equals the moles of salt removed from the feed in one half cycle and V_d is the volume of feed desalinated in that half cycle. This parameter is crucial as it gives the extent of desalination and depends on the applied current/voltage, the flowrate of the feed and the ion transport in the cell, as explored in the later chapters.

2. Water recovery, *WR*

Water recovery, *WR*, gives the amount of desalinated water produced as a fraction of total volume processed by the CDI cell during one desalination cycle, and is defined as

$$WR = \frac{V_d}{V_d + V_c}, \tag{1.2}$$

where V_c is the volume of feed concentrated in one cycle. So, if a CDI cell produces the same amount of brine and desalinated water in one cycle, the *WR* in that cycle will be 50 %.

1.2.2 Performance metrics

These parameters act as the yardsticks against which the cell performance is measured. The metrics used in this work are defined as follows:

1. Volumetric energy consumption, E_v

The energy E_v consumed by a CDI cell for every m³ of desalinated water produced is given as

$$E_v = \frac{1}{V_d}\int_{\Delta t_{\text{cycle}}} IV dt\,, \tag{1.3}$$

where Δt_{cycle} is the duration of one desalination cycle and the product of current and voltage (power), IV, is positive. The unit of E_v is Wh/m³.

2. Productivity, P

Productivity, P, defined as the volume of the diluate produced per cycle time and projected face area of the electrodes in the cell, in L/h/m², is calculated as

$$P = \frac{V_d}{A\Delta t_{\text{cycle}}}, \tag{1.4}$$

where A is the projected face area of the electrodes. The use of P makes a CDI cell system independent of the feed flowrate, Q (ml/min), resulting in comparable operational parameters. This facilitates easy comparison between two different sets of data taken at different Q.

3. Average salt adsorption capacity, *ASAR*

The average salt adsorption rate is calculated over one full desalination cycle and is defined in two ways:

ASAR (mg/g/min)

$$\frac{\text{SAC}}{\Delta t_{\text{cycle}}}, \tag{1.5}$$

and *ASAR* (μmol/cm²/min)

$$\frac{N_d}{A\Delta t_{\text{cycle}}}. \tag{1.6}$$

where SAC is a performance indicator, defined as the salt adsorption capacity of an electrode, as explained below. The two different normalizations of ASAR presented here neatly highlight

the effect of the weight (g refers to $g_{\text{both-electrodes}}$) and the area ($cm^2$ refers to $cm^2_{\text{both-electrodes}}$) of the electrode, respectively, on the final salt adsorption rate obtained during desalination.

1.2.3 Performance indicators

These performance indicators help to understand the operation of a CDI cell. The ones used in this work are defined as follows.

1. Salt adsorption capacity, *SAC*

The salt adsorption capacity is one of the most-quoted values in CDI literature. In essence, it gives the amount of salt (in mg) absorbed during one half cycle, normalized by the weight of both the electrodes involved in the operation. It is calculated as

$$\frac{QM}{m}\int_{\Delta t_{\text{HCT}}}(c_{\text{in}}-c_{\text{out}})dt\,, \tag{1.7}$$

where Q is the flowrate, m is the weight of the two electrodes, M is the molecular weight of the salt being removed and c_{in} and c_{out} are the inlet and outlet concentrations of the feed solution. Typically, the unit of *SAC* is $mg/g_{\text{both-electrodes}}$. As categorised, it is merely an indicator of desalination performance. It is good to have a high SAC, but there are caveats around it such as: what is the Δc, P, and *ASAR* at which the SAC is being reported? A SAC value quoted without these metrics is difficult to contextualize and therefore, has limited practical use. On a related subject, the SAC must not be confused with equilibrium SAC (eq-SAC), a quantity that represents the maximum salt electrodes can adsorb.[20] The eq-SAC is usually measured under CV at various voltages. It is a useful quantity as it gives an indication of how much capacity is being used during a desalination operation by the SAC obtained with the eq-SAC.

2. Charge and coulombic efficiency, Λ and η

CDI operation requires charge from an external circuit, delivered via an applied current or voltage. To keep an account of this charge supply, indicators such as charge and coulombic efficiencies are introduced. This basic accounting helps keep a track of the ion adsorption and charge input/output, indicating the overall efficiency of the process. *Charge efficiency*, Λ is calculated as

$$\Lambda=\frac{F\Delta N_d}{q_{\text{in}}}, \tag{1.8}$$

where F is the Faraday constant, ΔN_d is the moles of target ion adsorbed by the electrode during the desalination half cycle and q_{in} is the amount of charge supplied to the cell via the external circuit, calculated as

$$q_{\text{in}}=\int_{\Delta t_{\text{HCT}}} I dt\,, \tag{1.9}$$

where $I > 0$.

Unlike charge efficiency, coulombic efficiency, η, does not consider the adsorption of ions during desalination. To the contrary, η represents the ratio of the input and output of charge, q_{in}/q_{out}, to and from the cell, in one full desalination cycle. This ratio indicates the extent of electrode regeneration. Therefore, while the Λ can be calculated for every charge/discharge half cycle, η is calculated only for complete desalination cycle.

With the above-mentioned background information, non-selective deionization can be understood and contextualized. Selective ion separation via CDI also utilizes similar parameters and operation conditions and is usually performed on feed solutions containing multiple (and possibly multivalent) ions. To complete the description of ion selectivity, the preference of one ion, be it cation or anion, over another is reported. This metric has been calculated in different ways in literature.[3] The most common definitions are tabulated below.

Table 1.1: Selectivity based on most definitions in literature. Here, i and j designate two competing ions.[3]

Symbol	Equation	Description
ρ	$\frac{\frac{c_{i,in}-c_{i,f}}{c_{i,in}}}{\frac{c_{j,in}-c_{j,f}}{c_{j,in}}}$	$c_{i,in}$ and $c_{i,f}$ are initial and final concentrations of the target ion. $c_{j,in}$ and $c_{j,f}$ are initial and final concentrations of the competing ion.
$S_{i/j}$	$\frac{\int_0^t (c_{i,inf}-c_{i,eff})dt/c_{i,inf}}{\int_0^t (c_{j,inf}-c_{j,eff})dt/c_{j,inf}}$	$c_{i,inf}$, $c_{i,eff}$, $c_{j,inf}$, $c_{j,eff}$ are concentrations (c) of influent (inf) and effluent (eff) of two competing ions, i and j, respectively.
R	$\frac{R_i}{R_j}$	R_i and R_j are calculated by dividing the effluent concentration by feed concentration of each ion.

1.3 Research objectives

The broad objectives of this work include the fabrication, characterization, and application of next-generation electrode materials for (selective) ion separation via CDI. In more detail, this dissertation aims to:

1. Explore PBA electrodes and their properties in CDI, and to compare them with carbon electrodes.
2. Obtain cation selectivity using PBA electrodes in CDI and explore the structure-property relation of PBAs.

3. Investigate simultaneous anion and cation selectivity from a symmetrical CDI cell.
4. Generate theoretical insights into the working of a symmetric CDI cell containing cation intercalating electrodes.

Below follows a brief introduction to the literature on (selective) deionization of water that forms a backdrop for the research problems to be tackled and presented in the next seven chapters of this thesis.

1.4 Scope and context of the research

In recent years, CDI has gained much attention in water desalination, even though the concept has existed since 1960s.[111] This focus is due to the ease of operating a CDI cell and regenerating the electrode, potential for energy recovery,[112] and more recently, a vast potential for selective ion separation.[3] Originally conceived with porous carbon electrodes due to their fast adsorption and desorption of ions in an electrical double layer,[3,20,113] the field of CDI has incorporated elements from the field of energy storage as well to augment the ion removal and storage capacity of carbon electrodes.[101] It must be pointed out that concerted efforts on improving carbon as an electrode material has also led to an increase in its capacity for ion storage. Nevertheless, the use of capacitive, energy storage materials in CDI intensified over the last decade and required comprehensive chronicling to understand the research already done and extrapolate for the future investigation ideas. **Chapter 2** records the rise in the use of non-carbon intercalation materials, presents insights on the common trends, and provides an outlook on future research focus. It becomes clear from this comprehensive review that the increased attention on the non-carbon electrodes has had a two-pronged effect on the state-of-the-art: (i) the salt adsorption capacities being reported are vastly higher than those reported using porous carbon, and (ii) inherently ion-selective CDI cells have been developed. Consequently, tailor-made ion-selective CDI cells can be fabricated, depending on the application demand. In this thesis, both topics are addressed in detail.

The first effect of energy storage materials on the CDI state-of-the-art is observed in the indiscriminate ion adsorption that enables water desalination. Use of intercalation (or other non-carbon) materials has enhanced the SACs delivered by the cells. In addition, a number of studies reporting desalination of feeds with salinity beyond the range of brackish water have also come up. However, with the rapid proliferation of reports on the use of new non-carbon materials, it becomes imperative to objectively compare them with carbon to weigh their merits. In this thesis, a class of one such intercalation material, PBA, is tested for its potential for (selective) water desalination. **Chapter 3** embarks upon one such comparative investigation by pitting a state-of-the-art intercalation electrode based on nickel hexacyanoferrate (NiHCF), a PBA, against the conventional, activated carbon electrodes. This investigation addresses **Aims - 1 -** and **- 4 -** of this research, as mentioned in **Section 1.3**. The NiHCF electrodes were assembled in a symmetric CDI cell, also referred to as a rocking chair cell,[56,69,114,115] illustrated

in **Figure 1.2d**, while the activated carbon electrodes were assembled in an MCDI configuration, as illustrated in **Figure 1.2b.** The symmetric/rocking chair cell contains two geometrically, physically and chemically identical NiHCF electrodes separated by an AEM. This configuration allows one electrode to adsorb cations while the other regenerates. As a result, the cell produces concentrated and diluted streams simultaneously, and does not require a separate regeneration step, as usually obtained with (M)CDI cells with carbon electrodes. The experimental conditions for both the electrode materials were matched and their desalination performance was measured according to the metrics described in **Section 1.2.2** to arrive at an objective comparison. Furthermore, the individual performance of the NiHCF electrodes in a rocking-chair cell was quantified by systematically operating it under various operational conditions and comparing it with the state-of-the-art to contextualize the results and highlight the benefits of using a symmetric, two-chamber cell for water desalination in CDI.

The second of the two effects of the use of intercalation electrodes in CDI, as described before, is the development of ion-selective CDI cells. The intrinsic ability of these intercalation electrodes to differentiate ions (usually cations) of the same charge can potentially revolutionize the use of CDI cells in applications where one ion is preferred over the others. While techniques like ED use membranes to achieve this selectivity, carbon electrodes in CDI and membranes in MCDI use surface functionalization to gain ion selectivity. On the other hand, intercalation electrodes in CDI can obviate any such need for a membrane or a surface modification to deliver ion selective desalination. Intercalation electrodes possess an inherent filter (ion size/hydration energy, ion charge) that may facilitate preferential adsorption of one (cat)ion over another. Understanding ion selectivity of PBA electrodes was one of the aims of this research, noted as **Aim - 3 -.** Towards this end, the ion selectivity of NiHCF electrodes in a symmetric CDI cell is reported in **Chapter 4**, along the lines of the aim where Na^+ was selectively adsorbed from a ternary aqueous mixture that also contained divalent Ca^{2+} and Mg^{2+}. In practical terms, such a separation will be crucial in controlling the concentration of Na^+ ions in irrigation water that can potentially harm the soil and plant health.[11,116,117] The results obtained showed a correlation between the preference of the Na^+ and its size/hydration energy, in relation to the other two divalent ions present in the feed solution. Remarkably, this selectivity towards Na^+ remained largely independent of its concentration in the solution, relative to that of the divalent ions.

The ion selectivity with PBA electrodes was further explored by altering the chemical composition of the material, within the scope of **Aim - 3 -** of this thesis. **Chapter 5** presents these findings with altered chemistry of PBAs. The replacement of nickel in the NiHCF lattice with vanadium altered the selectivity of the resulting VHCF electrodes. This observation was further supported by preliminary theoretical calculations based on density functional theory (DFT). The results presented in this chapter open exciting new opportunities for manipulating ion selectivity of PBA electrodes by tinkering with their chemical composition. In addition, the

successful use of DFT calculations to explain the experimentally observed phenomena facilitates a better understanding of preference of ions by intercalation electrodes in general.

From the above discussion, it is easy to note that the conversation on ion selectivity has focused only on cations so far. It is because anions intercalate in few, layered intercalation materials. Furthermore, no report on anion selectivity with intercalation materials has emerged. On the contrary, carbon can be made selective towards different anions via surface functionalization. **Chapter 6** addresses this lack of anion selectivity in CDI cells constructed with intercalation electrodes and provides a method to implement simultaneous anion and cation selectivity, firmly in line with **Aim - 4 -** of this thesis. The assembled cell resembled the symmetric cell depicted in **Figure 1.1d** and had two flow channels interfacing two identical NiHCF intercalation electrodes. The channels were further separated from each other by an AEM. The surface of this AEM was modified by charged polymers, also known as polyelectrolytes.[118] This resulted in an extra layer of charge on top of the AEM that imparted an anion-selective property to the cell. The NiHCF electrodes, on the other hand, remained the cation-selective element of the cell. Upon polarization, the electrodes selectively adsorb/desorb cations, while the anions selectively electro-migrate through the modified membrane. This arrangement resulted in simultaneous differentiation between cations and anions and each element of the cell became functional. Such a configuration carries a vast potential when it comes to tunable cation as well as anion selectivity.

Chapters 2 – 6 primarily present experimental investigations into (selective) CDI. However, development of a quantitatively precise model to understand and predict cell performance is necessary in the development and commercialization of (selective) CDI.[119,120] In addition to aiding in understanding and predicting the performance of a CDI cell, such a model can be used to optimize cell design elements (*e.g.* electrode and spacer thickness) and operation parameters (*e.g.* applied current/voltage, feed flow rate). Finally, mathematical models can serve as a great tool in comparison of desalination performance across different desalination technologies, such as RO, ED, and CDI, as recently attempted in literature.[121,122] This is the reason behind the **Aim - 4 -** of this thesis that is pointed towards developing a theoretical, system-level understanding of a symmetric CDI cell with intercalation materials. **Chapter 7** of this thesis presents the first mathematical model developed to understand and predict desalination by a symmetrical CDI cell, with two intercalation electrodes interfacing with two flow channels and separated by an anion-exchange membrane as depicted in **Figure 1.2d**. The model hinges around a Nernst-Planck equation to account for the ion transport in the flow channels, electrodes and the membrane. The modes of ion transport modelled were diffusion, advection, and electro-migration. While all the three modes influenced ions in the feed flow channels, advection was assumed to be absent within the electrodes and the membrane, separating the two compartments. In addition to ion transport, an isotherm (Frumkin adsorption) was used to account for the storage of ions into the intercalation particles. When solved for a specified cell design, mode of operation and conditions, the model predicted the effluent concentration and the overall cell voltage, providing insight into the Δc

and E_v of desalination. Moreover, it also provided insight into quantities that are not directly measured such as the fraction of electrode filled with cations over time. This mathematical framework was also used in **Chapter 3** to predict and explain the desalination performance of the two chamber CDI cell constructed with NiHCF electrodes. Recently, an extension of this model was reported by our group that attempted at explaining the cation selectivity delivered by intercalation materials such as NiHCF.[3] This augmented model explains the preferential adsorption of one monovalent cation over the other, based on the difference in their size/hydration energy. The model predicts very high selectivity, more than 12 times towards the smaller cation over the larger one, at short timescales (within 1 second of the commencement of the adsorption operation). As the adsorption progresses, uptake of the bigger cation increases, readily reducing the initial high selectivity. The mathematical framework neatly describes the dependence of selectivity on the moment in the adsorption cycle and has implications for the electrode design and operation conditions to realize the full potential of ion selectivity of intercalation electrodes.

The last chapter of this thesis, **Chapter 8**, presents discussions and perspectives on interesting leads for future work by taking inspiration from the results of this thesis. This discussion outlines how the findings on energy efficient water desalination and ion selectivity, as put forward in this thesis, can act as a platform to facilitate development of more efficient and customizable CDI cells. This chapter is followed by a **Summary** that recounts the highlights of each chapter and describes the essence of each chapter and the investigation presented in them.

An over-arching theme in **Chapter 8**, and the **Summary** of this thesis is sustainable development and how the results and outlook of this thesis contribute towards the global efforts towards realizing a sustainable future. This contribution is highlighted by drawing a connection between the outcomes of this thesis (both results and the outlook inspired by them) and the sustainable development goals (SDGs) put forward by the United Nations (UN). A total of 17 SDGs were adopted in 2015 by the UN to work towards ensuring global peace and prosperity by 2030. Not only the findings of this thesis contribute directly towards some of the SDGs, but the future work, inspired from these findings, will also contribute to the goal of improving water desalination and harvesting of resources from waste water, summarized under the 6th SDG : Clean water and Sanitation. As stated, international cooperation should be built-up around water desalination, harvesting, recycling, and reuse technologies. The research themes of energy efficient water desalination and selective ion recovery as explored in this thesis, together with an outlook on the future on the CDI state-of-the-art, constitute a direct contribution toward global sustainable development efforts.

2 Timeline on the Application of Intercalation Materials in Capacitive Deionization

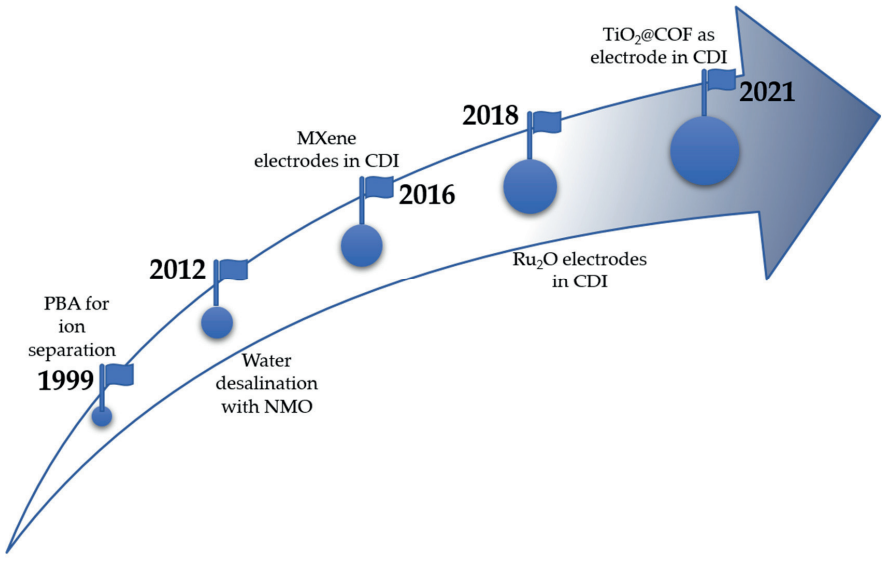

This chapter has been published as:
Singh, K., Porada, S., de Gier, H. D., Biesheuvel, P. M., & de Smet, L. C. P. M. (**2019**). Timeline on the application of intercalation materials in Capacitive Deionization. *Desalination*, *455*, 115-134.

Since the publication of this study (Spring 2019), new reports on the use of intercalation materials as electrodes for desalination have appeared in literature as highlighted in the graphic above. Short summaries of the selected reports are appended to this chapter.

Abstract

Capacitive deionization is a water desalination technology in which ions are stored in electrodes in an electrochemical cell construction, connected to an external circuit, to remove ions present in water from various sources. Conventionally, carbon has been the choice of material for the electrodes due to its low cost, low contact resistance and high specific surface area, electronic conductivity, and ion mobility within pores. The ions in the water are stored at the pore walls of these electrodes in an electrical double layer. However, alternative electrode materials, with a different mechanism for ion and charge storage, referred to as ion intercalation, have been fabricated and studied. The salt adsorption performance exhibited by these materials is in most cases higher than that of carbon electrodes. This work traces the evolution of the study of redox activity in these intercalation materials and provides a chronological description of major developments in the field of Capacitive Deionization (CDI) with intercalation electrodes. In addition, some insights into the cell architecture and operation parameters are provided and an outlook is presented.

2.1 Introduction

The electrochemical technology of Capacitive Deionization (CDI) has witnessed an exponential increase in research and development efforts over the past years. It employs porous electrodes to remove ions of interest from water. These ions are driven to the interior of the electrodes by the electrical current, where they are stored. The mechanism of ion storage in CDI depends on the type of electrode material. The mechanism can be ion adsorption next to a charged interface, or ion insertion into a host lattice, which may or may not be followed by a change in the redox state of an element constituting the lattice. The first category consists of carbon-based electrodes which have been studied[51,123–125] and reviewed thoroughly.[18,20,126] Similar literature is available for non-carbon electrodes for applications in energy storage[92,105] and desalination.[46,101,127][46] However, no attempt has been made to record the use of intercalation materials in the rapidly growing field of CDI. The current work intends to fill this gap by providing a review in the form of a timeline overview on the use of inorganic ion intercalation materials as electrodes for water desalination by CDI. We also address selected papers from other fields (*e.g.*, energy storage) that inspired the use of such materials for water desalination.

Research into cheaper alternative materials for Li-ion batteries led to research into aqueous sodium and potassium ion batteries, due to their low cost and easy availability.[92] As a consequence, transition metal compounds such as $NaMnO_2$,[128] $Na_2Fe_2P_2O_7$, [129] and $Na_2Ni[Fe(CN)_6$ (NiHCF)[79] were nominated as promising candidates for aqueous ion batteries. Since CDI requires storage of ions in the electrodes of a desalination cell, the electrode materials used for batteries satisfy this condition of being capable of ion storage as well. Carbon as an electrode material has been in use in CDI since the 1960s.[111,130] However, intercalation materials have certain key advantages in comparison to carbon as electrodes in CDI. The first advantage is the ability of intercalation materials such as nickel hexacyanoferrate (NiHCF) to provide the same salt adsorption capacity (SAC) at a lower voltage. Therefore, these materials have a lower energy input than carbon electrodes. This is attributed to a higher differential charge, $\frac{\partial Q}{\partial E}$ where Q is the charge input/output and E is the corresponding change in the electrode potential, in comparison to carbon.[54] Differential charge values are reported to be an order of magnitude higher for NiHCF electrodes than those for carbon electrodes.[54] Therefore, the use of intercalation materials may potentially reduce energy consumption while keeping SAC unchanged. Secondly, carbon electrodes suffer from co-ion expulsion, a phenomenon where co-ions are depleted from the electrical double layer (EDL) during ion removal from the salt solution.[131] With carbon electrodes, it has been observed that an increase in the salinity of the water leads to a decrease in the salt adsorption, and consequently leads to a decrease in the charge efficiency (*i.e.* the moles of salt adsorbed/moles of charge input).[119,131] This effect can be minimized by placing ion-selective membranes in between the electrodes and the salt solution as done in (M)CDI[132] or by surface modification of carbon electrodes.[133,134] The use of intercalation materials is another approach to obtain a high charge

efficiency without requiring membranes or surface modification, which reduces the complexity of cell design and electrode preparation.

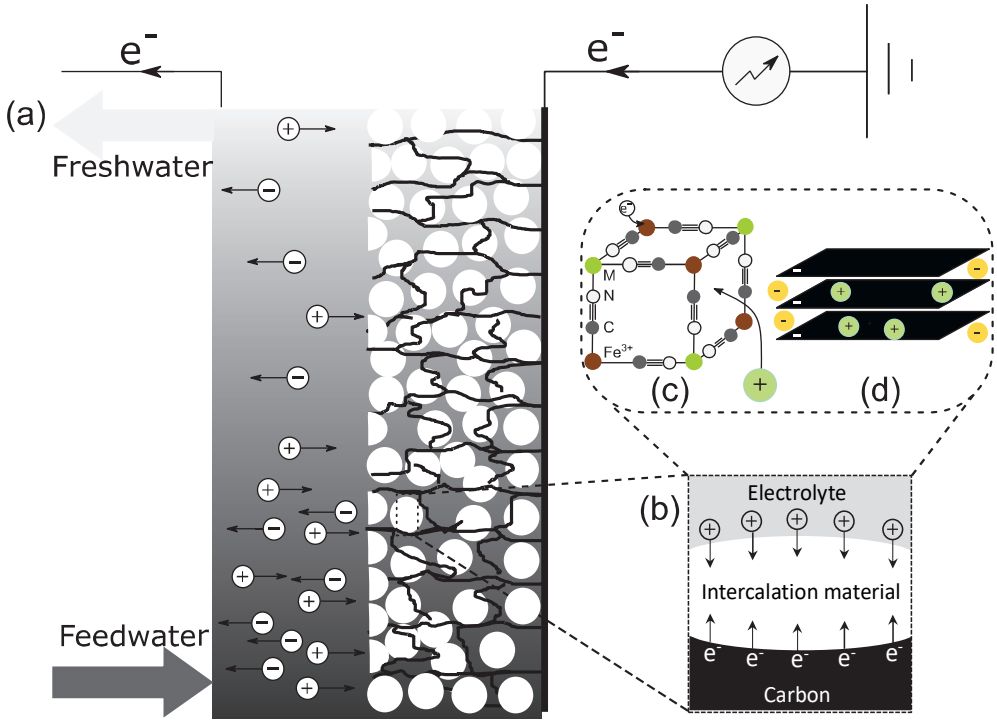

Figure 2.1: (a) Schematic illustration of an intercalation material being used as an electrode in a CDI cell. Salt concentration in the flow channel adjacent to the electrode undergoing intercalation decreases with time, indicated by the grey-scale gradient. Black lines in the electrode area represent the conductive carbon which provides an electronic link between the intercalation particles (white circles) and the current collector. **(b)** Schematic representation of intercalation of cations and inclusion of electrons in the electrode. **(c)** Illustration of redox-active cation intercalation, as seen in sodium hexacyanoferrate (NiHCF) electrodes with a cage-like lattice. **(d)** Intercalation through electrostatic interaction between intercalant and host material as seen in MXene electrodes.

In intercalation materials, the mechanism of ion storage via insertion into the interstitial lattice sites is different from that for carbon electrodes. In most types of intercalation materials, only cations or anions are adsorbed, and thus the co-ion expulsion effect is avoided leading to an enhanced charge efficiency of desalination. In addition, the use of intercalation materials facilitates size-based selective separation of ions bearing a certain valence and charge.[135] In contrast, porous carbon electrodes demonstrate a limited selectivity towards different ions.[73,136–141] As a substitute to the carbon electrode in CDI, intercalation materials have now been successfully employed as porous electrodes in a CDI cell setup.[56,95,97]

A schematic picture illustrating an operational CDI cell with an intercalation material as an electrode is shown in Figure 1 (a). It depicts a flow-by configuration in which the electrolyte flows parallel to the porous electrode in an adjacent flow channel.[109] **Figure 2.1** represents a moment in time when cations intercalate into the cathode. This process can be controlled by the application of a current or voltage difference across the electrodes. As a consequence of cation intercalation, the salt concentration in the flow channel adjacent to the electrode decreases. Electrode regeneration can be easily accomplished by reversing the electrical current. Different configurations with an altered placement of the flow channel have also been explored.[142] The inset **b** in **Figure 2.1** represents the ion storage mechanism of intercalation electrodes. The cation and an electron are included into the intercalation material to preserve the overall electroneutrality. A closer look into this mechanism is provided in the insets **c** and **d** that describe different types of intercalation material. In **Figure 2.1c** a cation is inserted into a lattice vacancy while one of the lattice atoms is reduced,[102] whereas in **Figure 2.1d** cations intercalate in between the negatively polarized sheets of a layered structure.[87]

A specific example of ion-intercalation followed by a redox reaction is observed in electrodes prepared from Prussian Blue (PB) and its analogues (PBAs.)[108] These materials (in their reduced form) generally have an ideal formula of $A_2M[Fe(CN)_6]$ where A is an alkali metal (Na, K). For PB, the element M is Fe whereas for PBAs, M can be Ni, Cu, Mn and other transition metal elements.[82] Upon (de)intercalation of an alkali metal into/out of the interstitial site, the carbon-coordinated Fe undergoes a corresponding redox transformation, as shown in **Figure 2.1b**, and it ensures an electroneutral environment for the lattice. PBAs, which resemble zeolites in their structure, have crystal lattices with fixed dimensions (*e.g.*, the diameter, *d*, of the entrance to the interstitial site in the PBA NiHCF is d=1.6 Å),[143] and can filter out ions with a size that is above this diameter, making the electrodes ion-selective.[144]

Another method of intercalation, as illustrated in **Figure 2.1d**, is observed with materials such as MXene. These are transition metal carbides, nitrides and carbonitrides (MXene phases) which are 2-D materials of the form $Ti_3C_2T_x$ (where T refers to a surface terminated group such as O, OH or F) with layered structures. Ions of different size and valence have been demonstrated to intercalate in between such sheets.[87] The ion storage in these materials is not necessarily accompanied by a redox reaction. However, it has been argued that in the case of Li intercalation, charge transfer occurs between the carbon atoms in the carbide sheets and the Li-ion.[145]

Cation intercalation in the electrode, resulting in desalination, depends on the ion storage capacity of the electrode. If an electrode is perfectly selective to only adsorb either cations or anions, the ion storage capacity is directly proportional to the capacity to store charge, expressed in mAh/g. The utilization of this capacity depends on many factors, primary amongst them are the current density (in a constant current experiment)[137] and voltage (in a constant voltage experiment) and the salt concentration of the water. The operational conditions, dictated by these parameters, determine the actual realized charge capacity of the electrode as well as the retention of this capacity with number of cycles. In addition, these parameters influence the resistance in the cell and as a consequence, the rate of salt removal

and the energy consumption in a desalination experiment.[56,95] An ideal CDI cell should have sufficient salt adsorption capacity, a high salt removal rate and low energy input.

This timeline overview attempts to chronicle the advances in the use of non-carbon intercalation materials in the field of CDI. In our view, this is an efficient method to map the progress in new electrode materials for CDI. We also include selected works about aqueous ion batteries that have had a direct consequence to the field of CDI. In the final section, we extrapolate from the literature and provide a brief outlook for future directions of research. Our work is intended to help in consolidating the efforts of the CDI community towards achieving improved solutions to selective and energy-efficient water desalination.

2.2 Timeline for intercalation materials in CDI

In this section we provide a chronological description of published studies that investigate the properties of intercalation materials (with and without redox activity) and employ these materials in a desalination process based on the principles of CDI. The order in which they are described here is determined by their date of submission, to provide an overview of how the field developed. Our descriptions are intended to give a clear picture of the idea behind every study, the reported observations, and the operational conditions. To this end, keywords are also provided for each entry. The default system (which is *not* indicated with keywords) is as follows: the paper is an experimental study including data for the characterization of the electrode (three-electrode setup), and data of desalination in a CDI cell (two-electrode setup), with an aqueous electrolyte, and a single salt solution. Operation is asymmetric (anode and cathode have different composition) and there is no membrane. Deviations from this default system are addressed with keywords as listed in **Table 2.1**.

Table 2.1: Keyword number and description, used to categorize all timeline entries.

Number	Description
1(a)	Only theory
1(b)	Theory and experiments combined
2	Only characterization in a 3-electrode setup; no desalination data
3	Symmetric operation, *i.e.*, same chemical composition anode + cathode
4	Non-aqueous electrolyte
5	Solution with multiple ions
6	Including Ion-exchange membrane

Besides these numerical keywords, information is provided on the mode of operation *i.e.*, constant voltage (CV) or constant current (CC), typical salt concentration, typical voltage or current, a specified value of salt adsorption capacity (SAC) in mg/g and the electrode material, if not mentioned in the title of the paper.

1. Neff, V.D., **1978**. **Electrochemical Oxidation and Reduction of Thin Films of Prussian Blue.**
   Journal of the Electrochemical Society
   Kent state University, USA; *Submitted:* Sep. 29, 1977; *Revised:* Dec. 1, 1977.[102]
   Keyword: (2)

   This study ignited the interest in electronic activity of Prussian blue (PB) by demonstrating its redox properties. A 100 mM KCl solution was used as an electrolyte to perform cyclic voltammetry for thin film PB electrodes. The oxidation of the redox active center of the PB lattice with the applied potential was the cause of the reversible change in color of the electrode film from blue to colorless. This hinted at the reversible nature of the redox reactions in the thin film electrode. It was the first evidence of cation intercalation in the interstitial sites of a PB lattice. The study was restricted to PB and did not investigate its derivatives (Prussian blue analogue, PBA).

2. Bocarsly, A.B. and Sinha, S., **1982. Effects of surface structure on electrode charge transfer properties: Induction of ion selectivity at the chemically derivatized interface.**
   Journal of Electroanalytical Chemistry and Interfacial Electrochemistry
   Princeton University, USA; *Received:* Aug. 17, 1982.[146]
   Keywords: (2), (5), NiHCF
   The capability of Nickel hexacyanoferrate (NiHCF) thin film electrodes to intercalate alkali metal cations is reported in this work. The experiments were performed for electrolytes of respective alkali metal ions, at a concentration of 1 M. The half-cell potential increased with increasing cationic size following the trend $Li^+ > Na^+ > K^+ > Rb^+ > Cs^+$ in aqueous media. This implied that there was an inherent preference based on size towards the cations being inserted into the lattice of the thin film electrode. Fast (de)intercalation of Cs^+ ions against Li^+ ions was reported hinting clearly towards a size dependent affinity of the electrodes for the cations in a non-aqueous electrolyte. Works to follow would establish the size-based selectivity of PBAs towards different cations.

3. Schneemeyer, L.F., Spengler, S.E. and Murphy, D.W., **1985. Ion selectivity in nickel hexacyanoferrate films on electrode surfaces.**
   Inorganic Chemistry
   AT&T Bell Laboratories, USA; *Submitted:* Nov. 16, 1984; *Accepted:* Sep. 1985.[143]
   Keywords: (2), (5)
   This work made the first advance towards demonstrating the dependence of cation size on intercalation in NiHCF, a PBA. The authors identified the diameter of the interstitial site to be 3.6 Å and that of the lattice channel connecting this site, to be ~ 1.5 Å. Under the presence of an organic electrolyte, it was observed that Li^+ ions and Na^+ ions could intercalate reversibly but the insertion of K^+ ions was inhibited. The ions bigger than K^+,

which are Rb^+ and n-tetra ethylammonium (TEA^+), did not intercalate at all. It was reported that a wider spectrum (in size) of cations was inserted into NiHCF in aqueous electrolyte and there was no clear size dependence trend, as seen for non-aqueous electrolytes. It was concluded that the role of water, in this departure from the observed trend of size selectivity in non-aqueous electrolyte is unclear.

4. Ikeshoji, T., **1986. Separation of Alkali Metal Ions by Intercalation into a Prussian Blue Electrode.**
   Journal of the Electrochemical Society
   Government Industrial Research Institute, Tohoku, Japan; *Submitted:* Nov. 16, 1984*; Accepted:* Sep. 1985.[135]
   Keywords: (2), (5)

   This work focuses on selective separation of alkali metal ions from an aqueous mixture of Li^+, Na^+, K^+, Rb^+, and Cs^+ ions by using $KFe_2[(CN)_6]$, a PB, as an electrode material. A platinum plate (area ~ 20 cm^2) with PB coatings on both sides was used to intercalate cations from a mixture in batch mode. The reduction steps were performed for a 100 mM ion solution for 10 minutes at a current of 1 mA. The regeneration step with alkali ion deintercalation was performed with a 100 mM acetic acid solution, giving rise to the effluent stream. It was reported that the total number of moles of cations removed was 95 % of the total moles of charge input to reduce the oxidation state of the redox active iron in the PB lattice. The selectivity for the alkali metal cations, was reported to follow the order $Li^+ << Na^+ < K^+ < Rb^+ << Cs^+$. No explicit quantification of selectivity was provided but the mole fractions of the alkali ions in the effluent solution was reported as an indicator of the ionic selectivity. This trend is opposite to what was observed in [146] for non-aqueous electrolytes. An inhibition of charge transfer due to the presence of Na^+ ions was observed during cyclic voltammetry of the PB film electrode in a K^+ - Na^+ mixture. However, this observation was not explained.

5. Lilga, M.A., Orth, R.J., Sukamto, J.P.H., Haight, S.M. and Schwartz, D.T., **1997. Metal ion separations using electrically switched ion exchange.**
   Journal of the Electrochemical Society
   Pacific Northwest National Laboratory, USA; *Submitted:* Sep. 21, 1995*; Accepted*
   Feb. 26, 1996.[147]
   Keywords: (2), (5), NiHCF

   This study describes the practicality of the metal ion separation method defined as "Electrically switched ion-exchange" (ESIX).

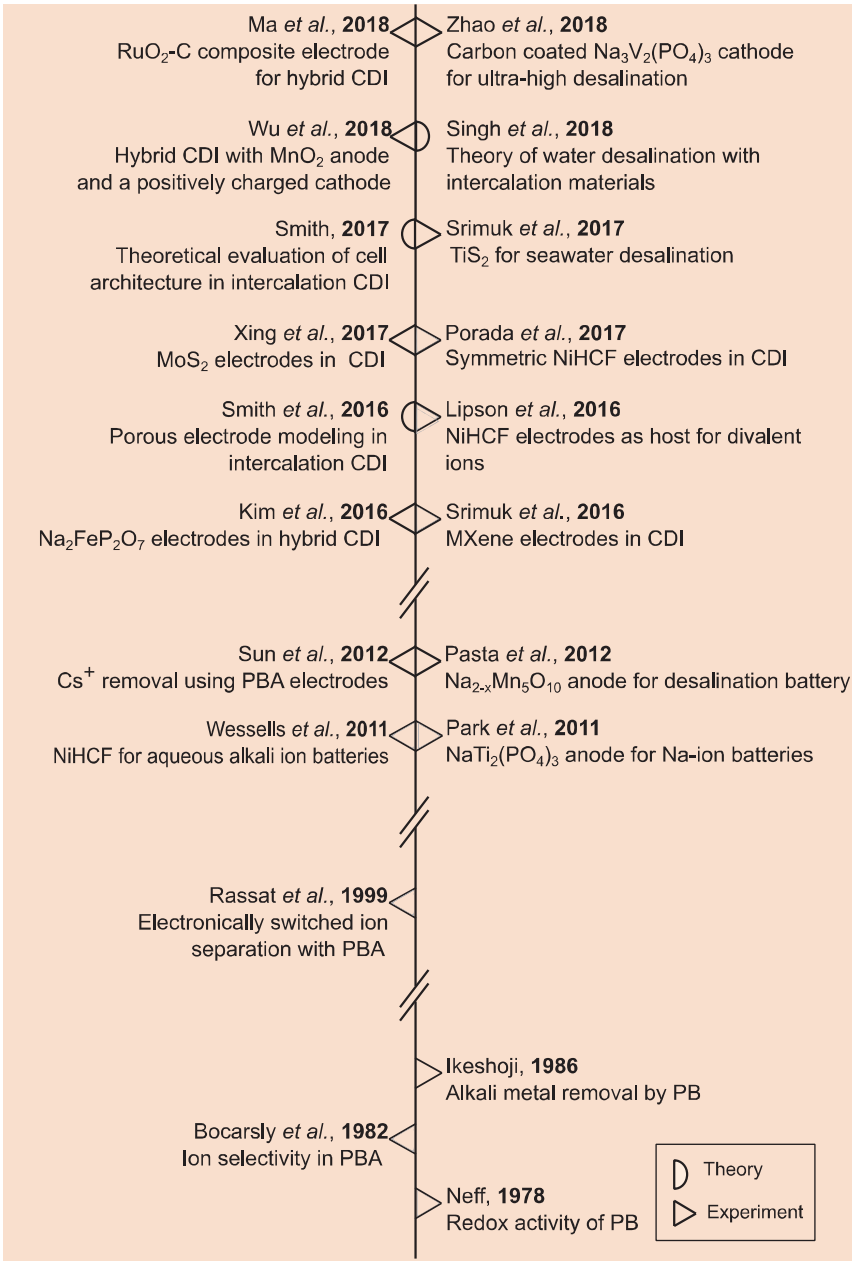

Figure 2.2: A brief chronology describing the development of intercalation materials based on selected papers.

A thin film of nickel hexacyanoferrate (NiHCF), electro-deposited on a nickel surface, was studied for alkali metal ion insertion. It was demonstrated that the hexacyanoferrate film was selective towards Cs^+ in a Na^+ rich electrolyte. An earlier reported film fabrication

procedure, carried out by applying a voltage of 1 V (*vs.* standard calomel electrode) to a nickel surface exposed to 5 mM $K_3Fe(CN)_6$ and 100 mM KCl solution for 300 s, was modified to yield films of higher capacity and improved cycling rates. These modifications were termed as PNNL and were detailed in the work due to their proprietary source. During the discharge step, which is referred to as the load cycle by the authors, Cs ions were inserted into the NiHCF lattice. The charge step, referred to as unload cycle, lead to de-insertion of Cs^+ ions. The rate of diffusion of ions through the film was reported to be different for the charge and discharge steps. It was attributed to the solvent exchange process, but no further explanation was delivered. It was reported that the presence of Cs^+ ions in the interstitial sites of NiHCF made it stable in a highly basic medium. Based on previously observed trend of size dependent ion intercalation in PBA, as described elsewhere,[102,146] the authors expected the Cs^+ ion to be the preferred cation for (de)insertion in NiHCF lattice from a mixture of multiple ions.

6. Rassat, S.D., Sukamto, J.H., Orth, R.J., Lilga, M.A. and Hallen, R.T., **1999. Development of an electrically switched ion exchange process for selective ion separation.**
Separation and Purification Technology
Pacific Northwest National Laboratory, USA; *Submitted:* April 20, 1998*; Accepted:* July 15, 1998.[148]
Keywords: (2), (5), NiHCF

This work focuses on depositing an ion exchange film on an electrode surface followed by ion uptake into it and their subsequent elution. This is accomplished by changing the electrochemical potential of the deposited film. The film material used was NiHCF, a redox-active intercalation material. The improved film fabrication procedure from[147] was employed, leading to a higher capacity retention for the electrode. In addition, the authors attempted to quantify the selectivity of alkali-metal ions in pairs. The selectivity of K^+ and Cs^+ ions over Na^+ ions was systematically investigated for different salt mixture compositions using cyclic voltammetry (CV) and quartz crystal microbalance (for quantification of intake of ions by the NiHCF film). Very high selectivity ($\alpha_1^2 = \frac{x'_2/x'_1}{x_2/x_1}$, where the numbers *1* & *2* serve as an identifier for the types of ions, x'_1 and x'_2 are mole fractions of ions *1* and *2* in the film; x_1 and x_2 are mole fractions of ions *1* and *2* in the bulk) was reported for Cs^+ ions over Na^+ ions for a salt solution with low (2300:1 Na^+:Cs^+ mole ratio) Cs^+ concentration. A sharp decrease in α was observed with an increase in the relative concentration of Cs^+ ions over Na^+ ions in the salt solution. It was argued that an estimation of separation factors was sensitive to the fluctuations in a apparent molar weights of pure species. A detailed discussion about the use of peak currents in a CV experiment for cation selectivity was also provided.

7. Yang, J., Zou, L., Song, H. and Hao, Z., **2011. Development of novel MnO_2/nanoporous carbon composite electrodes in capacitive deionization technology.**
Desalination
University of South Australia, Australia; *Submitted:* Feb. 24, 2011*; Accepted:* March 16, 2011.[149]
Keywords: CV, 1.2 V, 50 mM NaCl, 17 μmol/g-active material

This work uses MnO_2/nanoporous carbon composite for removal of ions from brackish water using CDI. It was claimed by the authors that this was the first application of such a composite as an electrode for desalination purposes. Physical characterization revealed a smaller Brunauer–Emmett–Teller (BET) surface area (total surface area including micro and meso-pores) and pore volume, for the composite in comparison to the activated carbon (AC). However, the meso-surface area (area of the meso-pores with size in between 2 and 50 nm) was found to be larger and was argued to be the effective area for desalination. Electrochemical characterization revealed a capacitive behaviour with a rectangular voltammogram for the composite electrodes and in general, higher capacitance was reported for these electrodes compared to AC. The authors claimed that MnO_2 can provide a high pseudo-capacitance. The desalination experiments were done at constant voltage and the electrochemical cell had only one flow channel, thus interrupting the supply of desalinated water during the regeneration step. The salt adsorption of the composite electrodes (17 μmol/g) was roughly three times the value observed for carbon electrodes (5 μmol/g), for a 50 mM NaCl solution and a maximum salt removal efficiency of ~ 81 % was observed. The mechanisms for charge storage in MnO_2 were identified to be based on electrical double layer formation on pore surface, and intercalation of ion in the MnO_2 lattice followed by, as indicated by the authors, a faradaic reaction which must involve an electron transfer from the external circuit to the MnO_2 electrode. This may result in the change in the valence of the intercalated cation as specified in.[150] The contribution of each mechanism in the reported salt adsorption capacity of the composite electrodes were not specified or deliberated further.

8. Park, S.I., Gocheva, I., Okada, S. and Yamaki, J.I., **2011. Electrochemical Properties of $NaTi_2(PO_4)_3$ Anode for Rechargeable Aqueous Sodium-Ion Batteries.**
Journal of the Electrochemical Society
Kyushu University, Japan; *Submitted:* May 11, 2011*; Accepted:* June 17, 2011.[151]
Keywords: (4), (6)

This study reports on the use of $NaTi_2(PO_4)_3$ as anode material for sodium-ion batteries. Experiments were performed to ascertain the capacity of these anode materials in a Na_2SO_4 electrolyte. In addition, it was demonstrated that the loss of capacity of electrodes with charge/discharge cycle was higher for cells with aqueous electrolytes against those using organic electrolytes at low applied current densities. With increasing current density, the

capacity retention for the electrode decays quicker in the organic electrolyte than aqueous electrolyte. In organic electrolyte, the electrodes lost ~ 70 % of their initial capacity after 30 cycles at 20 A/m^2. In comparison, only 40 % capacity loss was observed for aqueous electrolytes. A smaller over-potential for charge/discharge cycle was observed for aqueous electrolyte in comparison to organic electrolyte. The authors attributed this to the smaller impedance and viscosity in the aqueous medium. It was also observed that the decay in the capacity was accelerated at pH > 9 which was attributed to an easier decomposition of phosphate group in aqueous electrolyte. The authors identified the next step towards preparing a sodium ion battery is to find a Na^+ accepting electrode, stable in aqueous electrolyte.

9. Wessells, C.D., Peddada, S.V., Huggins, R.A. and Cui, Y., **2011. Nickel Hexacyanoferrate Nanoparticle Electrodes for Aqueous Sodium and Potassium Ion Batteries.**
Nano Letters
Stanford University, USA; *Submitted:* Sept. 13, 2011*; Accepted:* Nov. 01, 2011.[152]
Keywords: (2), (5)

This study was one of the first to demonstrate that NiHCF is an attractive material for grid-scale batteries due to its low cost, fast kinetics (because of its open framework structure) and long cycle life. The fabrication of NiHCF was carried out by a co-precipitation method where the reactants were added dropwise to a common liquor to maintain a fixed reactant ratio and consequently, constant composition of the precipitate. The NiHCF electrodes were characterized in a three-electrode cell with NiHCF as a working electrode, an oversized NiHCF electrode as counter electrode Ag/AgCl electrode as a reference and aqueous 1 M solutions of $NaNO_3$ and KNO_3 as an electrolyte. The potential for insertion of Na^+ and K^+ into the NiHCF lattice was reported as 0.59 and 0.69 (*vs.* SHE). The capacity of NiHCF electrodes, for both the cations, was reported to be 60 mAh/g at a charging rate of C/6 (1 C is the electrode charging rate at which the electrode is charged to its full, theoretical capacity in one hour). The authors reported a capacity retention of 87 and 67 % at charging rates of ~ 8C and 42C, respectively, in a $NaNO_3$ solution. A similar performance was observed when the cycling was performed in a KNO_3 solution. This led the authors to conclude that NiHCF can sustain high charge/discharge rates. The open framework structure, enabling fast ion diffusion, led to a low voltage hysteresis during cycling. An increase in the applied current density (and therefore the charging rate) resulted in a linear increase in voltage hysteresis. Most of this was attributed to the electrolytic resistance. The NiHCF electrode showed no capacity loss after 5000 cycles in the $NaNO_3$ solution sodium electrolyte at 8.3C. However, after 1000 cycles in the KNO_3 solution, capacity loss was observed. The authors also measured the effect of the state of charge on the NiHCF electrodes by ex-situ XRD spectra obtained for the electrodes at different states of charge. It was reported that the lattice parameters increased with charging (cation deintercalation) in the KNO_3 solution. This increase corresponded to an increase in the radius of

[$Fe^{2+}(CN)_6^{3-}$] ion. The authors argued that the interaction of the so-called zeolitic water in the NiHCF lattice with water in the hydration shell of the (de)intercalating ions make the transport process complex and less understood.

10. Pasta, M., Wessells, C.D., Cui, Y. and La Mantia, F., **2012**. **A Desalination Battery.**
Nano Letters
Stanford University, USA; *Submitted:* Nov. 4, 2011*; Accepted:* Jan. 23, 2012.[153]
Keywords: (5), CC, 5.0 A/m², seawater salinity, NaMNO

This study proposed a desalination battery for salt removal using a $Na_xMn_5O_{10}$ ($2<x<4$ [128]) nanorod intercalation cathode and an Ag/AgCl anode. The desalination was performed in batch mode. The initial salt solution had a concentration equal to that of sea water and it was regularly changed after the cation uptake and removal half cycles. The NMO electrodes showed removal for ions other than Na^+ as well, notably Ca^{2+}, Mg^{2+} and K^+ ions. However, the K^+ ion was observed to be less preferred over other cations. The authors attributed this to the larger size of K^+ ions (without the hydration shell) in comparison to Ca^{2+}, Mg^{2+} and Na^+ ions. This finding is in contrast to what was reported in works before[135] and after this study[54] about the size of cation and their selectivity. The coulombic efficiency of the process was reported to be around 80 % with the rest of the charge being diverted to side reactions such as the reduction of oxygen. The authors claimed that the efficiency values give information about the selectivity of the electrodes towards intercalating cations. Finally, energy values for the desalination battery and reverse osmosis were compared and it was found that the energy required for 25 % reduction in salt concentration was 0.3 Wh/L, a value that, according to the authors, is comparable to that obtained for reverse-osmosis under similar conditions (0.2 Wh/L).

11. Lu, Y., Wang, L., Cheng, J. and Goodenough, J.B., **2012. Prussian blue: a new framework of electrode materials for sodium batteries.**
Chemical Communications
The University of Texas at Austin, USA; *Submitted:* March 10, 2012*; Accepted:* May 4, 2012.[79]
Keywords: (2)

This work is one of the first to indicate that PB and its analogues, prepared by replacing the Fe atoms in PB with transition metals such as Cu, Ni, Mn, Co, and Zn, can be a feasible electrode material for sodium-ion batteries. From the X-ray diffraction characterization, it was concluded that different transition metal ions change the cubic lattice parameter. The electrochemical characterization was performed in an organic liquid carbonate electrolyte at a rate of C/20 (C is the current density in mA/g which can charge/discharge the electrode in an hour). The charge (deintercalation) capacity was reported to be higher than the discharge (intercalation) capacity for all the analogues. Insertion of Na^+ ions in $KFe_2(CN)_6$ showed a capacity of 100 mAh/g and the capacity remained stable for 30 cycles. The charge

capacity declined with increasing number of cycles and plateaued at 120 mAh/g. It hints at the capacity of PB being higher than any of its analogues prepared by replacing Fe atoms with a transition metal element.

12. Sun, B., Hao, X.G., Wang, Z.D., Guan, G.Q., Zhang, Z.L., Li, Y.B. and Liu, S.B., **2012**. **Separation of low concentration of cesium ion from wastewater by electrochemically switched ion exchange method: Experimental adsorption kinetics analysis.**
Journal of Hazardous Materials
Taiyuan University of Technology, China; *Submitted:* May. 21, 2012*; Accepted:* July 3, 2012.[154]
Keywords: (3), (6), CV, 0-7 V, salinity 10-30 mg/L, NiHCF

NiHCF precipitated on porous three-dimensional carbon felt (PTCF) substrate is used in this work to remove Cs^+ ions from a salt solution in a continuous mode. The electrochemical cell comprised of two similar NiHCF electrodes separated by an AEM. The effect of variation in applied potential, salt concentration and pH were studied. Low concentrations of Cs^+ in the solutions, rarely encountered in literature (10-30 mg/L), were used to study cation adsorption. The removal of Cs^+ ions is reported to increase when the applied potential was increased from 0 to 7 V. Such high values of potentials are rarely seen in ion separation/removal studies involving redox-active electrodes and in CDI with aqueous salt solutions. Following the potentials, a variation in salt concentration resulted in no observable difference in the percentage adsorption of Cs^+ ions and a full 100% removal of Cs^+ ions was reported. A decrease in pH resulted in a decrease in the adsorption of Cs^+ ions. It was attributed to the increase in the concentration of H_3O^+ which may result in Cs^+ ions being repelled away from the electrodes, reducing their adsorption.

13. Chen, R., Tanaka, H., Kawamoto, T., Asai, M., Fukushima, C., Na, H., Kurihara, M., Watanabe, M., Arisaka, M. and Nankawa, T., **2013. Selective removal of cesium ions from wastewater using copper hexacyanoferrate nanofilms in an electrochemical system.**
Electrochimica Acta
National Institute of Advanced Industrial Science and Technology, Japan; *Submitted:* June 29, 2012*; Accepted:* Aug. 31, 2012.[155]
Keywords: (2), (5)

This study employs electrodes prepared by coating a titanium + gold substrate with copper hexacyanoferrate (CuHCF) to selectively remove Cs^+ ions from wastewater in a three-electrode cell. The Cs^+ ion removal was followed by regeneration of the electrode. The system was operated by switching the voltage between 0 and 1.3 V. A poor regeneration of active particles in the conventional system (using CuHCF powders in a Cs^+ solution), in comparison to the proposed three-electrode cell, was demonstrated. Metal removal was identified as a three-step process. These steps were described as: bulk phase diffusion; film

diffusion; and intra-particle diffusion. Diffusion in the particle, which the authors agreed was a slow process, was still not explicitly mentioned as the rate-limiting step. It was also claimed that the uptake capacity of the electrode decreased with an increase in electrode thickness due to active sites remaining unutilized. The removal efficiency however increased with increasing electrode thickness. This observation was attributed to an increase in surface area. Removal efficiency and uptake capacity saw no appreciable change in the pH range of 0 - 9. A sharp decline in these values was observed at a pH of 12. A preference for Cs^+ over Na^+ ions was reported but no quantitative discussion was provided.

14. Lee, J., Kim, S., Kim, C. and Yoon, J., **2014**. **Hybrid capacitive deionization to enhance the desalination performance of capacitive techniques.**
Energy & Environmental Science
Seoul National University, South Korea; *Submitted:* July 28, 2014*; Accepted:* Aug. 28, 2014.[95]
Keywords: (6), CV, 1.2 V, 10-20 mM NaCl, SAC 31 mg/g-both electrodes, NMO

A novel hybrid desalination cell architecture is proposed in this work. The authors used $Na_4Mn_9O_{18}$ (NMO), a battery material, to fashion a cathode and chose a porous carbon anode. The design includes a single channel for the flow of water. Consequently, there is no provision for a continuous supply of desalinated water. A high salt removal capacity of 31 mg was reported per grams of total electrode weight for a 10 & 20 mM salt solution when desalinated at a constant voltage of 1.2 V. The authors claimed this value to be twice as high as the one reported for conventional porous carbon CDI systems (*i.e.*, ~ 14 mg/g). However, the exact operation conditions for the carbon electrodes used for comparison were not mentioned. In addition, the use of AC as an anode material, which has a lower salt adsorption capacity than the NMO electrode was not a limiting factor in the desalination experiment. The ion-removal capacity was reported to remain constant with changes in salt concentration. The ion-removal rate and capacity increased with an increase in operational voltage. It was attributed to the increase in the electro-sorption capacity of AC electrode and an enhancement in the rate of reaction in the NMO electrode. The authors concluded that the proposed hybrid system can be used to desalinate water with high concentration (~100 mM).

15. Smith, K.C. and Dmello, R., **2016. Na-Ion Desalination (NID) Enabled by Na-Blocking Membranes and Symmetric Na-Intercalation: Porous-Electrode Modeling.**
Journal of The Electrochemical Society
University of Illinois at Urbana-Champaign, USA; *Submitted:* June 16, 2015*; Accepted:* Jan. 5, 2016.[142]
Keywords: 1(a), (6), NiHCF

This study introduces a new electrochemical cell design for sodium ion desalination (NID). A precursor to this design has already been discussed in [156]. It presents a theoretical study of a symmetric cell with two similar intercalation electrodes used for desalination of a NaCl salt solution. The materials modelled in simulation were $NaTi_2(PO4)_3$ (NTP) and $Na_{0.44}MnO_2$ (NTP). A cell with an anion-exchange membrane and one with a non-selective membrane, separating the two electrode compartments, were compared for cation-removal performance. The equilibrium potentials for these electrode materials were estimated from their potentials against an Ag/AgCl reference electrode measured during a charge/discharge cycle. The study used the Butler-Volmer equation to model the current density because of cation intercalation into the redox-active electrodes. A modified expression for the exchange current density, derived from literature on the modelling of Li-ion batteries, was used with a dependence on electrolyte concentration and the intercalation degree of the electrodes. The current density obtained from the Butler Volmer equation was then used to model the time dependence of intercalation degree of the electroactive material in the electrode. A mass balance on the salt was written using Darcy's law for a flow through porous media with an additional term for the flux (in the form of current) due to (de)intercalation. The simulation results showed that the proposed cell can desalinate water of a salinity resembling seawater. It was concluded that ion selectivity in the separator membrane was essential for a high degree of desalination. It was also observed that increasing the applied current density increases polarization of electrodes leading to a rapid rise in voltage. The energy consumption was observed to decrease with increasing concentration and decreasing electrode thickness.

16. Chen, R., Tanaka, H., Kawamoto, T., Wang, J. and Zhang, Y., **2017**. **Battery-type column for cesium ions separation using electroactive film of copper hexacyanoferrate nanoparticles.**
Separation and Purification Technology
University of Chinese Academy of Sciences, China; *Submitted:* Aug. 10, 2015*; Accepted:* Sep. 10, 2016.[157]
Keywords: (2)

The authors in this work propose a device for electrochemical removal of Cs^+ ions, referred to as battery-type column. The electrodes used for cation removal were fabricated by depositing CuHCF nano-particles on a stainless-steel electrode through spray coating. The battery setup consisted of a platinum reference electrode, CuHCF nano-particle coated stainless steel as the working electrode and a stainless-steel sheet as a counter electrode, like a three-electrode cell setup. Two different salt concentrations for Cs^+ ions were tested (4 and 6 ppm) and the removal efficiency in both cases was reported around 97 %. The voltage was switched between 0 and 0.4 V to adsorb and desorb Cs^+ ions into the redox-active electrode. The kinetics of the redox reaction was divided in two parts and fitted with a pseudo-first and second order model. The authors argue that the Cs^+ ion removal is

dominated by electro-static attraction in the initial stages of the reaction and gradually, as the opposite charge of the electrode is compensated, chemical reduction of Fe(III) to Fe(II) becomes the dominant cation removal mechanism. The reduction of iron in the beginning of the experiment was not considered. A stability analysis for the CuHCF film was performed by CV. The oxidation and reduction peaks were shifted away from each other and towards higher potentials. However, the changes were not discussed quantitatively further.

17. Chen, B., Wang, Y., Chang, Z., Wang, X., Li, M., Liu, X., Zhang, L. and Wu, Y., **2016**. **Enhanced capacitive desalination of MnO_2 by forming composite with multi-walled carbon nanotubes.**
RSC Advances
Fudan University, China*; Submitted:* Dec. 11, 2015*; Accepted:* Jan. 4, 2016.[158]
Keywords: CV, 1.4-1.8 V, salinity 30 mg/L, SAC 7mg/g-active material

The authors use an electrode fabricated out of a composite of a multi-walled carbon nanotubes and MnO_2 for water desalination. The electrode was referred as a capacitor in this study. Its performance was also compared to that of the electrode with only MnO_2. A physical characterization revealed an increase in surface area in the composite against the regular MnO_2. A higher capacitance for the composite was reported and this was attributed to an enhanced surface area of MnO_2 together with a reduced internal resistance. The desalination experiments were performed in batch-mode for a solution with 30 mg/L NaCl. Activated carbon was used as anode. The operation was performed at different voltages between 1.4 - 1.8 V. The salt removal was reported as ~ 7 mg/g-total active materials weight in both electrodes. This adsorption capacity was 4 times higher than that observed for electrodes made of only MnO_2. This led the authors to conclude that the modified MnO_2 electrodes can be considered in CDI.

18. Lipson, A.L., Han, S.D., Kim, S., Pan, B., Sa, N., Liao, C., Fister, T.T., Burrell, A.K., Vaughey, J.T. and Ingram, B.J., **2016. Nickel hexacyanoferrate, a versatile intercalation host for divalent ions from non-aqueous electrolytes.**
Journal of Power Sources
Argonne National Laboratory; USA, *Submitted:* Jan. 27, 2016*; Accepted:* June 5, 2016.[77]
Keywords: (2), (4), (5)

This study employs NiHCF based electrodes to remove divalent ions from non-aqueous electrolyte solutions. The capacity of the electrode when cycled with Ca^{2+}, Mg^{2+}, and Zn^{2+} ions was reported to be around 50 mAh/g, similar to aqueous solutions with Na^{+} ions. The capacity also varied with the number of cycles. For a solution with Mg^{2+} ions the capacity increased to 80 mAh/g with increasing number of cycles whereas in case of Ca^{2+} ions, the capacity declined with increasing number of cycles. The capacity for the solution with Zn^{2+}

ions was reported to be constant with the number of cycles. During cyclic voltammetry experiments, Ca^{2+}, Mg^{2+}, and Zn^{2+} ions gave a redox potential of 2.9, 2.6 and 1.2 V, respectively. The Na:Fe content in the electrodes was measured using EDX. The ratio dropped from 0.6 to 0.2 following the charging of electrodes (Charging here is referred to as the process of removing Na^{+} ions from the Prussian blue lattice by subjecting it to high positive voltages). The elemental composition of the electrodes was also measured during charging and discharging by energy-dispersive X-ray spectroscopy. An increase in the content of Ca^{2+}, Mg^{2+}, and Zn^{2+} ions was reported upon discharge (Discharging is referred to the process of insertion of cations in the NiHCF lattice). The change in lattice structure was monitored using XRD. As the change in lattice parameter was less than 1 %, it was concluded that repeated cycling is unlikely to cause any mechanical degradation in the lattice structure.

19. Kim, S., Lee, J., Kim, C. and Yoon, J., **2016**. **$Na_2FeP_2O_7$ as a Novel Material for Hybrid Capacitive Deionization**.
Electrochimica Acta
Seoul National University, South Korea; *Submitted:* March 5, 2016*; Accepted:* April 11, 2016.[97]
Keywords: (6), CV, 0.9-1.5 V, 10-100 mM NaCl, SAC 30 mg/g-cathode

This study proposes a hybrid capacitive desalination system (HCDI) with $Na_2FeP_2O_7$ as the primary redox-active cathode material. It consisted of an electrochemical cell with one inlet, a redox-active cathode and an AC anode with an anion-exchange membrane separating them. The system was operated under constant-voltage conditions. The salt solution was continuously pumped into the cell and the delivery of freshwater was interrupted during regeneration of the electrodes. The electro-chemical characterization comprised of CV and galvanostatic intermittent titration (GIT). The capacity of the cathode, observed during GIT at a charging rate of 0.5 C, was 56 mAh/g. The salt adsorption capacity (SAC) of this HCDI system was reported at 30 mg/g- $Na_2FeP_2O_7$ electrode. Different salt concentrations (10, 50, and 100 mM) were tested for three different voltages (0.9, 1.2, and 1.5 V). The rate of deionization increased by 40% when the concentration was increased from 10 to 100 mM. This was attributed to the decrease in ionic resistance of the electrolyte solution. The HCDI system was claimed to have a higher SAC to the membrane capacitive deionization (MCDI) systems with symmetric carbon electrodes at low applied current densities. The difference in performance between these two systems decayed at higher current densities. Thus, the authors concluded that at high current densities, the HCDI system cannot utilize the available capacity of the $Na_2FeP_2O_7$ for desalination. Therefore, the operation parameters are crucial for the performance of the proposed HCDI system.

20. Srimuk, P., Kaasik, F., Krüner, B., Tolosa, A., Fleischmann, S., Jäckel, N., Tekeli, M.C., Aslan, M., Suss, M.E. and Presser, V., **2016**. **MXene as a novel intercalation-type pseudocapacitive cathode and anode for capacitive deionization**.
Journal of Materials Chemistry A
Saarland University, Germany; *Submitted:* Sep. 9, 2016*; Accepted:* Nov. 2, 2016.[89]
Keywords: (3), CV, 1.2 V, 5 mM NaCl, SAC 13 mg/g-active material

This study reports on a new intercalation electrode material, modelled along the lines of an ideal supercapacitor, for CDI. It was referred to as MXene and was used in the form of nanosheets to intercalate anions as well as cations. The MXene electrodes were prepared by first fabricating Ti_3AlC_2 (referred to as the MAX phase) and then treating it with hydrofluoric acid. The electrode was directly cast on the separator used to isolate the anodic and the cathodic compartments, for CDI experiments. The authors point out that this work was the first to adopt such an electrode preparation method in CDI. The galvanostatic charge/discharge of MXene resembles to that of a capacitor due to a linear rise in voltage with current (and therefore, the charge input). The capacitance of MXene when compared to AC electrodes, was attributed to the intercalation of ions in between the MXene sheets. The authors argue that this feature qualifies MXene as a pseudo-capacitor material. It was observed that the voltage is not evenly distributed between the cathode and the anode and as a result, the potential is shifted to negative values. This observation was explained by the presence of groups terminating in –OH, =O and –F on MXene surface giving it a negative static charge. The salt adsorption was reported as 13 mg/g-active material for a 5 mM salt solution during a constant voltage operation at 1.2 V. The average salt adsorption rate was reported to be 1 mg/g/min. The electrodes were observed to be highly stable over 30 cycles. The authors identify the ion (de)intercalation and oxidation of the sheets as two primary sources of the observed morphological changes in the MXene.

21. Smith, K.C., **2017. Theoretical evaluation of electrochemical cell architectures using cation intercalation electrodes for desalination.**
Electrochimica Acta
University of Illinois at Urbana-Champaign, USA; *Submitted:* Sep. 21, 2016*; Accepted:* Feb. 2, 2017.[159]
Keywords: (1a), (3), (6), NiHCF

This theoretical study tries to predict the performance of NiHCF electrodes for various electrochemical cell architectures. The author demonstrated that the NiHCF electrodes are capable of efficiently desalinating water with seawater level salinity. The model was set up in a manner similar to that in.[142] For this work, a thermodynamic factor (activity γ) was included in the existing model relating the ionic current in the electrolyte to, as proposed by the authors, intercalation reaction current density derived from the Butler-Volmer equation. The activity coefficient was included to account for the concentrated nature of

the salt solution which marked the shift from dilute to concentrated solution treatment. Experimentally measured bulk diffusion coefficient of salt along with revised bulk ion conductivity for a concentrated solution was included in the model. This, as the author claimed, aided in explaining the electrode polarization due to ohmic resistance as well as concentration changes in saltwater flowing through the cell. The simulations were done for three cell designs: A flow-through (FT) cell, in which the water flows through the electrodes; A flow-by (FB) cell, in which the water flows along the electrodes in a channel; and a membrane flow by (MFB) cell in which an extra cation exchange membrane (CEM) is introduced between the flow channel and the electrode. The simulation results showed the MFB cell, with polarization and cation intake capacity, was comparable to the FT cell and better than the FB cell. A decrease in the discharge capacity of the FB cell was attributed to an increased polarization, due to the absence of a CEM. The enhanced performance of the MFB was attributed to its ability to retain salt within the electrodes. A similar explanation, however, not provided, can be expected for the flow through electrodes which have similar performance as the MFB and employ only one membrane. It was claimed that the concentration in the FB cell decreases over time as compared to the MFB cell in which the concentration remains constant at the same initial salinity level when averaged across the cell width. The study went further to claim that the NiHCF electrode can be used to desalinate a 700 mM stream in an electro-dialysis stack.

22. Xing, F., Li, T., Li, J., Zhu, H., Wang, N. and Cao, X., **2017**. **Chemically exfoliated MoS_2 for capacitive deionization of saline water.**
Nano Energy
National Center for Nanoscience and Technology, China; *Submitted:* Nov. 11, 2016*; Accepted:* Dec. 7, 2016.[99]
Keywords: (2)

Stimulated by a study showing that chemically exfoliated nanosheets of MoS_2 (ce-MoS_2) containing a high concentration of the so-called metallic 1T phase can electrochemically intercalate a series of group 1 ions with extraordinary efficiency [160], Xing et al. explore these 2D materials for electrode fabrication to remove ions from wastewater through CDI. In more detail, a comparison between electrodes made from, what is referred to as bulk MoS_2, and ce-MoS_2 was formulated. The exfoliation was performed on the 2H phase MoS_2 to obtain ultra-thin 1T phase MoS_2 nanosheets. The phases and properties themselves were not detailed in the work but can be found in.[160] Salt solutions from 50 to 400 mM were desalinated using the ce-MoS_2 and bulk MoS_2 electrodes. The maximum salt adsorption capacity observed was ~ 9 mg/g for a 400 mM NaCl salt solution at 1.2 V. The weight used to normalize the SAC value was not explicitly mentioned. This was claimed to be the highest in comparison to a series of five selected carbon-based electrodes. The comparison was hindered by the fact that the exact conditions (salt concentration, applied voltage) for the carbon electrodes were not mentioned. Nevertheless, this work does show the potential

of using 2D ce-MoS_2 in CDI. Considering the high mass and volume-specific CDI performance, the authors believe that the as-prepared multilayer 1T phase ce-MoS2 nanosheets will be favourable for the miniaturization of commercial CDI device.

23. Lee, J., Kim, S. and Yoon, J., **2017**. **Rocking Chair Desalination Battery Based on Prussian Blue Electrodes**.
ACS Omega
Seoul National University, South Korea; *Submitted:* Dec. 19, 2016*; Accepted:* April 13, 2017.[56]
Keywords: (6), CC, 5 A/m², 500 mM NaCl, SAC 60 mg/g-both electrodes

This study focuses on desalinating high salinity water by CDI in a continuous manner using two PBA electrodes. The desalination cell consisted of nickel and iron hexacyanoferrate ($Na_2Ni[Fe(CN)_6]$ and $Na_2Fe[Fe(CN)_6]$) separated by an anion exchange membrane. The system had an intake of water from two channels which ran parallel to the electrodes. This ensured that the cell always produced a desalinated stream during operation. The main mechanism of cation removal was via intercalation into the interstitial lattice sites of the PB electrodes. In this system, when one electrode intercalates (takes cations in), the other deintercalates (releases cations out). The anions move from the cation deficient compartment to the cation rich compartment through the anion exchange membrane. It was reported that for a 500 mM NaCl salt solution at 5 A/m², the SAC was 60 mg/g-both electrodes. This number represents the salt adsorbed during intercalation in both the channels in one desalination cycle, where one desalination cycle comprises of intercalation and deintercalation steps. In this study, sodium citrate was added in the precipitation reaction mixture during the preparation of PBA. It coordinates with the metal ions and then, releases them slowly from the complex for reaction with the hexacyanoferrate ions. This, in theory, leads to a slow and ordered crystallization. At the same time, it did not make a significant improvement in the capacity which was reported to be 56 mAh/g-active particles. Therefore, addition of citrate during precipitation did not enhance the capacity of the PBA electrodes. It was concluded that the development of a flow type reactor would lead to enhancement of water treatment capacity for the proposed rocking chair desalination technique.

24. Porada, S., Shrivastava, A., Bukowska, P., Biesheuvel, P.M. and Smith, K.C., **2017. Nickel Hexacyanoferrate Electrodes for Continuous Cation Intercalation Desalination of Brackish Water.**
Electrochimica Acta
University of Illinois at Urbana-Champaign, USA;
Submitted: May 2, 2017*; Published:* Sep. 22, 2017[54] (*Electrochimica Acta*)
Submitted: Dec. 25, 2016*; Published:* Dec. 25, 2016[161] (ArXiv.org).
Keywords: (1b), (3), (5), (6), CC, 1.4-2.8 A/m², 20 mM NaCl, SAC 34 mg/g-both electrodes

This study presents an electrochemical cell prepared using two similar NiHCF cathode and anode for desalination purposes. This symmetric cell architecture for ion separation was referred to as cation intercalation desalination (CID) and this work is the first experimental demonstration of such a system. Two similar NiHCF electrodes interfacing the current collector on one side and a flow channel on the other were separated by an anion exchange membrane. This enabled the system to desalinate during the charge and discharge steps in a continuous mode. The total charge intake capacity of these electrodes was determined to be ~ 60 mAh/g, using the galvanostatic intermittent titration (GIT) technique. The presence of water in the interstitial sites of NiHCF indicated by elemental analysis was identified by the authors as one of the causes behind low intercalation of Na^+ ions in the lattice. Differential capacitance (as done in[103]) calculated from the GIT data gave a peak value of 1000 F/g which was claimed to be tenfold higher than a conventional carbon electrode used in CDI. This implied that NiHCF based electrodes can store the same amount of charge as the carbon electrodes at one tenth of the voltage. The desalination experiments were performed for a 20 mM salt solution at 1.4 and 2.8 A/m^2 in a constant current mode of operation. Higher current densities were avoided as they result in an increase in concentration polarization for a given salinity. The highest SAC reported (for one half cycle) was 34 mg of NaCl per gram of both electrodes and was 2.5 times higher than that reported for carbon electrodes in CDI. The deviation of current efficiency (moles of salt removed per mole of charge input) form unity was partly attributed to side-reactions occurring at high overpotential. A mixture of K^+ and Na^+ ions was also fed to the cell. The inherent selective nature of the NiHCF electrodes was demonstrated. For an equimolar salt solution, K^+ adsorption was three times higher than of Na^+ ions.

25. Erinmwingbovo, C., Palagonia, M.S., Brogioli, D. and La Mantia, F., **2017. Intercalation Into a Prussian Blue Derivative from Solutions Containing Two Species of Cations.** *ChemPhysChem*
University of Bremen, Germany; *Submitted:* Jan. 8, 2017*; Accepted:* Jan. 25, 2017.[103]
Keywords: (1b), (2), (5)

This work uses NiHCF in a mixed aqueous electrolyte solution to observe the (de)intercalation of ions and the corresponding potentials. The measurements were done in a three-electrode cell. NiHCF electrodes were chosen to be the counter and the working electrode with an Ag/AgCl reference. It was claimed that in a mixture of cations, separate potentials corresponding to (de)intercalation of each constituent ions are not necessarily observed. The potential for intercalation of cations into NiHCF was measured by galvanostatic cycling in respective electrolytes of Na^+, K^+, and NH_4^+ ions with the total ion concentration of 500 mM. The potentials obtained increased in the order $Na^+ < K^+ < NH_4^+$. It was argued that a more favourable intercalation process corresponded to a higher intercalation potential. The authors claimed that the cations present in the interstitial sites were completely exchanged with those from the solution during the repeated

charging/discharging of the electrodes. Different experiments performed with mixtures of ions (with differing ratios) indicated a transition from an average potential (single peak) of one cation to a combined potential according to the respective concentrations. Upon changing the concentration, the intercalation potential shifted, quasi-logarithmically, from one value to another. A simplified model to predict the single peak potential, observed for a cation mixture, was also presented. In more detail, a simple lattice model which assumes no interaction between intercalated species was adopted as the starting point. It was extended for solutions containing a mixture of intercalating species. The calculations implied that during intercalation, both the cations in the mixture were inserted in a defined ratio which was proportional to the concentration of cations in the solution. An expression for the average potential, in line to the one obtained from the simplified model, was calculated for a solution with two cations. The authors concluded, upon comparison of the model with experimental data that the values of single peak potentials were satisfactorily close to those reported in literature.

26. Nam, D.H. and Choi, K.S., **2017. Bismuth as a New Chloride-Storage Electrode Enabling the Construction of a Practical High Capacity Desalination Battery.**
Journal of the American Chemical Society
University of Wisconsin–Madison, USA; *Submitted:* Feb. 1, 2017*; Accepted:* Aug. 4, 2017.[162]
Keywords: CC, 10 A/m^2, 600 mM NaCl, SAC 80 mg/g-bismuth

This study presents bismuth foam electrodes as a prospective candidate for Cl^- ion storage, to be coupled with the cation-accepting $NaTi_2(PO_4)_3$, for water desalination. The bismuth anode stores Cl^- ion as BiOCl while the cathode stores Na^+ by intercalation. It was reported that the reduction kinetics of BiOCl to Bi were slower than the oxidation. It was observed that ~ 50 % of the Bi electrode was electrochemically active. Based on this, the Cl^- storage capacity was reported to be ~ 80 mg/g of Bi. The faradaic efficiency of Cl^- adsorption was reported to be nearly 100 % since there were no competing oxidation processes. The desalination experiments were carried out by coupling Bi and $NaTi_2(PO_4)_3$ electrodes with no separation. The salt solution was 600 mM NaCl and operation was carried out at a constant current density of 10 A/m^2. The reduction of BiOCl requires an energy input (or an overpotential) in 600 mM NaCl. To facilitate this process and reduce the energy input, a 70 mM HCl was used to regenerate the Bi electrode. The evolution of cell voltage with capacity was reported and it was concluded that the capacity of the cell remains constant up to 200 cycles.

27. Chen, F., Huang, Y., Guo, L., Ding, M. and Yang, H.Y., **2017. A dual-ion electrochemistry deionization system based on AgCl-$Na_{0.44}MnO_2$ electrodes.**
Nanoscale
University of Technology and Design, Singapore; *Submitted:* March 16, 2017*; Accepted:* June 2, 2017.[163]

Keywords: CC, 100 mA/g, salinity 890 mg/L NaCl, SAC 57 mg/g-active electrode

This work employs an Ag/AgCl and a sodium manganese oxide electrode $Na_{0.44}MnO_2$, (NMO) to prepare an electrochemical cell for water desalination. The Ag/AgCl electrode was used as a Cl^- donor/acceptor and the NMO electrode was used to (de)intercalate cations. The cell architecture consisted of the electrodes separated by a flow channel. The adsorption step was initiated with Na^+ ions being adsorbed faradaically, as claimed by the authors, in NMO and Cl^- ions doing the same in the Ag/AgCl electrode. The desorption step involves a current reversal which leads to Na^+ and Cl^- ions being released from the respective electrodes resulting in their regeneration. The value for charge capacity for the NMO electrode was reported to be ~ 390 C/g-active material (~ 110 mAh/g) at 100 mA/g current density. It was reduced to 260 C/g (~ 70 mAh/g) after 30 cycles. The salt concentration was 890 mg/L (15 mM) and the recovery efficiency was reported to be approximately 100 %. A maximum value of 57 mg/g was reported for SAC and was claimed to be higher than those from the conventional and hybrid CDI. It must be noted that the channel does not produce desalinated water continuously due to interruptions during the regeneration steps. The salt adsorption decreased with increasing number of cycles and eventually settled to a final value of 57 mg/g-active electrode at the lowest applied current density of 100 mA/g. This adsorption, and the charge efficiency, decreased with increasing current density.

28. Srimuk, P., Lee, J., Fleischmann, S., Choudhury, S., Jäckel, N., Zeiger, M., Kim, C., Aslan, M. and Presser, V., **2017. Faradaic deionization of brackish and sea water via pseudocapacitive cation and anion intercalation into few-layered molybdenum disulfide.**
Journal of Materials Chemistry A
Saarland University, Germany; *Submitted:* April 10, 2017*; Accepted:* July 4, 2017.[164]
Keywords: (3), CV, 0.8 V, 5-500 mM NaCl, SAC 25 mg/g-both electrodes

Electrodes fabricated from molybdenum disulfide (as used in [99] for CDI) and carbon nanotubes (MoS_2-CNT) are used in this study to desalinate water of high salinities. The salt adsorption results from the indiscriminate (de)intercalation of anions as well as cations in the layered 2-D structure of MoS_2. A similar mechanism was highlighted for electrodes made out of MXene.[89] The desalination operation was performed in constant-voltage mode at 0.8 V and the regeneration was done at 0 V. The salt concentration varied from 5 mM to 500 mM. The CDI cell consisted of two electrodes separated by a porous membrane and the solution was introduced in the cell in a flow-by mode, also discussed in.[142] The salt adsorption capacity reported by the authors was normalized by the total weight of both the electrodes. It was argued that the pseudo-capacitive behaviour of the MoS_2-CNT electrode was confirmed by the triangular galvanostatic charge/discharge cycles and the high specific capacitance of 200 F/g was primarily attributed to the charge storage by

intercalation into the MoS_2 sheets. An in-situ Raman spectroscopy analysis revealed that the ion insertion into MoS_2 expands the structure because the ions are bigger than the inter-layer spacing. The SAC value was reported to increase with salt concentration and the largest value of 25 mg/g-both electrodes was reported for a salt concentration of 500 mM and a constant voltage of 0.8 V. This was claimed to be higher than electrodes prepared from AC only. Charge efficiency varied from 80 % (for 5 mM salt concentration) to 95 % (for 500 mM). The authors acknowledged the difficulty in comparison of different SAC values due to differing weights used for normalization. It was suggested to use the skeletal density of the materials to get around this problem.

29. Kim, S., Yoon, H., Shin, D., Lee, J. and Yoon, J., **2017. Electrochemical selective ion separation in capacitive deionization with sodium manganese oxide.**
Journal of colloid and interface science
Seoul National University, South Korea; *Submitted:* May 6, 2017*; Accepted:* July 16, 2017.[165]
Keywords: (5), CC, 10 mA/g, salinity 30 mM

This study deals with selective removal of ions from a mixed salt solution by using manganese oxide, an intercalation material, in CDI. The electrodes made from $Na_{0.44}MnO_2$ (NMO) were used in aqueous mixtures of Na^+, K^+, Mg^{2+}, and Ca^{2+} ions to selectively absorb Na^+ ions. The electrochemical cell consisted of $Na_{0.44}MnO_2$ cathode and an Ag/AgCl anode. The authors describe the salt removal process in two steps. The first one, the capture step is identified as the one during which, a pre-treated NMO cathode intercalates cations from a 30 mM mixture of NaCl, KCl, $MgCl_2$, and $CaCl_2$ while the Ag/AgCl anode reacts with the Cl^- ions. In the second one, the release step, the intercalated ions get released into a 30 mM LiCl solution, marking the regeneration of the cathode. The operation was performed under constant-current conditions. It was claimed that 49-57 % of the charge was used to release and capture Na^+ ions in contrast to 35-37 % involved for the divalent cations. Only 5 % of the charge went towards capturing and releasing K^+ ions. Therefore, the selectivity towards Na^+ ions was reported to be 13 times higher than that for K^+ ions and 6-8 times higher than that for Mg^{2+} and Ca^{2+} ions. A preference towards Na^+ ions by NMO was inferred from the selectivity numbers and the cyclic voltammetry experiments which showed peak currents for Na^+ (de)intercalation into the cathode. A reason for such a preference was not provided.

30. Guo, L., Mo, R., Shi, W., Huang, Y., Leong, Z.Y., Ding, M., Chen, F. and Yang, H.Y., **2017. A Prussian blue anode for high performance electrochemical deionization promoted by the faradaic mechanism.**
Nanoscale.
Singapore University of Technology and Design, Singapore; *Submitted:* May 19, 2017*; Accepted:* July 30, 2017.[166]

Keywords: (6), CC, 125-1250 mA/g, salinity 10-200 mM NaCl, SAC 120 mg/g-active material

This study uses a hybrid (asymmetric) configuration with one AC electrode and one based on pure PB particles ($Na_xFe_2(CN)_6$) in combination with both an anion exchange membrane and cation exchange membrane. The detailed chemical synthesis of the composite electrode, also containing graphene oxide, binder, and carbon black, was describe. The PB forms nanocubes of about 200 nm size. In the 3-electrode experiment, cyclic voltammetry (CV) was used as well as galvanostatic charge/discharge. In CV, redox peaks at +0.15/+0.05 V vs Ag/AgCl, show relate to Na^+ (de)intercalation. In the CDI experiment, the current was varied between 125 and 1250 mA/g resulting in a cell voltage ranging between -1.4 V to +1.4 V. Salt concentration was in the range of 10-200 mM. A schematic was provided explaining the charge/discharge cycle, and ion adsorption/desorption in CDI with PB and AC. Removal capacity was shown to be stable at ~40 mg/g up to 600 cycles. A maximum SAC of 120 mg/g was reported.

31. Yoon, H., Lee, J., Kim, S. and Yoon, J., **2018. Electrochemical sodium ion impurity removal system for producing high purity KCl.**
Hydrometallurgy.
Seoul National university, S. Korea; *Submitted:* May 29, 2017; *Accepted:* Dec. 20, 2017.[167]
Keywords: (5), CC, 3 A/m², salinity 20-40 mM NaCl, KCl, KFeHCF, NMO

This study presents an electrochemical system comprised of $NaMnO_2$ and $K(Fe[CN_6])$ (KFeHCF) electrodes to selectively remove sodium impurities from a KCl solution to produce KOH of high purity. Two target solutions were used as feed: the first one consisted of 20 mM NaCl and 40 mM KCl and the second one contained 20 mM NaCl in 4 M KCl solution, replicating industrially relevant conditions. The impurity removal was done in four steps. In the first step, the electrochemical cell with a completely deintercalated NMO electrode and a fully intercalated KFeHCF electrode was operated in a constant current mode, such that the NMO electrode (cathode) intercalated ions from the target solution. Concomitantly, the anode deintercalates K^+ ions in the feed. In the second step, the feed solution was replaced with a 20 mM KCl solution to prepare for the regeneration of NMO electrode. In the third step, the direction of the applied current was reversed to regenerate the NMO electrode (anode). In the fourth and final step, the feed was replaced with the target solution. This completes one (four-step) cycle of operation. After the first step, the concentration of Na^+ ions in the target solution decreased by ~ 20 % with a charge efficiency of ~ 76 %. The efficiency reduced to 54 % for the feed solution containing 4 M KCl. This difference was attributed to the interference from K^+ ions in the electrolyte. Next to this decrease in the Na^+ ion concentration, K^+ ions increased in the solution by ~ 12% due to deintercalation at the anode. Despite the decreased efficiency, the authors claimed that the NMO/KFeHCF system was capable of removing Na^+ impurities

from industry grade KCl solutions as ~ 36 % of Na^+ ions were removed from it after three full cycles (12 steps).

32. Byles, B.W., Cullen, D.A., More, K.L. and Pomerantseva, E., **2018. Tunnel structured manganese oxide nanowires as redox active electrodes for hybrid capacitive deionization.**
Nano Energy.
Drexel University, USA; *Submitted:* June 7, 2017*; Accepted:* Dec.10, 2017.[168]
Keywords: (5), (6), CV, 1.2 V, salinity 15 mM, SAC 44 mg/g-both electrodes (KCl)

This work presents a hybrid CDI system comprised of a redox active MnO_2 electrode paired with AC in a flow-by cell configuration. The anode and the cathode were separated from the flow channel by an AEM and a CEM respectively. Four different types of MnO_2 with different crystal structures were tested to find an appropriate electrode material. The tunnel structure of different MnO_2 materials were found to be stabilized by different cations. These stabilizing cations were reported to facilitate repeated (de)insertion of cations from the feed solution. The CDI operation was performed under constant voltage of ± 1.2 V in batch mode for 15 mM individual solutions of Na^+, K^+ and Mg^{2+} ions. The MnO_2 phase with the most diverse tunnel sizes demonstrated the maximum SAC in NaCl (28 mg/g), KCl (44 mg/g) and $MgCl_2$ (43 mg/g). This led the authors to conclude that the structure with larger tunnels had higher capacity for ion storage. The relation between the salt removal and the tunnel size is not straight forward as the stabilizing ions was also reported to play a role in ion storage. The ion removal, which is linked to the reduction of Mn atoms, is reduced by the stabilizing ions may also partially reduce the oxidation states of Mn in the lattice. The charge efficiency was reported to be above 80 % for each tested material. The ion removal by the MnO_2 electrodes was attributed to two mechanisms: First was the pseudo-capacitive adsorption of cations on the surface of the MnO_2 electrode; second was the diffusion controlled ion intercalation of ions in the crystal structure of MnO_2 electrode. The fast pseudo-capacitive adsorption of ions is followed by the slow intercalation into the MnO_2 lattice. This work successfully demonstrated the application of different MnO_2 electrodes for hybrid CDI.

33. Lee, J., Srimuk, P., Aristizabal, K., Kim, C., Choudhury, S., Nah, Y.C., Mücklich, F. and Presser, V., **2017. Pseudocapacitive Desalination of Brackish Water and Seawater with Vanadium-Pentoxide-Decorated Multiwalled Carbon Nanotubes.**
ChemSusChem
Saarland University, Germany; *Submitted:* July 5, 2017*; Accepted:* July 25 2017.[169]
Keywords: CC, 33 mA/g, salinity 600 mM NaCl, SAC 24 mg/g-both electrodes

This study uses a multiwalled carbon nanotube (MWCNT) electrode, modified with vanadium pentaoxide (h-V_2O_5) to store Na^+ via pseudocapacitive intercalation. The

electrochemical cell also consisted of an AC which was used to store Cl^- ions via electrosorption in the pores. The capacity of the MWCNT-hV_2O_5 electrodes were estimated to be ~ 45 mAh/g. The mass of AC electrode was twice that of the MWCNT-hV_2O_5 electrode because of the low capacity of AC. The desalination operation was performed at a constant current of ~ 33 mA/g-both electrodes for 200 and 600 mM salt solution. The SAC for a 200 mM NaCl solution was reported to be ~ 23 mg/g-both electrodes. The authors claimed that the high SAC value resulted from Na^+ ion intercalation into the hV_2O_5 electrode. A decrease in the SAC value with increasing number of cycles was attributed to structural degradation of V_2O_5. The SAC for a 600 mM NaCl solution was reported to be ~ 24 mg/g-both electrodes. The energy consumption value, reported for the 200 and 600 mM NaCl solution, were claimed to be lower than that for a MCDI cell. Finally, the study introduced another method for normalizing the SAC values to make a fair comparison between different electrode materials. The authors argue that the weight of the electrode adsorbing Na^+ ions should be used to normalize the salt removal capacity in the cell since it is the Na^+ removal which drives the whole process. This line of argument is applicable for systems with different materials for cathode and anode.

34. Srimuk, P., Lee, J., Tolosa, A., Kim, C., Aslan, M. and Presser, V., **2017. Titanium Disulfide: A Promising Low-Dimensional Electrode Material for Sodium Ion Intercalation for Seawater Desalination.**
Chemistry of Materials.
Saarland University, Germany; *Submitted:* Aug.8, 2017*; Accepted:* Nov. 11, 2017.[170]
Keywords: CC, 0.1 A/g, 5-600 mM NaCl, SAC 14 mg/g-both electrodes

This work focuses on a composite electrode fabricated by blending titanium disulfide (TiS_2) with carbon nanotubes (CNTs) to desalinate water of high salinity. The 2-D layered structure of TiS_2 facilitates cation intercalation between the layers. The electrodes were prepared without the addition of a polymeric binder. Electrochemical characterization was performed in a standard three-electrode cell configuration through cyclic voltammetry (CV) and GIT. The desalination experiments were done in a conventional two-electrode CDI configuration. The TiS_2-CNT electrode was paired with a carbon electrode in a flow-by cell configuration, as illustrated in Figure 1 (a). The electrodes were separated by a porous separator. No IEM was employed in this cell setup. The experiments were performed at a single flow rate for 5, 50 and 600 mM NaCl solution. The salt removal was done at a constant current of 0.1 A/g in the potential window of 0.2 - 0.8 V. The TiS_2-CNT composite electrode exhibited a charge storage capacity of 68 mAh/g which was higher than the capacity observed for a pristine TiS_2 electrode (40 mAh/g). This was attributed to the addition of CNTs, which would provide a highly conducting network for ion (de)intercalation. The TiS_2-CNT electrodes were reported to suffer from poor capacity retention at voltages lower than -0.3 V. Repeated cycling at -0.4 V caused volume expansion, leading to an unravelling of the layered TiS_2 structure. The reason provided for

the capacity decay at -0.6 V was change in phase from TiS_2 to TiO_2. During desalination experiments, the TiS_2-CNT//carbon cell exhibited a SAC value of ~ 11, 13 and 14 mg/g for a feed of 5, 50 and 600 mM NaCl, respectively. The charge efficiency of the process was reported to be in the range of 78-92 %. The authors also argued to normalize the SAC values with the mass of the ion-selective electrode (TiS_2-CNT in this case) to give a fair assessment of the desalination performance of the electrode, because in a hybrid cell, the TiS_2-CNT electrode is paired with an electrode with low capacity. Therefore, normalization with the total electrode weight may not reflect the qualities of TiS_2-CNT composite electrode. This method of normalization resulted in a sodium ion removal capacity of 36 $mg_{Na}/g_{negative\text{-}electrode}$.

35. Kim, T., Gorski, C.A. and Logan, B.E., **2017. Low Energy Desalination Using Battery Electrode Deionization.**
Environmental Science & Technology Letters
Pennsylvania State University, USA; *Submitted:* Sep. 3, 2017; *Accepted:* Sep. 18, 2017.[137]
Keywords: (3), (6), CC, 3 A/m², 50 mM NaCl, SAC 100 mg/g-both electrodes, CuHCF

This study uses two copper hexacyanoferrate (CuHCF) electrodes in a symmetric electrochemical cell to remove cations from an aqueous 50 mM NaCl solution. The cell architecture allows for a desalinated and a concentrated stream being produced simultaneously. The authors refer to this technique as battery electrode deionization. The CuHCF are a type of PBAs and their electrodes store and release ions via (de)intercalation. The study introduced 1, 3, and 5 ion-exchange membranes (IEMs) between the electrodes and claimed that the difference in the feed and outlet concentration increased from 4 mM (in single stack cell containing only one IEM) to 12 mm (triple stacked, containing 5 IEMs). The maximum salt adsorption capacity reported was 100 mg-NaCl/g-electrodes for an applied current density of ~ 3 A/m^2. The authors report this number to be the highest yet in the CDI literature. The charge efficiency was reported around 80 %. The salt adsorption capacity for a single-stacked cell was not provided. The authors also observed that only 60 % of the full capacity of CuHCF was utilized. The total capacity was reported around 57 mAh/g-active material (205 C/g) when cycled in 1 M NaCl and 53 mAh/g-active material (205 C/g) when cycled in 50 mM NaCl electrolyte. The energy consumption with a triple-stacked cell was reported to be an order of magnitude lower than that observed in CDI and MCDI experiments for the same inlet and outlet concentrations. The authors concluded that the addition of extra membranes reduced the energy consumption by ~ 30 %.

36. Bao, W., Tang, X., Guo, X., Choi, S., Wang, C., Gogotsi, Y. and Wang, G., **2018. Porous Cryo-Dried MXene for Efficient Capacitive Deionization.**
Joule.
Drexel University, USA; *Submitted:* Oct. 3, 2017; *Accepted:* Feb.16, 2018.[171]

Keywords: (3), CV, 1.2 V, 170 mM NaCl, SAC 45 mg/g

This research paper presents an enhanced porous MXene ($Ti_3C_2T_x$, $T_{xz}(OH)_xO_yF_z$) electrode, as used in[89] for CDI applications. The layered nanosheets of MXene were prevented from restacking, due to Van der Waals forces, by a vacuum freeze drying process to obtain an aerogel-like material. This led to the fabrication of a porous electrode with a large surface area (~ 290 m^2/g) in comparison to regular MXene electrodes (30 m^2/g). In addition, the porous MXene had larger pores in the range of 15-40 nm. The non-porous MXene lacked pores in this range. The authors speculated that this larger pore size gives sufficient space for the intercalation of Na^+ and Cl^- ions. The porous MXene was electrochemically characterized through CV in a three-electrode cell configuration. The charge storage capacity was found to be 156 F/g, which was twice as high as the value reported for untreated MXene. The CDI cell prepared using the porous MXene electrodes exhibited a SAC value of 45 mg/g for a 170 mM NaCl solution under an applied voltage of 1.2 V. We note that the SAC normalization weight was not explicitly mentioned. The ion storage was attributed to a combination of EDL formation on the nanosheets of exfoliated MXene and the intercalation of ions in between the sheets, along the lines reported by Srimuk *et al*.[89]

37. Wu, T., Wang, G., Wang, S., Zhan, F., Fu, Y., Qiao, H. and Qiu, J., **2018. Highly Stable Hybrid Capacitive Deionization with a MnO_2 Anode and a Positively Charged Cathode.** *Environmental Science & Technology Letters*
Dalian University of Technology, China; *Submitted:* Nov. 30, 2017*; Accepted:* Jan. 22, 2018.[94]
Keywords: CV, 1.4 V, 8 mM NaCl, SAC 14 mg/g-both electrodes

This work uses a cation-selective MnO_2 anode coupled with anion-selective quaternized poly-(4-vinylpyridine)-coated AC cathode in a CDI cell setup not separated by an ion-exchange membrane. The intercalation of Na^+ ions was reported into the MnO_2 structure by the means of a reduction reaction and its oxidation would follow deintercalation of Na^+ ions during the charging step. The salt adsorption capacity of the cell with MnO_2 electrode was reported to be 14 mg/g-both electrode for a ~ 8 mM solution desalinated at 1.4 V. The SAC values were shown to increase upon increasing the applied voltage. In addition, it was demonstrated that these values were higher than those observed for the cell made of only carbon electrodes (10 mg/g). A decrease in charge efficiency was observed for an increasing applied voltage and it was attributed to an increase in the parasitic reactions in the cell. It was also argued that a higher amount of charge was consumed in the parasitic reactions during the charging step resulting in a higher charge efficiency for discharging step. A cyclic performance step revealed that the cell with MnO_2 anode retained a higher percentage of SAC after 350 cycles in comparison to the cell with both electrodes made from carbon. The improvement in the cyclic stability of the MnO_2 cell was attributed to the elimination of the carbon oxidation reactions prevalent in the cell with carbon anode.

38. Liu, S. and Smith, K.C., **2018. Quantifying the trade-offs between energy consumption and salt removal rate in membrane-free cation intercalation desalination**.
Electrochimica Acta.
University of Illinois at Urbana-Champaign, USA; *Submitted:* Dec. 15, 2017*; Accepted:* March 11, 2018.[172]
Keywords: (1a), (3), NiHCF

This theoretical study makes a two-dimensional numerical analysis of symmetric CDI with PBA intercalation materials where water flows through the pores of the electrode (*i.e.*, without a flow channel), with the two electrodes separated by a diaphragm, *i.e.*, an uncharged porous layer. Performance was analysed in terms of ASAR for the rate of desalination, and ENAS for the energy to desalinate, and were related to the dimensionless Péclet number and Damköhler numbers which describe fluid flow in relation to the diffusional rates. The flow-through design was compared with calculation results from a flow-by and a flow-behind configuration (where the water flows either in between the electrode and the diaphragm, or on the backside of the electrode). Flow-through was found to have superior desalination performance because in this geometry, ions advected with the water, and ion transport was not limited by diffusion and migration. Regular solution theory was used to describe the electrosorption process into the intercalation material, while also analytical results were presented.

39. Marzak, P., Yun, J., Dorsel, A., Kriele, A., Gilles, R., Schneider, O. and Bandarenka, A.S., **2018. Electrodeposited $Na_2Ni[Fe(CN)_6]$ Thin-Film Cathodes Exposed to Simulated Aqueous Na-Ion Battery Conditions.**
Journal of Physical Chemistry C
Technical University of Munich, Germany; *Submitted:* Jan. 12, 2018*; Accepted:* April 4, 2018.[108]
Keywords: (2)

This study investigates an electrochemically deposited layer of NiHCF in aqueous and organic electrolytes to understand its degradation and propose a mechanism for it. The electrode film NiHCF were electrodeposited directly from the reactants and were used in a three-electrode cell setup with a platinum wire as counter electrode. The electrodes were characterized, during operation, by atomic force microscopy to identify any morphological changes in the NiHCF lattice due to (de)intercalation of Na^+ ion. It was concluded, from the images which showed no difference in the morphology after repeated cycling, that the mechanical degradation is not the factor behind the loss of electrochemical capacity of the film over a period of use. A chemical change in the active material in the form of oxidation of nickel, into its oxide NiO_x at high pH, was claimed to be the primary cause in loss of electrochemical capacity of the electrodes. A change in the color of the film, from goldish to blackish, provided a visual confirmation of nickel oxidation. A mechanism for this

degradation was also suggested. According to the study, the OH^- ions are adsorbed at nickel sites. The reaction of OH^- with Ni atoms destabilizes the lattice and leads to the extraction of iron centres. The intercalation capacity of an electrode is proportional to the amount of Fe centers and therefore, their removal makes the electrode inactive towards intercalation.

40. Srimuk, P., Lee, J., Fleischmann, S., Aslan, M., Kim, C. and Presser, V., **2018. Potential-Dependent, Switchable Ion Selectivity in Aqueous Media Using Titanium Disulfide.**
ChemSusChem
Saarland University, Germany; *Submitted:* March 5, 2018*; Accepted:* May 1, 2018.[100]
Keywords: (3), (5)

Electrodes fabricated from a composite of titanium disulfide and carbon nanotubes (TiS_2-CNT) are used in this study to selectively remove Cs^+ ions from a salt solution containing Cs^+ and Mg^{2+} ions. CV revealed different potentials associated with intercalation of different ions. The highest potential was observed for Cs^+ ions and the lowest was seen for Mg^{2+} ions, indicating an inherent preference of the electrode towards Cs^+ ions. It was reported that the electrodes exhibited different potentials for different cation concentrations due to their dependence on the activity of the redox species. A linear trend suggesting an increase in redox potential, associated with (de)intercalation of different cations in the electrode, with concentration was reported. For a multi-cation system, the potentials for (de)intercalation were shifted from the values observed during operation with a single cation system. The potential difference observed between Cs^+ and Mg^{2+} ions was ~ 140 mV which had shifted from an expected value of ~ 65 mV. Multi-cation systems such as these were also studied in.[103] The authors argue that the change in potentials of Cs^+ and Mg^{2+} ions in a multi-cation system does not render the system unsuitable for selective ion removal. An applied potential of −200 mV was suggested as an appropriate operating potential. The authors concluded the study by identifying three regimes of electrode potentials (vs Ag/AgCl) in which removal pf one cation was preferred over the other. In the potential range of −220 to −390 mV (*vs.* Ag/AgCl), Mg^{2+} ions were preferred with a molar selectivity of ~ 30 against Cs^+ ions. In the potential range of −220 to −160 mV, TiS_2-CNT electrode showed a weak preference towards Mg^{2+} ions (molar selectivity ~ 6). Finally, in the potential range of −220 to +26 mV, Cs^+ ions were removed with a molar separation factor of ~ 2. It was therefore concluded that the potential applied to a TiS_2-CNT electrode can be manipulated to selectively remove cation of choice from a multi-cation mixture.

41. Singh, K., Bouwmeester, H.J.M., de Smet, L.C.P.M., Bazant, M.Z. and Biesheuvel, P.M., **2018. Theory of Water Desalination with Intercalation Materials.**
Physical Review Applied
Wageningen University, Netherlands; *Submitted:* March 22, 2018*; Accepted:* May 4, 2018.[109]

Keywords: (1a), (3), (6)

The authors present a comprehensive mathematical model of water desalination for a complete electrochemical CDI cell, with two electrodes interfacing with two flow channels separated by an anion exchange membrane. The authors implement the Nernst-Planck (NP) equation for ion transport on a complete desalination cell by neglecting any transport limitation within the intercalation material and assuming a dilute electrolyte. The transport processes modelled were: diffusion and migration of ions through the pores of the electrode; ionic transport in the flow channels; ion transport across the membrane. In addition to the NP equation, a Frumkin isotherm was implemented to relate the difference in potential between the cations in the electrode and the electrolytic phase with the intercalation degree (i.e the ratio of concentration of cation in the intercalation particle and the maximum cation concentration in the intercalation particle) and the concentration of cations in the local electrolyte. The transport in the membrane was also described by the NP equation by assuming that only diffusion and electromigration occur in the membrane. The simulations were performed in the same manner as a constant- current desalination experiment is executed. Concentration profiles for different times were provided for (de)intercalation steps. In addition, the variation in intercalation degree with time was also demonstrated. The authors argued that the same starting value of the intercalation degree of the modeled electrodes gave them a symmetric character in terms of desalination and energy consumption. Therefore, the actions of one electrode were mirrored in the other electrode. Consequently, the authors claimed that an authoritative labeling of these operations as charging and discharging step lacked a definite criterion. A prediction of cell voltage with time also hinted at the possibility of energy recovery.

42. Choi, S., Chang, B., Kim, S., Lee, J., Yoon, J. and Choi, J.W., **2018. Battery Electrode Materials with Omnivalent Cation Storage for Fast and Charge-Efficient Ion Removal of Asymmetric Capacitive Deionization.**
Advanced Functional Materials.
Seoul National university, S. Korea; *Submitted:* April 19, 2018*; Accepted:* July 11, 2018.[173]
Keywords: (5); CV, 1.2 V, 500 mM salt mixture, SAC 20 mg/g-both electrodes, CuHCF

This study presents an IEM-free asymmetric CDI cell with a cathode fabricated out of a metal organic framework (MOF) and porous carbon anode. The MOF material used to fabricate an electrode was $K_{0.03}Cu[Fe(CN)_6]_{0.65}\cdot 0.43H_2O$, which has a comparable structure to the previously observed PBAs.[54,137] The MOFs were mixed with carbon and a polymer binder. Electrochemical tests were performed in a three-electrode cell configuration through CV and GIT to assess the charge storage performance of the MOF-containing electrodes prior to their use in a two-electrode CDI cell with MOF cathode and an AC anode, MOF//AC. The electrochemical characterization and the desalination performance of the CDI cell was monitored in 1 M salt solutions of K^+, Na^+, Mg^{2+} and Ca^{2+} ions as well as

a 4000 ppm (~ 68 mM) mixture of all the these cations. The desalination capacity of the MOF cell was tested at a constant applied voltage of 1.2 V. The authors concluded from the characterization experiments that the MOF-containing electrodes could intercalate all the tested cations within the water stability window, from their individual solution and from their mixture. The charge storage capacity obtained for the cations during galvanostatic charging at 50C were 52, 45, 36 and 40 mAh/g, respectively for K^+, Na^+, Mg^{2+} and Ca^{2+}. The difference in the observed capacities can be understood from the difference between the sizes of the cations and consequently, their ionic mobility in the solution. It was reported that AC//AC cell predominantly removed divalent ions from the mixture. The MOF//AC cell exhibited invariant intercalation for mono and divalent ions. However, K^+ and Na^+ were removed 70 % and 26 % more, respectively, than Mg^{2+}. The authors also noticed that intercalation of water molecules in association with the incoming cation from thermo-gravimetric analysis (TGA) of electrodes before and after complete discharge. The amount of intercalated water molecule was higher for divalent cations due to their strong electrostatic interaction with water molecules. A charge efficiency of 76 % was obtained for a MOF//AC cell which was significantly higher than a AC//AC cell (33 %) without an IEM. The MOF//AC cell exhibited a similar ion removal capacity of 20 mg/g in a 500 mM mixture of ions. This was higher than the SAC value obtained from the AC//AC cell (5 mg/g). It was concluded that the open framework structure of the MOF crystals facilitated fast ion kinetics leading to a rapid ion and charge transfer. This enhanced the salt-removal rate and made it possible to utilize the maximum of the charge storage capacity available.

43. Ma, X., Chen, Y.A., Zhou, K., Wu, P.C. and Hou, C.H., **2018**, **Enhanced desalination performance via mixed capacitive-Faradaic ion storage using RuO_2-activated carbon composite electrodes.**
Electrochimica Acta.
Xiamen University, China; *Submitted:* May 12, 2018*; Accepted:* October 29, 2018.[174]
Keywords: CV, 1.2 V, 5 mM NaCl, SAC 11 mg/g-both electrodes

This study deals with a composite of ruthenium oxide (RuO_2) and AC to prepare a high-performance hybrid CDI electrochemical cell. A combination of electrostatic deposition of ions on an EDL and faradaic processes were claimed to participating mechanisms behind the salt removal by the proposed system. RuO_2 was electro-deposited on AC through CV to prepare the composite electrodes. The amount of deposited RuO_2, and hence also the specific surface area available for EDL electrodeposition of ions, was controlled by the number of deposition cycles in CV. This study advocates a balance between retaining the specific surface area of the composite electrode available from the CNTs and the amount of electrodeposited RuO_2 on the CNT surface to make the most out of the two participating storage mechanism. The study presents two sets of experiments. The first one utilizes a setup is a three-electrode cell used for electrochemical characterization of the RuO_2-AC electrode (working electrode) through CV and GIT in a potential range of -0.4 to 0.6 V. The

second setup consisted of a desalination cell comprising of two electrodes separated by a spacer channel. A 5 mM feed solution was recirculated through the cell and the salt removal was performed at a constant voltage of 1.2 V. The electrode regeneration was performed by the short circuiting of electrodes. In the electrochemical characterization experiments, an enhanced charge/discharge cycle time for the composite electrode in comparison to the regular AC electrodes indicated an increase in the storage capacity of the RuO_2-AC electrodes by the active RuO_2 particles. It was also claimed by the authors that the addition of RuO_2 facilitated electron transfer and therefore, reduced resistance of the electrode. The CV experiments for RUO_2-AC composite electrode yielded a higher charge storage capacity (60.6 F/g) than the AC electrodes (31.1 F/g). It was concluded that the deposited RuO_2 was active and can enhance the charge storage capacity of the electrode due to its pseudo-capacitance charge storage. The desalination experiments employed RuO_2-AC electrode as a cathode to remove Na^+ ions. The SAC obtained after operating the cell at 1.2 V for 1 hour in a 5 mM NaCl solution is reported to be ~ 11 mg/g-electrodes. The relative contribution of the capacitive and faradaic salt adsorption by the electrodes was calculated as 18 % and 82 %, respectively. The charge efficiency of the RuO_2-AC//AC cell, at 60 %, was reported to be higher than that of a regular AC//AC cell, at 27%. A tabulated summary was provided to demonstrate a superior performance of the RuO_2-AC electrodes in comparison to MnO_2 based composite electrodes. However, the exact redox reactions behind the claimed pseudo-capacitance of the composite electrodes were not provided.

44. Byles, B.W., Hayes-Oberst, B. and Pomerantseva, E., **2018. Ion Removal Performance, Structural/Compositional Dynamics, and Electrochemical Stability of Layered Manganese Oxide Electrodes in Hybrid Capacitive Deionization.**
ACS Applied Materials & Interfaces.
Drexel University, USA; *Submitted:* June 10, 2018; *Accepted:* September 5, 2018.[175]
Keywords: (5), (6), CV, 1.2 V, 15 mM NaCl, SAC 31-50 mg/g-both electrodes

This work utilizes two-layered manganese oxides (LMOs) stabilized by hydrated Na^+ ions (Na-birnessite) and Mg^{2+} ions (Mg-buserite) in a HCDI cell configuration, similar to those reported in [95][97]. The difference in the structure of Na-birnessite and Mg-buserite arises from the structural water layers residing in between the layers with the stabilizing ions. The LMO electrodes, prepared by mixing the active materials with carbon black and poly(tetrafluoroethylene) (PTFE), were used as cathodes with AC anodes. The electrodes were mounted in a HCDI cell with the flow channel separated from cathode and anode with a cation and an anion exchange membrane, respectively. The ion-adsorption was performed for two separate NaCl and $MgCl_2$ salt solutions (both 15 mM) in a constant voltage mode of operation. The SAC recorded within the first 10 adsorption/desorption cycles for a NaCl solution with Na-birnessite and Mg-buserite were 31.5 and 37.2 mg/g-total electrode weight, respectively. For a $MgCl_2$ salt solution, Na-birnessite and Mg-buserite demonstrated a SAC of 50.2 and 39 mg/g-total electrode weight. It is interesting

to realize that both electrode materials removed higher amounts of NaCl than $MgCl_2$. This result was correlated to the larger size of hydrated Mg^{2+} ions in comparison to the size of Na^+ ions. In addition, it was also observed that HCDI cell with Mg-buserite delivered higher SAC values when operated in a NaCl solution. This was attributed to a higher interlayer spacing in the Mg-buserite. In contrast, the HCDI cell comprising of Na-birnessite, with smaller interlayer spacing, delivered higher SAC in $MgCl_2$ solution. This counter-intuitive observation could not be explained by the current study. Extended cycling revealed that the SAC reduced upon increasing number of cycles. In addition, the SAC retention for the NaCl solution was found to be higher than $MgCl_2$, which was rationalized by an easier diffusion of smaller and single charge carrying Na^+ ions in comparison to Mg^{2+} ions. It was claimed that the ion removal proceeded via surface adsorption and redox reaction with the electrode material itself. This was postulated based on EDX spectroscopy, which showed the presence of the stabilizing ion as well as the cation from the salt solution in the composition of the electrode. Therefore, the change in interlayer ion content and consequently, the interlayer spacing, were argued as significant factors to be considered for extended cycling of HCDI cell with Na-birnessite and Mg-buserite electrodes and their SAC in desalination experiments.

45. Kim, T., Gorski, C.A. and Logan, B.E., **2018. Ammonium Removal from Domestic Wastewater Using Selective Battery Electrodes.**
Environmental Science & Technology Letters.
Pennsylvania State University, USA; *Submitted:* July 2, 2018; *Accepted:* Aug. 2, 2018.[106]
Keywords: (5), (6), CV, 0.1-0.3 V, ion concentration 5 mM NH_4^+, 20 mM Na^+, CuHCF

An electrochemical cell assembled with two intercalation electrodes fabricated using CuHCF, a PBA, is used in this study to selectively remove NH_4^+ ions from a mixture of ions. The cell used the same materials for both the electrodes which were separated by an anion-exchange membrane. This was achieved by manipulating the applied voltage. Such treatment of a multi-cation salt solution has been described for TiS_2 electrodes in[100] and cyclic voltammetry has been used to demonstrate different potentials of intercalation in a CuHCF electrode for different ions.[144] Electrochemical analyses have demonstrated that various cations such as Li^+, Na^+, K^+, and NH_4^+ intercalate into PBAs, such as CuHCF, at different potentials. One of the studies reviewed here reported extensive observations on this phenomenon and attempted to support the experimental data of ion intercalation with a thermodynamic model.[103] It was proposed that the higher intercalation potential observed for NH_4^+ ions (*vs.* SHE) in comparison to that of Na^+ ions should result in its preferential adsorption. The electrodes used in this study were prepared by the method similar to that in.[137] Two salt solutions with varying and similar concentrations for NH_4^+ and Na^+ ions were treated to ascertain the selective removal performance of the cell. For the salt solution with NH_4^+ concentration of 5 mM and Na^+ concentration of 20 mM, an increase in the applied voltage from 0.1 V to 0.3 V increased the removal of NH_4^+ ions from

65 to 93 %. However, an increase in voltage resulted in a decrease in the selectivity towards NH_4^+ ions, reflected by the decrease in the separation factor (*i.e.*, % NH_4^+ removed / % Na^+ removed) from 6 to 2. Non-selective MnO_2 electrodes tested for the same salt concentration at 0.2 V were reported to show a separation factor < 2. The CuHCF electrodes produced a separation factor of ~ 3. The concentration of ions was varied and it was claimed that the selectivity increased upon increasing NH_4^+ concentration. The authors identified the operation potential of 0.2 V to be optimal for NH_4^+ ion removal (80 %) and selectivity (separation factor ~ 3).

46. Shi, W., Zhou, X., Li, J., Meshot, E.R., Taylor, A.D., Hu, S., Kim, J.H., Elimelech, M. and Plata, D.L., **2018. High-Performance Capacitive Deionization via Manganese Oxide-Coated, Vertically Aligned Carbon Nanotubes.**
Environmental Science & Technology Letters.
Yale University, USA; *Submitted:* July 31, 2018; *Accepted:* September 25, 2018.[176]
Keywords: CV, 1.2 V, 100 mg/L NaCl, SAC 28 mg/g-one electrode

This work focuses on the fabrication of MnO_2-coated, vertically aligned carbon nanotube (VACNTs) electrodes prepared via Atomic Layer Deposition (ALD) for capacitive deionization. The technique of ALD was chosen to deposit thin films of MnO_2 on the VACNTs in order to enhance their SAC while still retaining a high electronic conductivity. Two sets of experiments were performed to assess the performance of the composite electrode. The first was electrochemical characterization performed in a three-electrode cell configuration through CV. The second set of experiments were done to ascertain the salt removal performance of the electrode. A 100 mg/L (~ 1.8 mM) flow solution was recirculated, in a batch mode, through a two-electrode cell, with a VACNT-MnO_2 as cathode and AC as anode to study the salt removal at a constant voltage of 1.2 V. The electrochemical characterization yielded a charge storage capacity of 220 F/g for VACNT-MnO_2, which was higher than that for uncoated VACNTs (53 F/g). This increase was attributed to the intercalation of alkali metal ions in the MnO_2 crystal lattice. The charge storage capacity of the cathode decreased upon increasing thickness of the MnO_2 coating. This was attributed to an increase in the ohmic resistance and reduced accessible functional area in the electrode, like the proposition made in.[174] The desalination experiments yielded an optimized SAC of 490 μmol/g-cathode (~ 28 mg/g-cathode), which is higher than the SAC obtained by using pristine VACNTs (~15 mg/g-cathode).

47. Zhao, W., Guo, L., Ding, M., Huang, Y. and Yang, H.Y., **2018. Ultrahigh Desalination Capacity Dual-ion Electrochemical Deionization Device Based on $Na_3V_2(PO_4)_3$@ C-AgCl Electrodes.**
ACS Applied Materials & Interfaces.

Singapore University of Technology and Design, Singapore; *Submitted:* August 15, 2018*; Accepted:* Oct. 29, 2018.[177]

Keywords: (6), CC, 0.1-0.5 A/g, 1 g/L NaCl, SAC 98 mg/g-both electrodes

This work deals with $Na_3V_2(PO_4)_3$ (NVP) as a cathode material in a dual-ion electrochemical deionization (DEDI). The origin of the term dual is not specifically motivated. The authors claim that the electrode materials for EDI achieve high SAC values by participating in redox reactions with either sodium or chloride ions in the feed solution. The electrochemical cell proposed in this work uses carbon-coated NVP as a Na^+ faradaic electrode and Ag/AgCl as anode. Three different types of NVP structures were tested: sphere-, wire- and flower-shaped NVPs. The NVP-C electrodes were electrochemically characterized via cyclic voltammetry (CV). The desalination experiments were performed in an EDI cell with the cathode and anode separated from the flow channel by a CEM and an AEM, respectively. The feed contained 1000 mg/L NaCl (~18 mM) and the desalination step was performed by applying a constant current of 100 – 500 mA/g. The wire-shaped NVP exhibited a better SAC value and the removal rate was comparable to the other two NVP structures. At an applied current density of 100 mA/g, the SAC value observed for wire-shaped NVPs was 98 mg/g; in both cases after 50 cycles. Bare NVP, without any carbon coating exhibited a reduced capacity of 70 mg/g. The salt adsorption rates varied from 0.04 to 0.14 mg/g/s with increasing applied current. The SAC value was claimed to be higher than the values reported in literature using DEDI technology.

48. Agartan, L., Hayes-Oberst, B., Byles, B.W., Akuzum, B., Pomerantseva, E. and Kumbur, E.C., **2019. Influence of operating conditions and cathode parameters on desalination performance of hybrid CDI systems.**[178]

Desalination

Drexel University, USA; August 22, 2018*; Accepted:* October 31, 2018

Keywords: (6), CV, 1.2 V, 10 mM NaCl, SAC 23-26 mg/g-both electrodes, NMO

This study reports on the effect of operational parameters like feed flow rate and half cycle time (time given to the system for ion (de)intercalation) and cathodic parameters like cathode thickness as well as the loading of a conductive additive on the salt removal performance of a hybrid CDI cell. A faradaic cathode, prepared from α-MnO_2 and a capacitive anode, prepared out of AC, were separated by an IEM to assemble a water desalination cell. Two salt removal mechanisms were suggested to be functional in the cathode namely, pseudo-capacitance and ion intercalation in the crystal structure of the α-MnO_2. The desalination performance of the cell was tested in experiments under constant voltage of ±1.2 V in a batch mode with a 10 mM NaCl solution. To test the influence of each of the experimental parameters mentioned above, their values were systematically altered and the corresponding system response was recorded. The comparison between the salt adsorption rate (SAR) values obtained for the half cycle times 120 and 240 minutes made

the authors to conclude that the electrode was saturated after the 120 min cycle length and the salt removal had become diffusion controlled, leading to a decrease in the SAR. Increase in feed flow rate (from 5 mL/min to 40 mL/min) led to an increase in the SAC values (from 18 to 23 mg/g). This was attributed to a more effective ion transport to the electrodes at higher flow rates. Systematic increment in the electrode thickness (from 150 to 450 μm) resulted in a small increase in the SAC of the electrode (from 23 to 26 mg/g). However, further increase in electrode thickness to 600 μm resulted in a SAC of 13 mg/g. This decrease was attributed to an increase in electronic resistance and increase in the diffusion path length in the electrode. These factors resulted in an incomplete utilization of the active material in the electrodes. Finally, an increase in the loading of the conductive additive (from 10 wt. % to 50 wt. %) to the electrode led to an increase in their SAC from 23 to 25 mg/g. This increase was observed even with a decreasing amount of active material in the electrode. The authors observed that the trends in salt removal performance of the composite electrode cell for electrode thickness and half cycle time aligned with the trends reported for CDI systems. However, those obtained for different flow rates and the loading of conductive additives were opposite of what has been observed in the CDI literature.

2.3 Insights

The timeline overview, presented in **Section 2.2**, gives a concise description of the main findings reported by the studies on intercalation electrode materials. To provide a better insight into the functioning of intercalation electrodes in CDI, we highlight recurring aspects that have been addressed in the studies related to the cell architecture (**Section 2.3.1**) and operation parameters (**Section 2.3.2**).

2.3.1 Cell architecture

The studies described in this work employed different architectures for the desalination cell in terms of the materials used to fabricate the cathode and the anode for ion adsorption. A CDI process can be performed with a two-electrode cell configuration where the electrodes may or may not be separated by an ion-selective membrane. However, several works reported here also used a three-electrode cell to characterize the intercalation electrodes. These papers are usually encountered very early in the timeline, when the properties of intercalation materials were not yet well understood,[102,135] or when new avenues were being explored later.[77,103,108] The two-electrode cell configuration, relevant for desalination applications, can employ different types of cathodes and anodes. A common theme among these cell configurations is the use of intercalation materials as the positive electrode to adsorb cations. This adsorption is usually accompanied by the reduction of one of the lattice elements of the electrode material. An exception is the system reported in[89,179] where an indiscriminate ion adsorption occurs without a redox reaction.

Desalination cells consisting of a cathode and an anode with the same chemical composition with two flow channels on either side of an ion-exchange membrane, are referred to as *symmetric* cells, explored more than one decade.[156] If operational conditions such as the water flow rate in the two channels are also symmetric, a symmetric cell leads to symmetric operation, where the processes in one compartment in one half of the cycle, are the same as in the other channel in the other half of the cycle, making the cell easy to operate.[142]

An interesting point relevant for symmetric systems with intercalation electrodes, is that the desalination performance depends on the initial charge of the electrode. If for instance both electrodes are initially almost fully deintercalated (low concentration of adsorbed cations) and thus the redox-active atoms in the lattice almost fully oxidized, the cycle will be far from optimal, because quickly after charging one electrode relative to the other, one electrode will have released all cations, and then the process stops (voltages get very high). Therefore, intercalation materials must be pre-charged in a suitable way such that the full capacity of the pair of electrodes can be used.[54]

For *asymmetric* electrodes, with cathode and anode fabricated from different materials, anodes have been constructed from:

1. Ag/AgCl
2. Activated carbon (AC)
3. Bismuth, Bi/BiOCl
4. MnO_2

The most common choices for anode materials in cells with an intercalation cathode is Ag/AgCl and AC electrodes. The Ag/AgCl electrode only operates with the Cl^- ions and therefore, it lacks the versatility provided by the AC or cells with the same electrodes. The use of AC provides a predictable capacitive behavior to the cell. Recently, bismuth (Bi) has been reported to be a potential anode material which can be coupled with an intercalation electrode.[162] In more detail, it has been demonstrated that Bi/BiOCl as an anode material can store ~80 mg of Cl^- ions per gram of Bi (for a 600 mM NaCl solution) which is significantly higher than reported for conventional CDI systems. Slow reduction kinetics and loss of capacity (60 % retention after 200 cycles at 20 A/m^2) were identified as the shortcomings of Bi/BiOCl as an anode. The electrical potential for the reduction step was reported to be in between 1.2 and 1.5 V *vs.* Ag/AgCl, which is more negative than values usually reported in literature. A CDI cell with MnO_2 electrode has also been proposed as an alternative to CDI cells with carbon electrodes.[94] The use of such a cell with a modified AC cathode gave an enhanced stability in terms of SAC retention, in addition to increasing the value of SAC (14 mg/g) and reducing the parasitic reactions associated with carbon anodes. The redox reaction typically observed in MnO_2 is similar to that seen for PBAs.[82] It is worth noting that more effort has been put into the development of cathode materials in comparison to that for the anode. However, if the symmetrical electrode cell architecture would be further optimized, there may not be a need for a separate anode material.

2.3.2 Operation parameters

The desalination of brackish water depends on several operation parameters. Most important among them are the current density (*i.e.*, the current applied per unit electrode area, A/m^2) and the salt concentration. These two factors have consequences for the SAC of the desalination cell. The studies reported in this review use different values for these parameters resulting in different capacities for salt adsorption. A glimpse of such differences in operating conditions and their effect on cell performance is illustrated in **Figure 2.3** which provides an overview of the SACs reported in different studies and the corresponding operational conditions such as the applied current/potential and the salt concentration. In addition, it also indicates the electrode (*E*) materials (anode (*A*) and cathode (*C*)) used in the desalination cell. A common characteristic observed during desalination experiments is the dependence of the total SAC on the salt concentration, the current density (for a constant current operation as shown in orange) and the voltage (for a constant voltage operation as shown in blue). A usual trend observed for constant-current operations is that an increase in the current density, while keeping the cut-off voltage and concentration the same, will increase the rate of salt adsorption but decreases the total salt adsorption in a cycle. This is due to an increase in the Ohmic drop (*IR*) in the cell which raises the cell voltage closer to the cut-off value leading to a reduction in the cycle time. For a given value of the applied current/voltage, an increase in the salt concentration increases the salt adsorption capacity only up to a certain extent.[95] An increase in salt concentration should decrease the energy consumed by the cell for desalination due to reduction in ionic resistance.

It is interesting to realize that CDI with intercalation materials, in terms of the high SAC values observed, has been successfully applied to systems with salinities as low as 5 mM[89] and as high as 600 mM.[162] The largest value of 86 mg/(g-active material) for SAC was reported for a CDI cell with a Bi anode and a $NaTi_2(PO_4)_3$ cathode for a 600 mM salt solution, operating at a constant current of 10 A/m^2. Similarly, for a constant-voltage operation, the highest SAC of ~30 mg/(g-both electrodes) was reported for a salt solution with concentration from 10-100 mM operated at 1.2 V.[95] The charge capacity (usually reported in mAh/g) of the electrodes must also be considered along with the SAC values as it provides an idea about the system's ability to use the potential of the electrode for desalination. In addition to giving insight in the performance of the intercalation electrodes, **Figure 2.3** also provides an estimate about the range of values for SAC (and the operation parameters at which they were obtained) for carbon electrodes in CDI. It is difficult to find a common ground for comparison between the intercalation and carbon electrode performance, but some general features can be highlighted. The SAC values recorded for intercalation electrodes tend to be higher than those reported for carbon electrodes (values plotted in Figure 3, with dashed data points, can be found in [119][134][180][181][182]). For instance, intercalation electrodes prepared from NiHCF, when immersed in a 20 mM salt solution, result in a SAC of 34 mg/g at an operating current of 1.4 A/m^2. [54] On the other hand, carbon electrodes immersed in a 20 mM salt solution and operated at 37 A/m^2 achieved a SAC of 12 mg/g.[119] For constant voltage experiments, SAC values of 20 mg/g were

reported for carbon electrodes for a salt concentration of 9 mM[134] and 20 mM,[181] These values were still smaller than those reported for intercalation electrodes operated under constant voltage for a similar salt concentration.[95] In addition to SAC, the average salt adsorption rate (ASAR) (reported in mg/g/s) is also an important parameter in CDI.[18] This parameter is influenced by the applied current or voltage. Consequently, ASAR in a constant current process increases with the current density.[18,183] Carbon electrodes can sustain high current densities and reach a high SAC at the same time.[119,182] However, unlike carbon electrodes, intercalation electrodes are not capable of maintaining a high SAC at high current densities as the charge capacity (in mAh/g) decreases with the charging rate.[97] It is indicative of the presence of limitations in one of the transport processes involved in desalination with intercalation electrodes.[109] Therefore, for intercalation electrodes, at the moment an increase in the ASAR value comes at the expense of the SAC (reported in a Ragone plot in Figure 7 of[97]). This is an interesting opportunity for the optimization of cell design and operation parameters to ensure both a high salt adsorption capacity and a high salt adsorption rate.

In addition to illustrating the performance numbers reported in literature, **Figure 2.3** also highlights the underlying difficulty in comparing different studies. This is due to different materials, experimental conditions, modes of operation (constant current *vs.* constant voltage) and reporting of results. The performance metrics for an objective assessment of the CDI performance and their comparison has been recently described in[40] highlighting certain general characteristics which may be helpful in comparing two desalination systems with different designs. This timeline attempts to provide clear information on the mass by which the SAC values are normalized. It usually varies from the mass of both electrodes[54,137] to the mass of active particles,[162,163] which may be very different, particularly when (inactive) electrode supports are used. Therefore, to begin a meaningful comparison of desalination cell performances, parameters such as salt concentration, applied current/voltage, mass used for normalization of SAC, and cell architecture, must be explicitly mentioned.

2.4 Outlook

The discovery of redox activity in Prussian Blue (PB) in 1978 turned out to be a key moment in the development of intercalation electrodes. Since then, the study of the electrochemical properties of intercalation electrodes gradually expanded, with a systematic effort to understand and explain the redox-active behavior of intercalation electrodes. Remarkably, the electrochemical characteristics of the analogues of PB were studied soon after the electronic activity of pure PB was discovered. As a result, a considerable amount of literature exists which explains the characteristics of various PBAs. However, these materials were not immediately employed for water desalination. This occurred only after it was demonstrated that they were suitable for sodium batteries. In addition to PB(A), redox-activity has been discovered more recently in other materials, including MnO_2, $Na_2FeP_2O_7$, and MoS_2, which subsequently were successfully used in CDI. All these electrode materials show high rate capabilities and capacities and have potential for application in aqueous media.

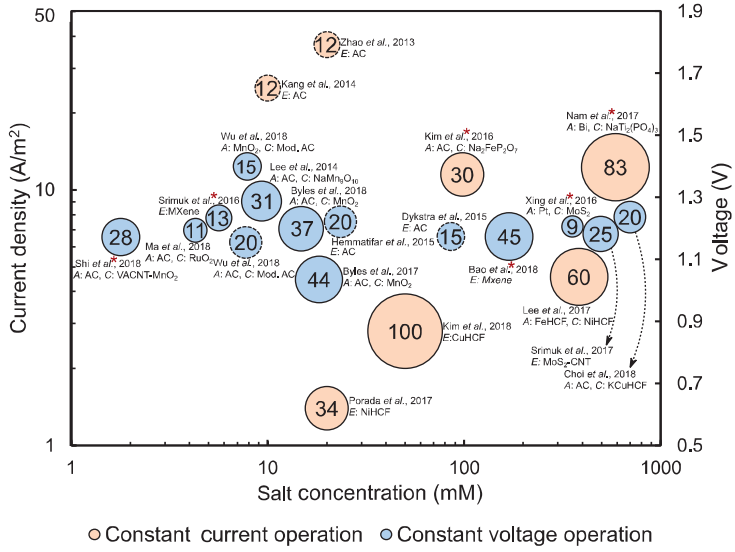

Figure 2.3: An overview of salt adsorption capacities (SAC) in mg/g (total electrode mass, unless marked by a *), reported in literature for constant current (blue - left y-axis) and constant voltage (orange - right y-axis) operation as a function of applied current density (A/m²), salt concentration (mM) and applied voltage (V). The area of the circles is proportional to SAC (value given within the circles) reported in the associated studies. The data labels give the information about the publication reporting the value along with the electrode (*E*) materials, indicated as cathode (*C*) and anode (*A*), used for the cell. A dashed circumference of the data-point circle represents SAC for carbon electrodes, added for comparison purposes.

A general rule for the optimization of intercalation materials and electrodes is that a high rate of salt removal must be achieved, while the salt adsorption capacity must at least be reasonable. To achieve this optimum, a systematic study is required of the dependence of cell performance on applied current/voltage and salt concentration. Furthermore, different studies have utilized different configurations of the desalination cell design. This includes the use of different cathode and anode materials (*e.g.*, Ag/AgCl, carbon or another intercalation electrode), use of multiple membranes between the electrodes, and the position of the flow channel. A definitive optimization of geometric parameters, along with a standardized set of metrics for performance measurement of a desalination cell will be crucial to the development of intercalation electrodes in CDI. This will also make performance comparison with existing technologies more convenient. Accepting the major differences between intercalation and carbon electrodes, nevertheless inspiration for optimization of desalination with intercalation electrodes can still be derived from the extensively developed CDI literature on carbon electrodes.

The chemistry of intercalation electrode materials offers avenues for the further development of the electrode structure, for example in terms of their stability, loading capacity, and selectivity. Depending on the type of electrode material and the electrode properties of interest, (pre)synthetic and/or post-synthetic strategies may be followed. Following literature on energy storage applications[101] and medical diagnosis and treatment,[184] NiHCF and other PBAs used in CDI studies are usually prepared via co-precipitation and, to a lesser extent, thin film electrodeposition, where water is the solvent of choice. In aqueous approaches it is a challenge to control the size of the particle agglomerates, which is relevant because of its role in controlling the accessibility both of ions and electronic charge to the active site. It is anticipated that the CDI field will benefit from recent developments in controlling PB and PBA nanostructure formation and morphology.[184]

So far in CDI applications, NMO has been synthesized under high-temperature conditions using a solid-state reaction,[95] before mixing with carbon black and a binder to obtain sheet-type electrodes. Given the versatility of the NMO system and its derivatives,[185] there is a considerable research activity in this area, and chemical recipes from the field of energy storage will also become available to the field of CDI.

The MXene sheets[186] that have been introduced in CDI [89,171] are made by wet etching from their layered precursors. Delamination of MXene via intercalation approaches using polar organic molecules or large organic base molecules have been reported, and bottom-up methods such as chemical vapor deposition (CVD) are within reach.[186] In the case of another 2D material, MoS_2 nanosheets were prepared via an exfoliation technique, before depositing them onto gold-covered, flexible electrodes.[187]

While the above-mentioned electrode materials have (some) size-based selectivity, the preparation of composite materials and post-synthetic treatments have the potential to further tune the intercalation of certain ions. In this regard, CDI can benefit from surface modification strategies already applied to carbon electrodes,[188,189][189] but also to the field of water purification membranes.[190] Interestingly, polymer coatings can not only be tailored to control ion selectivity,[191] but also to reduce fouling.[192] Another interesting development is the use of graphene-based materials in CDI technology.[193] Given its unique physicochemical properties, including the exceptionally high surface area, electron mobility, and mechanical strength, graphene is expected to be further integrated with intercalation materials, both in terms of composites as well as surface modification.

For further development of CDI technology, it is anticipated that more and more inspiration will be taken from the ever-increasing, but already highly developed energy storage field.[101] Composites containing intercalation materials are interesting to achieve enhanced conductivity and higher structural stability. Post-synthetic surface modifications to obtain materials such as polymers and graphene layers with a thickness in the nanometer scale, are attractive to deposit thin membrane layers on intercalation materials. The number of materials that are available as electrode building blocks, *i.e.*, intercalation materials, polymers and fillers – is already very large, while continuing to increase rapidly. The main challenge is to develop chemical schemes which combine aspects related to the high structural stability

and ionic-selectivity, and thus enabling the fabrication of electrodes with a long-term cycling stability that can also be applied in the selective removal and recovery of specific ions.

In addition, mathematical (theoretical) modelling of a complete CDI cell based on intercalation electrodes, has only recently been initiated. Theoretical modeling of ion transport and adsorption is of relevance to bring the technology further, as it leads to a better understanding of the underlying physical processes and because it provides a tool for quantitative optimization of the parameters involved. Physics-based modeling uses a sufficiently detailed picture of the basic microscopic phenomena in ion transport and adsorption and implements this information in a large-scale model of a CDI cell. Therefore, it can analyze full CDI cycles and provide predictions for desalination, energy use and pH fluctuations. Such models exist for CDI with carbon-based electrodes, but their development is still in its early stages for CDI with intercalation materials.[109,142,194]

For CDI with intercalation materials, on a microscopic level, questions to be addressed relate to the rate-limiting steps in ion adsorption in the electrodes. This limitation can have many causes, such as: the ion transport process within macropores that connect to the active particles;[109] the ion intercalation at the active particle-electrolyte interface;[195] the ion diffusion within the active particles;[196] or perhaps, dependent on electrode design, the electronic transport to and through the active particles.[197] A related question is about the choice for the most suitable framework for a CDI cell model: is a model based on approaches similar to those used for batteries more suitable,[142,159] or are the models based on dilute solutions and classical carbon electrodes[132] a better starting points? Other elements in a theoretical model that must be considered are the fluid flow pattern in the flow channels, and ion transport in the IEMs. An empirical description for the IEMs can be provided with a fixed value for ion selectivity, or a more detailed model can be used that describes diffusion and electromigration of all ions in the membrane. For the flow channels, a *single stirred tank* approach may suffice, but more detailed models can be used which include concentration gradients across the channel, as well as fluid flow patterns. Existing models[109,142,194] are based on one and two-dimensional numerical frameworks. Although this level of description is relevant, such models are also complicated to implement if experience in numerical programming is not available. Therefore *zero-order models* are also relevant to develop. Such models include the basic phenomena of ion transport and adsorption, but only use *stirred tank* approaches and describe transport limitations by an equivalent of Ohm's law or a *film layer*. Therefore, the model mainly consists of algebraic equations supplemented with macroscopic balances (described by ordinary differential equations) which describe the accumulation of ions in electrode and spacer. Such a model is easier to develop and implement than the higher-order models. Another future model extension is to consider separation of salt mixtures with intercalation materials.[54][103]

The models discussed so far can be classified as *mean-field* or *engineering* models. Advanced theoretical tools and numerical methods could be of relevance both on a small and larger scale. On the molecular scale, Molecular Dynamics (MD) simulations can give insight in the intercalation process by looking at ion distributions and the capacity to store charge and ions. On the cell level, computational fluid dynamics (CFD) can help in describing fluid flow

patterns inside the macropores of the electrode and in the flow channels. Knowledge obtained by these advanced tools must be translated (*e.g.*, via empirical equations) for meaningful application in mean field/engineering models.

To conclude, studies on CDI with intercalation materials have been appearing in literature faster than ever. Experimental data for various operation parameters with different types of electrode materials are now readily available. This should significantly facilitate the task of validating theoretical models against suitable experimental data. This may lead to faster system optimization and a better design of electrodes and cell, resulting in reduced energy consumption while improving desalination performance. For intercalation materials in CDI, endeavours in this direction will become important over the coming years.

Appendix

Since the publication of this chapter, new reports on the use of intercalation materials as electrodes for desalination have appeared in literature. Short summaries of selected reports are appended below, as an update to the original 48 summaries provided in the chapter above. The papers summarized below are solely selected on the basis of the use of a new intercalation material as an electrode. Therefore, new reports on the electrodes previously described in literature are not included.

49. Lee, J., Srimuk, P., Zwingelstein, R., Zornitta, R.L., Choi, J., Kim, C. and Presser, V., **2019**. **Sodium ion removal by hydrated vanadyl phosphate for electrochemical water desalination**. *Journal of Materials Chemistry A*
Saarland University, Germany; *Submitted:* October 19, 2018*; Accepted:* January 27, 2019
Keywords: (6), CC + CV, 50 mA/g-cathode, 100 mM NaCl, SAC 31 mg/g-cathode[198]

    Vanadyl phosphate was used as a working electrode material with AC electrodes as a counter to desalinate 100 mM feed water. The working and the counter electrodes were separated from the feed flow channel by a CEM and an AEM, respectively. The specific charge storage capacity of the vanadyl phosphate electrode was found to increase from 23 to 33 mAh/g over 150 cycles in a cyclic voltammetry characterization. The authors claimed that repeated cycling in NaCl electrolyte resulted in a phase change of the working electrode and led to the formation of a phase with higher capacity. The desalination experiments were performed in a CC + CV mode of operation. In addition, a time was given to the cell in between the charge and discharge cycles to determine the baseline concentration. A maximum SAC of 31 mg/g-cathode was obtained after 280 cycles, without any sign of performance fade.

50. Sriramulu, D. and Yang, H.Y., **2019. Free-standing flexible film as a binder-free electrode for an efficient hybrid deionization system**. *Nanoscale.*
SUTD, Singapore; *Submitted:* November 12, 2018*; Accepted:* March 3, 2019
Keywords: (6), CC, 1 – 8 A/m², 51 mM NaCl, SAC 129 mg/g-both electrodes, $Na_2Ti_3O_7$-CNT@rGO[199]

    This study used a $Na_2Ti_3O_7$ (NTO) to prepare a composite electrode also containing carbon nanotubes and reduced graphene oxide (rGO). This composite formed the binder-free working electrode and was paired with an AC electrode to serve as a counter electrode. The working and the counter electrodes were separated from the feed via CEM and AEM, respectively. The hybrid cell treated a ≈ 50 mM NaCl feed in CC mode. The authors determined the SAC to be 129 mg/g at the lowest applied current density of 145 mA/g, which reduced to ≈ 30 mg/g when the applied current was increased by a factor of 5. The salt adsorption rate increased at a commensurate rate with increasing current density. The

high SAC and the adsorption rates were attributed to the combination of high surface area provided by the rGO (≈ 442 m^2/g) and intercalation sites for sodium provided by NTO. The authors observed that the films remained structurally intact for 80 desalination cycles.

51. Younes, H., Ravaux, F., El Hadri, N. and Zou, L., 2019. Nanostructuring of pseudocapacitive $MnFe_2O_4$/Porous rGO electrodes in capacitive deionization. *Electrochimica Acta*.
Khalifa Univesity of Science and Technology , UAE; *Submitted:* December 06, 2018*; Accepted:* March 14, 2019
Keywords: (6), CV, 1.6V, 0.85 mM NaCl, 9 mg/g, MnFe2O4/ rGO[200]

This work presented the use of $MnFe_2O_4$ (MnF) as an active particle in a composite electrode that also contained rGO to treat 100 mL of low salinity (50 mg/L) NaCl feed solution. The MnF/rGO cathode was paired with an rGO anode to form a hybrid CDI cell. The authors determined the SAC of the MnF/rGO electrode to be ≈ 9 mg/g and observed that it was higher than the one of the MnF only electrode (6.5 mg/g). This highlighted the added value of combining MnF with rGO.. The authors claimed reversible and stable operation of the HCDI cell for 6 hours of continuous desalination.

52. Lee, J., Srimuk, P., Zornitta, R.L., Aslan, M., Mehdi, B.L. and Presser, V., 2019. High electrochemical seawater desalination performance enabled by an iodide redox electrolyte paired with a sodium superionic conductor. *ACS Sustainable Chemistry & Engineering*.
Saarland University, Germany; *Submitted:* March 26, 2019*; Accepted:* May 8, 2019
Keywords: (6), CC, 0.1 – 1 A/g, 600 mM NaCl, SAC 35-60 mg/g, NaI+AC[201]

In this study, an iodide couple (I^-/I_3^-) was used as a redox-active electrode element in a hybrid cell to desalinate NaCl feed with seawater concentration (600 mM). An AC electrode was soaked in NaI to form the cathodic compartment, separated from the feed channel by a ceramic NASICON membrane that only allowed sodium to pass through it. The cathode was paired to an AC electrode, soaked in NaCl solution and separated by the flow channel by an AEM. The authors tested the setup using CC mode at currents in the range of 100 to 1000 mA/g and reported SAC values in the range of 40 – 80 mg/g. The cell performance was assessed by operating the cell continuously for a month in CC mode and a stable SAC (70 mg/g) was determined. Furthermore, the charge efficiency of the cell remained close to 80 % throughout this testing period.

53. Yue, Z., Ma, Y., Zhang, J. and Li, H., 2019. Pseudo-capacitive behavior induced dual-ion hybrid deionization system based on Ag@rGO‖$Na_{1.1}V_3O_{7.9}$@ rGO. *Journal of Materials Chemistry A*.
Ningxia University, P. R. China; *Submitted:* April 4, 2019*; Accepted:* June 21, 2019
Keywords: (6), CV, 0.8 – 1.2 V, 5 – 10 mM NaCl, SAC 15 – 40 mg/g, $Na_{1.1}V_3O_{7.9}$ [202]

A hybrid CDI cell with Ag as a chloride-adsorbing anode and $Na_{1.1}V_3O_{7.9}$ (NVO) as a sodium-intercalating cathode was introduced in this study for water desalination. Both Ag and NVO were blended with rGO to prepare the anode and the cathode to desalinate a NaCl feed solution (5 – 10 mM) in a batch mode from a 45 mL reservoir. The HCDI cell was operated in CV mode and the voltage was varied from 0.8 – 1.4 V. The authors reported that the SAC increased from 15 to 40 mg/g when the voltage increased from 0.8 to 1.4 V. Furthermore, it was also observed that the charge efficiency of the cell was close to 100 %. The cycling performance of the cell was deemed to be stable for 1000 minutes, at 1.2 V.

54. Li, Y., Ding, Z., Li, J., Li, J., Lu, T. and Pan, L., 2019. Highly efficient and stable desalination via novel hybrid capacitive deionization with redox-active polyimide cathode. *Desalination*.
East China Normal University, China; *Submitted:* May 2, 2019; *Accepted:* August 2, 2019
Keywords: (6), CV, 1 – 1.8 V, 5 – 17 mM NaCl, SAC 5 – 30 mg/g, Polyimide[203]

This study introduced the use of a redox-active polyimide, poly[N,N-(ethane-1,2-diyl)-1,4,5,8 naphthalenetetracarboxiimide] (PNDIE), as a cathode in a hybrid CDI cell for desalination. The PNDIE cathode was paired with an AC anode, separated by an AEM from the NaCl feed solution. Desalination was performed in a batch mode from a 80 mL feed reservoir. The cell was operated in CV mode and the voltage was varied from 1 – 1.8 V to desalinate a 250 ppm (≈ 5 mM) NaCl feed solution. The equilibrium SAC was reported to increase from 5 to 30 mg/g with the increasing cell voltage. In addition, a maximum SAC of 50 mg/g was reported when the inlet concentration of the NaCl feed solution was increased to 1000 ppm (≈ 17 mM) at the highest applied cell voltage of 1.8 V. The cell was operated at 1.8 V for 100 continuous cycles in a 5 mM feed solution to test its stability. The decline in the SAC from 30 to 17 mg/g after 100 cycles was attributed to the parasitic reactions at the AC anode, resulting in their degradation.

55. Kim, N., Hong, S.P., Lee, J., Kim, C. and Yoon, J., 2019. High-desalination performance via redox couple reaction in the multichannel capacitive deionization system. *ACS Sustainable Chemistry & Engineering*.
Seoul National University, Republic of Korea; *Submitted:* June 3, 2019; *Accepted:* September 4, 2019
Keywords: (3), (6), CV, 0.8 – 1.2 V, 10 mM NaCl, SAC 20 – 60 mg/g, $Fe(CN)_6^{3-/4-}$ [204]

A ferro/ferri-cyanide couple was used in this study as a redox-active electrolyte to compliment the salt adsorption capacity of regular AC electrode in a multi-channel CDI cell. The anode and cathode contained an AC electrode and a ferricyanide/ferrocyanide electrolyte was recirculated between them. These compartments were isolated from the feed channel by an AEM and a CEM. The authors claimed that the combination of the EDL and redox couple resulted in higher adsorption capacity. As a result, the cell had three

compartments with flow and the authors introduced the term multichannel redox CDI (MC-RCDI). The concentration of the redox couple, used as the electrolyte here, was varied from 0 – 100 mM, with 100 mM NaCl as the supporting electrolyte, while the concentration of the NaCl feed was fixed at 10 mM. The feed was desalinated in CV mode in the range of 0.8 – 1.2 V. The authors observed that the SAC increased from 20 to 60 mg/g when the concentration of the redox couple in the side chambers, containing the AC electrodes, was increased from 0 to 100 mM. The authors reported SAC of 68 mg/g and claimed that this value was more than 3 times higher than that delivered by the cell containing only AC electrodes.

56. Li, Y., Ding, Z., Zhang, X., Li, J., Liu, X., Lu, T., Yao, Y. and Pan, L., 2019. Novel hybrid capacitive deionization constructed by a redox-active covalent organic framework and its derived porous carbon for highly efficient desalination. *Journal of Materials Chemistry A*.
East China Normal University, P. R. China; *Submitted:* July 8, 2019*; Accepted:* October 9, 2019
Keywords: (6), CV, 1 – 1.6 V, 8 – 100 mM NaCl, SAC 10 - 30 mg/g, DAAQ-TFP-COF[205]

This study uses redox-active 2,6-diaminoanthraquinone (DAAQ) embedded in β-keto-enamine-linked covalent organic frameworks (COFs) for the first time in CDI for desalination. The DAAQ-TFP-COF cathode was paired with a nitrogen-doped carbon anode, basically obtained by the carbonization of DAAQ-TFP-COF, isolated from the flow channel by an AEM, in a hybrid CDI cell. The HCDI cell was operated in a CV mode to treat a 100 mL NaCl feed, with concentration between 8.5 – 100 mM, in a batch mode operation. The authors found the SAC in the range of 10 – 30 $mg/g_{\text{active material in both electrodes}}$ with a tenfold increase in the inlet concentration. While keeping the concentration constant at 8 mM, an increase in applied voltage from 1 – 1.6 V increased the SAC from 7 to 23 $mg/g_{\text{active material in both electrodes}}$ with a charge efficiency staying maintained at 60 %. Finally, the HCDI cell was claimed to be stable for up to 5000 cycles when operated in a cyclic manner at 0 and 1.6 V, treating a 8 mM NaCl feed in batch mode.

57. Wen, X., Zhao, M., Zhang, M., Fan, X. and Zhang, D., 2019. Efficient capacitive deionization of saline water by an integrated tin disulfide nanosheet@graphite paper electrode via an in-situ growth strategy. *ACS Sustainable Chemistry & Engineering*.
Shanghai University, P. R. China; *Submitted:* November 5, 2019*; Accepted:* December 24, 2019
Keywords: (6), CV, 0.8 – 1.2 V, 8.5 mM NaCl, SAC 21 - 30 mg/g, SnS_2[206]

In this work, tin sulfide (SnS_2) was grown on a graphite paper to fabricate a binder-free electrode to treat a 8.5 mM NaCl solution in batch mode. The cell was operated in a CV mode with cell voltages varying from 0.8 – 1.2 V. The authors claimed that anchoring SnS_2 on graphite enhanced the overall conductivity of the electrode and high surface area.

During desalination at 1.2 V, the cell delivered the maximum equilibrium SAC of 30 $mg/g_{electrode\text{-}weight}$. Furthermore, the cell delivered this SAC and retained a reversible operation for 5 cycles. The authors observed that the SAC values reported here (up to ≈ 30 mg/g) were higher than those reported with other metal sulfide electrodes namely WS_2, MoS_2, and TiS_2 in CDI literature.

58. Tan, G., Lu, S., Xu, N., Gao, D. and Zhu, X., 2020. Pseudocapacitive behaviors of polypyrrole grafted AC and MnO2 electrodes to enable fast and efficient membrane-free capacitive deionization. *Environmental science & technology*.
Louisiana State University, USA; *Submitted:* November 26, 2019*; Accepted:* April 3, 2020
Keywords: CV, 0.8 – 1.4 V, 9 – 15 mM NaCl, SAC 20 – 34 mg/g, PPy & MnO_2 [207]

This work reports on an HCDI cell comprising a polypyrrole (PPy) grafted AC as an anode and an MnO_2 cathode, without the use of a membrane. A batch of 50 mL brackish water feed (9 – 15 mM) was treated in CV mode at different applied voltages, ranging between ±0.8 to ±1.4 V. The HCDI cell delivered a maximum equilibrium SAC of 34 mg/g at 1.4 V for a 15 mM NaCl solution. The authors claimed this SAC to be among the highest reported for a HCDI cell and attributed this result tot the pseudocapacitive nature of PPy and MnO_2, resulting in enhanced ion adsorption capacities. Moreover, this was also assumed to be the reason behind the high rates of salt removal, over an order of magnitude higher than the previous reports, as claimed by the authors.

59. He, F., Hemmatifar, A., Bazant, M.Z. and Hatton, T.A., 2020. Selective adsorption of organic anions in a flow cell with asymmetric redox active electrodes. *Water Research.*
Massachusetts Institute of Technology, USA; *Submitted:* January 7, 2020*; Accepted:* May 19, 2020
Keywords: CV, 0.05 – 0.7 V, 0.25 mM benzoate + 12.5 mM perchlorate, pPy-DBS-CNT and **PVFc-CNT**[208]

This study reports on the use of two different materials as a cathode (polypyrrole (pPy) doped with anion surfactant, dodecylbenzenesulfonate (DBS)) and an anode (polyvinylferrocene (PVFc) polymer complexed CNTs), assembled in an asymmetric CDI cell to selectively remove benzoate from perchlorate, present as a background anion in water. The cell was reported to be functioning reversibly when cycled in a CC and a CV mode of operation in a 10 mM perchlorate solution. During the selectivity experiment, a mixed feed of benzoate (0.25 mM) and perchlorate (12.5 mM) was desalinated. The cell was operated in a CV mode with the potential of the anode modulated using a reference electrode. The authors claimed that the PVFc preferential adsorption of benzoate was 3-fold higher than that of perchlorate, even though the concentration of perchlorate was 50-fold higher than that of benzoate. Furthermore, presence of benzoate in the electrolyte

was also claimed to be responsible for an increased charge efficiency during desalination.

60. Sebti, E., Besli, M.M., Metzger, M., Hellstrom, S., Schultz-Neu, M.J., Alvarado, J., Christensen, J., Doeff, M., Kuppan, S. and Subban, C.V., 2020. Removal of Na^+ and Ca^{2+} with Prussian blue analogue electrodes for brackish water desalination. *Desalination*.
Lawrence Berkeley National Laboratory, USA; *Submitted:* February 14, 2020*; Accepted:* April 1, 2020
Keywords: CV, 1 V, 17 mM NaCl, 9 mM $CaCl_2$, SAC 20 – 45 mg/g-active material, MnHCF & ZnHCF[209]

This work reports the use of manganese hexacyanoferrate (MnHCF) and zinc hexacyanoferrate (ZnHCF) as cathodes in HCDI for a single-pass desalination of brackish water, containing either a 17 mM solution of NaCl or a 9 mM solution of $CaCl_2$, in a CV mode. An oversized carbon electrode was used as counter in the cell. The authors discovered rapid dissolution of ZnHCF cathodes upon repeated (de)intercalation of both Na^+ and Ca^{2+}. The authors observed MnHCF delivering a higher SAC and salt adsorption rate when cycled in a monovalent ion feed while CuHCF performed better on the same metrics in divalent ion feed. After 280 cycles of (de)intercalation in both NaCl and $CaCl_2$, MnHCF was found to retain a higher fraction of its initial capacity when compared with CuHCF, leading the authors to conclude that MnHCF was more robust than CuHCF in desalination.

61. Chen, F., Wang, J., Feng, C., Ma, J. and Waite, T.D., 2020. Low energy consumption and mechanism study of redox flow desalination. *Chemical Engineering Journal.*
University of New South Wales, Australia; *Submitted:* March 22, 2020*; Accepted:* June 26, 2020
Keywords: CC, 1.2 – 2.4 A/m², 50 mM NaCl, $Fe(CN)_6^{3-}/Fe(CN)_6^{4-}$[210]

In this work, a redox-active solution of ferri-/ferrocyanide (1:1 ratio) was used in a 4-compartment flow cell to desalinate a ≈ 50 mM NaCl solution continuously, resulting in a fresh water of 2.5 mM concentration. In the cell, the redox-active Fe solution was recirculated between the cathode and the anode, which were separated from the two flow channels by a pair of CEMs. The flow channel was separated from each other via an AEM. The cell was operated in a CC mode to treat a 25 mL batch of NaCl feed solution under recycling conditions. During desalination, ferrocyanide was oxidized at the anode while ferricyanide was reduced at the cathode. The recycling of the redox mediators maintained low operating potential (~100 mV) and facilitated continuous salt removal from the recycled feed with no upper limit on the adsorption capacity of the system. Furthermore, an increase in the concentration of the redox mediators decreased the energy consumption of the 4-compartment cell. The authors claimed that the recirculation of the redox mediators also prevented a change in the solution pH and that the low energy

consumption was due to the rapid rate of electron transfer between the ferri-/ferrocyanide redox couple.

62. Pan, Y., Yao, L., Wu, D., Bentalib, A., Li, J. and Peng, Z., 2020. Sulfonated nickel phthalocyanine redox flow cell for high-performance electrochemical water desalination. *Desalination*.
University of Akron, USA; Submitted: May 14, 2020; Accepted: September 10, 2020
Keywords: (6), CC + CV, 2 – 2.8 A/m², ±0.5 V, 50 mM NaCl, 0.25 – 0.7 $g_{NaCl}/mol_{NiPcTATS}$ [211]

This study reports on the use of a nickel phthalocyanine tetrasulfonic acid tetrasodium salt (NiPcTATS)-based redox flow desalination cell. The redox-active electrolyte, a combination of aqueous NiPcTATS in the pristine form and in an oxidized form ($NiPcTATS^+$) with a total concentration of 35 mM, was separated from the feed solution via two CEMs and recirculated between the cathodic and the anodic compartments. The flow channels were separated from the electrode compartments by an AEM. The 50 mM NaCl feed solution was recirculated in the two feed chambers and the cell was operated under different currents (2 – 2.8 A/m²) and a pair of cell voltage (±0.5 V). In CC mode, the authors found that the ASAR increased with increasing current while concomitantly the SAC reduced. In CV mode, the conductivity of the feed gradually reduced with time and reached below the value of drinkable water to around 500 μs/cm in 800 minutes. The cell was also found to be stable for 50 charge/discharge cycles and delivered a charge efficiency of ≈ 90%. While the focus of this chapter is on intercalation materials, it is interesting to mention that this redox flow desalination cell (RFDC) was powered with a solar panel.

63. Guo, L., Ding, M., Yan, D., Pam, M.E., Vafakhah, S., Gu, C., Zhang, W., Alvarado, P.V., Shi, Y. and Yang, H.Y., 2020. High-speed capacitive deionization system with flow-through electrodes. *Desalination*.
Singapore University of Technology and Design, Singapore; Submitted: June 22, 2020; Accepted: September 03, 2020
Keywords: CV, 0.05 – 0.7 V, 0.25 mM benzoate + 12.5 mM perchlorate, TiO_2@CNT[212]

This study presents the use of TiO_2 encapsulated carbon nanofibers (TiO_2@CNF) as a flow-through electrode (both cathode and anode) in a CDI cell. The brackish water feed solution (4 – 85 mM) flows through the electrodes and emerges desalinated at the outlet after crossing the two electrodes. The cell was operated in CV mode in the cell voltage range of 0.8 – 1.4 V. The authors reported an equilibrium SAC in the range of 8 – 14 $mg/g_{both\ electrodes}$ when the cell voltage was increased from 0.8 V to 1.4 V. In addition, the equilibrium SAC was also found to increase with increasing feed concentration and flow rate. The highest charge efficiency value of 66 % was obtained at the largest applied voltage of 1.4 V. Finally, the TiO_2@CNT electrodes were found to be stable for 15 charge discharge cycles.

64. Liu, X., Zhang, S., Feng, G., Wu, Z.G., Wang, D., Albaqami, M.D., Zhong, B., Chen, Y., Guo, X., Xu, X. and Yamauchi, Y., 2021. Core–shell MOF@ COF motif hybridization: selectively functionalized precursors for titanium dioxide nanoparticle-embedded nitrogen-rich carbon architectures with superior capacitive deionization performance. *Chemistry of Materials.*
University of Queensland, Australia; Submitted: October 23, 2020; Accepted: January 25, 2021
Keywords: CV, 1.2 – 1.6 V, 0.8 – 2.5 mM NaCl, 33 mg/g$_{\text{effective-weight-both-electrodes}}$[213]

In this report, a carbonaceous hybrid of Ti-based MOF (NH_2-MIL-125) and triformylphloroglucinol (TP) + 2,6-diaminoanthraquinone (DQ) COF was used as an electrode in an HCDI cell with AC anode to desalinate a 40 mL NaCl solution in batch mode. The concentration of the recirculated feed ranged from 0.8 – 2.5 mM and the cell was operated in CV mode. The equilibrium SAC of the cell was found to increase with increasing feed concentration as well as the applied cell voltage. The highest equilibrium. SAC of 33 mg/g$_{\text{cathode-weight}}$ was achieved at 1.6 V. Finally, the stability of the cell was tested by operating it in a 2.5 mM NaCl solution at 1.4 V. The cell was found stable in performance for 40 cycles that lasted close to 2 days.

65. Si, W. and Li, H., 2021. Understanding the enhanced capacitive desalination performance of spherical $ZnCo_2O_4$ electrode. *Advanced Materials Interfaces.*
Ningxia University, P.R. China; Submitted: January 24, 2021; Accepted: February 18, 2021
Keywords: (6), CC + CV, 10 mA/g, 1.2 V, 18 mM NaCl, 40 – 75 mg/g$_{\text{effective-weight-both-electrode}}$[214]

In this report, spinel ZnCo2O4 (ZCO) was used in an HCDI cell with AC anode to desalinate a batch of 18 mM NaCl feed solution. The cell was operated in both CV as well as CC modes. The authors reported an increasing equilibrium SAC with increasing applied cell voltage. In CC mode, the SAC was found to decrease with increasing applied current with maximum value obtained at 10 mA/g and minimum at 40 mA/g. The authors attributed the high SAC at lower applied currents to the longer adsorption time and less resistance under low current. The electrodes, during cycling, lost 20 % of their initial capacity after 20 cycles, performed under a constant current of 20 mA/g, in NaCl. Finally, the authors also found a preference of ZCO towards smaller monovalent K^+ over larger monovalent Na^+ and divalent Mg^{2+} .

3 Water Desalination with Nickel Hexacyanoferrate Electrodes in Capacitive Deionization: Experiment, Model and Comparison with Carbon

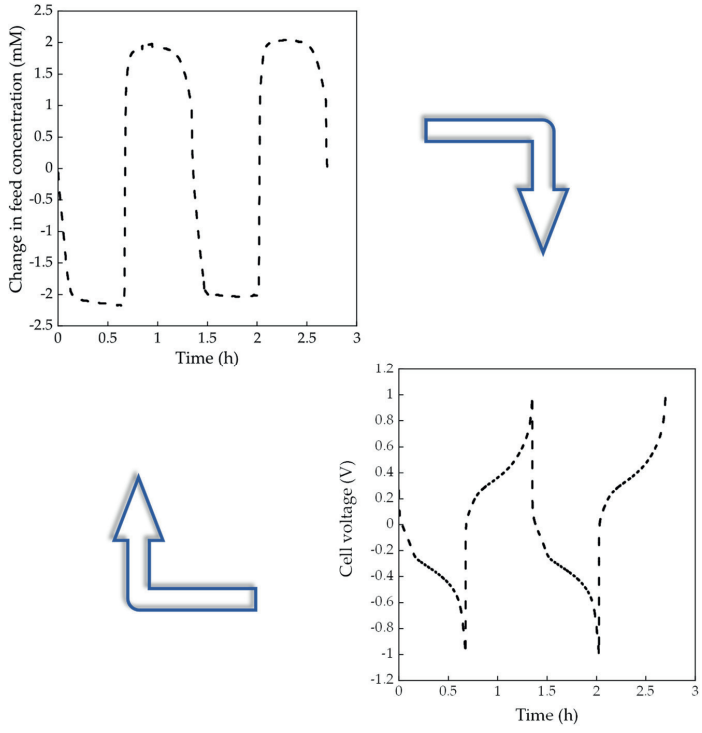

This chapter has been published as:

Singh, K., Zhang, L., Zuilhof, H., & de Smet, L. C. P. M. (**2020**). Water desalination with nickel hexacyanoferrate electrodes in capacitive deionization: Experiment, model, and comparison with carbon. *Desalination*, *496*, 114647.

Abstract

Capacitive deionization (CDI) is a water desalination technology in which ions are removed from water by creating a potential difference between two capacitive electrodes. Porous carbon has been extensively used as an electrode material in CDI. However, recent developments in the field of intercalation materials have led to their application in CDI due to their large ion storage capacity. One such intercalation material, nickel hexacyanoferrate (NiHCF), was used in this study as the electrode material. A symmetrical cell was assembled with two identical NiHCF electrodes separated by an anion-exchange membrane. The effect of operational parameters such as current density, feed concentration and flow rate on the desalination characteristics of the cell was investigated. The highest salt adsorption capacity of ≈ 35 $mg/g_{both\text{-}electrodes}$ was measured at a current density of 2.5 A/m^2 in a 20 mM NaCl feed solution. Furthermore, a Nernst-Planck transport model was successfully used to predict the change in the outlet concentration and cell voltage of the symmetric CDI cell. Finally, performance of the symmetric NiHCF CDI cell was compared with an MCDI cell with porous carbon electrodes. The NiHCF cell, on average, consumed 2.5 times less energy than carbon-based MCDI cell to achieve similar levels of salt removal from saline water in CDI.

3.1 Introduction

Capacitive deionization (CDI) is an electrochemical water desalination technique in which the anions and cations are removed from water and temporarily stored in capacitive electrodes by creating a potential difference between them.[18,20,123] Regardless of the similarities between the design of different desalination setups, the mechanism of ion storage in the capacitive electrodes marks the difference between CDI and other electrochemical technologies such as electrodialysis, ED, where desalination is driven by faradaic reactions occurring at the electrodes. Therefore, desalination *via* ED can function continuously, provided the reaction conditions are maintained. On the other hand, conventional CDI cells produce desalinated water in an intermittent manner and the electrode voltage changes with charge accumulation. Once saturated, the capacitive electrodes are regenerated by either short-circuiting or reversing the polarities. This regeneration step interrupts the desalinated water supply. However, a different cell architecture such as flow electrodes and rocking chair can enable CDI to continuously produce desalinated water,[54,69,142] like ED and reverse osmosis. Moreover, it has been demonstrated that a part of the electrical energy supplied to the electrodes during the ion adsorption step can be recovered, after adjusting for the resistive losses, during the desorption step.[44,112]

Table 3.1: List of symbols.

Nomenclature			
Applied current density (A/m^2)	I	Intercalation degree	ϑ
Inlet concentration (mM)	c_{in}	Spacer/electrode porosity	ρ_s/ρ_e
Change in concentration (mM)	Δc	Spacer/electrode tortuosity	$\varepsilon_s/\varepsilon_e$
Average concentration change (mM)	$\langle\Delta c\rangle$	Dimensionless potential	ϕ
Maximum cation concentration (M)	c_{max}	Dimensionless potential in electrode	ϕ_{ec}
Reference concentration (mM)	c_{ref}	Inter-ionic repulsion factor	g
Concentration in active particle (mM)	c^+	Fluid velocity in flow direction (m/s)	v_y
Interfacial area (m^2)	A	Ion valency, i	z_i
Active particle volume fraction	ε_a	Intercalation flux (mol/m^{3}s)	aJ_{int}
Volumetric flow rate (mL/min)	Q	Productivity (L/h/m^2)	P
Half cycle time (s)	Δt_{HCT}		

The recovery of the energy released during the electrode regeneration can enhance the thermodynamic energy efficiency of CDI,[215] making capacitive electrodes attractive for water desalination applications.

Conventionally, porous carbon has been used as an electrode material in CDI,[51,216–218] due to its low cost, high specific surface area and electronic conductivity. Ion storage in these electrodes proceeds via an electrical double layer (EDL) formation on the pore surface.[219] However, carbon electrodes in CDI suffer from co-ion expulsion *i.e.* the depletion of co-ions from the EDL during counter-ion adsorption.[220] This results in only a partial use of the applied current or the potential difference in storing counter-ions in the micropores of the carbon electrodes, as the remaining part is diverted towards the removal of co-ions from the micropores. Consequently, the thermodynamic efficiency of the process decreases. It can be solved by placing ion-exchange membranes, IEMs, in between the electrodes and the flow channel, effectively blocking the release of the co-ions from the micropores.[131] This is called membrane capacitive deionization, MCDI. Furthermore, the ion storage in the electrical double layers shows limited inherent selectivity towards different ions,[73,221,222] restricting its use in selective ion removal applications.

Recently, intercalation materials, explored in the field of energy storage, have found application as an alternative electrode material to the porous carbon in CDI.[41,101] The ion storage in these materials involves insertion of an ion, mostly cation, in interstitial sites.[105] This mechanism is advantageous, as it has the desirable characteristics of adsorption in carbon such as ease of fabrication, fast kinetics,[104] and improves upon the ion storage capacity,[97] while eliminating the co-ion repulsion. In addition, desalination systems based on intercalation materials provide more flexibility for selective removal of ions of choice without any chemical modifications of the electrode.[11,100,106,165] Finally, the intercalation electrodes are capable of storing the same amount of charge at a lower voltage, which can lower their energy consumption in comparison to their carbon-based counterparts, as argued in[54] and recently predicted theoretically in [223]. Here, we focus on this energy aspect of the intercalation materials and compare them with carbon electrodes.

Among all the intercalation materials, the so-called Prussian blue analogues (PBAs) have been most commonly used to fabricate electrodes for CDI cells.[54,56,137,153] These materials have attracted attention due to their non-toxic nature, open framework structure, customizable chemistry, and stability at high cycling rates.[82] The process of intercalation in these materials proceeds via the insertion of a cation in an interstitial lattice site and a simultaneous reduction of a redox-active species in the cubic lattice structure.[82] The deintercalation of the inserted ion, during regeneration, is accompanied by the oxidation of the same redox-active species, thus maintaining the electro-neutrality of the lattice. An ideal PBA unit cell has an empirical formula of $A_2M[Fe(CN)_6]$ where A is an alkali metal (Na, K) and M can be Ni,[77] Cu,[144] V,[104] or other transition metal element.[82,86] This highlights the versatility of the chemical composition of PBAs. In addition, PBAs have demonstrated an ability to intercalate ions of

multiple valences such as Na^+, Ca^{2+}, and Y^{3+} among others.[77,80] One such PBA, NiHCF, with $Na_2Ni[Fe[(CN_6)]$ as empirical formula of its reduced form, is used in this study as an electrode material for water desalination. The lattice structure in this material is important since a highly crystalline structure would result in a higher charge storage capacity, which is inversely proportional to the defects in the crystal structure such as the absence of $Fe(CN)_6$ from the lattice. The loss of storage capacity in NiHCF electrodes has been attributed to the irreversible oxidation of the redox-active materials instead of the process of (de)intercalation.[108]

The use of intercalation materials such as NiHCF as an alternative to porous carbon in CDI relies upon **(a)** desalination performance metrics such as energy consumption and productivity, *P*, defined as the volume of desalinated stream produced over a cycle for a given electrode area and **(b)** desalination objectives such as an average reduction in concentration with respect to inlet feed, c_{in}, ⟨Δ*c*⟩, and water recovery (*WR*) for a given inlet feed concentration. The desalination performance indicators such as the salt adsorption capacity, SAC, and the charge efficiency in combination with the metrics can further help in assessment of electrode material performance in CDI. Many studies have reported a higher SAC for intercalation electrodes in comparison to that of carbon.[54,129,137,175] However until now, there has been no effort to compare the performance of intercalation electrodes with that of carbon electrodes, in terms of well-defined performance metrics, under equivalent separation conditions and cell design elements.[40,41] The current study bridges this gap by providing a direct comparison between an intercalation electrode based-symmetric cell and a porous carbon electrode-based MCDI cell with respect to specific performance metrics, indicators, and separation conditions as described elsewhere.[40] The cell used in this study is termed symmetric as the electrodes in the cell intercalate the same kind of ion *i.e.* cation.[142] A comparison, as presented in this work, will help to put the performance of intercalation electrodes in perspective with that of porous carbon electrodes. In addition, it will facilitate the comparison of CDI systems based on symmetric intercalation electrodes with other desalination technologies as the comparisons currently presented in literature, with reverse osmosis and electrodialysis, take neither the intercalation materials nor the symmetric cell configuration in CDI into account.[224,225]

In this study, we use two NiHCF electrodes, with identical chemical and ionic composition, in a symmetrical CDI cell configuration to desalinate feed water containing NaCl. The electrodes are referred to as identical here if their ionic content is the same. An estimate of their state of charge/discharge is defined as the intercalation degree, ϑ, which ranges between 0 and 1, and is calculated by taking a ratio of the actual charge transferred to or from the electrode and the equilibrium charge storage capacity of the electrode. A $\vartheta \approx 0$ indicates a state of minimum Na^+ content (charge) and $\vartheta \approx 1$ indicates the maximum Na^+ content (discharge) inside the NiHCF particles. A schematic in **Figure 3.1a** shows the symmetric cell with NiHCF electrodes under operation in a desalination cell. The figure shows the moment during which a current applied via the external circuit results in a synchronized expulsion and introduction of electrons from the left and the right electrode, respectively. In this moment, Na^+ deintercalates from the left electrode into the solution. It is mirrored in the right compartment

where Na^+ intercalates into the electrode. Both processes occur simultaneously to preserve the electroneutrality. The electric field drives the Cl^- in the direction opposite to that of Na^+ from the spacer channel. Therefore, an anionic flux is directed through the anion-exchange membrane (AEM) towards the electrode on the left. The Na^+ deintercalating from the anode combines with the Cl^- migrating through the membrane to give a concentrated stream in the anodic compartment and a freshwater stream in the cathodic compartment. This study includes the influence of c_{in} and applied current densities I on the ⍰Δc⟩, energy consumed per cubic meter of the desalinated water E_v, and the SAC. A theoretical model for symmetric CDI cell with intercalation materials such as NiHCF, developed in [109], was used to describe the results obtained from experiments.

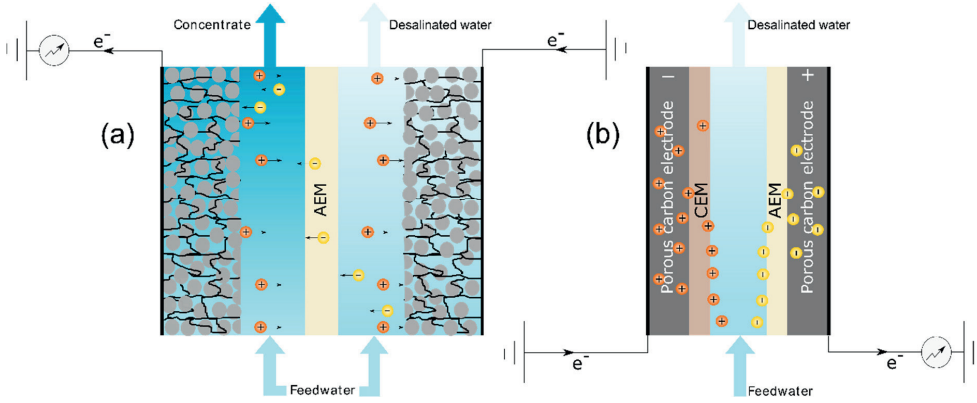

Figure 3.1: Schematics of the two CDI setups, one with PBA and the other with porous carbon electrodes **(a)** A two-compartment symmetric cell assembled with identical NiHCF electrodes separated by a pair of flow channels and an AEM. The active particles, grey spheres, are presented as an agglomerate connected to each other and to the current collector, black solid line adjacent to the electrodes, by the conductive carbon, represented by twisted black lines running across the width of the electrode. **(b)** A one-compartment MCDI cell with identical porous carbon electrodes. In this configuration, an AEM and CEM are placed in front of the carbon electrodes, separating them from the flow channel in the middle.

The theoretical description, reported here with the experimental results, gives insight into desalination by the symmetric NiHCF cell. Finally, a comparison between symmetric CDI cell with NiHCF electrodes and an MCDI cell with porous carbon electrodes, as depicted in **Figure 3.1b**, was performed. The MCDI cell resembled the symmetric cell with the PBA electrodes by having the same geometric surface area (cm^2) and loading ($g_{active\text{-}material}/cm^2$), spacer porosity and thickness along with the graphite current collectors and the polymeric end-plates. In addition to an AEM, the MCDI cell had a cation-exchange membrane, CEM, for the cathode. The performance metrics and indicator mentioned in [40] such as the energy consumption, P, and ⍰Δc⟩, respectively, were evaluated under identical experimental conditions for the

symmetric cell with NiHCF electrodes and for the MCDI cell with porous carbon electrodes to highlight the differences between them.

3.2 Materials and methods

3.2.1 NiHCF synthesis and characterization

A co-precipitation method[152] was adopted to prepare the NiHCF powder. A 200 mL solution of 24 mM $NiCl{\cdot}6H_2O$ (Alfa Aesar) and 12 mM $Na_4Fe[(CN)_6]{\cdot}10H_2O$ (Sigma Aldrich) each was added drop-wise to a 200 mL reaction medium containing 99 % milliQ water and 1 % 1 M HCl, by volume, under vigorous stirring. The reaction mixture was stirred at 1000 RPM for ≈ 12 h. The precipitate formed was washed three times with milliQ water using a vacuum filtration unit and dried overnight in a vacuum oven at 40 °C. The chemical composition of the powder was determined by dissolving a small amount of NiHCF precipitate in ≈ 70 % (by volume) solution of HNO_3 and using inductive coupled plasma optical emission spectrometry (ICP-OES) to analyze the resulting solution. The surface morphology of the NiHCF was observed using a scanning electron microscope (SEM). The particles were coated with gold and imaged under the microscope for two different magnifications. The Brunauer-Emmett-Teller, BET, surface area of the NiHCF powder and the YP 80F carbon was measured by Tristar 3000 surface area analyzer (Micromeritics). The crystallinity of the NiHCF particles was assessed by powder X-ray diffraction (XRD) analysis, performed using a copper source for diffraction angles in the range of $10° < 2\theta < 70°$.

3.2.2 Electrode preparation and characterization

The dried NiHCF precipitate, obtained from the co-precipitation reaction mentioned in **Section 3.2.1**, was used as an active material in preparing free-standing electrodes for desalination experiments. These electrodes comprised of conductive carbon black (Cabot), to enhance the electronic conductivity of the electrodes, and poly-tetrafluroethylene (PTFE) (Sigma Aldrich), to provide them shape and bind the components together. The NiHCF precipitate and the conductive carbon were milled together. The fine NiHCF-carbon blend was mixed with the 60 % (by weight) PTFE dispersion and ethanol as a solvent. The slurry formed contained the NiHCF powder, carbon black and the binder in a ratio of 8:1:1 by weight. The slurry was kneaded until most of the solvent evaporated. The electrode mass left behind, in form of a wet dough, was cold rolled into 200 μm sheet electrodes with stainless steel rollers in a rolling machine (MTI corp.) at room temperature. Finally, the electrodes were cut into rectangles of 10 cm × 2 cm, dried in an oven at 60 °C for 2 h to eliminate any residual ethanol from the fabrication procedure and weighed. The weight of the electrodes was kept between 0.42-0.45 g.

Electrodes were electrochemically characterized by an *ex-situ* Galvanostatic Intermittent Titration Technique, GITT. A three-electrode cell setup was employed in this technique containing the NiHCF electrode as the working electrode (WE), a platinum-coated titanium mesh as the counter electrode (CE) and an Ag/AgCl electrode as the reference electrode (RE). A 1 M Na_2SO_4 solution, bubbled with nitrogen, was used as an electrolyte. The pH of the electrolyte was monitored at specific intervals and kept acidic (pH = 3). Current was applied in pulses via a potentiostat (IviumStat.h standard, IVIUM Technologies), and the corresponding voltage response was recorded. These current pulses were interrupted by an equilibration time, during which the circuit was left open, and the open circuit voltage (OCV) was measured. The number of pulses applied to the cell corresponds to the charge capacity of the WE. Each pulse carried a charge of 5 C (at a current of ≈ 60 mA/g_{NiHCF}). The charge storage capacity of the electrodes was determined by the product of the number of (de)intercalation steps and the charge transferred to the electrodes in these steps.

The carbon electrodes used in the MCDI cell were prepared in a similar manner as the NiHCF electrodes. In place of NiHCF, fine YP 80F carbon powder was used. The ratio of YP 80F and PTFE in the resulting electrodes was 0.95: 0.05. The thickness of carbon electrodes was kept at ≈ 700 μm to keep their area and weight equal to that of the 200 μm thick NiHCF electrodes. The electrochemical characterization of the YP 80F carbon electrodes has been reported in detail elsewhere.[226]

3.2.3 Cell assembly and experiments

The NiHCF electrodes were pre-treated prior to the assembly of the desalination cell. One of the two NiHCF electrodes used in the desalination cell, as shown in **Figure 3.1a**, was put in a three-electrode cell configuration and charged to 0.9 V to deintercalate the cations, Na^+ in this study, from the interstitial sites in it. The other electrode was assembled in an identical cell and discharged to −0.2 V to intercalate cations in the interstitial sites of the active particles bringing the electrode to a state of maximum discharge. These charged and discharged electrodes were then assembled in the desalination cell of **Figure 3.1a** together with spacer channels, an AEM, graphite current collectors and PVC end plates to sandwich the arrangement together. After the assembly, the cell was short-circuited for 1 h. This step before starting the desalination experiment was performed to equalize the ion content in the two, fully intercalated and deintercalated, electrodes. This ensures that the desalination starts with two identical electrodes, resulting in symmetrical and mirrored operation in the two cell chambers.

The MCDI desalination cell with carbon electrodes was assembled according to the schematic presented in **Figure 3.1b**. The cell design elements including the electrode weight of 0.45 g, projected area of 20 cm^2 and spacer thickness of 500 μm were kept identical to the

symmetric CDI cell with NiHCF electrodes. The spacer channel was separated from the anode and cathode by the AEM and the CEM (CMX Neosepta), respectively. The carbon electrodes were soaked in the feed water for 0.5 h before the assembly.

Two sets of experiments were performed to investigate the performance of NiHCF electrodes and to allow comparison with literature. In the first set, constant current was applied to the symmetric cell with NiHCF electrodes in the cell voltage window of ±1 V to desalinate feed with c_{in} of 5, 20, and 50 mM NaCl. For all these concentrations, I was varied from 2.5 to 15 A/m^2. The current was normalized with the projected electrode area of 20 cm^2. The change in effluent concentration was monitored using a probe, connected to a conductivity meter (Orion Versa star, Thermo Scientific), at the two outlets of the desalination cell. The SAC obtained during a half cycle was determined as

$$\frac{QM}{m}\int_{\Delta t_{HCT}}(c_{in}-c_{out})dt\,, \tag{3.1}$$

where c_{out} indicates effluent concentration, M is the molar mass of NaCl, Q is the feed flow rate through each spacer channel, Δt_{HCT} is the half cycle time for the adsorption/desorption steps and m is the weight of both electrodes in the desalination cell. The symmetric cell with the NiHCF electrodes removes salt from both compartments over the entire duration of the desalination cycle. Therefore, the total salt removed in one full cycle is different from the SAC and is obtained by the addition of the SAC obtained during the adsorption half cycles of each electrode. The MATLAB code developed to calculate SAC for a desalination cycle is provided in the section S 3.1 of the supporting information.

In the second set of experiment, the half cycle time, Δt_{HCT}, of the adsorption and desorption steps was fixed. The NiHCF cell was operated under both constant current and constant voltage modes. The c_{in} of the feed was kept constant at 20 mM NaCl. During the operation, I was varied in the range of 10 to 30 A/m^2, and the Q was varied in the range of 4 - 12 mL/min. For operation in constant voltage mode, the cell voltage was varied from 0.4 to 1.2 V. For example, in one cycle, +0.4 V was applied in the first half and −0.4 V was applied in the second half of the cycle. This procedure was repeated for the cell voltages 0.6, 0.8, 1, and 1.2 V. For all these experiments, the c_{in} and Q was kept constant at 20 mM and 7.8 mL/min, respectively.

Finally, for direct performance comparison, the symmetric cell with NiHCF electrodes and the MCDI cell with carbon electrodes were operated under the identical constant current conditions for the same c_{in}, Δt_{HCT} and Q. The ⍰Δc⟩ was calculated as

$$\langle \Delta c \rangle = \frac{N_d}{V_d}, \tag{3.2}$$

where N_d are the moles of salt removed from the feed in one cycle and V_d is the volume of feed desalinated in one cycle. The average salt adsorption rate (*ASAR*) over a desalination cycle was calculated in two ways,[40]

ASAR (mg/g/min)

$$\frac{\text{SAC}}{\Delta t_{\text{cycle}}}, \tag{3.3}$$

and *ASAR* (μmol/cm²/min)

$$\frac{N_d}{A\Delta t_{\text{cycle}}}. \tag{3.4}$$

where A is the projected area of the desalination cell and Δt_{cycle} is the cycle time. The use of two definitions of the *ASAR* help to evaluate and compare the design requirements of a desalination system by highlighting the influence of electrode mass and area used to achieve the removal rate.

The volumetric energy consumption was determined as

$$\frac{1}{V_d}\int_{\Delta t_{\text{cycle}}} IV dt\,, \tag{3.5}$$

where $IV > 0$.

Productivity, P, defined as the volume of the diluate produced per unit time and projected face area of the desalination cell was calculated as

$$P = \frac{V_d}{A\Delta t_{\text{cycle}}}, \tag{3.6}$$

In this work, the P of the symmetric cell with NiHCF electrodes is twice as high as that for the MCDI cell with carbon electrodes at the same Q as the desalinated water is produced in the entire duration of the desalination cycle for NiHCF cell. Furthermore, the water recovery *WR*, defined as the ratio of the volume of desalinated water produced during one cycle and the total volume of water treated in one cycle,[40] was fixed at 50 % for both the systems.

3.2.4 Theory

The theoretical understanding of the desalination performance of porous carbon electrodes in MCDI has been extensively reported in literature.[50,181,227] Recently, the theoretical framework has been extended to intercalation electrodes.[109] This theory is used in the current work to understand the desalination performance of present system. In short, we model the transport of ions in the spacers and the electrodes and the intercalation dynamics in the active particles.

First, the transport of ions in the spacer channel is described by a mass balance including an advective term for the inflow in the y-direction:

$$\varepsilon_s \frac{\partial c}{\partial t} = \frac{\varepsilon_s}{\tau_s} D_i \left\{ \frac{\partial^2 c}{\partial x^2} + z_i \frac{\partial}{\partial x}\left(c_i n \frac{\partial \phi}{\partial x} \right) \right\} - v_y \frac{\partial c}{\partial y}. \tag{3.7}$$

The ion flux in x-direction is described by the Nernst-Planck equation. The transport of ions in the pores of the electrodes is modeled in a similar manner:

$$\varepsilon_e \frac{\partial c}{\partial t} = \frac{\varepsilon_e}{\tau_e} D_\mathrm{i} \left\{ \frac{\partial^2 c}{\partial x^2} + z_i \frac{\partial}{\partial x}\left(c \frac{\partial \phi}{\partial x} \right) \right\} + a J_\mathrm{int}, \tag{3.8}$$

where aJ_int is the intercalation flux from the pores into the active particles normalized by the surface area of the active particles per unit volume of the electrode, a. Then the intercalation degree, ϑ, is governed by

$$c_\mathrm{max} \varepsilon_v \frac{\partial \vartheta}{\partial t} = a J_\mathrm{int}, \tag{3.9}$$

where c_max is the maximum theoretical concentration of the cations in the active particles. Finally, we assume an equilibrium between the cations in the active particle and the electrolyte where the potential difference is given by the Frumkin isotherm

$$\phi_\mathrm{ec} - \phi = \mu_c^\dagger - \ln \frac{\vartheta}{1-\vartheta} + \ln \frac{c^+}{c_\mathrm{ref}} - g(\vartheta - 0.5), \tag{3.10}$$

where ϕ_ec is the dimensionless potential in the conductive carbon in the electrode and g is a cation-dependent constant, signifying the inter-cation repulsion in the active particles. The model predicts the effluent concentration from both spacer channels and the evolution of the cell voltage, V, in time. The cell voltage is calculated as the difference between the ϕ_ec at the anode and the cathode of the desalination cell. The parameters used in the model are given in **Table 3.2.**

Table 3.2: Input values for the parameters in the model used to predict the desalination behaviour of a symmetric cell with NiHCF electrodes, adopted from. [109]

Parameter	Value
Electrode thickness, (μm)	200
Electrode porosity, ε_e	500
Spacer thickness, (μm)	0.5
Spacer porosity, ε_s	0.7
Maximum cation concentration, c_max (M)	4.4
NiHCF volume fraction in electrode, ε_v	0.55

Interfacial area, A (cm^2)	20
Inter-ionic repulsion factor, g	4
Initial intercalation degree, $\vartheta_{initial}$	0.5
Diffusion coefficient in membrane, D_m (m/s)	5.5×10^{-9}
Flowrate, Q (mL/min)	6.4 – 11.8

3.3 Results and discussion

3.3.1 Characterization of NiHCF powder and electrodes

The surface morphology of the NiHCF active particles after milling, observed under SEM, revealed a grainy structure of the active particles, as shown in **Figure S 3.1a** in the supporting information at the end of the chapter, that may have been formed due to inter-particle agglomeration. Imaging at different magnifications revealed particle sizes in the range of 0.5 to 5 µm. The porosity of these agglomerates affects the kinetics of ion transfer from the bulk to the active particles.[109] The SEM images revealed a combination of smooth and rough surfaces with micron-sized cracks. No evidence of active particle agglomeration and formation of island-like structures was observed.

An elemental analysis of the NiHCF active particles with ICP revealed the presence of Ni, Fe, and Na in the ratio of 1.9 : 1.2 : 1. A deficiency in the amount of Na per formula unit, in comparison to the theoretical value can be attributed to the fast precipitation of NiHCF during synthesis.[104] This results in the formation of defective lattices with inclusion of water in them which can compete with sodium for insertion, as reported before.[54,86] The crystalline nature of the particles was confirmed by their X-ray diffractogram, which is comprised of sharp peaks at positions consistent with those of materials in the Fm3m space groups, as shown in **Figure S 3.1b**. In addition, the spectrum obtained was consistent with literature.[152] Finally, a N_2 adsorption analysis performed on the NiHCF powder revealed a BET surface area of ≈ 14 m^2/g, which is two orders of magnitude lower than the surface area of ≈ 2300 m^2/g, measured for the YP 80F carbon used in this study, which is also comparable to values reported in literature.[226] This shows that the mechanism of ion storage in the electrodes used is intercalation into the interstitial lattice sites of NiHCF electrodes.

3.3.2 Electrochemical characterization

The GIT technique, described in **Section 3.2.2**, was utilized to determine the total charge storage capacity of the NiHCF electrodes. The results of the electrochemical characterization of the NiHCF electrodes are presented in Figure **S 3.2**. A negative current applied across the

electrodes drives the Na^+ from the feed channel, through the macropores in the WE and into the interstitial sites of the NiHCF particles. Simultaneously, a Fe^{3+} in the lattice reduces to Fe^{2+} by transfer of an e^- from the current collector to the site of active particle *via* the conductive carbon. Such redox reactions accompanying ion intercalation are commonly observed for PBAs.[84–86] The equilibrium voltage (open circuit voltage, OCV) of the NiHCF electrode (WE) relative to a Ag^+/AgCl electrode decreases as intercalation proceeds in time, making the electrode less favorable to the incoming Na ions. A reversal in the direction of the I results in the deintercalation of the adsorbed Na^+ and an increase in the OCV. During (de)intercalation, the NiHCF electrode acts as an anode/cathode, which makes it prone to pH-dependent faradaic reactions. These reactions degrade the electrode during deintercalation by oxidizing the nickel in the NiHCF into one of its oxides.[108] The pH of the electrolyte was kept around 3 to inhibit parasitic faradaic reactions. On average, a charge storage capacity of ≈ 55 mAh/g was recorded for the NiHCF electrode in this work, which is close to values reported in literature.[54,56,152] A lack of sodium in the synthesized PBA lattice, described in **Section 3.2.1** is reflected in the capacity of the electrode obtained from the GITT, as it is lower than the theoretical charge storage capacity of ≈ 80 mAh/g, calculated for single cation intercalation per unit cell.

3.3.3 Desalination results

The first set of desalination tests, as mentioned in Section 3.2.3, were performed at three different c_{in} values: 20 mM (defined as the optimum CDI concentration[40]), 5 mM, and 50 mM for four I values: 2.5, 5, 10, and 15 A/m². The I changes direction when the cell voltage reaches a cutoff value of either −1 or 1 V. A sample data set, showing the concentration of the diluate, is given in **Figure 3.2a** & **b** for a feed of 20 mM treated in constant current mode at I = 10 A/m².

The salt concentration at the outlet from the cell changes in response to the I. This is confirmed in **Figure 3.2a** which gives Δc at the outlet for the diluate. At this I and Q, the ⟨Δc⟩ obtained was 2 mM, which increased and decreased with the I. Such dependence of Δc on I has been shown before for carbon electrodes in MCDI.[228] The Δc predictions from the ion transport model, with the parameter values mentioned in **Table 3.2**, are plotted as continuous red line. Clearly, these predictions agreed with the values obtained experimentally.

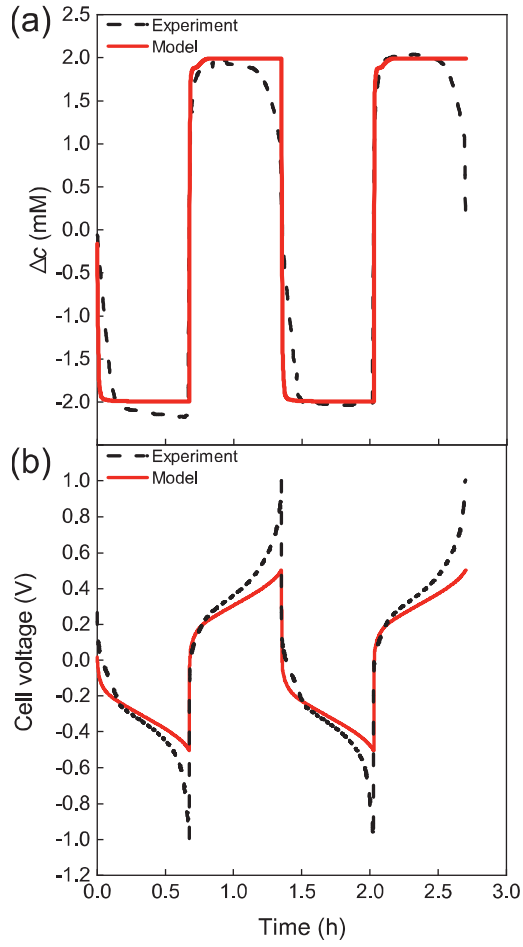

Figure 3.2: Results of the desalination experiments (black dots) with superimposed model predictions (solid red line). The experimental data was obtained at the following conditions: c_{in} = 20 mM, I = 10 A/m² **(a)** Change in effluent concentration from one channel (Δc) with time for two desalination cycles **(b)** The cell voltage response between −1 and 1 V for two desalination cycles.

Figure 3.2b gives the corresponding change in the cell voltage during the constant current desalination at 10 A/m². The model prediction for the cell voltage is shown as a continuous red line. The voltage response of the cell was predicted in the model by an ion adsorption isotherm for monovalent ions given in **Equation (3.10)**. The trend in the cell voltage was qualitatively predicted and only lacked agreement with the experimental data at voltages approaching 1 and −1 V.

Figure 3.3a & **b** provide the SAC and the energy consumption data obtained for four different current densities: 2.5, 5, 10, and 15 A/m² at three different feed water concentrations: 5, 20, and 50 mM at a constant flowrate of 6.4 mL/min.

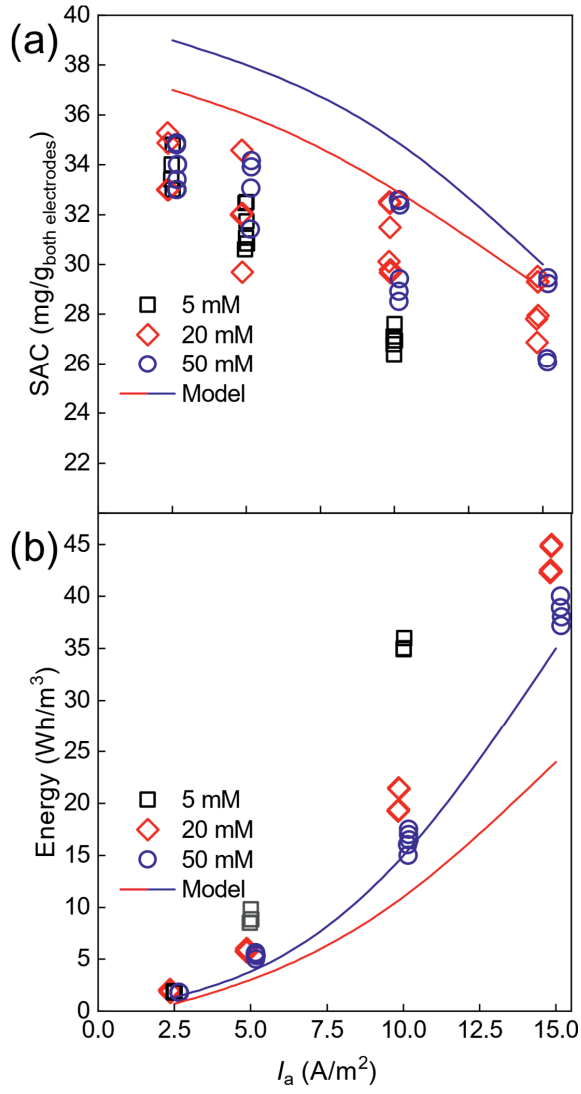

Figure 3.3: Desalination results for symmetrical CDI cell with identical NiHCF electrodes. The experimental data is given for c_{in} = 5 (black squares), 20 (red diamonds), and 50 mM (blue circles). The corresponding model predictions for c_{in} = 20 and 50 mM are shown by solid red and blue lines **(a)** Single-channel SAC for different c_{in} as a function of I **(b)** Energy consumed in Wh/m³ during (de)intercalation half cycles for different c_{in} as a function of I.

The maximum SAC in one half cycle was measured at ≈ 35 mg/$g_{both\text{-}electrodes}$. for the cell at the lowest I of 2.5 A/m^2. This corresponds to a single electrode charge storage capacity of 40 mAh/g-NiHCF which is ≈ 72 % of the 55 mAh/g equilibrium charge storage capacity measured per electrode. In one full desalination cycle, the total salt removed from the feed water was ≈ 70 mg/$g_{both\text{-}electrodes}$. This highlights the advantage of a symmetric cell with two identical NiHCF electrodes that can continuously desalinate water without interrupting the process for regeneration. The SAC value for the intercalation half cycle decreased to 27 mg/$g_{both\text{-}electrodes}$ when the I was increased to 15 A/m^2, as shown in **Figure 3.3a**. At the same time, the ⟨Δc⟩ increased, as is shown in Figure **S 3.3b**. The decrease in SAC has also been observed for other intercalation materials during desalination,[129] as the cut-off voltage is reached faster at higher I, resulting in a reduced half cycle time, as shown in **Figure S 3.3a**. During desalination, the concentration in the electrolyte-filled pores in the electrode may drop very low (< 1 mM) in the intercalation compartment.[109] So, at c_{in} = 5 mM, the highest I of 15 A/m^2 generates a high voltage drop in the cell, resulting in insignificant salt removal. Therefore, the salt removal for this condition was not included in **Figure 3.3**. The model predictions, superimposed on the experimental data in **Figure 3.3**, provide a qualitative estimate of the SAC obtained from the experiments. The overestimation in values can be attributed to the imperfect concentration prediction, as illustrated in **Figure 3.2b**. The model estimates identical SAC values for I of 2.5 and 5 A/m^2. The SAC reduces at higher I, as obtained in the experiments as well. The theoretical results were omitted for the case of c_{in} = 5 mM and I = 15 A/m^2, as the model predicted a very high voltage drop over the cell and as a result, a low Δt_{HCT} and SAC.

Figure 3.3b represents the energy consumption for the desalination tests presented in **Figure 3.3a**. The concentration increase reduces the ionic resistance in the cell and as a result, the energy consumption. In addition, a decrease in the half cycle times, Δt_{HCT}, with increasing I reduces the amount of treated water in one half cycle, increasing the volumetric energy consumption. The model predictions come close to the experimentally measured energy values for low I values, but lack a complete agreement at higher I. Therefore, a better understanding of an increase in the resistance of the system at high I and low c_{in} will be necessary in the future to accurately predict the energy consumption. The results from the second set of experiments with symmetric NiHCF cell, for fixed Δt_{HCT}, are given in **Figure 3.4a & b**. The dependence of the volumetric energy consumption on P is shown in panel **(a)** for two ⟨Δc⟩ values. The trend for each ⟨Δc⟩ shows an increase in the energy consumption with increasing P. Such dependence has also been reported before for carbon electrodes as well.[40] When the ⟨Δc⟩ was doubled from ≈ 1 to 2 mM, the energy consumption also doubled in the range of $50 \leq P \leq 125$. To maintain a ⟨Δc⟩, I also increases with increasing P. The dependence of the energy consumption on I is plotted in **Figure S 3.4**. The predicted energy consumption by the model, given as a solid red line in **Figure 3.4a**, matches with those obtained from the experiments. This follows from the agreement between the voltage curves obtained from the model and experiments, shown in **Figure 3.4b**. Since the fixed Δt_{HCT} for the second set of experiments was only a fraction of the time it usually takes to saturate or empty the NiHCF

electrodes, the model predictions closely match the energy values. This remains the case for all P at which the cell delivers ⍰Δc⟩ of ≈ 1 mM, and for a majority of P for ⍰Δc⟩ of ≈ 2 mM.

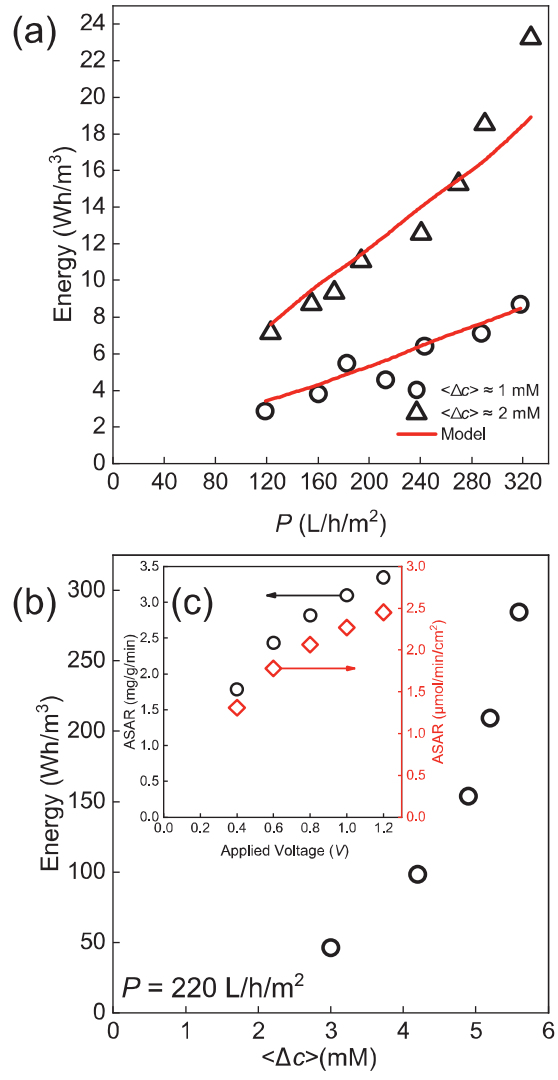

Figure 3.4: Performance of the symmetric CDI cell with NiHCF electrodes during fixed Δt_{HCT} desalination tests in constant current and constant voltage modes **(a)** Variation of energy consumption of the cell under **constant current operation** as a function of P for ⍰Δc⟩ of ≈ 1 and 2 mM. The solid red line represents the predictions from the model for the identical operation conditions. **(b)** Energy consumption of the symmetric cell under **constant voltage operation** as a function of ⍰Δc⟩ at a fixed P of 220 L/h/m². The inset **(c)** gives the ASAR as a function of applied cell voltage in mg/g/min (left y-axis in black) and μmol/cm²/min (right y-axis in red).

The performance of the CDI cell under constant voltage operation for a fixed Δt_{HCT} and P is given in **Figure 3.4b**. The Q for these experiments was kept constant at 7.8 mL/min. The ⟨Δc⟩ increased with an increase in the applied voltage from 0.4 to 1.2 V. The maximum Δc, *i.e.*, the difference between the lowest concentration recorded during adsorption and c_{in}, was ≈ 6 mM for the applied cell voltage of 1.2 V. This corresponds to a ⟨Δc⟩ of ≈ 5.5 mM for a fixed Δt_{HCT} of 3 mins. The energy consumption increased with the applied voltage in a similar manner as shown in **Figure 3.4b**. Since the energy was normalized by the Δt_{HCT}, the actual duration of the half cycle had no influence on the energy consumption calculations. For the ⟨Δc⟩ of 5 mM, the NiHCF cell consumed ≈ 170 Wh/m^3 of energy at a P of 220 L/h/m^2. For comparison, data given in Figure 5 of [40] shows that an MCDI cell with carbon electrodes consumes ≈ 140 Wh/m^3 (without recovery), and ≈ 60 Wh/m^3 (with recovery), to achieve a ⟨Δc⟩ of 5 mM at a P of 70 L/h/m^2, for a system with c_{in} = 20 mM and WR of 50 %. Such comparisons are crucial to compare the performance of symmetric NiHCF cell with the data reported in CDI literature. In addition to the energy consumption, the rate of salt adsorption, ASAR, is also provided in **Figure 3.4**. The rate doubles from 1.6 mg/g/min, obtained at 0.4 V, to 3.2 mg/g/min, obtained at 1.2 V. The values of ASAR obtained here for the NiHCF cell are higher than the maximum ASAR of ≈ 1.8 and 2.5 mg/g/min, reported in literature for MCDI with carbon electrodes.[119,229]

Finally, the results from the experiments performed to directly quantify the differences between NiHCF and carbon-based symmetric and MCDI cells is given in **Figure 3.5a** & **b**. It must be pointed out that the Q was the same for the NiHCF and carbon cells. A sample data set containing the concentration and IV profiles from the NiHCF and carbon electrode cells, obtained during the fixed Δt_{HCT} comparison experiments, is given in **Figure S 3.5**. The desalination performance was evaluated based on the volumetric energy consumption as a function of ⟨Δc⟩, given in **Figure 3.5a**, and the ASAR as a function of I, given in **Figure 3.5b**. From panel **(a)**, it can be concluded that for ⟨Δc⟩ ≤ 2.5 mM and the same electrode weight, spacer thickness, and Δt_{HCT}, the MCDI cell with carbon electrodes consumed, on average, 3 times more energy than symmetric cell with NiHCF electrodes. As a specific example, the NiHCF cell consumes ≈ 22 Wh/m^3 at a P of 220 L/h/m^2 to deliver a ⟨Δc⟩ of 2.5 mM. The MCDI cell with carbon electrodes on the other hand consumes ≈ 65 Wh/m^3 to deliver the same ⟨Δc⟩ at a reduced P of 110 L/h/m^2. It must be pointed out that the symmetric NiHCF cell delivered twice as high P as the carbon-based MCDI cell at the same Q. For ⟨Δc ⟩ > 2.5 mM, the MCDI cell still consumed more than 2 times the energy consumed by the NiHCF cell. The relative increase in the energy consumption of the NiHCF cell, in comparison to the carbon-based MCDI cell, can be attributed to the transport limitations at higher adsorption or discharging rates, as has been reported before for other intercalation materials.[129] However, even at the highest I and ⟨Δc⟩ tested and achieved here, respectively, the MCDI cell with carbon electrodes consumed twice as much energy as the symmetric cell with NiHCF electrodes. The conclusion remains the same when the energy consumption is calculated in Wh/mol-NaCl, as shown in **Figure S 3.6**. This finding is in line with the conclusion of a thermodynamic comparison of

energy consumption between intercalation and carbon electrodes, recently performed in reference.[223]

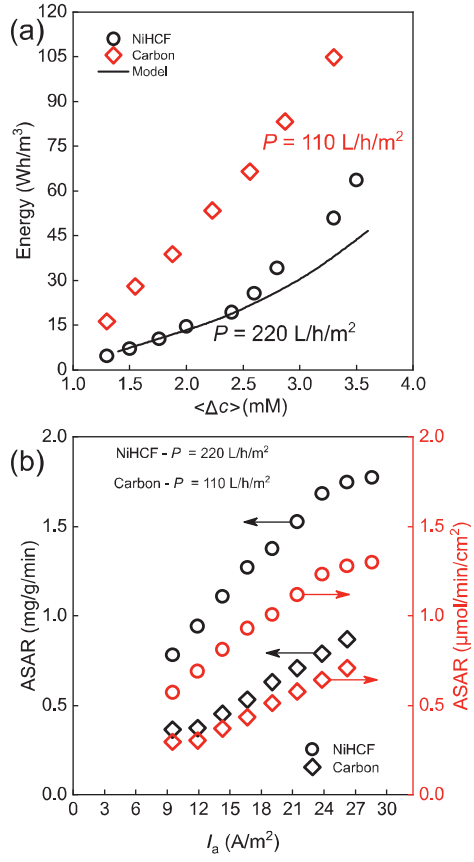

Figure 3.5: Comparison of the symmetric CDI cell with NiHCF electrodes (circles) and MCDI cell with carbon electrode (diamonds) during fixed Δt_{HCT} desalination tests **(a)** Variation of energy consumption of the symmetric and MCDI cell under constant current operation with ⟨Δ*c*⟩ for the same *Q*. The solid black line represents the predictions from the model for the symmetrical CDI cell with NiHCF electrodes **(b)** Variation of ASAR values in mg/g/min and μmol/min/cm² with the *I* for the symmetric and MCDI cell, obtained at the same *Q*.

Furthermore, this finding also serves as an experimental proof for claims made in [230] about intercalation-based CDI cell being more energy efficient than a carbon based MCDI cell. Charge efficiency, Λ, another important parameter defined as the ratio of charge adsorbed by the electrode to the external charge input to the electrode, provides an interesting insight in this comparison. For low *I*, therefore low Δc, the symmetric NiHCF cell exhibited a high Λ of 96 %. However, with increasing *I*, the Λ reduced and settled at ≈ 75 %. This was observed for the highest *I* of 30 A/m². An increased resistance in the cell at high *I* may be behind the drop in Λ. This explains the relative increase in the energy consumption of the symmetric NiHCF cell at high Δc over the MCDI cell, which exhibited a Λ of 92 % at the lowest *I* and settled at a

Λ of 86 % for the highest I of 27.5 A/m^2. The Λ values of both the systems, for all I, is provided in **Table S 3.1**. Furthermore, the model predictions for the NiHCF cell, given by solid black line in **Figure 3.5b** match with the values obtained from experiments, especially for the ⟨Δc⟩ ≤ 2.5 mM. At higher ⟨Δc⟩ values, the model underestimates the energy consumption, as has been observed earlier from the data in **Figure 3.3** and **Figure 3.4**.

In addition to energy consumption, the ASAR values obtained with the NiHCF and carbon MCDI cells as a function of I are presented in **Figure 3.5b**. The ASAR values, calculated for one full cycle of desalination for both cells, show that the NiHCF cell removed ions at a rate twice as high as that obtained for MCDI cell with carbon electrode. This further highlights the advantage of a two-chamber symmetric cell over a single-chamber MCDI cell: the NiHCF cell desalinated water in the entire cycle and delivered higher ASAR and P at the same Q. Comparison of ASAR values obtained during the constant current and constant voltage operation of the NiHCF cell shows that higher ASAR was achieved in the constant voltage mode in comparison to the constant current mode. This can be seen from **Figure 3.4b** and **Figure 3.5b**. However, the energy consumption of the cell, plotted as a function of ASAR for constant current and voltage mode of operation in **Figure 3.4c**, was also found to be higher during the constant voltage operation. It is clear from the data in the figure that the constant voltage mode of operation renders higher rates of adsorption at the expense of the energy consumption.

3.4 Conclusion

In this study we demonstrated the intrinsically high energy efficiency of symmetric CDI cells with nickel hexacyanoferrate (NiHCF) electrodes compared to carbon-based MCDI cells by typically obtaining a 2.5-fold reduced energy consumption. In addition, the average salt adsorption rate (ASAR) of the NiHCF cell was typically 2-fold higher than that of a carbon-based MCDI cell for identical separation conditions. The set-up contained identical NiHCF electrodes which reversibly intercalate Na ions. This allowed for continuous desalination, and a removal of 70 mg NaCl/$g_{\text{both-electrodes}}$ in one full cycle at an applied current of 2.5 A/m^2. An even higher ASAR was obtained in constant voltage mode in comparison to constant current mode, but at the expense of a higher energy consumption. A Nernst-Planck transport model, with Frumkin adsorption isotherm, was successfully used to accurately predict the SAC, via the effluent concentration. In addition, it provides a qualitative description of the energy input, via the cell voltage prediction, especially for the lower current densities tested here. A better theoretical understanding of the resistance in the NiHCF cell will be required to improve the energy input predictions also at higher current densities.

Supporting information

3 S.1 Calculation of salt adsorption capacity and charge efficiency of a **symmetric** desalination cell containing two identical PBA electrodes

The analysis of the concentration and current *vs.* time data gives the salt adsorption capacity (SAC) and the energy efficiency (Λ) associated with a desalination process. While the current vs time data is usually obtained from software that also provide the charge input per cycle (calculated as the area under the current – time curve), calculation of SAC from the concentration *vs.* time data requires further processing. A MATLAB code appended below was used in this work to calculate the SAC and Λ values associated with the desalination experiments. The executable code is in black and the accompanying comments, explaining the code is in green.

```
clear all
close all
%Define flowrate – Q (mL/min)
%Define the total weight of both electrodes – m (g)
%Define the total cycle time – t_cycle (s)
%Define the molecular weight, M (mg/mol), of the salt being adsorbed e.g. M = 58.5 fot NaCl
%Calculate the charge input per cycle (C_input) via the external circuit from the area under
the current – time curve
%Faraday constant F – 96487 C/mol
%Valence of an ion – z – e.g. 1 for Na and 2 for Ca
```

```
concentration_time_data_sheet; %Calling data file containing concentration data points
collected as a function of time. The array containing these points is named conc_data with
units of mM. The data file should be in the same folder as the code file.
time =1:length(conc_data); %creates an array for operation time
figure(1)
plot(time_time, conc_data,'b') %Plots the concentration vs time data
```

```
%Calculation of Δc – the reduction in concentration – variable name – delta_conc
 %Baseline = concentration of the feed solution = c_inlet
for i=1:length(conc_data)
  delta_conc(i)=sqrt((c_inlet – conc_data(i))^2); %Calculation of Δc
end
delta_time =1:length(delta_conc); %Array for the

%Figure presenting Δc of the desalination process
```

```
figure(2)
plot(time_conc_salt_bare,delta_conc_bare,'r')
```

```
%SAC and Λ calculation
disp ("Area  under the curve of one full adsorption cycle")
t_start = t_s; %The time at which the cycle started,
t_finish = t_s + t_cycle;
area=trapz(delta_time (t_start:t_finish),delta_conc (t_start:t_finish)); %Area under the curve for one complete cycle
SAC= (M/m)*((area)*(Q/60000))/2; %Gives the SAC of the cycle analysed in mg/g both-electrodes
charge_adsorbed = SAC*(m/M)*F*z/1000; %Gives the amount of charge actually adsorbed by the electrodes.
charge_efficiency= charge_adsorbed_bare/C_input%Gives the Λ for the cycle being analysed
disp (“The SAC of the cell in the analysed cycle is :” ) SAC
disp(“The energy efficieny of the cell in the analysed cycle is :”) energy_efficiency
%End of code
```

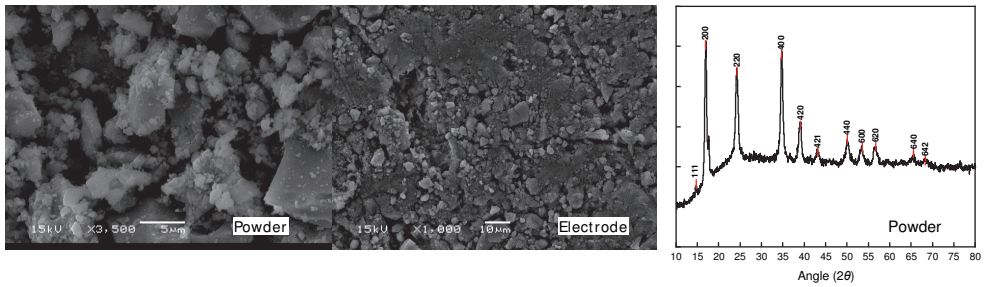

Figure S 3.1: (a) SEM images of powdered NiHCF particles (left) and an NiHCF electrode (right); **(b)** XRD spectrum of powdered NiHCF particles.

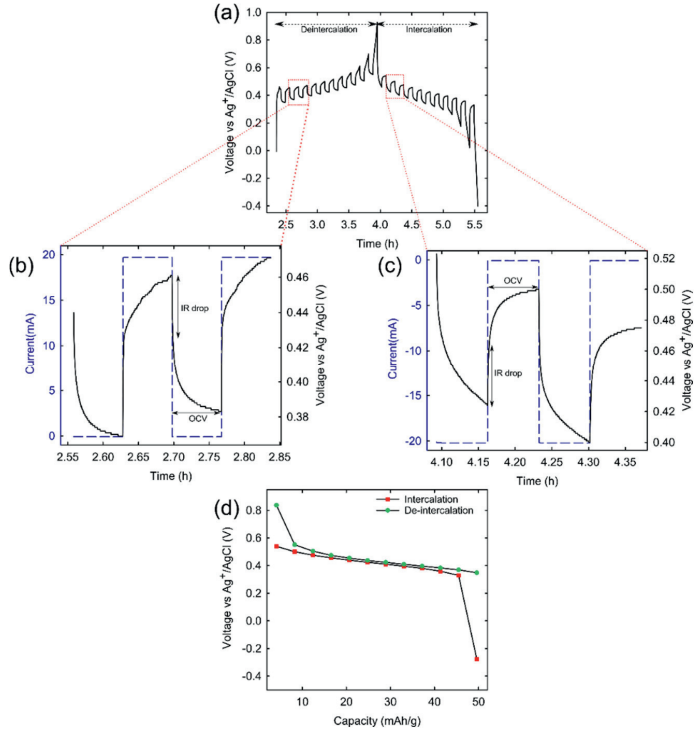

Figure S 3.2: Galvanostatic intermittent titration (GIT) data of NiHCF electrodes in a three-electrode cell configuration for a 1 M Na_2SO_4 electrolyte. **(a)** The voltage response for an intercalation cycle of the WE (NiHCF) **(b,c)** Two intercalation steps with a negative and positive applied current (blue) and the corresponding voltage response (black), interrupted by the open circuit equilibration step. The voltage drop during the open circuit is divided into the IR drop and the steady-state voltage change. **(d)** The open circuit voltage (OCV) plotted against the amount of charge (in mAh/g-NiHCF) (de)-intercalated during the repeated titration.

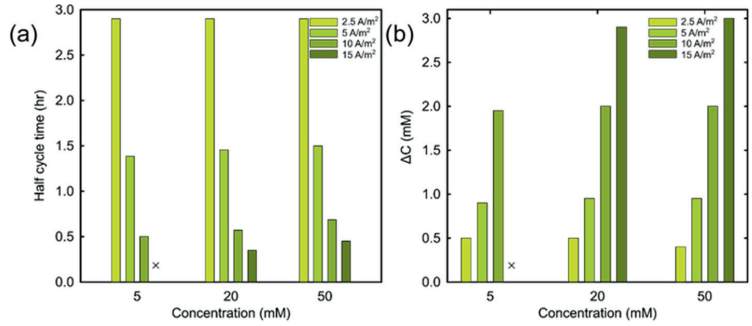

Figure S 3.3: Desalination performance results for the cell with symmetric NiHCF electrodes. The experimental data is given in gradients of solid green bars. **(a)** The Δt_{HCT} for the desalination half cycles for different c_{in} as a function of I. **(b)** The corresponding ⟨Δc⟩ (de)intercalation half cycles for different c_{in} as a function of the I. The symbol × indicates a failure in operating the system for that set of operational parameters.

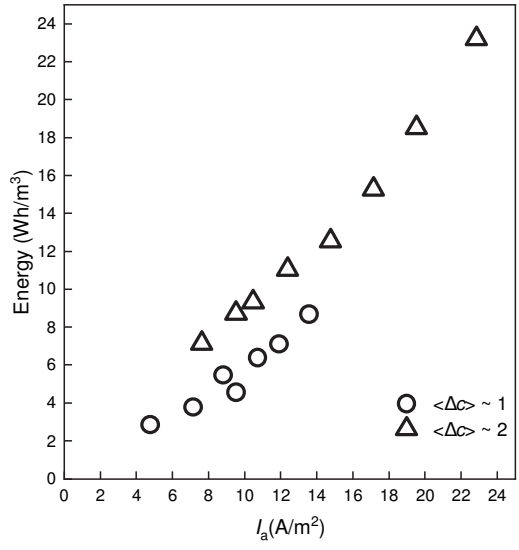

Figure S 3.4: Energy consumption of the symmetric CDI cell with NiHCF electrodes as a function of I for two ⟨Δc⟩ values.

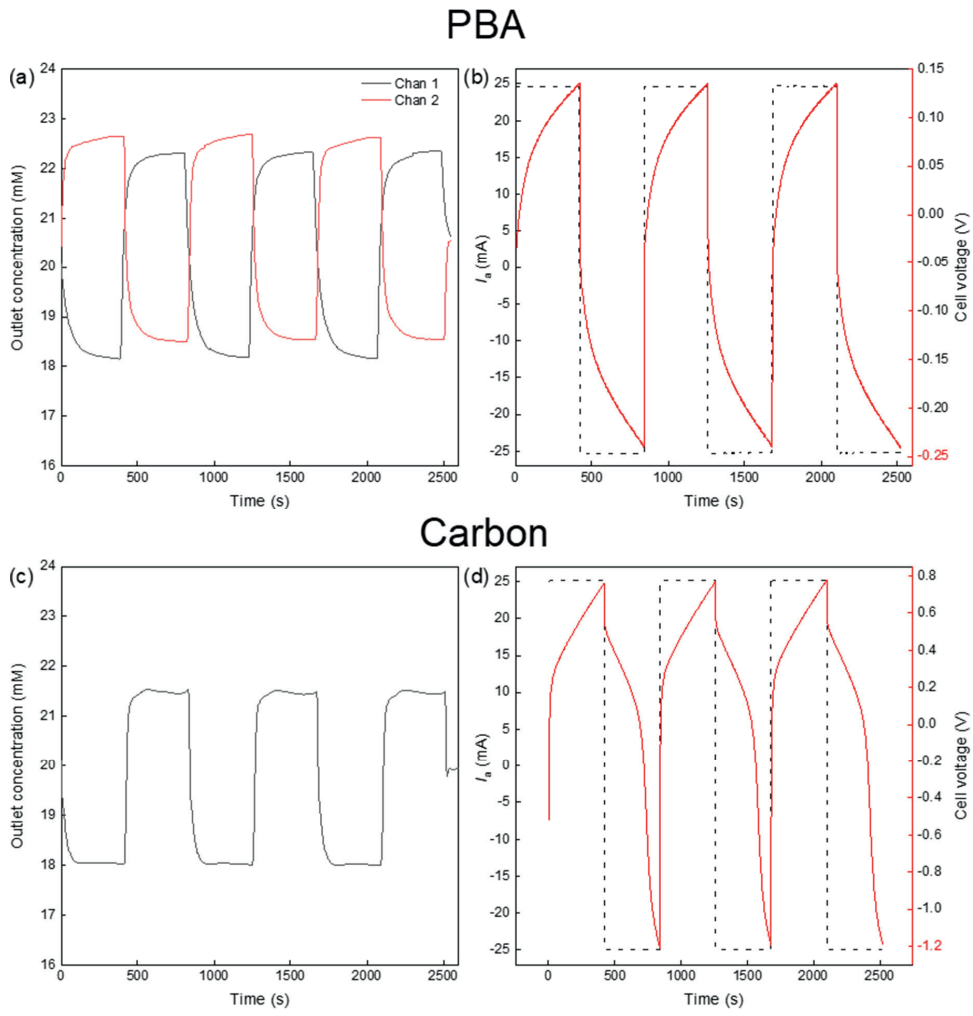

Figure S 3.5: Sample dataset obtained for comparison experiments between carbon and intercalation electrodes with equivalent operation parameters **(a)** Outlet concentration as a function of time for both channels in the NiHCF intercalation electrode cell **(b)** Constant *I* (black dash line) of 25 mA (12.5 A/m^2) and the cell voltage response (solid red line) for desalination of a 20 mM feed solution with NiHCF intercalation electrodes in a symmetric cell configuration **(c)** Outlet concentration as a function of time for the MCDI cell with carbon electrodes **(d)** Constant *I* (black dash line) of 25 mA (12.5 A/ m^2) and the cell voltage response (solid red line) for desalination of a 20 mM feed solution with carbon electrodes in an MCDI cell configuration.

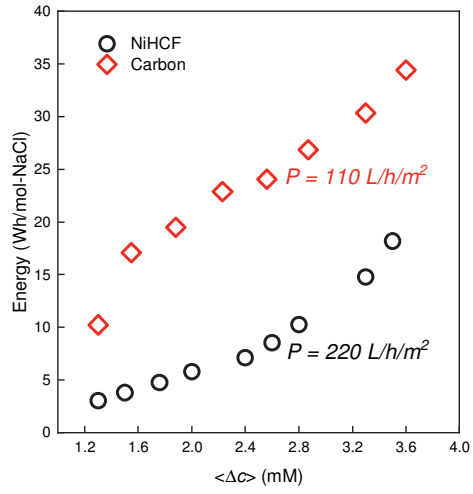

Figure S 3.6: Variation of energy consumption of the symmetric NiHCF cell and the MCDI cell, under constant current operation, with ⟨Δc⟩ for the same *Q*.

Table S 3.1: Charge efficiency, Λ, obtained during fixed half cycle experiments, performed with the symmetric NiHCF cell and the carbon based MCDI cell

NiHCF cell	
I (A/m²)	Λ (%)
10	96
12.5	93
15	92
17.5	91
20	87
22.5	87
25	85
27.5	80
30	75

MCDI cell	
I (A/m²)	Λ (%)
10	93
12.5	82
15	83
17.5	83
20	86
22.5	86
25	86
27.5	86
30	--

4 Nickel Hexacyanoferrate Electrodes for High Mono/Divalent Ion-Selectivity in Capacitive Deionization

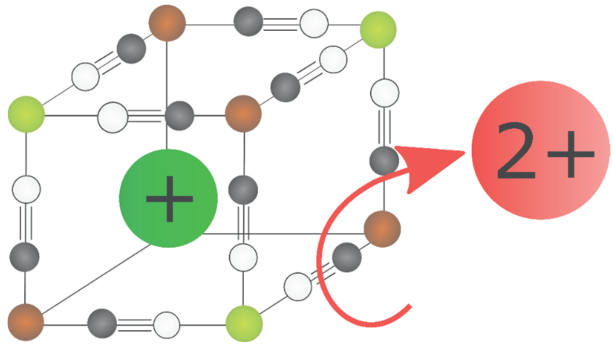

This chapter has been published as:

Singh, K., Qian, Z., Biesheuvel, P. M., Zuilhof, H., Porada, S., & de Smet, L. C. P. M. (**2020**). Nickel hexacyanoferrate electrodes for high mono/divalent ion-selectivity in capacitive deionization. *Desalination*, *481*, 114346.

Abstract

Selective ion removal has been a point of focus in capacitive deionization because of its industrial applications such as water purification, water softening, heavy metal separation and resource recovery. Conventionally, carbon is used as electrode material for selectivity. However, recent developments focus on intercalation materials such as Prussian Blue Analogues, due to their size-based preference towards cations. Selectivity of nickel hexacyanoferrate electrodes from a mixture of Na^+, Mg^{2+}, and Ca^{2+} ions was studied in this work. Here, a CDI cell with two identical NiHCF electrodes was operated in two desalination modes: (a) cyclic, in which ions are removed from and released into the same water reservoir and thus, the ion concentration remains the same after one cycle, and (b) continuous, in which ions are removed from one water reservoir and released back in a different reservoir. An average separation factor of ≈ 15 and 25, reflecting the selectivity of the electrodes, was obtained for Na^+ over Ca^{2+} and Mg^{2+} from an equimolar solution of Na^+, Ca^{2+} and Mg^{2+} in both, cyclic and continuous desalination. It was concluded that NiHCF, used in a symmetric CDI cell, is a promising material for highly selective removal of Na+ from a multivalent ion mixture.

4.1 Introduction

Capacitive Deionization (CDI) is an electrochemical technique in which polarized electrodes remove ions from water.[20,41] Conventionally, these electrodes are fabricated out of porous carbon[18,51,125,188,231] with ions stored in micropores with sizes just above and below 1 nm. Recently, research into intercalation materials for aqueous ion energy storage[79,92,105] has led to their application in CDI.[56,97,101,153,175] The ion storage in these materials proceeds via intercalation of ions into the interstitial lattice sites or in between the layers of the host electrode material. In some intercalation materials, such as Prussian Blue Analogues (PBAs),[54,104,166] the ion insertion is accompanied by the electrochemical reduction of a redox-active element in the lattice. These intercalation materials retain the attributes of porous carbon-based electrodes, such as a non-toxic nature, easy preparation, and fast charge transfer kinetics,[104] while improving upon the charge adsorption capacity[83] and eliminating co-ion expulsion from the electrode.[18] The use of PBAs in CDI is of interest because of their open framework structure, customizable chemical composition, and size-based selectivity towards cations.[82] Selective removal of ions using CDI has already been explored with carbon electrodes.[73,232–234] Only recently, it has been studied with electrodes based on intercalation materials as well.[106,165,235] However, much of this focus has been on the separation between cations with the same valence, and very few studies are available on the selective removal of a cation from a mixture of ions with different valency. This contrasts with the research focus towards carbon electrodes, where selective removal of ions from a mixture has been extensively studied.[10,47,236,237] This work aims at filling this gap in literature.

The electrodes used for selective ion-removal here contain nickel hexacyanoferrate (NiHCF) particles as the active material. It is a PBA that has been successfully used for desalination[54,56] and was found to a have size-based preference for cations in CDI[54] and other electro-chemical techniques.[135,146,148] In more detail, the trends observed for alkali metal ions suggest that the affinity of NiHCF particles towards ions decreases with an increase in their hydrated size in aqueous electrolytes. Studies[135,146,147] have shown that in a mixture of alkali metal ions, PB and its analogues demonstrate the strongest affinity towards Cs^+, and the affinity reduces for the alkali metals above Cs^+ in the group.

In this study, we demonstrate the performance of electrodes fabricated using NiHCF in CDI experiments to selectively remove monovalent (Na^+) over divalent (Ca^{2+}, Mg^{2+}) ions. The preferential removal of Na^+ from a mixture of Na^+, Ca^{2+}, and Mg^{2+} is crucial to maintain the quality of irrigation water as an increase in its Na^+ can result in adverse effects on the physical properties of soil[238] and plant growth.[239,240] This was achieved with a symmetric two-compartment CDI cell,[142] constructed with two NiHCF electrodes of the same mass, and identical physical, chemical and electrochemical composition. These electrodes were separated by an anion-exchange membrane inside the cell. The use of identical electrode materials avoids

the need for an anode with an equivalent charge storage capacity and allows for an uninterrupted selective ion removal in the adsorption and regeneration steps by reversing the electrode polarities. Part of the potential of the presented electrochemical setup lies in the cheap, non-toxic, and facile fabrication of ion-selective NiHCF particles, and subsequently, of the electrodes, and in their easy application in a symmetric, two-compartment deionization cell. Figure 1a illustrates the intercalation compartment of the symmetric desalination cell, illustrated elsewhere[109], during the operation. The other half of the cell undergoes a mirrored deintercalation operation simultaneously, evident from the outlet concentrations measured during the desalination cycles. The inset schematic indicates the size-based exclusion of cations by the NiHCF lattice.

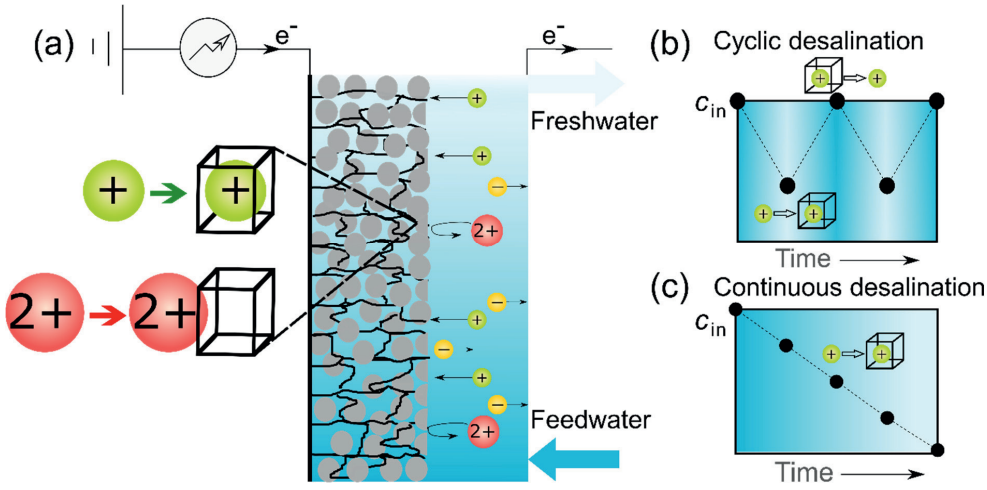

Figure 4.1: Schematic overview of capacitive deionization with NiHCF electrodes in monovalent/divalent ion mixtures with two different operational modes. **(a)** Intercalation compartment from the two-compartment CDI cell[40] assembled with identical, free-standing NiHCF electrodes fed with feed water containing a mixture of Na^+, Ca^{2+}, Mg^{2+}. The redox-active NiHCF particles are present as grey agglomerates and the black lines running around them indicates the carbon black in the electrode. The schematic depicts the selective intercalation of monovalent cations in the cathode. The Cl^- electro-migrates to the deintercalating compartment of the cell. **(b)** Schematic of the change in concentration of one feed reservoir paired with an electrode during the cyclic mode of desalination. The ion concentration decreases during the intercalation half cycle and is restored during the deintercalation half cycle. Therefore, the concentration remains unchanged after one full cycle. **(c)** Schematic presenting the change in concentration of the feed reservoir during the continuous mode of desalination. The ion concentration decreases with every half cycle due to switching of the reservoir along with the electrode polarity. This leads to a permanent pairing of a reservoir with a cathode resulting in a continuous decrease in the concentration of ions.

4.2 Experimental section

4.2.1 NiHCF preparation and characterization

The synthesis of NiHCF active particles was performed by a co-precipitation method.[79,241] Briefly, a 200 mL solution of 24 mM $NiCl_2 \cdot 6H_2O$ (Alfa Aesar) and 12 mM $Na_4[Fe(CN)_6] \cdot 10H_2O$ (Sigma Aldrich) each was drop-wise added to a (1% by volume) 1 M HCl solution. The reaction mixture was stirred at a 600 RPM for ≈ 12 hrs. Addition of HCl during the reaction has been reported to induce higher levels of crystallinity in the cubic lattice NiHCF structure.[16] The precipitate formed was washed three times with water in a vacuum filtration unit and the collected residue was dried overnight in a vacuum oven at 40 °C. The surface morphology of the NiHCF particles was studied using scanning electron microscopy (SEM). An elemental analysis was performed using energy-dispersive X-ray spectroscopy (EDS) to identify the elements in the active particles. The crystallinity of the NiHCF particles was assessed by powder X-ray diffraction (XRD) analysis, performed using a copper source for diffraction angles in the range of $10° < 2\theta < 70°$.

4.2.2 Electrode fabrication

The dried NiHCF powder was milled together with conductive carbon black (Cabot) and mixed with poly-tetrafluoroethylene (PTFE) (Sigma Aldrich) in ethanol as a solvent, in a weight ratio of 8:1:1 and subsequently cold-rolled into highly conductive, free-standing electrodes. The thickness of these electrodes was kept at 200 μm with an area of 20 cm^2. The electrodes were dried in an oven at 55 °C to evaporate any residual solvent left from the cold-rolling procedure. The weight of the electrodes was between 0.42 – 0.45 g.

4.2.3 Electrochemical characterization and desalination

The galvanostatic intermittent titration was performed in a three-electrode cell configuration with NiHCF as the working electrode (WE), a platinum-coated titanium mesh as a counter electrode (CE) and an Ag/AgCl electrode as the reference electrode (RE) mounted close to the WE. The pH of the electrolyte solution (1 M solution of NaCl, $MgCl_2$, and $CaCl_2$) was kept at pH ≈ 3 by adding HCl. The equilibrium voltage was measured by interrupting the charging and discharging steps with an open circuit and measuring the cell voltage. In addition to assessing the capability of electrodes towards intercalation of cations, the three-electrode cell configuration was also utilized to control the charging degree, ϑ, of the electrodes. The assembly was used to set the ϑ values to either 0 or 1 (by setting the WE potential to 1 or 0 V *vs.* Ag/AgCl, respectively).

The dependence of ionic selectivity of the electrodes on the relative concentration of mono- and divalent ions in the feed solution was explored by varying their concentration from equimolar mono- and divalent ions (optimum CDI concentration[40] of 20 mM) to an excess of divalent over monovalent ions (concentration ratio monovalent ions : divalent ions = 1 : 3). These concentrations are given in Table 1. The desalination tests were run for solutions F1 – F6 with a symmetric CDI cell.[54,109] The solutions were fed to the two compartments from two separate 70 mL reservoirs. Before starting the tests, the CDI cell was short-circuited for 1 h to equilibrate the charge concentration in the electrodes with $\vartheta \approx 0$ and 1. As a result, ϑ in both the electrodes becomes ≈ 0.5. This step is necessary to ensure that the electrodes start operation from an identical state of charge, resulting in a symmetric deionization from both electrode compartments. The (de)intercalation steps were performed under constant current, followed by a constant cell voltage applied via a potentiostat (n-stat, IVIUM technologies).

Table 4.1: Composition of the feed F1 – F6 in the two-compartment deionization cell to investigate the dependence of electrode selectivity on the relative concentration of mono- and divalent ions in the electrolyte.

Feed number	Na^+ (mM)	Mg^{2+} (mM)	Ca^{2+} (mM)
F1	20	20	--
F2	20	--	20
F3	10	30	--
F4	10	--	30
F5	20	20	20
F6	40	40	40

The desalination experiments were performed in two operational modes: *cyclic* and *continuous*. In cyclic desalination, the symmetrical cell was fed by two reservoirs containing identical solutions. A constant current of 10 A/m² (30 mA/g-NiHCF in both electrodes) was applied until the cell voltage reached a cut-off of 1.0 V. This was followed by applying a constant voltage of 1.0 V over the cell for 1 h. This concluded the first step. Once the electrodes were saturated, a current of –10 A/m² was applied in the opposite direction until the voltage reached a cut-off of –1 V. Following this, a voltage of –1 V was applied over the cell for 1 h to saturate the electrode. This second step completed one full cycle. One such cycle is given in **Figure S 4.3** of the supporting information, given at the end of this chapter, as a sample data set. The main characteristic of cyclic mode of operation is the periodic switching of electrode polarities only while keeping the feed reservoirs the same. In contrast, the continuous mode of operation allows for the switching of electrode polarities as well as the feed reservoirs. Therefore, after the first step of current and voltage application, the feed reservoirs are manually exchanged between the electrodes by simply changing the pipes connecting the cell compartments to the reservoirs. This manual swapping of reservoirs between the desalination

steps is the defining feature of the continuous desalination. Once the electrodes reached equilibrium, samples were taken from both the reservoirs for ICP analysis. These equilibrium concentrations were used for selectivity calculations.

4.3 Results and Discussion

The surface morphology of the NiHCF particles, observed under SEM (**Figure S 4.1**), shows inter-particle agglomeration, and BET analysis shows a small surface area (≈ 13 m^2/g). While such a small area would be highly detrimental for carbon-based electrodes in CDI, it does not hamper the performance of intercalation-based materials, in view of the different mode of ion storage, *i.e.*, inside the lattice of the intercalation material rather than only near its surface. An elemental analysis of the NiHCF particles with ICP revealed the presence of Ni, Fe and Na in the ratio of 1.9 : 1.2 : 1. A deficiency in the amount of Na per formula unit, in comparison to the theoretical value (1 : 1: 2) can be attributed to the fast precipitation of NiHCF during synthesis.[104]

EDS mapping of powdered PBA revealed the presence of Ni, Fe and Na (in decreasing order) in the crystal lattice which qualitatively supports the results obtained from the elemental analysis. The crystalline nature of the particles and the presence of cubic lattices were confirmed by the X-ray diffraction spectra, which display sharp peaks at positions consistent with those of materials in the *Fm3m* space groups (**Figure S 4.1**), and consistent with literature.[242]

To demonstrate the capability of the electrodes in intercalating mono- and divalent ions, a galvanostatic intermittent titration (GIT)[54,144,241,243] was performed with 1 M solutions of NaCl, $MgCl_2$ and $CaCl_2$ in a three-electrode cell configuration. The equilibrium voltages measured during the open-circuit regime of the titration is plotted against the charge input of the electrode in Figure 2. The results indicate a single-phase (de)intercalation for both monovalent (Na^+) and divalent ion (Mg^{2+}) (data for Ca^{2+} in **Figure S 4.2**) into the NiHCF particles of the electrodes, in line with literature.[152,244] A similar charge intake capacity of ≈ 55 mAh/g was measured for NiHCF electrodes in sodium electrolytes as in magnesium electrolytes, which is close to the reported maximum capacity of ≈ 60 mAh/g.[54,152] This result demonstrates the ability of the NiHCF electrodes to successfully (de)intercalate both mono- as well as divalent ions with similar, reversible capacities. The hysteresis observed in the voltage profiles for the larger Mg^{2+} is attributed to the rate-limiting dehydration step necessary for the intercalation of cations into the NiHCF lattice.[245] It has been reported that a dehydration step is necessary for the insertion of cations into the PB lattice.[80,246,247] Therefore, the larger Mg^{2+} requires more energy for dehydration to intercalate. This barrier to cation insertion into the NiHCF lattice results in the shifting of the intercalation curve to lower values of voltage, as measured in Mg electrolyte.

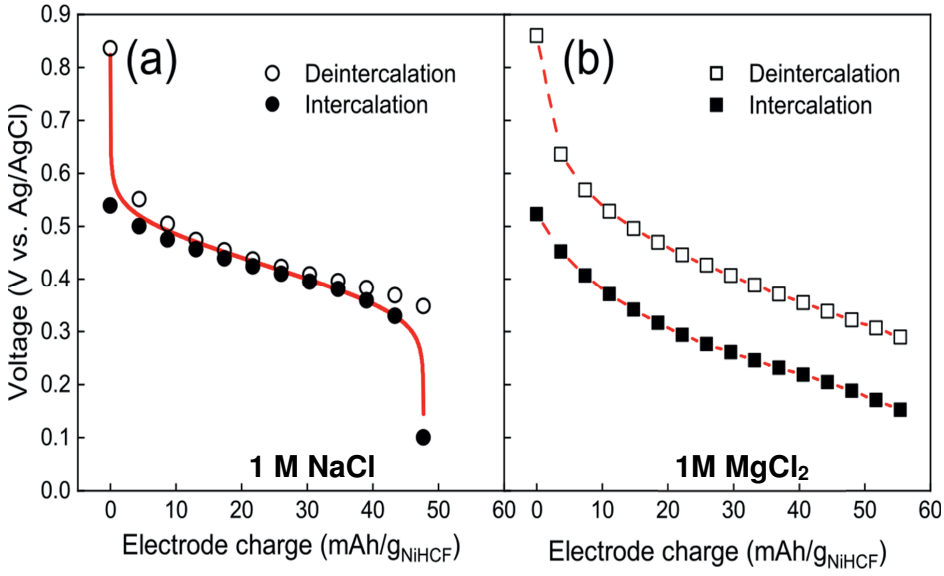

Figure 4.1: Charge intake capacity of NiHCF electrodes, measured by GIT, for **(a)** 1 M NaCl, **(b)** $MgCl_2$ solution in a three-electrode cell with platinum coated titanium electrode as counter and a Ag/AgCl electrode as reference. Solid line in (a) represents the Frumkin adsorption isotherm fitted to the GIT data for monovalent Na^+ cation. Dashed line in (b) serves as a guide

The electrode potentials measured during the GIT experiments in NaCl were correlated with the charge content of the electrode ϑ, a dimensionless number which ranges from 0 to 1 with 0 referring to the minimum cation content in the electrode (charged) and 1 referring to the maximum cation content in the electrode (discharged). The correlation follows from the Frumkin isotherm for monovalent cations[109]

$$E = E_{\text{ref}} - \frac{RT}{F}\left[\ln\frac{\vartheta}{1-\vartheta} - \ln\frac{c_+}{c_{\text{ref}}}\right] - g(\vartheta - 1/2), \tag{4.1}$$

where the values of parameters E_{ref} (reference potential dependent upon the intercalating ion and its interaction with the lattice of intercalating material) and g (which is positive here and accounts for the inter-ionic repulsion in the intercalation particle) were 425 and + 90 mV respectively, to get the best fit for both (de)intercalation voltage curves for NaCl, in line with previous reports.[54] The Frumkin adsorption isotherm however does not provide a similar insight into the (de)intercalation of divalent ions in the NiHCF lattice as in its current form, it does not account for the hysteresis associated with divalent ion insertion. Therefore, the isotherm can provide a qualitative insight into the (de)intercalation process of only the monovalent ions into the NiHCF electrodes.

The desalination tests with the symmetric CDI cell were performed in two operational modes referred to as *cyclic* and *continuous* desalination. The difference between these modes is reflected in the outlet concentration profiles obtained during these operations, presented in **Figure 1b** & **c**. In the cyclic desalination mode, after the completion of intercalation half cycle, the electrodes were regenerated (deintercalated) in the same reservoir by reversing their polarities. Therefore, the concentration of ions in the reservoirs changed in a cyclic manner, as presented in Figure 1b, because the reservoirs were permanently paired to one electrode regardless of its polarity. Therefore, after one full cycle, which comprised of an intercalation and a deintercalation step, the reservoir concentration was restored back to its original value.

The results of cyclic desalination on the feed solutions F1 – F5 in cyclic desalination are presented in **Figure 4.3**. The actual concentration profiles obtained during cyclic desalination are presented in **Figure S 4.4** & **S 4.5**. Feeds F1 – F4 contained a mixture of Na^+ and one of the divalent ions. Feed F5 contained all the three ions. The operation with a symmetric CDI cell resulted in a change in the concentration of Na^+, Ca^{2+}, and Mg^{2+} in the feed reservoirs. The closed circles, open triangles and squares represent the average change in concentration, Δc), of Na^+, Ca^{2+}, and Mg^{2+}, respectively, after every (de)intercalation half cycle. An average $\Delta[Na^+]$ of ≈ 7 mM was obtained after every half cycle for every tested feed sample, regardless of its initial relative concentration with the divalent ions (Na^+/D^{2+} ratio, with D = Ca, Mg). This corresponds to 0.5 mmol-Na^+/(g-both electrodes) being removed in every half cycle. In comparison, during the same desalination tests, the uptake of the divalent ions by the electrodes remained consistently low at ≈ 0.1 mmol/(g-both electrodes) *i.e.* $\Delta[Ca^{2+}]$ and $\Delta[Mg^{2+}]$ were in the 0.5 - 1 mM range. The data presented in Figure 3 demonstrate the high affinity of the NiHCF particles towards monovalent ions, which is quantified with a separation factor[47,106,148], β, calculated as

$$\beta_{M/D} = \left(\frac{c_{M,\text{initial}} - c_{M,\text{final}}}{c_{D,\text{initial}} - c_{D,\text{final}}}\right)\left(\frac{c_{D,\text{initial}}}{c_{M,\text{initial}}}\right) \tag{4.2}$$

where M and D represent the monovalent (Na^+) and divalent (Mg^{2+} or Ca^{2+}) ions, $c_{M,\text{initial}}$, $c_{M,\text{final}}$, $c_{D,\text{initial}}$, and $c_{D,\text{final}}$ are the concentrations of the mono- and divalent ions in the beginning and at the end of the intercalation half cycle, respectively. A high average $\beta \approx 15$ was measured for feeds with equimolar ion concentration (F1, F3) and feeds with the concentration of divalent ions three times as much as that of the monovalent ions (F2, F4). Such β value clearly indicates a strong preference of NiHCF electrodes towards monovalent Na^+. This trend is in contrast to values reported for carbon electrodes which are more selective towards divalent ions: β values of ≈ 7 and 24 were reported towards Ca^{2+} over Na^+ from a 1:5 Ca : Na solution for different adsorption times[136]; a β value of ≈ 1.5 was reported towards Ca^{2+} over Na^+ from a 1:1 Ca : Na solution.[248] Furthermore, the obtained selectivity here for Na^+ over Mg^{2+} and Ca^{2+}, $13 < \beta < 17$, is twice as high in comparison to a CDI cell, $6 < \beta < 8$, constructed with $Na_{0.44-x}MnO_2$ another widely used intercalation material.[165] This selectivity is also

comparable to other systems such as electrodialysis in which ion-selective membranes are used to achieve preferential ion adsorption.[249,250]

In addition to the selective removal of Na^+ from a binary mixture with Mg^{2+} and Ca^{2+}, the ability of the NiHCF electrodes to selectively remove Na^+ from an equimolar mixture of all three ions was also investigated. The feed F5 was desalinated to test the influence of the presence of multiple ions on the selectivity of the NiHCF electrodes. In this case, an average β value ≈ 20 and 25 was obtained for Na^+ over Ca^{2+} and Mg^{2+} respectively. Similar results in CDI have been reported for preferential removal of Cs^+ over Mg^{2+} with titanium disulfide as intercalation materials.[100] However, it must be pointed out that the monovalent ion removed in this study is Na^+, the second largest hydrated alkali metal ion that is considerably larger than Cs^+. In addition, these β values also indicate that the presence of more than one divalent ion in the feed has no adverse influence on the Na-removal performance of the electrodes. To the contrary, the selective ion separation becomes more pronounced with all three ions present in the solution. An increase in the number and type of divalent ions that are difficult to intercalate may work in the favor of Na^+ resulting in its preferential removal from a ternary mixture. A similar phenomenon of competition between intercalating and non-intercalating ions has been reported before.[251] However, we do not have experimental evidence to support this claim and therefore, this only remains a hypothesis.

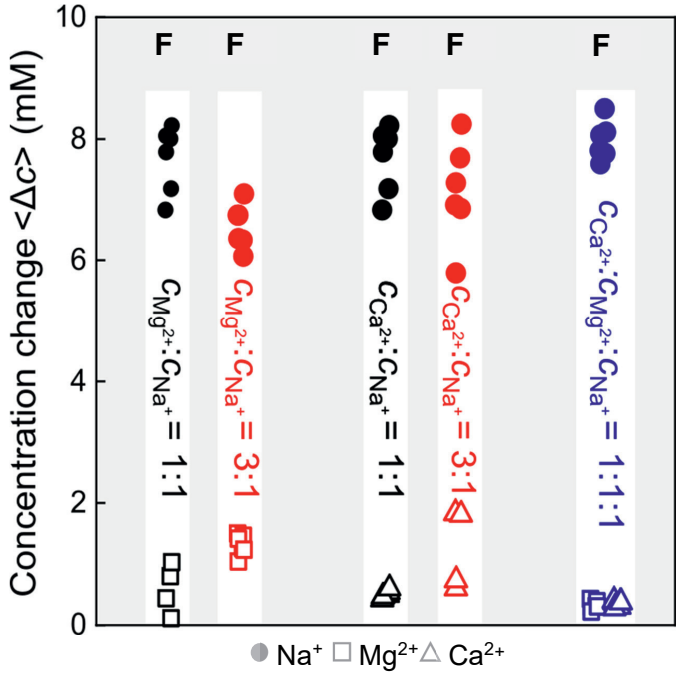

Figure 4.2: Results of all the cyclic desalination experiments performed with the feed solutions F1 – F5. The average change in the concentration of Na^+ (closed circles), Mg^{2+} (open squares), and Ca^{2+}(open triangles) is plotted on the y-axis. The separation factor β, calculated by Equation (2), was found to be 15 ± 2 for binary io mixtures (F1 – F4) and ≈ 25 for ionic mixture of all three ions (F5).

It can be concluded that within the bounds of the tested concentrations of the three ions in the feed solution, the NiHCF active particles remain highly selective towards Na^+ ions. **Tables S1 – S6** in the Supporting Information provide all the information of the achieved concentration reduction, ⟨Δ*c*⟩, calculated for each ion for every intercalation half cycle performed with the feeds F1 – F5 for the left and the right compartments of the symmetric CDI cell. Charge efficiency during intercalation Λ, calculated as the ratio of ion uptake and charge input, was found between 85 – 95 %. These values have been tabulated and provided in **Table S7** of the supporting information.

The second mode of operation, namely continuous desalination, is of more practical relevance because it results in uninterrupted desalination of the feed reservoirs. This mode requires a manual switching of the reservoirs between the cell compartments, simultaneously along with the switch in the electrode polarities. As a result, reservoirs are permanently paired with either a positive or a negative electrode, resulting in a continuous deionization or enrichment of the reservoir. The symmetric nature of the CDI cell becomes highly desirable because desalination can continue without being interrupted for electrode regeneration. A schematic of the expected concentration profile in the depleted reservoir (diluate) is shown in Figure 1c. In contrast to cyclic desalination, this mode of operation permanently removes ions from one reservoir and concentrates them in the other reservoir.

Average concentrations (from two separate runs) of Na^+, Ca^{2+}, and Mg^{2+} in the diluate and the concentrate output streams from the cell, during the desalination experiments performed in continuous mode, is reported in **Figure 4.4**. The decrease and increase in the concentration of the ions obtained in either of the reservoirs supports the claim of symmetric operation of the presented CDI cell configuration. It can be seen from **Figure 4.4a** that more than 85 % of Na^+ (a reduction in concentration from 40 mM to 5 mM) was removed from the solution within the first 7 half cycles. During these seven half cycles, less than 10 % of Ca^{2+} and Mg^{2+} was removed. On an average, a separation factor of 20 ± 5 was obtained for Na^+ over Ca^{2+} and Mg^{2+}. Remarkably, there was no drastic reduction in the preference towards Na^+ even after its concentration in the mixture was reduced by more than 90%, as evident from Figure 4a. Therefore, it can be inferred that the selectivity of NiHCF electrodes towards Na^+ does not strongly depend on the concentration of Na^+ in the ionic mixture.

Figure 4.4b presents the concentration of all the ions in the concentrate reservoir. The decrease in the diluate concentration is associated with an equivalent increase in the number of ions in the concentrate. This clearly support the claim of symmetric CDI operation with identical NiHCF electrodes. As a finer point it may, additionally, be noted that a slight difference in the performance of the two electrodes may arise from an unequal distribution of the cell voltage between them, or an asymmetric charging degree, ϑ, in the electrodes, leading to an incomplete use of one half of the desalination cell.

Another consequence of the (de)intercalation of cations is dissolution of the metallic components of the lattice in the treated water. This results in the loss of capacity of the

electrodes over time. Such losses have previously been reported in literature as well.[42,53] It has been recently reported that Mg^{2+} can replace Ni^{2+} in the lattice resulting in dissolution of the Fe centers of the lattice as well.[247] This can enhance the fade in capacity of the electrodes. **Figure S 4.6** gives the concentration profile of Ni and Fe in the treated water for both cyclic as well as continuous desalination modes. While the continuous mode results in the accumulation of Ni and Fe in the concentrate and dilute chamber, respectively. In contrast, the build-up of Ni during the cyclic desalination mode is slowed down by its partial adsorption by the electrode. This further shows the ability of the NiHCF electrodes to intercalate ions of multiple valences.

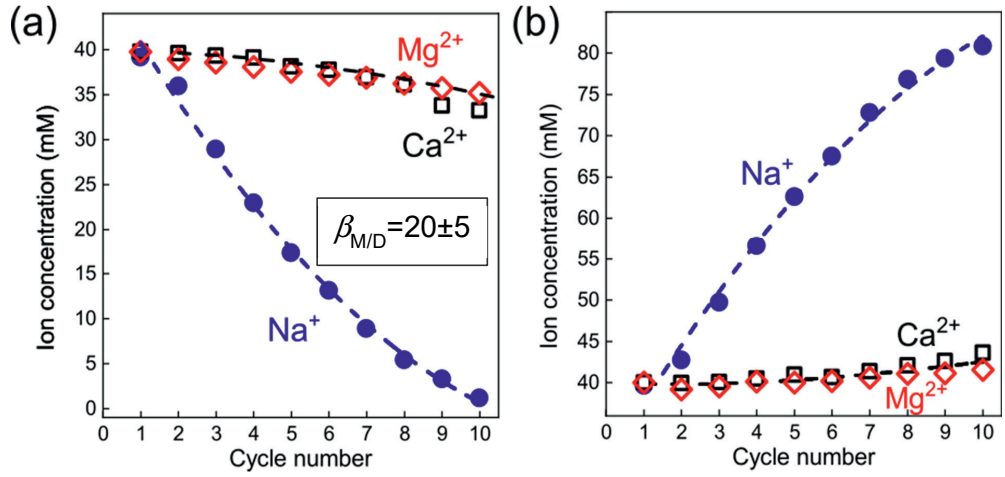

Figure 4.3: Continuous desalination via symmetric CDI cell with identical NiHCF electrodes **(a)** Result from the intercalation compartment (**diluate**) during the continuous desalination of F6, containing 40 mM each of Na^+, Mg^{2+}, and Ca^{2+} with the symmetrical CDI cell. **(b)** Result from the deintercalation compartment (**concentrate**) during the continuous desalination of F6. Average separation factor of **20 ± 5** between monovalent (Na^+) and divalent (Ca^{2+} and Mg^{2+}) ions was obtained during continuous desalination of F6. The dashed lines serve as a guide to the eye.

The preference of NiHCF electrodes towards monovalent ions was also tested after the electrodes were run for 200 cycles. The concentration profile obtained from this experiment is given in the **Figure S 4.7** of the supplementary information. The preference towards monovalent Na^+ ions was clearly preserved. However, after 200 cycles, the divalent ions were removed in larger amounts (≈ 20 %) in comparison to the time when fresh electrodes were used (≈ 10 %). In the same interval, Na^+ concentration dropped by ≈ 90 %. This resulted in a small reduction in the separation factor β for monovalent Na^+ over divalent Ca^{2+} and Mg^{2+} to ≈ 11 ± 4 in comparison to the value of 20 ± 5 obtained using fresh electrodes, as depicted in **Figure**

4.4. Therefore, it can be concluded that as far as long-term selectivity is considered, the preference of NiHCF electrodes towards monovalent ions over divalent ions was preserved.

The selectivity of NiHCF electrodes towards Na^+ from a mixture containing Ca^{2+} and Mg^{2+} ions can be primarily attributed to their different dehydration energies with divalent ions having higher energies than monovalent ions[252] (which follows from their hydrated ionic radii: Na^+ = 3.58 Å; Ca^{2+} = 4.12 Å; Mg^{2+} = 4.28 Å).[253] The intercalation of these ions in the NiHCF lattice requires partial dehydration of the inserting ion.[80] Thus, a larger dehydration energy would make the intercalation of a divalent ion thermodynamically unfavorable in comparison to the monovalent ion, present in the ionic mixture. Another, entropic, barrier to the intercalation of divalent ions in the NiHCF lattice is their requirement for the simultaneous reduction of two Fe^{3+} atoms in the lattice. In contrast, Na^+ intercalation only requires one Fe^{3+} center to be reduced. These combined effects yield the high selectivity of the NiHCF electrodes observed here for monovalent Na^+ ion.

4.4 Conclusion

A symmetrical CDI cell was assembled with identical electrodes fabricated with NiHCF as active particles. Six different concentrations of Na^+, Ca^{2+}, and Mg^{2+} were desalinated in cyclic and continuous mode. In the cyclic mode, high values of the selectivity factor (calculated as the ratio of the amount of monovalent and divalent ions removed relative to their initial concentration) $\beta_{Na/Ca}$ and $\beta_{Na/Mg}$, between 13 – 17 were obtained for the feed solution containing a mixture of Na^+ with Ca^{2+} and Mg^{2+}, respectively in the ratio of 1:1 (equimolar) and 1:3 (divalent ions three times as much as the monovalent ions). The selective removal of Na^+ remained unaffected by the increase in the concentration of divalent ions in the solution. An equimolar mixture of all three ions, when desalinated in cyclic mode, resulted in a high average $\beta \approx 20$ and 25 towards Na^+ over the divalent Ca^{2+} and Mg^{2+} ions, respectively. During the continuous desalination of the equimolar solution containing all three ions, a symmetrical increase and decrease in ion concentration was obtained in the reservoirs feeding the two compartment CDI cell. In addition, more than 95 % of all Na^+-ions was removed from the solution while only 10% of Mg^{2+}-ions and Ca^{2+}-ions was removed. The average β varied between 15 - 25 for Na^+ over Ca^{2+} and Mg^{2+}. Furthermore, the preference towards Na^+ did not decrease with its decreasing concentration in the diluate stream out of the continuous desalination experiment. Therefore, the developed electrochemical system serves as an elegant solution for continuous, highly selective removal of monovalent ions from a mixture of monovalent and divalent ions via capacitive deionization.

Supporting information

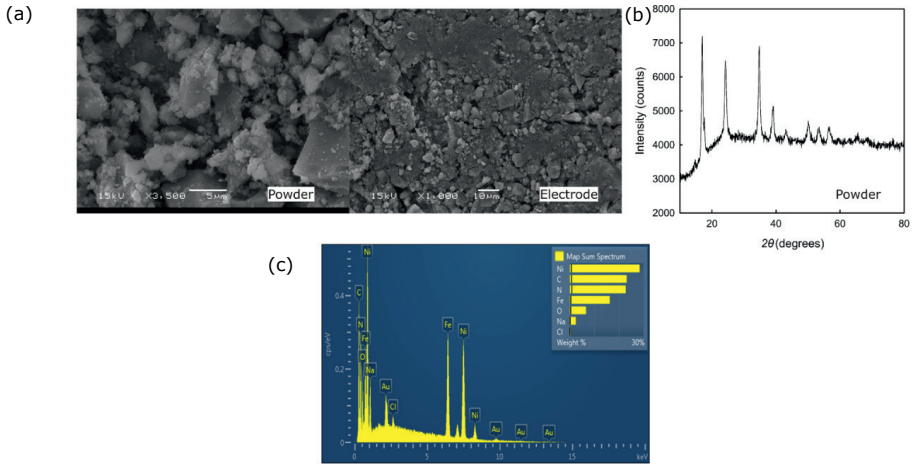

Figure S 4.1: Results from characterization analysis performed on NiHCF and electrode. The top row presents **(a)** the SEM images acquired for the NiHCF particles and the electrodes along with **(b)** an XRD spectrum of powdered NiHCF. The last row **(c)** provides relative compositions of elements in the NiHCF lattice from an EDS elemental mapping of NiHCF powder.

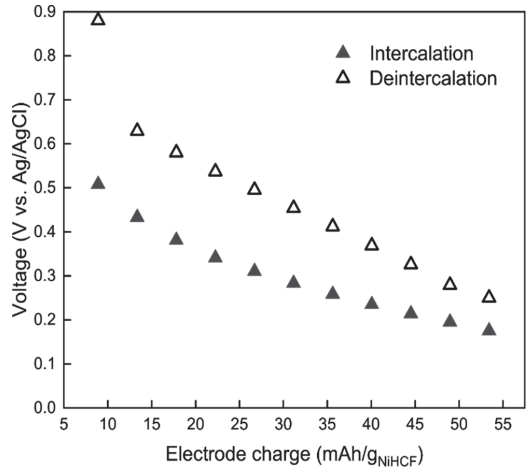

Figure S 4.2: Charge intake capacity of NiHCF electrodes, measured by GITT, for 1 M $CaCl_2$ solution in a three-electrode cell with platinum coated titanium electrode as counter and an Ag/AgCl electrode as reference.

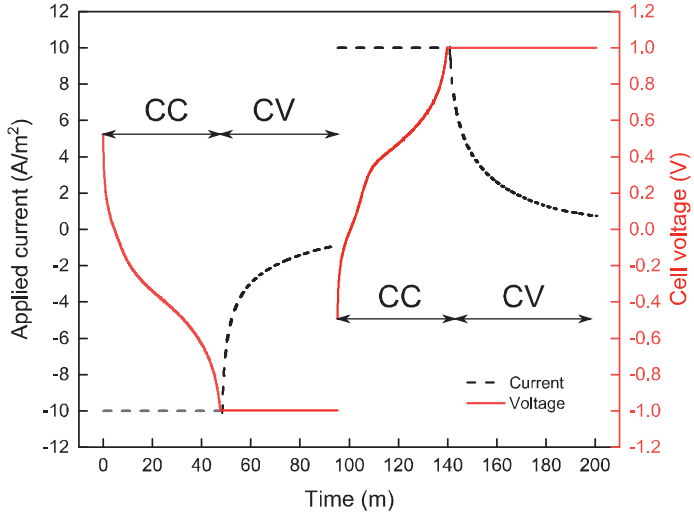

Figure S 4.3: The implemented constant current (CC)/constant applied voltage (CV) operations for deionization and enrichment in both cyclic as well as continuous modes of desalination.

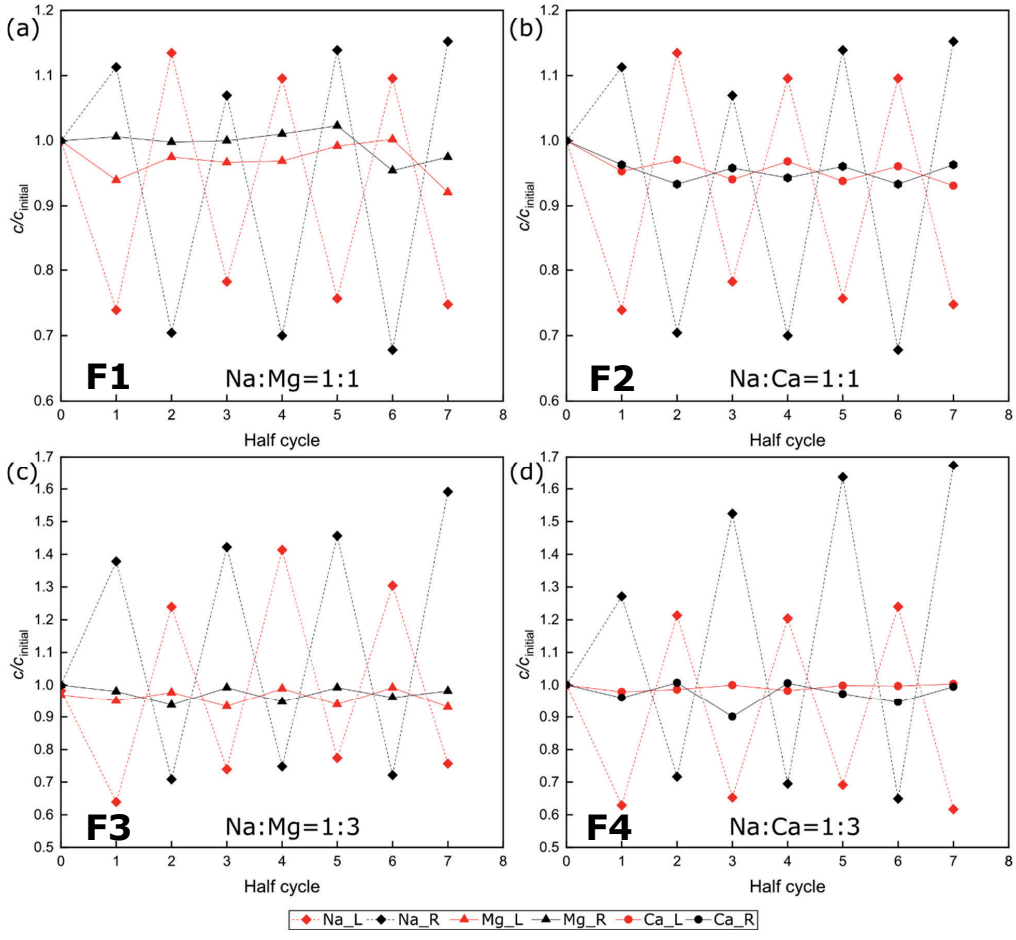

Figure S 4.4: Results of cyclic (de)intercalation from binary ionic mixtures (F1, F3) and (F2, F4) of Na^+ (diamonds)/Mg^{2+} (triangles) and Na^+/Ca^{2+}(circles), respectively from both channels (red: left, subscript **L**; black: right, subscript **R**) of the two-compartment cell. Operation on equimolar solution of the monovalent and divalent ions resulted in changes in concentration reported in panels **(a)** and **(b)**. Operation performed on feed with concentration ratio of 1:3 between monovalent and divalent ions resulted in changes in concentration as reported in panels **(c)** and **(d)**. The y-axis of each graph is normalized with the feed concentration of the respective ion

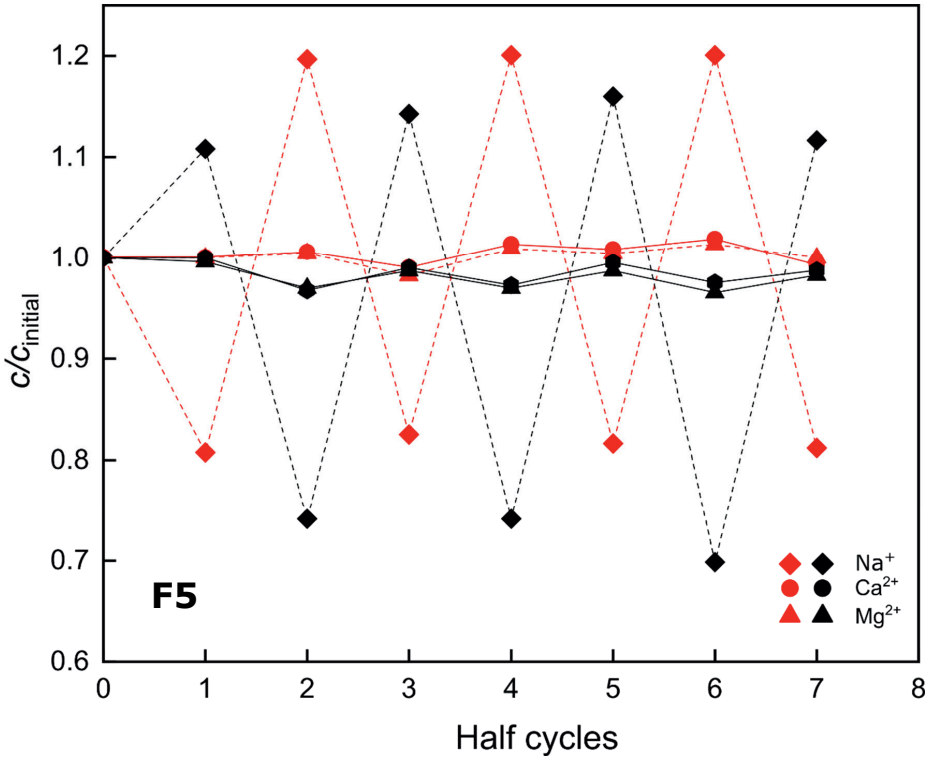

Figure S 4.4: Results from cyclic desalination experiments containing 20 mM each of NaCl, $MgCl_2$ and $CaCl_2$ with the symmetric, two compartment CDI cell with identical NiHCF electrodes. The red and black colour codes for the data points indicate the concentration from the outlets connected to the two cell compartments.

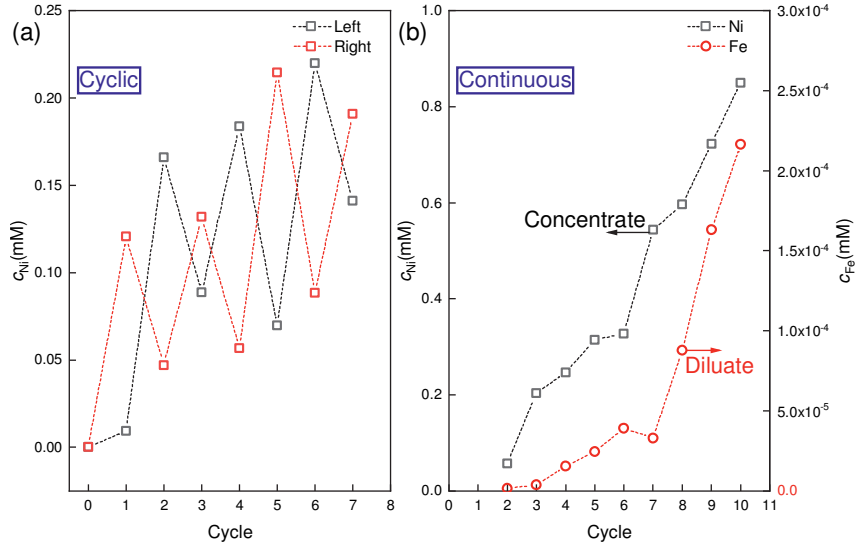

Figure S 4.6: Ion-concentration during **(a)** cyclic mode for Ni in both reservoirs and **(b)** continuous desalination for Ni (black squares) and Fe (red circles) in concentrate and diluate, respectively. The concentration of Fe during cyclic desalination was too small to be accurately measured.

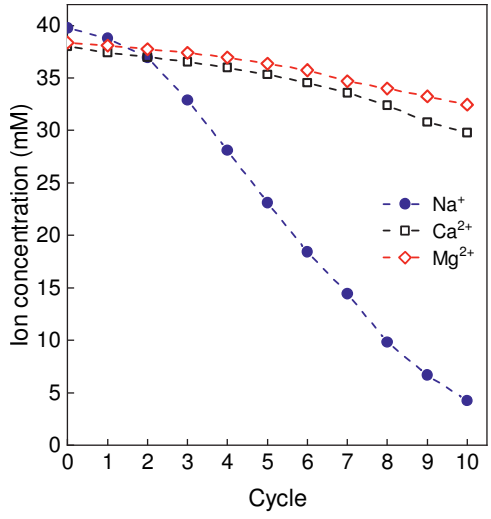

Figure S 4.5: Ion concentration in depletion reservoir (**diluate**) after 200 cycles.

Table S 4.1: Average change in concentration (⟨Δc⟩) of Na^+ from the outlet of the right compartment of the CDI cell for three deionization/enrichment half cycles presented in **Figure S 4.4.**

Half cycle	F1 (mM)	F3 (mM)	F2 (mM)	F4 (mM)	F5 (mM)
1→ 2	8.0	6.3	8	6	7.5
3→ 4	6.8	6.7	6.9	7	7.8
5→ 6	8	6.3	8	7.7	8.5

Table S 4.2: Average change in concentration (⟨Δc⟩) of Na^+ from the outlet of the left compartment of the CDI cell for three deionization/enrichment half cycles presented in **Figure S 4.4.**

Half cycle	F1 (mM)	F2 (mM)	F3 (mM)	F4 (mM)	F5 (mM)
2→ 3	7.2	6.1	7.2	6.8	7.7
4→ 5	7.8	6.7	7.9	7.3	8
6→ 7	8.2	7.1	8.2	8.2	8

Table S 4.3: Average change in concentration (⟨Δc⟩) of Mg^{2+} from the outlet of the right compartment of the CDI cell for three deionization/enrichment half cycles presented in **Figure S 4.4.**

Half cycle	F1 (mM)	F3 (mM)	F5 (mM)
1→ 2	0.4	1	0.3
3→ 4	--	1.5	0.4
5→ 6	0.8	1.3	0.3

Table S 4.4: Average change in concentration (⟨Δc⟩) of Mg^{2+} from the outlet of the left compartment of the CDI cell for three deionization/enrichment half cycles presented in **Figure S 4.4.**

Half cycle	F1 (mM)	F3 (mM)	F5 (mM)
2→ 3	0.1	1.5	0.4
4→ 5	--	1.4	0.2
6→ 7	1	1.2	0.3

Table S 4.5: Average change in concentration (⍰Δc⟩) of Ca^{2+} from the outlet of the right compartment of the CDI cell for three deionization/enrichment half cycles presented in **Figure S 4.4.**

Half cycle	F2 (mM)	F4 (mM)	F5 (mM)
1→ 2	0.5	0.6	0.4
3→ 4	0.4	1.8	0.4
5→ 6	0.5	--	0.3

Table S 4.6: Average change in concentration (⍰Δc⟩) of Ca^{2+} from the outlet of the left compartment of the CDI cell for three deionization/enrichment half cycles presented in **Figure S 4.4.**

Half cycle	F2 (mM)	F4 (mM)	F5 (mM)
2→ 3	0.5	1.8	0.4
4→ 5	0.5	0.7	0.3
6→ 7	0.6	--	0.4

Table S 4.7: Charge efficiency obtained during intercalation from three feed solutions.

Na + Ca		Na + Mg		Na + Mg + Ca	
Cycle	Λ (%)	Cycle	Λ (%)	Cycle	Λ (%)
2→ 3	91	2→ 3	99	2→ 3	87
4→ 5	87	4→ 5	88	4→ 5	85
6→ 7	83	6→ 7	94	6→ 7	86

5 Divalent ion selectivity in capacitive deionization with vanadium hexacyanoferrate: Experiments and quantum-chemical computations

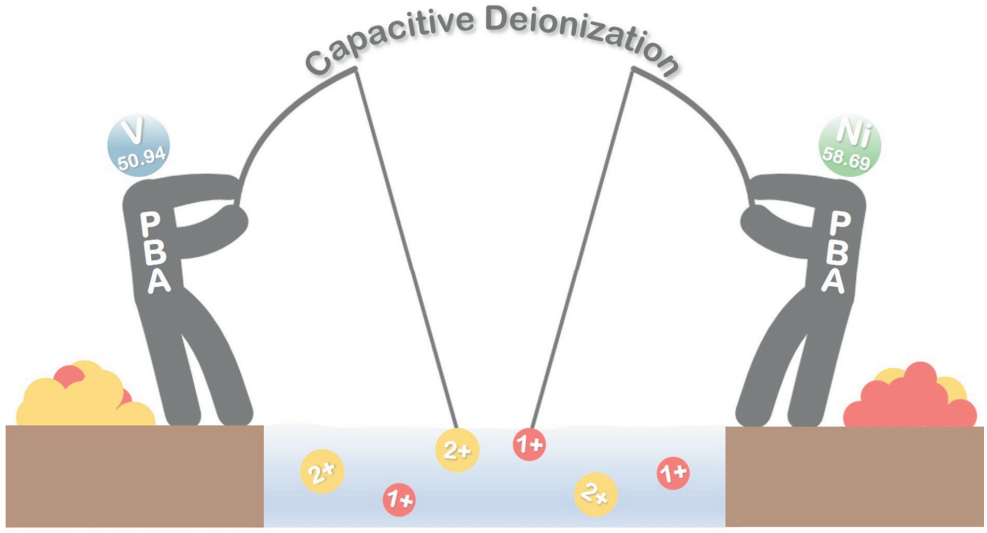

This chapter has been published as:

Singh, K., Li, G., Lee, J., Zuilhof, H., Mehdi, B. L., Zornitta, R. L., de Smet, L. C. P. M. (**2021**), Divalent Ion Selectivity in Capacitive Deionization with Vanadium Hexacyanoferrate: Experiments and Quantum-Chemical Computations. *Adv. Funct. Mater.*, 31(41), 2105203.

Abstract

Selective removal of ions from water, via capacitive deionization (CDI), is relevant for environmental and industrial applications like water purification, softening, and resource recovery. Prussian blue analogues (PBAs) are proposed as an electrode material for selectively removing cations from water, based on their size. So far, PBAs used in CDI have been selective towards monovalent ions. Here, we introduce vanadium hexacyanoferrate (VHCF), a PBA, as a new electrode material in a hybrid CDI setup, to selectively remove divalent cations from water. These electrodes preferred divalent Ca^{2+} over monovalent Na^{+}, with a separation factor, $\beta_{Ca/Na} \approx 3.5$. This finding contrasts the observed monovalent ion selectivity by PBA electrodes. This opposite behaviour was understood by Density Functional Theory (DFT) simulations. Furthermore, the coating of the VHCF electrodes with a conducting polymer (poly-pyrrole, doped with poly-styrenesulphonate, PPy/PSS) prevented the contamination of the treated water following the degradation of the electrode. This facile and modular coating method can be effortlessly extended to other PBA electrodes, limiting the extent of treated water contamination during repeated cycling. This study paves the way for tunable selectivity while extending the library of electrodes that can be successfully used in (selective) CDI.

4.1 Introduction

Capacitive deionization (CDI) is a water desalination technology in which two porous electrodes remove ions from water under the influence of an applied electric current or voltage.[20,41] Once removed, these ions are stored inside or at the surface of the capacitive electrodes. These electrodes can be fabricated out of the same materials with the same ion storage mechanism, like in conventional CDI, or from materials with different ion storage mechanism, as demonstrated in hybrid CDI (HCDI).[95,97] The choice of materials for electrode fabrication plays a crucial role in the performance of a CDI setup. Conventionally, carbon has been the material of choice for electrodes. The ions are removed from the water and stored in the micro/mesopores of the carbon.[50,64] Carbon has been the material of choice because of its low cost, easy availability, high conductivity, amphoteric behavior, and high surface area.[51,65] These attributes make it suitable for water desalination applications.[18,50,125] Carbon electrodes are, however, of limited utility for two reasons: First, they suffer from an unproductive reaction caused by the expulsion of ions with the same charge as that of the electrode, referred to as co-ion repulsion or ion swapping.[60,254] Second, they display an insufficient selectivity towards different ions.[73] Such selective removal of ions from water is, however, crucial for industrial applications like resource recovery, production of fine chemicals, water softening.[3]

A solution to a few of the above-mentioned issues of bare carbon is the use of ion-exchange membranes placed adjacent to it inside the desalination cell. This configuration is referred to as membrane capacitive deionization (MCDI).[132,255] The use of membranes in CDI cells has increased their ion removal and energy efficiency,[201] and enabled versatile new cell architectures.[3] However, the high cost of the membranes poses a practicality issue. Another alternative to carbon lies with electrodes based on intercalation materials for CDI.[41,54,56] The crucial difference between intercalation materials and carbon is the physical storage mechanism of ions. Unlike storage on the pore surface as seen in carbon, ions in intercalation materials are inserted either into an interstitial lattice sites[80,108] or in between the layers of the material[89,175] under an applied electric current or voltage. This ion storage mechanism prevents the co-ion repulsion encountered in carbon-based electrodes, eradicating the necessity of membranes in high-efficiency CDI cells.[41] In addition, these materials retain the positive attributes of carbon, such as easy electrode preparation and improve upon the salt absorption capacity[83] and energy efficiency.[91,223] Furthermore, intercalation materials have also demonstrated inherent selectivity towards various ions,[3,100,165] unlike carbon which requires either membranes or surface modifications to gain high selectivity. The current study explores this inherent selectivity, exhibited by one of the Prussian Blue Analogues (PBAs), a class of intercalation materials.[82]

Prussian blue (PB), one of the oldest synthesized pigments, has the chemical formula $A_2M[Fe(CN)_6]$ in reduced form, where A is an alkali metal (Na, K). For PB, the element M is Fe, whereas, for PBAs, M can be Ni,[152] Cu,[173] and V,[104] among other transition metal

elements.[256,257] The use of PBAs in CDI is interesting because of their open crystal structure, customizable chemical composition, and inherent selectivity towards cations.[3,11,54] Furthermore, these electrodes have also been reported to be stable for up to 80 cycles under brackish water desalination conditions.[137,258] The ions removed from the water are stored in the interstitial lattice sites of the PBAs. This insertion is accompanied by a change in the oxidation state of a redox-active constituent of the PBA lattice.[102] Different cations intercalate into the lattice at different (reduction) potentials within the stability window of water.[3] This intercalation potential serves as a useful indication of whether the intercalation of a cation will be easy or difficult relative to another ion. Studies have shown that in a mixture of alkali metal ions, PB and its analogues demonstrate the strongest affinity towards Cs^+. This affinity reduces in the case of the alkali metals above Cs^+ in the group.[135,143] This trend of reducing the affinity of the PBA towards cations follows their insertion potential.[106,259] Taking advantage of this property, recent studies in CDI have also successfully demonstrated the use of PBA electrodes in the selective separation of monovalent over divalent ions.[11,54,106,260] However, systems for the selective removal of divalent ions based on PBA electrodes, important for applications such as water softening, surely require further development. Another area that requires improvement is the stability of PBA electrodes during repeated cycling.[144] It has been hypothesized that the electrodes dissolve due to the exchange of CN^- in the PBA lattice with OH^- from the aqueous solution.[108] This dissolution results in the release of undesired species into the treated solution, demanding an extra post-treatment step. To enable a wider utilization of PBA based CDI technologies, this shortcoming must be addressed.

In this study we introduce vanadium hexacyanoferrocyanate (VHCF) as electrode material in CDI, explain its ion selectivity by quantum-chemical calculations, and develop a coating for the electrode to prevent treated water contamination. In brief, VHCF was synthesized, characterized, and used as an active electrode material for selective ion separation from a mixture of mono- and divalent ions, via hybrid CDI (HCDI). A schematic of the cell used for desalination is given in **Figure 5.1**. This cell configuration comprises a cathode, made of VHCF particles embedded in a conducting carbon additive, a spacer channel for feed flow and an oversized activated carbon anode,[169] isolated by an anion-exchange membrane (AEM) from the feed. The VHCF particles were characterized in detail using a variety of surface-sensitive, temperature-sensitive, and electrochemical methods. Selectivity experiments were performed on binary and ternary solutions of mono- and divalent cations. The stability of the VHCF electrodes was tested in single-salt solutions. Density functional theory (DFT) calculations on the crystal structures were performed within the VASP program[261] to elucidate the intercalation preference of the VHCF lattice towards different cations, and to compare it with that of nickel hexacyanoferrate (NiHCF), another widely used PBA in (selective) CDI.[3,41] Finally, the surface of VHCF electrodes was modified to prevent the release of ionic components of the electrode in the treated stream after electrode degradation. We show that this can be successfully achieved by coating the VHCF electrode with a protective layer of a conducting polymer polypyrrole-doped with poly(styrenesulfonate) (PPy/PSS), thereby reducing the direct contact of feed and the electrode. This study demonstrates the first-

time use of a PPy/PSS layer to prevent contamination of treated water, for a divalent cation selective PBA electrode, also shown in this study for the first time.

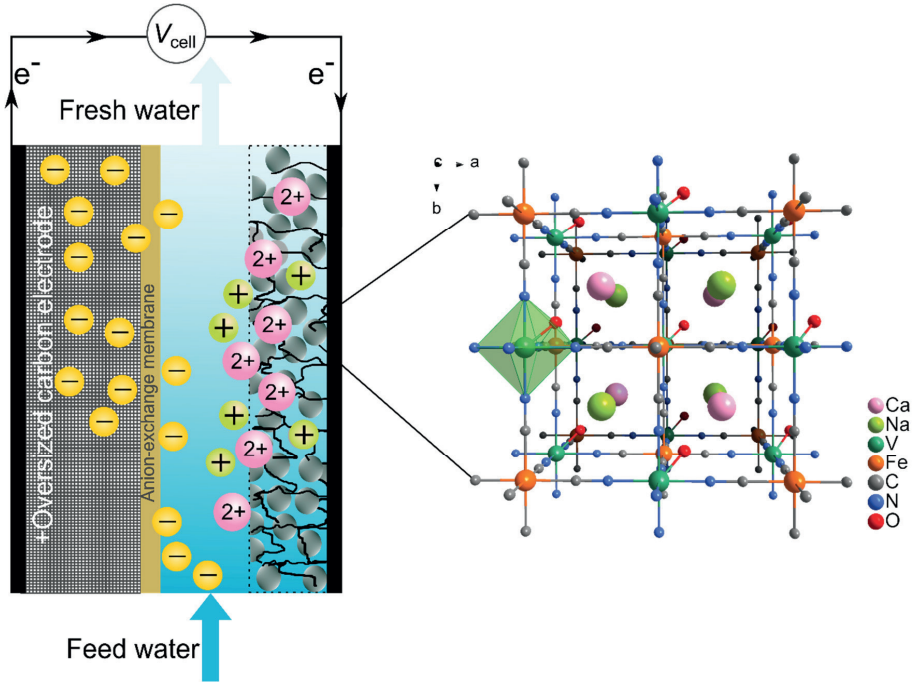

Figure 5.1: Schematic of a hybrid CDI cell with VHCF and an oversized carbon electrode, separated from the spacer by an anion-exchange membrane. A simplified version of the free-standing cathode shown here depicts its components as agglomerated VHCF particles (green spheres) interconnected by the conductive carbon additive (black irregular lines) to facilitate intra-particle electron transfer as well as that between the particles and the current collector. The schematic shows the moment of operation when cations (selectively) intercalate into the VHCF cathode and anions are adsorbed in the pores of the carbon anode, resulting in a desalinated feed at the outlet of the spacer channel. The inset depicts the unit cell structure of VHCF, modelled in the DFT calculations.

4.2 Materials and method

4.2.1 VHCF particles: preparation and characterization

The synthesis of VHCF-active particles was performed according to a modified co-precipitation adopted from literature.[104] A 40 mM solution of VCl_3 (Alfa Aesar) was prepared in 200 mL of water containing 1 % (*v*/*v*) HNO_3 (Sigma Aldrich). Simultaneously, a 20 mM solution of $Na_4[Fe(CN)_6]\cdot 10H_2O$ (Sigma Aldrich) was prepared in 200 mL of water containing 1 % (*v*/*v*) HCl (Sigma Aldrich). These acidified precursors were dropwise added to a 200 mL

of 10 % *v*/*v* HCl solution. The reactor was immersed in an oil bath, maintained at 70 °C, and the mixture inside was stirred at 600 RPM for ca. 12 h. The precipitate formed was washed with a vacuum filtration unit, and the residue was dried overnight in a vacuum oven at 80 °C. The morphology of the VHCF particles was examined by a JEOL JSM 7001F field emission scanning electron microscope (SEM) at an acceleration voltage of 10 – 15 kV. The chemical composition of the carbon electrodes was determined by energy-dispersive X-ray spectroscopy (EDS) with an INCA X-act EDS detector (Oxford Instruments). The spectra of ten spots on the different particles were measured using an accelerating voltage range of 15 kV and averaged. The crystallinity of the VHCF particles was assessed by powder X-ray diffraction (XRD), performed using a copper source for diffraction angles in the range of $10° < 2\theta < 70°$. infrared (IR) spectroscopy was performed on the VHCF powder by a Bruker Tensor 27 spectrometer with platinum attenuated total reflection accessory. The X-ray photoelectron spectroscopy (XPS) spectrum of the VHCF particles was obtained by a JPS-9200 photoelectron spectrometer (JEOL, Japan) under ultrahigh vacuum, using a monochromatic Al Kα source at 12 kV and 20 mA and was processed by CASA XPS software (version 2.3.16) with Shirley background fitting correction. The water content in the VHCF powder was estimated by thermo-gravimetric analysis (TGA), performed under N_2 environment at the rate of 5 °C /min from 25 to 700 °C.

4.2.2 Electrode fabrication

The dried VHCF powder was milled with the activated carbon (YP-80) (Kuraray corp.) in a ball mill for 20 min. The resulting fine powder was mixed with poly(tetrafluoroethylene) (PTFE) (60 % dispersion, Sigma Aldrich) in ethanol as a solvent and kneaded into a dough. The final composition of the dough added was 8.5: 1: 0.5 for VHCF, AC, and PTFE, respectively. The partially dried dough was cold rolled into 10 cm × 10 cm × 200 μm, free-standing sheets. The electrodes were dried at 120 °C overnight, under vacuum. Following the drying, the electrodes were stored in a desiccator.

4.2.3 PPy/PSS layer electrodeposition

The PPy/PSS layer was electrochemically deposited on the surface of the VHCF electrode to achieve a homogeneous layer. First, 150 mL of a solution containing 0.1 M PPy(Polymer, Sigma Aldrich) and 0.5 M PSS(Sodium salt, Sigma Aldrich) was prepared. The VHCF freestanding electrodes were pressed and deposited on a graphite current collector in a rolling machine (MTI Corp) at room temperature. This VHCF-graphite composite electrode was then dipped in a PPy/PSS solution as a working electrode (WE). An oversized activated carbon was used as a counter electrode (CE) along with an Ag/AgCl electrode in 3 M KCl as the reference (RE). The PPy/PSS layer electrodeposition was carried out in a constant-current operation during which, a current of ca. 150 mA/g was applied to the WE for 40 min. After the

electrodeposition, the VHCF and the current collector became completely black. The rear of the current collector was carefully polished to remove any excess of physically bound PPy/PSS. The composite electrode was labeled as VHCF-PPy/PSS.

4.2.4 Electrochemical characterization and (ion-selective) desalination

The electrochemical characterization of the electrodes was obtained from cyclic voltammetry (CV) experiments, carried out in a three-electrode cell with VHCF as WE, an activated carbon separated by an anion exchange membrane (AEM) as a CE and an Ag/AgCl electrode as RE mounted close to the WE. The electrolytes were two different, 1 M solutions of NaCl and $CaCl_2$ each, with pH values of ≈ 2 and 7. In addition, a dilute HCl solution of pH = 2, containing no other cation, was also used as an electrolyte for CV. The electrode potential was varied from −0.2 to 1.05 V at the scan rate of 1 mV/s by a potentiostat (n.stat, IVIUM technologies).

The selectivity experiments were performed in a hybrid CDI cell, as depicted in **Figure 5.1**, containing either the bare VHCF electrode or the PSS/PPy-coated VHCF electrode as cathode (0.1 - 0.2 g), and a YP-80F carbon electrode (10 cm × 10 cm × 500 μm, 0.6 - 0.8 g) as anode, separated by a porous spacer channel of thickness 500 μm. The weights of the cathode and anode were matched according to the adsorption capacities reported for PBAs (35 – 45 mg/g)[56,91,161] and AC (10 – 15 mg/g).[226,262] An AEM membrane was used to isolate the anode from the spacer channel, in order to prevent the influence of the carbon electrode on VHCF electrodes. Feed solutions with different kinds and concentrations of cations were treated by the cell to investigate the affinity of VHCF electrodes. The compositions of these feeds, namely **F1**, **F2**, **F3**, and **F4** and their corresponding pH are given in **Table 5.1**. The pH of the MilliQ water used to prepare the solutions was ≈ 6.5.

A batch of 50 mL of ion mixture was desalinated under a recycle condition by the VHCF hybrid cell. The ion removal was performed first under a constant-voltage operation. For absorption, a cell voltage of –1 V was applied for 0.5 h. The sample was taken after 0.5 h from the diluate reservoir to measure the ion concentration via ion chromatography (Eco IC, Metrohm). The VHCF electrode was regenerated by applying a cell voltage of +1 V for 0.5 h in a regeneration electrolyte containing the same cations as the ones in the diluate used during absorption. The end of these operations completed one full cycle. The chambers were flushed with MilliQ water in between the adsorption and desorption steps to prevent contamination of the diluate. Several cycles were performed to continuously reduce the concentration in the diluate.

Table 5.1: Concentration of cations and the pH of the feed solutions treated by a hybrid CDI cell to investigate the affinity of VHCF electrodes towards different ions.

Feed	Li^+ (mM)	Na^+ (mM)	Ca^{2+} (mM)	Mg^{2+} (mM)	pH
F1	--	10	10	--	6.1 – 6.2
F2	--	10	--	10	6.6 – 6.8
F3	--	10	10	10	7.3 – 7.4
F4	10	--	10	--	6.7 – 6.8

To understand how the VHCF electrodes performed upon continuous cycling, a hybrid cell containing a VHCF cathode, and a carbon anode was cycled continuously in 20 mM single-salt solutions of NaCl and $CaCl_2$, respectively. The reservoir volume was 5 L. The cell was run for 40 cycles in a constant-voltage mode with steps of 0.5 h of operation, each at 1 and -1 V and the conductivity was recorded at the outlet. The electrodes were analyzed via post-mortem XRD.

4.2.5 Quantum chemistry

All spin-polarized DFT calculations were performed using the Vienna Ab initio Simulation Package (VASP, version 5.4).[261,263] The Perdew–Burke–Ernzerhof (PBE) functional based on the generalized gradient approximation (GGA) was chosen to account for the exchange–correlation energy.[264] A plane-wave basis set in combination with the projected augmented wave (PAW) method was used to describe the valence electrons and the valence-core interactions, respectively.[265] The kinetic energy cut-off of the plane wave basis set was set to 400 eV. Gaussian smearing of the population of partial occupancies with a width of 0.05 eV was used during iterative diagonalization of the Kohn-Sham Hamiltonian. The threshold for energy convergence for each iteration was set to 10^{-5} eV. Geometries were assumed to be converged when forces on each atom were less than 0.05 eV/Å. Both atomic positions and lattice constants were fully optimized during the bulk calculation. The calculated lattice constants were 10.20 Å for the cubic NiHCF ($a = b = c$; $\alpha = \beta = \gamma = 90^\circ$) and 7.24 Å for the rhombohedral VHCF ($a = b = c$; $\alpha = \beta = \gamma \neq 90^\circ$) (detailed structural information available as .cif). The Brillouin zone integration and k-point sampling were done with a Monkhorst–Pack scheme of a 4×4×4 and 2×4×4 grid points for the unit cells and the 2×1×1 supercells of NiHCF and VHCF, respectively.[247,266] The DFT+U method was applied to deal with the on-site self-interaction error among the d electrons, and the U_{eff} values of Fe, Ni and V were set as 1 eV, 3 eV, and 3 eV, respectively. The Van der Waals (vdW) interactions were included by using Grimme's DFT-D3(BJ) method, as implemented in VASP.[267] The calculations were done with intercalated cations with no hydration shell and with cations with six water molecules around them to understand the effect of solvent on the selectivity.[268]

4.3 Results and Discussion

4.3.1 VHCF powder characterization

The proposed synthesis route was chosen so that the vanadium precursor remains as V(IV) during the reaction with the $[Fe^{2+}(CN)_6]^{4-}$ group in the acidified reaction mixture. The addition of HNO_3 in the vanadium precursor solution results in the oxidation of V(III) into V(IV), which is characterized by a final blue color of the precursor solution, as depicted in **Figure S 5.1**. The addition of V(IV) and $[Fe^{2+}(CN)_6]^{4-}$ precursors into an acidified aqueous reaction mixture, instead of adding one reactant to the other, kept the molar ratio of the reactant's constant in the reaction mixture during the addition process. The acidification of the reaction mixture has been shown to retard the rate of co-precipitation between the precursors.[104,152] The delayed formation of the first crystals during the reaction, after the dropwise addition, gave an indication of the retarded rate of co-precipitation, which helps in formation of lattices with higher crystallinity.[104] The acidified reaction mixture coupled with the easy availability of V(IV) results in a facile growth of VHCF particles. SEM images of the synthesized VHCF particles are given in **Figure 5.2a**, **b** and **Figure S 5.2**, showing an agglomeration of particles, as seen for other PBAs such as NiHCF.[91] The size of these agglomerates range between 0.5 and 5 µm. **Figure 5.2b** shows the particles at 22000× magnification, revealing that the agglomerates of ≈ 500 nm diameter have a flake-like morphology.

The XRD pattern of the VHCF powder was compared to that of the NiHCF powder to highlight the analogous nature of the two PBAs. The VHCF synthesis resulted in a well-defined and crystalline lattice, as seen in the XRD pattern of the VHCF powder in **Figure 5.2c**. A comparison of VHCF diffractogram (black) to that of NiHCF (red) confirms that the VHCF structure is that of a PBA. The peaks in the NiHCF diffractogram are characteristic of a cubic lattice,[152,269] while the structure of VHCF can be ascertained to fit either a cubic or rhombohedral lattice, considering the high degree of overlap between them. The exact structure of VHCF may vary between these two lattice types, as is usually seen for PBAs.[93] Nevertheless, the XRD patterns presented in **Figure 5.2c** agree well with the diffractograms reported elsewhere for an electrochemically deposited VHCF thin film,[270] and with the patterns predicted by the DFT calculations for the model crystals of both NiHCF and VHCF. The agreement between the experimental and the calculated diffraction pattern of VHCF is especially remarkable as it confirms our placement of O atom, present in the V=O bond, in the lattice towards the interstitial site, as illustrated in **Figure 5.1**. Interestingly, the peak positions appear to be shifted to higher angles for VHCF when compared to NiHCF. A closer look at the reflections of (200), (400), and (420) planes of VHCF and NiHCF particles, as shown in **Figure S 5.3**, confirms this observation. This results in a d_{100} lattice spacing, calculated using the (h00) peaks shown in **Figure 5.2c**, of 10.15 Å for VHCF, compared to 10.2 Å for NiHCF. This value is within the range of values reported in the literature for VHCF (10.1 Å[271] and 10.19 Å[272]).

An XPS wide scan, presented in **Figure 5.2d,** confirmed the presence of iron, vanadium, carbon, and nitrogen in the VHCF lattice. As expected, the most abundant elements in the powder were carbon and nitrogen, followed by oxygen, vanadium, and iron. The presence of vanadium at a peak position of 516.6 eV in the XPS spectrum implies the presence of V(IV).[270] The presence of oxygen in the structure may come from water molecules residing either in the interstitial sites in the center of the lattice, as confirmed by the TGA measurement of the VHCF powder (**Figure 5.2f**), or bound to the transition metal.[273] In addition, the presence of vanadium as vanadyl, VO^{2+}, in the lattice also contributes to the total oxygen content. The V/Fe ratio of 1.7 indicates a presence of the higher number of $Fe(CN)_6$ vacancies in the lattices or the presence of interstitial vanadyl ions, as hypothesized earlier in a work that reported a V/Fe ratio of 1.5 for a thin film electrode.[270] A similar trend in the elemental content of the VHCF powder was obtained by EDS measurements (**Figure S 5.2**). According to this result, carbon and nitrogen were the most-abundant elements, the V/Fe ratio was 1.61, comparable to the ratio obtained from XPS, indicating the similar elemental composition in the bulk and on the surface of the particles, and sodium, only detected by EDS, was the least-abundant element. The amount of iron was $1/6^{th}$ of both carbon and nitrogen, which can be attributed to the $Fe(CN)_6$ moieties in the lattice. A Fourier transform infrared (FTIR) spectrum, presented in **Figure 5.2e**, highlights the molecular vibrations in the VHCF lattice. The transmission peaks around 2090, 2165, and 440-520 cm^{-1} correspond to the characteristic stretching vibration of −Fe(II)−C≡N−, −Fe(III)−C≡N−, and −M−C− bonds, respectively, as reported elsewhere.[273–276] These peaks also prove the presence of both Fe(II) and Fe(III) in the as-prepared VHCF particles, as reported earlier.[277] This feature of the VHCF particles is also seen in narrow XPS scan of Fe, as shown in **Figure S 5.4**. The V=O stretching was observed at 978 cm^{-1}, in line with literature for vanadyl ions.[104,271] The broad peak around 3300 cm^{-1} and the sharp peak around 1600 cm^{-1} can be attributed to the zeolitic and coordinated water present in the VHCF lattice, respectively.[104] The FTIR spectrum of the prepared VHCF powder is comparable to that of the NiHCF, with the only exception of −M−C stretching, confirming the analogous nature of VHCF and NiHCF PBAs. Finally, the result of the thermogravimetric analysis (TGA) of the VHCF powder is provided and compared with that of NiHCF powder in **Figure 5.2f**. Weight loss was observed in three regimes. The first regime starts from 100 °C, indicating a weight loss of 22 % related to the loss of structural water, as indicated by the IR transmission peaks and the presence of extra oxygen in the XPS analysis of the VHCF powder. This is lower than the amount seen in NiHCF (≈ 30 %). The second and third regimes are associated with the evolution of HCN (180 – 280 °C) and decomposition of the electrode (> 300 °C), similar to the reports in literature.[277]

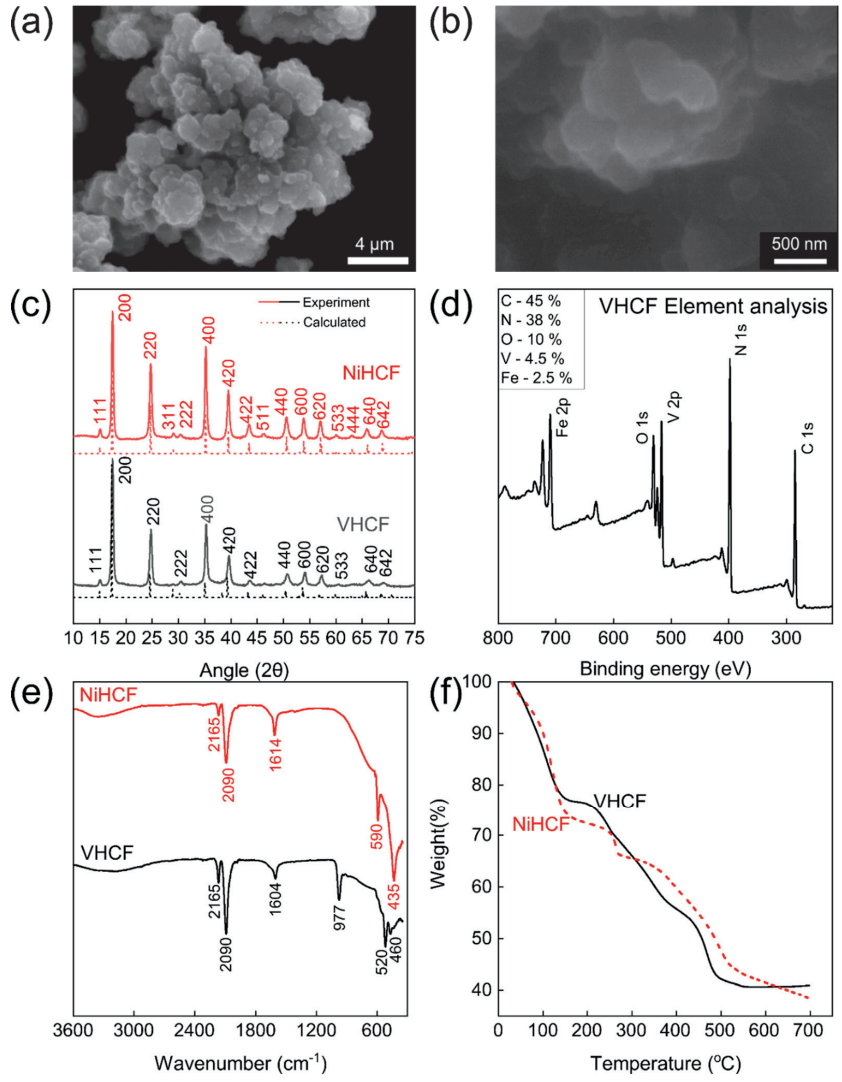

Figure 5.2: Characterization of the VHCF powder synthesized via a bulk co-precipitation reaction. Data for NiHCF, prepared via a similar co-precipitation method detailed elsewhere,[91] is also provided along with VHCF for comparison. **(a)** & **(b)** SEM images of VHCF powder obtained at 4,500× and 22,000× magnifications. **(c)** Measured (solid lines) XRD patterns of as-prepared VHCF (black) powder and NiHCF (red) powder and the predicted (dashed lines) XRD peaks from the $DFT_{crystal}$ models with labelled characteristic planes. **(d)** A wide XPS spectrum indicating the elements and their ratios in the VHCF powder. **(e)** IR spectra of the VHCF (black) powder compared with that of NiHCF (red) powder with labelled characteristic stretching. **(f)** TGA spectra of the VHCF (black) powder compared with that of the NiHCF (red) powder.

4.3.2 Electrochemical characterization of electrodes

The VHCF electrodes were electrochemically characterized by cyclic voltammetry (CV). Such characterization is crucial as (i) it provides insight into the redox activity of the electrode, associated here with cation intercalation, and (ii) it indicates the affinity of the electrode towards different ions.[100]

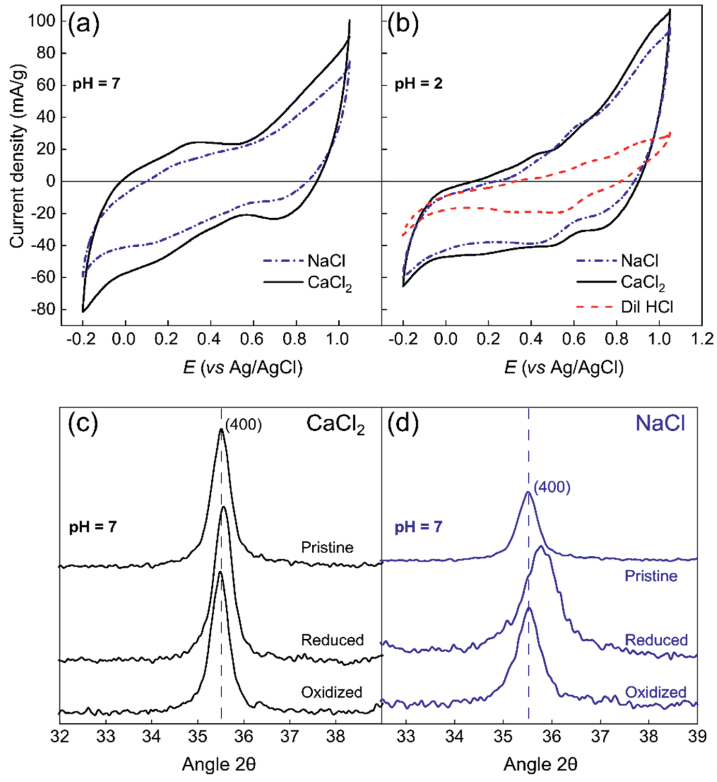

Figure 5.3: Electrochemical characterization of VHCF electrodes in a three-electrode cell by cyclic voltammetry in single-salt solutions of NaCl and $CaCl_2$ at **(a)** pH = 7 and **(b)** pH = 2, obtained at a scan rate of 1 mV/s. The voltammogram obtained in diluted HCl solution (pH = 2) is given by the red curve in panel. **(b)** The post-mortem XRD patterns comparing the (400) plane peak of the VHCF lattice in pristine electrode with the oxidized, and reduced electrodes cycled in **(c)** $CaCl_2$ and **(d)** NaCl solution under neutral pH conditions.

The voltammograms of VHCF electrodes, carried out in single-salt solutions of NaCl and $CaCl_2$ at two different pH of 2 and 7, are shown in **Figure 5.3a** and **b**. The voltammogram of $MgCl_2$ at pH = 2 is given in **Figure S 5.5**. For a neutral feed solution with pH = 7, the VHCF electrodes exhibited a higher capacity in $CaCl_2$ in comparison to NaCl, evident from the area enclosed by the respective voltammograms in panel **(a)** (25.4 ± 0.3 C/g_{VHCF} in NaCl *vs.* 42.8 C/g_{VHCF} in $CaCl_2$ solution). Interestingly, at pH = 2 the areas enclosed by the voltammograms of NaCl and $CaCl_2$,

as shown in panel **b**, increase to 38.2 ± 1.3 and 52.2 ± 1.7 C/g_{VHCF}, respectively. Interestingly, the reduction in pH increased the redox activity of the VHCF electrode resulting in more pronounced and distinct oxidation and reduction peaks related to (de)intercalation of Na^+ and Ca^{2+} in the lattice. This is, to the best of our knowledge, the first proof of the intercalation of any divalent ion in VHCF lattice at neutral and low pH. It also demonstrates a reliable operation of the electrodes at low pH, commonly encountered during recycling of metals in real-life applications. Furthermore, the voltammograms shown in **Figure 5.3b** give the first indication towards the relative preference of VHCF electrode towards divalent Ca^{2+} at $E_{red} \approx$ 0.55 V, against monovalent Na^+ ions, with $E_{red} \approx 0.4$ V *vs.* Ag/AgCl. A higher intercalation potential for the divalent ions indicates easier intercalation: after the deintercalation process, the ions with more positive reaction potential will be intercalated first. This voltammogram hints at the higher affinity of the VHCF electrodes towards divalent ions. The redox peaks which appear at pH = 2 cannot be due to extra H^+ (de)intercalation, as they remain absent from the voltammogram obtained in a dilute HCl solution that contains neither Na^+ nor Ca^{2+}. This implies that in the salt-containing solutions, Na^+ and Ca^{2+} remain the prominent adsorbing ions. The voltammograms presented in **Figure 5.3a** and **b** for NaCl differ from those previously reported in the literature for VHCF; for instance, the peak positions and the number of oxidation and reduction peaks.[104,270,271] These differences can be attributed to either (i) the type of electrode: thin film (order of 10 nm – seen in literature[270]) *vs.* sheet electrodes (200 – 300 μm- used in this study) or (ii) the CV conditions – acidic electrolytes (acid concentration > 3 M in literature) *vs.* neutral to mild acidic (pH = 2 - 7 electrolyte used here). Since – as mentioned earlier – this is the first time that divalent cations have been inserted into the lattice of VHCF, no such comparison can be made with literature for Ca ions.

Other than the CV peaks, the proof of insertion of both mono- and divalent cations into the lattice is provided by the post-mortem XRD of VHCF electrodes cycled in $CaCl_2$ and NaCl, as shown in **Figure 5.3c** and **d**, respectively. A closer look at the diffraction pattern of Ca^{2+} indicates a positive shift in the position of the (400) peak during intercalation (reduction of Fe^{3+} to Fe^{2+}) of Ca^{2+} from 35.53° for the pristine electrodes to 35.58° for the reduced electrodes, indicating a contraction of the lattice. The exact direction of contraction and expansion will depend on the lattice symmetry. During deintercalation (oxidization of Fe^{2+} to Fe^{3+}) of Ca^{2+}, the (400) peak shifts rather clearly to a lower angle of 35.48°, indicating an expansion of the lattice. A total change of 0.1° was obtained between VHCF electrodes, fully intercalated and deintercalated in $CaCl_2$ electrolyte. Remarkably, a similar contraction and expansion of the lattice during (de)intercalation, as presented here for VHCF electrodes, has been reported for Na^+ in NiHCF electrodes with a comparable difference in peak positions between the oxidized and the reduced electrode.[269] Similarly, the (400) peak shows a strong positive shift from 35.53° to 35.78° following the intercalation (reduction of Fe^{3+} to Fe^{2+}) of Na^+ into the lattice while the deintercalation of Na^+ (oxidization of Fe^{2+} to Fe^{3+}) brings the (400) peak back to the original position, as obtained for the pristine electrode. These observations support the inference that the VHCF electrodes, as prepared in this study, can store ions in their interstitial sites via

intercalation, like other PBAs, from a feed solution. The counter-intuitive expansion and contraction of the lattice following its deintercalation and intercalation, respectively, is characteristic of the PBAs and has been reported and explained in literature before.[86,278] For VHCF, the lattice contracts more during insertion of Na^+ in comparison to Ca^{2+}. This would indicate a higher strain for the (de)intercalation of Na^+ than that of Ca^{2+}, making it less attractive for the VHCF electrode. This observation is similar to the higher lattice strain associated with Na^+ (de)intercalation, in comparison to K^+, in a copper hexacyanoferrate (CuHCF) lattice which prefers K^+ over Na^+.[279]

4.3.3 Selective ion separation

The CV and post-mortem XRD analysis, although insightful, only provide an indication of the different affinity of the VHCF electrodes towards mono- and divalent ions. A more direct understanding of the selective ion separation was obtained by treating multivalent ion feeds **F1 – F3** with a hybrid CDI cell containing VHCF sheet electrodes as a cathode and activated carbon as anode, as shown in **Figure 5.1**. The concentrations of the feeds **F1 – F4** are given in **Table 5.1.** The feeds were either binary or ternary mixtures of monovalent alkali metal and divalent alkali earth metal ions. The concentration profiles of the dilute reservoirs containing Li, Na, Ca, and Mg ions are shown in **Figure S 5.6** and the concentration differences calculated during multiple adsorption steps for each cation is presented in **Figure 5.4**. It is clear from the four panels that among the ions tested here, VHCF electrodes prefer divalent ions over monovalent ions. This implies that the larger (hydrated) divalent Ca and Mg ions were preferentially absorbed over smaller (hydrated) monovalent Li and Na ions. This preference, or selectivity, can be quantified in terms of a separation factor[11,106,148], β, calculated as

$$\beta_{1/2} = \left(\frac{c_{1,\text{initial}} - c_{1,\text{final}}}{c_{2,\text{initial}} - c_{2,\text{final}}}\right)\left(\frac{c_{2,\text{initial}}}{c_{1,\text{initial}}}\right) \tag{5.1}$$

where 1 is the target ion, 2 is the competitive ion, $c_{1,\text{initial}}$, $c_{1,\text{final}}$, $c_{2,\text{initial}}$, and $c_{2,\text{final}}$ are the concentrations of the ions 1 and 2, respectively in the beginning and at the end of the intercalation step. The data presented in **Figure 5.4a** gives a $\beta_{Ca/Na}$ of ≈ 3.5, calculated for each pair of concentration differences and then averaged over the six absorption steps. This manifests as a difference in concentration profiles, as **Figure S 5.6a** shows, where in 7 adsorption steps, less than 30 % of the starting amount of Na^+ was removed while more than 50 % of Ca^{2+} was removed, clearly highlighting the preference of the VHCF ions. In **Figure 5.4a**, this is corroborated by the higher average Δc values for Ca^{2+} than Na^+. The average $\beta_{Ca/Na}$ value obtained here compares remarkably well with CDI – selectivity in the range of $2.5 < \beta_{Ca/Na} < 5.5$ was obtained with modified carbon electrodes.[3] In MCDI, where membranes are responsible for the selectivity, the values ranged between $3 < \beta_{Ca/Na} < 6$.[3] It must be pointed out that the $\beta_{Ca/Na} \approx 6$ was the highest and not the average value, performed with flow electrodes.[280]

The trend was maintained for the feed **F2**, as the divalent Mg^{2+} was removed more than the monovalent Na ions, as shown from the higher average Δc values for Mg^{2+} than Na^{+} in **Figure 5.4b**. However, the average $\beta_{Mg/Na}$ of 1.5 is lower than the $\beta_{Ca/Na}$. This may be attributed to the higher dehydration energy of Mg^{2+} (2000 kJ/mol) than Ca^{2+} (1600 kJ/mol),[281] which makes the intercalation of Mg^{2+} more difficult than that of Ca^{2+}.

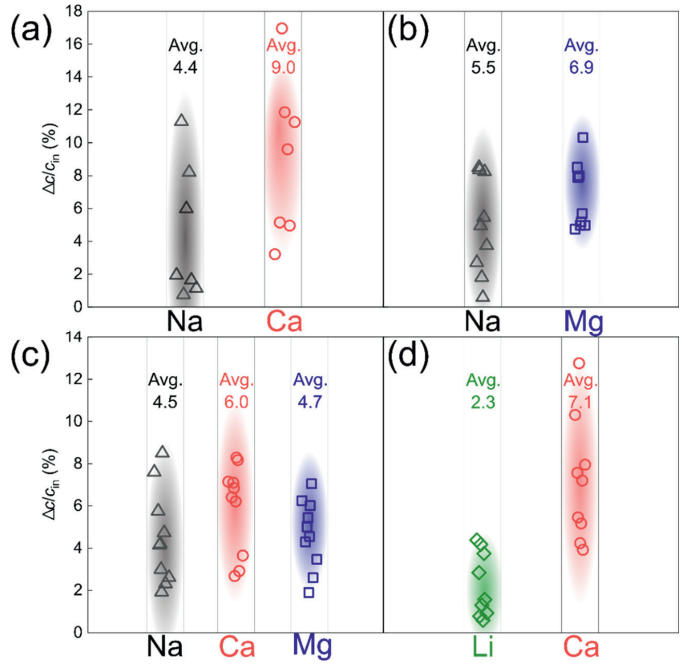

Figure 5.4: Change in cation concentration in the diluate relative to inlet concentration for feeds **(a) F1**, **(b) F2**, **(c) F3**, and **(d) F4** after each adsorption cycle. The pH of the feed solutions is given in **Table 5.1**.

This also becomes clear from **Figure 5.4c** where all three ions were present in one mixture. Clearly, divalent ions (Ca and Mg) together were adsorbed more than the monovalent Na^{+}. This contrasts with the affinity demonstrated by NiHCF, which shows high selectivity towards monovalent ions,[11] even though it has similar physical properties as VHCF, as described in **Section 5.3.1**. It is suggested that between the ions of the same valence, the selective separation is based on the dehydration energy of the ions. However, when ions of two different valences are present, the VHCF electrodes prefer divalent over monovalent ions. This is further supported by the result in **Figure 5.4d** where a further increase in the dehydration energy of the monovalent ion (from Na^{+} to Li^{+}) results in its increased rejection, apparent in the higher difference between the Δc values of Li^{+} and Ca^{2+} and the increased $\beta_{Ca/Li} \approx 4.5$. This becomes clearer in the concentration profile, given in **Figure S 5.6d**, where in seven intercalation steps, less than 20 % of Li^{+} was adsorbed while more than 50 % of Ca^{2+} was adsorbed by the VHCF electrode.

The DFT calculations paint a similar picture on ion-selectivity with VHCF electrodes to the experiments (**Figure 5.5**). For comparison, calculations on the intercalation in NiHCF electrodes were also studied. It is clear from **Figure 5.5a** that the intercalation of monovalent Na^+ into a NiHCF unit cell is thermodynamically more favorable than the divalent Ca^{2+}. The absorption energy for Na^+ (ΔE_{Na}) stabilized in the interstitial site of NiHCF was calculated to be −4.17 eV, while it was −3.72 eV for Ca^{2+} (ΔE_{Ca}), indicating a stronger interaction between Na^+ and NiHCF and the preference of the NiHCF towards Na^+ over Ca^{2+}. This observation is consistent with what has already been reported for experiments in literature about NiHCF electrodes in CDI.[11] In contrast, the intercalation of Ca^{2+} into a VHCF unit cell results in calculated absorption energy of −7.08 eV, indicating a stronger affinity of VHCF towards Ca^{2+} compared to the intercalation of Na^+ into the same lattice, of which the absorption energy was found to be −4.02 eV, as shown in **Figure 5.5b**. This result shows the opposite preference of the VHCF lattice towards divalent Ca^{2+} in comparison to the NiHCF lattice. Comparison of the absorption energies of Ca^{2+} into the lattices of NiHCF and VHCF reveals that the ΔE_{Ca} is larger for VHCF (−7.08 eV) than that for NiHCF (−3.72 eV). This implies that the Ca^{2+} is accommodated better in VHCF than NiHCF and will, therefore, be more likely to be preferred by the VHCF lattice.

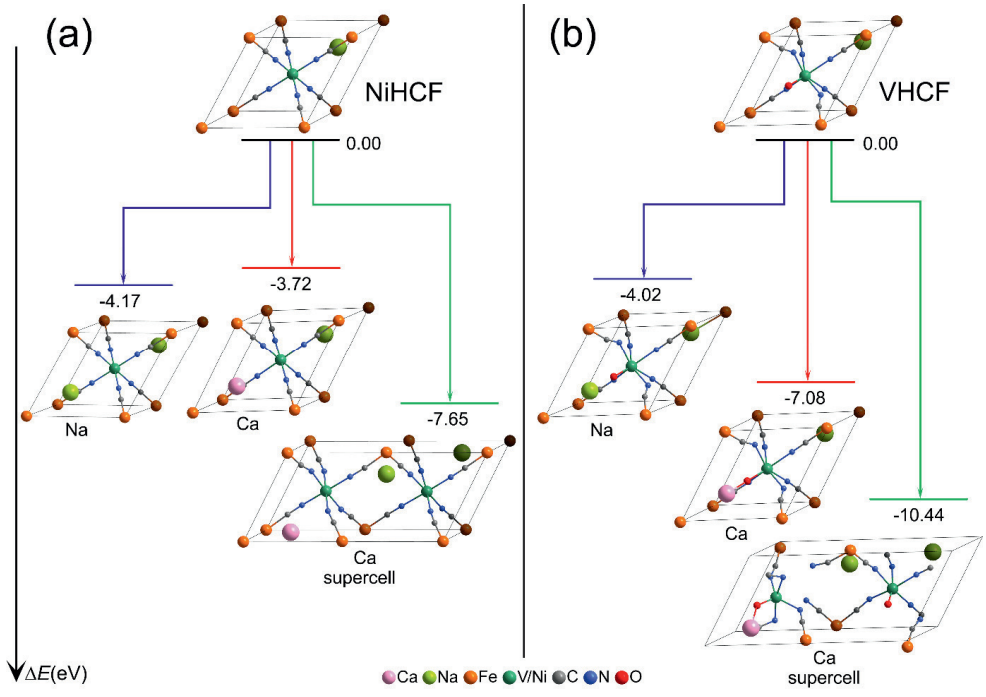

Figure 5.5: Results of DFT simulations performed to calculate the change in the energy of a unit cell and a 2×1×1 supercell, that is a combination of two unit cells of **(a)** NiHCF and **(b)** VHCF following absorption/intercalation of Na^+ and Ca^{2+} into the interstitial site.

This preference holds for both: a single unit cell where the $(V{=}O)^{2+}$ and the Fe^{3+} present in the lattice can, upon reduction, accommodate a divalent ion, according to the electrochemical reaction described by the expression of $Ca^{2+} + 2e^- + Na(VO)^{2+}Fe^{3+}(CN)_6 \leftrightarrows CaNa(VO)^{+}Fe^{2+}(CN)_6$. However, upon reduction, a 2×1×1 super cell is formed that is a combination of two unit cells. In this super cell structure, an intercalation of a divalent cation requires two Fe^{3+} per super cell to be reduced, according to the electrochemical reaction: $Ca^{2+} + 2e^- + (Na(VO)^{2+}Fe^{3+}(CN)_6)_2 \leftrightarrows Ca(Na(VO)^{2+}Fe^{2+}(CN)_6)_2$, as otherwise Ca^{2+} would need to be reduced, which is energetically highly unfavorable. Furthermore, the ΔE_{Ca} for the NiHCF and VHCF supercells were calculated to be −7.65 eV and −10.44 eV, respectively, making it evident that Ca^{2+} is the preferred cation for intercalation in VHCF over NiHCF. It can be argued, on the basis of similar ΔE_{Na} values for NiHCF and VHCF (−4.17 eV vs −4.02 eV, respectively), that the replacement of Ni with a V=O group has little influence on the intercalation of the monovalent Na^+, but a drastic influence on the intercalation of divalent Ca^{2+}, which is evident from the significant difference between ΔE_{Ca} values for NiHCF and VHCF, as presented in **Figure 5.5a** and **b** (−3.72 eV vs −7.08 eV for a unit cell, and −7.65 eV vs −10.44 eV for a supercell). In view of these predictions, it is proposed that the O atom in the interstitial lattice of VHCF may have a higher coulombic attraction with the divalent Ca^{2+} than the monovalent Na^+, leading to the switched preference of the VHCF lattice and a larger ΔE_{Ca}. However, this remains a hypothesis, and a further combination of experiments and simulations will be required to elucidate the exact selectivity mechanism in the VHCF lattice. Results from the calculation of the absorption energies of hydrated Na^+ and Ca^{2+} are summarized in the supporting information (**Figure S5.7**). The model again predicted that the intercalation of the hydrated Ca^{2+} in the lattice of VHCF is thermodynamically favorable over that of the hydrated Na^+. However, the hydration model also predicted slightly easier intercalation of Ca^{2+} into the NiHCF lattice, as can be seen by the ΔE_{Ca} and ΔE_{Na} numbers. This discrepancy could be because such simplified hydration models are not accurate enough to describe the solvent structures.[268]

4.3.4 Electrode stability

The long-term stability of the electrode was assessed by operating the hybrid CDI cell, containing the VHCF electrode in NaCl and $CaCl_2$ single salt solutions for 40 charge/discharge cycles, in a constant-voltage mode. A sample $CaCl_2$ concentration profile, along with the current, is presented in **Figure S 5.8a,** and the post-mortem XRD analysis of the oxidized electrodes, obtained after operation for 40 cycles in NaCl and $CaCl_2$, are provided in **Figure 5.6**. Nearly all the planes present initially in the pristine electrode were preserved after 40 charge/discharge cycles, demonstrating that the structural integrity of the VHCF lattice remained intact after the repeated (de)intercalation of both Na^+ and Ca^{2+}. Furthermore, a comparison of the position of the (400) peak in the X-ray diffractogram of the pristine electrode with that of the electrodes cycled in NaCl, and $CaCl_2$ shows that the lattice contracted after

cycling in NaCl, while remaining nearly the same after cycling in $CaCl_2$, indicating the smaller change in the lattice following Ca^{2+} (de)intercalation.

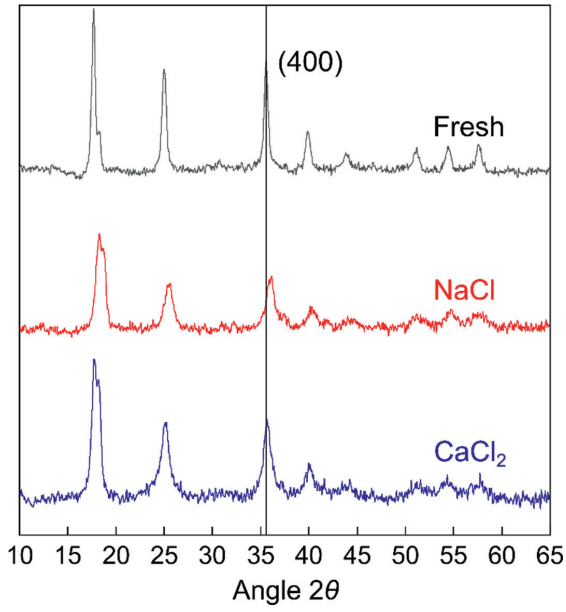

Figure 5.6: The XRD pattern of the pristine electrode before (black) and after 40 cycles in 20 mM single-salt solutions of NaCl (red) and $CaCl_2$ (blue). The (400) peak is marked by a straight vertical line.

During the long-term cycling experiments with bare VHCF electrodes, it was observed that in the absorption step of the desalination process, a part of the VHCF electrode degraded and dissolved into the treated solution. In more detail, the degradation was observed by the change in the color of the diluate to yellow, indicating that iron hexacyanoferrate had leached into the diluate. It can be attributed to the experimental conditions such as low electrolyte concentration (~ 20 mM) and neutral pH implemented in this study, against the high concentrations (1 M) and low pH (<1) as frequently used in literature[85,104] that can affect the stability of the electrodes.[108] This degradation is also reflected in the reduced capacity of the electrode to adsorb Ca^{2+} with the increasing number of cycles, and in the charge efficiency (Λ) values, as shown in **Figure S 5.8c.** The Λ values, calculated as the ratio of the ions adsorbed (in coulombs) and the charge input in one half cycle, gradually reduced with time, indicating electrode degradation. To prevent the leaching of the electrode into the treated water, an electro-polymerization of PSS-doped PPy conductive polymer, PPy/PSS, was carried out on the surface of the VHCF electrodes, inspired by the use of PPy as a protection against corrosion in metals.[282] A schematic that illustrates the coating, its structure and electrodeposition, is shown in **Figure 5.7a.** During the oxidation of pyrrole moieties in the polymer formation of PPy, their positive charge is counterbalanced by the negative charge of the PSS. During the reduction of the pyrrole moieties, however, PSS is

trapped in between the PPy, and thus, its negative charge will now need to be counterbalanced by the cations present in the solution. So, by doping the PPy with PSS, an anion exchanger was converted into a cation exchanger, matching the property of the VHCF electrodes.

A cyclic voltammogram of VHCF electrode, obtained in a 1 M $CaCl_2$ solution at pH = 7 is provided in **Figure 5.7b**. The VHCF electrode remained electrochemically unchanged after the electro-polymerization step, which is evident from the voltammogram (**Figure 5.7b**). The conductive polymeric layer did not contribute to any reversible/irreversible reactions during the oxidation as well as the reduction step; the area enclosed by the voltammogram was 40 mC/g_{VHCF}, comparable to values obtained for bare VHCF electrodes. A CV, performed in $CaCl_2$ on a graphite paper coated only with the PPy/PSS, shows no reaction peaks during the oxidation and the reduction steps (**Figure S 5.9**). This confirms that the PPy/PSS coating did not interfere with the preference of the electrode towards divalent ions, as shown in **Figure 5.7c**. When feed **F1** was treated with PPy/PSS-coated VHCF, the resulting cation concentrations in the diluate were like those obtained with bare VHCF electrodes (**Figure 5.4a**). The coated VHCF electrodes reduced the Ca^{2+} concentration by more than 50 % while removing less than 30 % of the Na^{+} in that same time. A sample concentration and current profile obtained from the desalination of 20 mM $CaCl_2$ feed with PPy/PSS-coated VHCF electrode is presented in **Figure S 5.8b**. The concentration profile shows improvement in calcium absorption, as confirmed by the calcium intake by the cathode, shown in **Figure S 5.8c**. However, after 25 cycles, the coated electrodes show a capacity fade. For bare electrodes, this happens after 20 cycles. **Figure 5.7d** shows the comparison between the UV-VIS spectrum of the fresh feed **F1** and the diluate produced after the selectivity experiments performed on feed **F1** using the bare VHCF (black curve) and the PPy/PSS coated VHCF electrodes (red curve). As expected, the fresh solution remained free of any iron impurity. The diluate produced after treatment with bare VHCF electrodes gave a strong absorption peak at ≈ 420 nm, confirming the presence of a $[Fe(CN)_6]^{3-}$ group in it.[283] This points to electrode degradation during intercalation. Lattices that lose a $[Fe(CN)_6]^{3-}$ unit will not undergo a reduction (intercalation), since the Fe^{3+} atom is removed from it, and as a result, the overall capacity of the electrode will decrease. The electrode degraded foremost in the beginning and then became stable after 4 cycles, as seen in the UV-VIS absorption spectra that converged at the same concentration level. A further look at the UV-VIS absorption spectra reveals that the PPy/PSS layer prevented the leaching of the $[Fe(CN)_6]^{3-}$ and kept its concentration significantly lower in the diluate, when compared with that for the bare VHCF electrode. In addition, no PPY was detected in the diluate. So, while the PPy/PSS was successful in preventing the contamination of the treated stream, its effect on preventing electrode degradation requires further improvement.

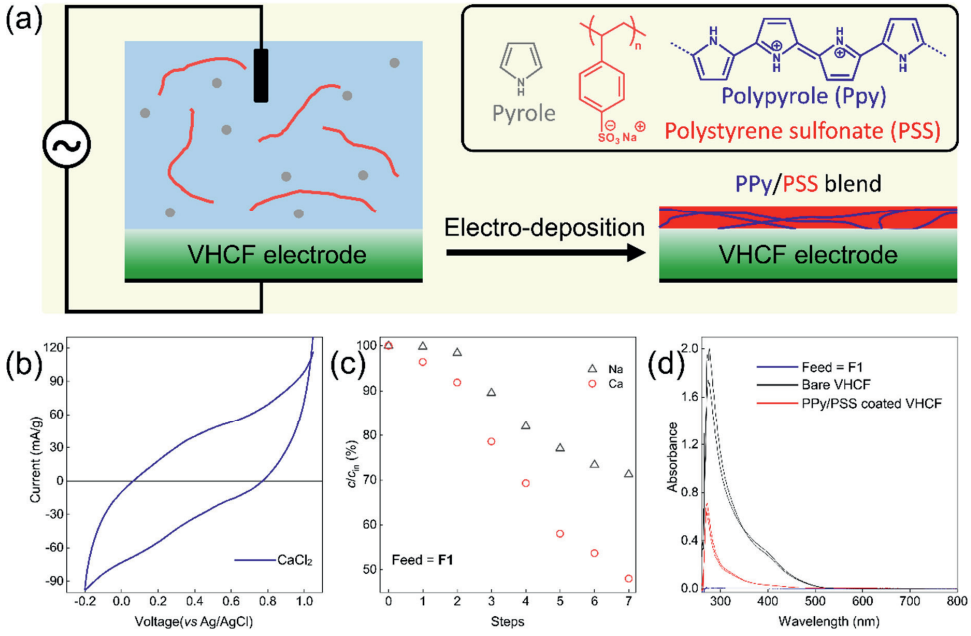

Figure 5.7: Enhanced stability of the VHCF electrodes by a protective layer of PSS-doped PPy on its surface. **(a)** Schematic of the VHCF electrodeposition with the conductive polymeric coating. **(b)** Cyclic voltammogram of the PPy/PSS coated VHCF electrode, obtained from CV performed in 1M $CaCl_2$ electrolyte at a scan rate of 1 mV/s. **(c)** Concentration of Na^+ and Ca^{2+} in the diluate reservoir prior to the treatment of feed **F1** by the hybrid cell containing PPy/PSS coated VHCF cathode and an activated carbon anode. **(d)** A UV-VIS spectra of the fresh feed **F1** (blue), the diluate treated by hybrid cell containing a bare VHCF electrode (black), and the diluate treated by a hybrid cell containing a PPy/PSS coated VHCF electrode (red).

Finally, as a check to establish that the PSS ion is held inside the PPy, and is not released into the treated solution, a bare piece of graphite (*i.e.*, without the VHCF electrode), electropolymerized with PPy/PSS was analyzed in XPS, after reduction and oxidation steps, as shown in **Figure S 5.10**. The nitrogen/sulphur ratio, representative of the PPy/PSS, was similar for both the oxidized as well as the reduced sample of PPy/PSS coated graphite plate, with a value of ≈ 1.7 for the oxidized and ≈ 1.5 for the reduced sample, indicating the stability of the layer. This provides a simple and elegant solution to the issue of feed contamination by electrode degradation.

4.4 Conclusion

The substitution of nickel with vanadium in the lattice of a Prussian blue analogue (PBA) switches its preference in CDI experiments from monovalent ions towards divalent ions. This finding provides the first correlation between the substituent transition metal ion in a PBA and

the preference of the resulting PBA towards different ions and opens vast possibilities for tuning PBA selectivity according to the desired application, within the framework of ion-selective CDI. A simple co-precipitation method was used to prepare VHCF with crystals of quality on par with those presented in the literature. In addition, divalent ions were selectively inserted into the VHCF lattice for the first time, proof of which was obtained by cyclic voltammetry, X-ray diffraction, and ion adsorption experiments. Furthermore, intercalation of cations was studied via DFT simulations, and the preliminary results indicated a preference of VHCF towards divalent ions, in contrast to what is usually observed for PBAs, likely resulting from the presence of an adjacent oxygen atom in the lattice. Finally, a simple solution to prevent leaching of the electrode into the treated water was provided by electro-polymerizing a conducting polymer poly-pyrrole, doped with poly-styrenesulphonate (PPy/PSS) on its surface, essentially cutting off the direct contact with the feed solution. This layer, as shown in this work, does not alter the characteristics of the VHCF electrode in any significant way, and effectively prevents the contamination of treated water due to electrode degradation, which has frequently been encountered in CDI with PBAs.

Supporting information

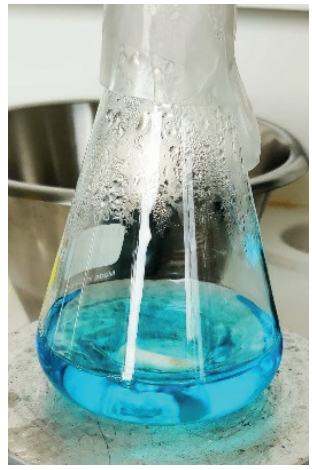

Figure S 5.1: Starting precursor solution, containing vanadium as V(IV), confirmed by the blue colour.

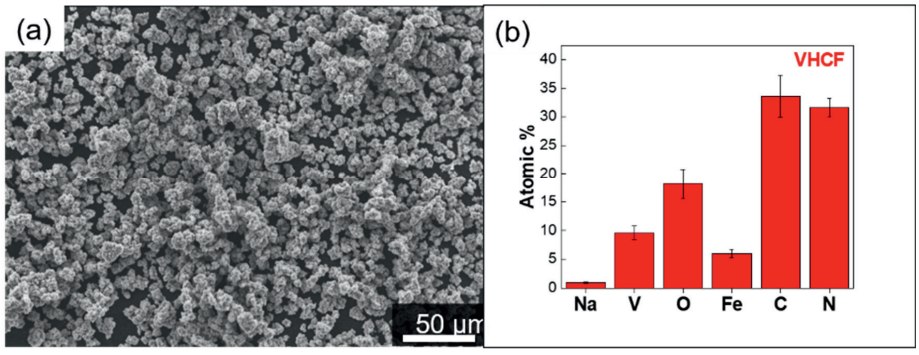

Figure S 5.2: Physical characterization of the VHCF particle chemical composition shown in the SEM image (a) SEM and (b) EDS cumulative mapping of the *e.g.* 5 areas demonstrating high C, N, O and V content.

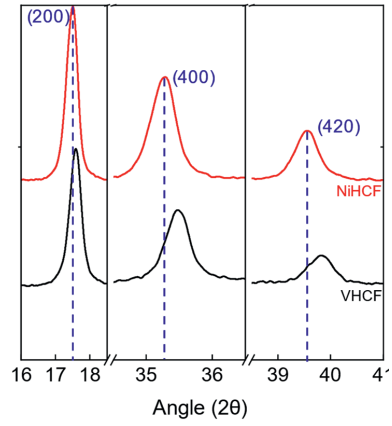

Figure S 5.3: XRD diffractograms of the NiHCF (red) and VHCF (black) powders, showing the (200), (400) and (420) plane peaks.

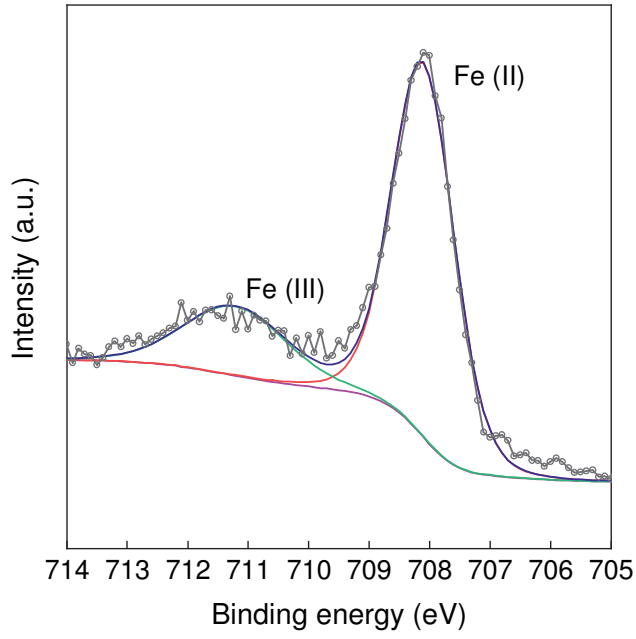

Figure S5.4: XPS spectrum of VHCF electrode showing the Fe $2p_{3/2}$ transitions for Fe(II) and Fe(III) ions present in the lattice.

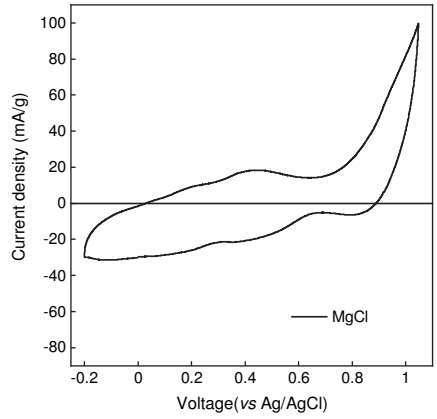

Figure S 5.5: Electrochemical characterization of VHCF electrodes in a three-electrode cell by cyclic voltammetry in a single-salt solution of $MgCl_2$ at pH = 2, obtained at a scan rate of 1 mV/s.

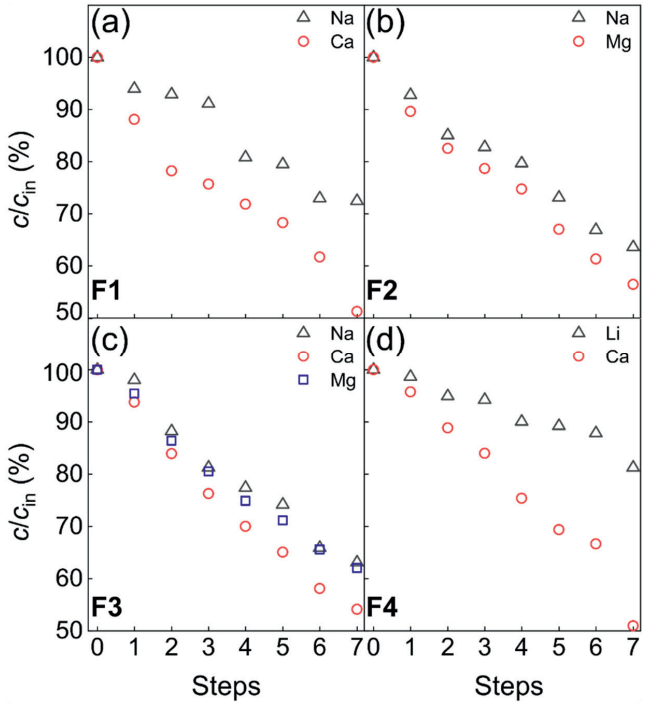

Figure S 5.6: Ion concentration in the diluate reservoir containing feed **(a) F1**, **(b) F2**, **(c) F3**, and **(d) F4** as a function of absorption steps. The feed solutions were at neutral pH.

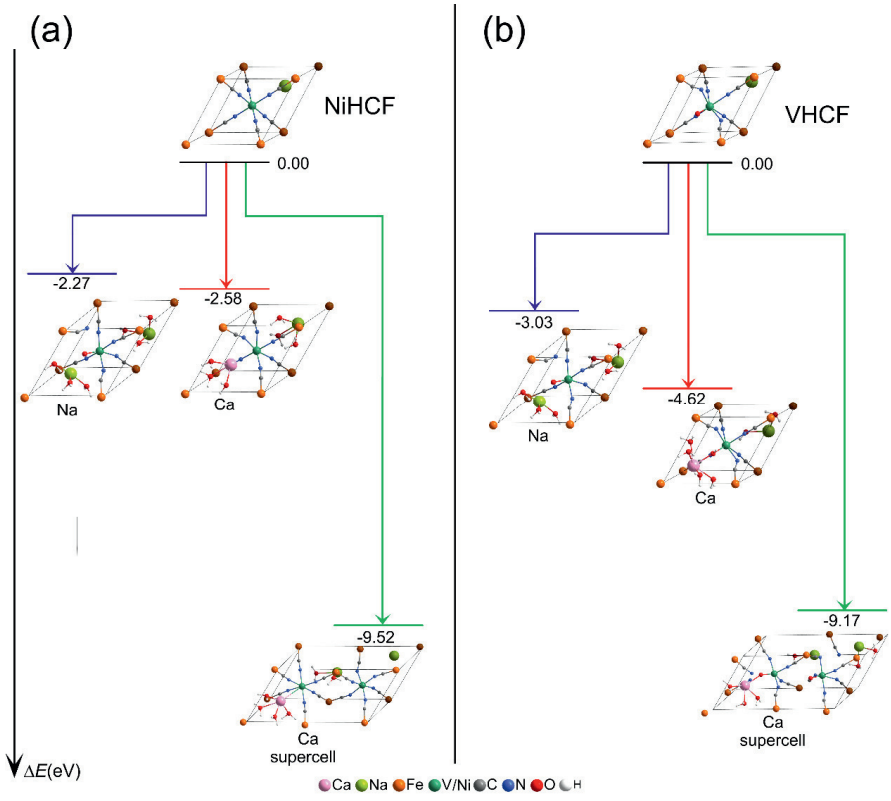

Figure S 5.7: DFT calculated adsorption energy for the hydrated Na and Ca ions in the interstitial space of **(a)** NiHCF and **(b)** VHCF, respectively.

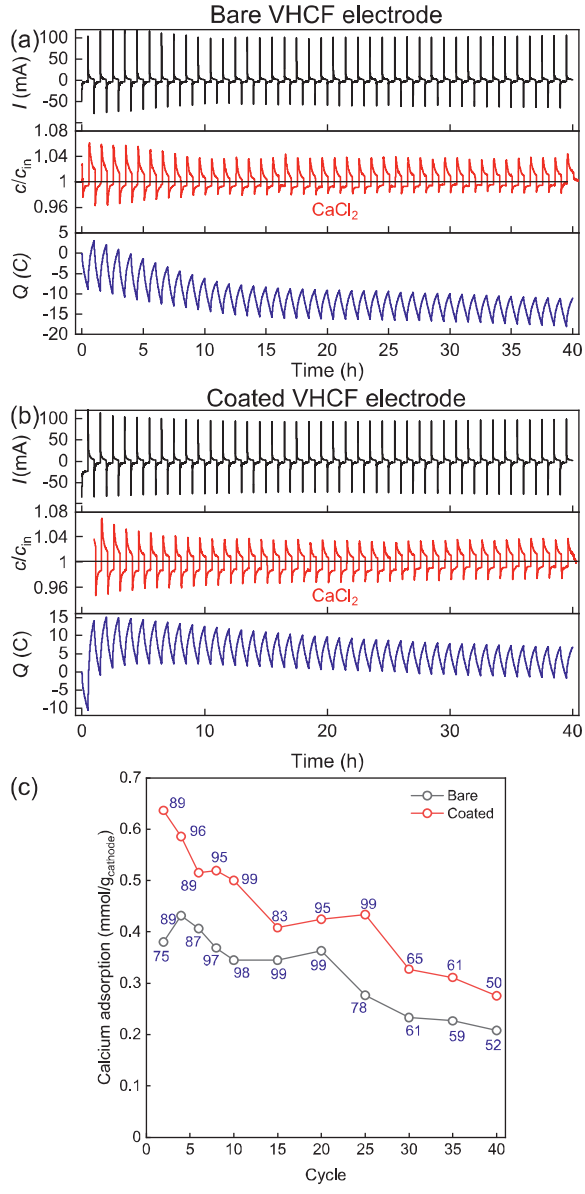

Figure S 5.8: Current and concentration profiles obtained during long term cycling of **(a)** bare VHCF electrodes and **(b)** PPy/PSS-coated VHCF electrode in 20 mM $CaCl_2$ solution under constant voltage (±1 V) operation. **(c)** Calcium adsorbed (mmol-Ca/g-cathode) as a function of ion adsorption cycle. The values in blue are charge efficiencies in %.

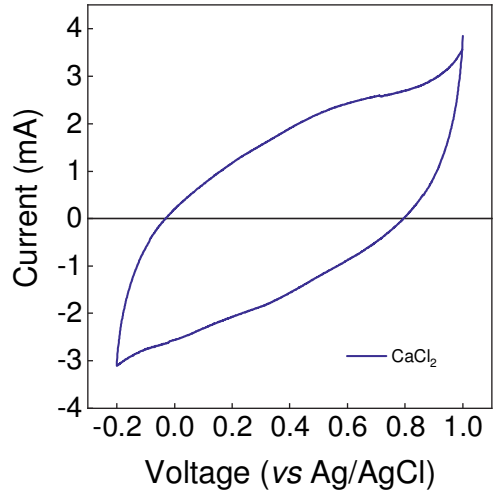

Figure S 5.9: Cyclic voltammogram obtained for a PPy/PSS-coated graphite plate, performed in 1 M $CaCl_2$ solution at a scan rate of 1 mV/s.

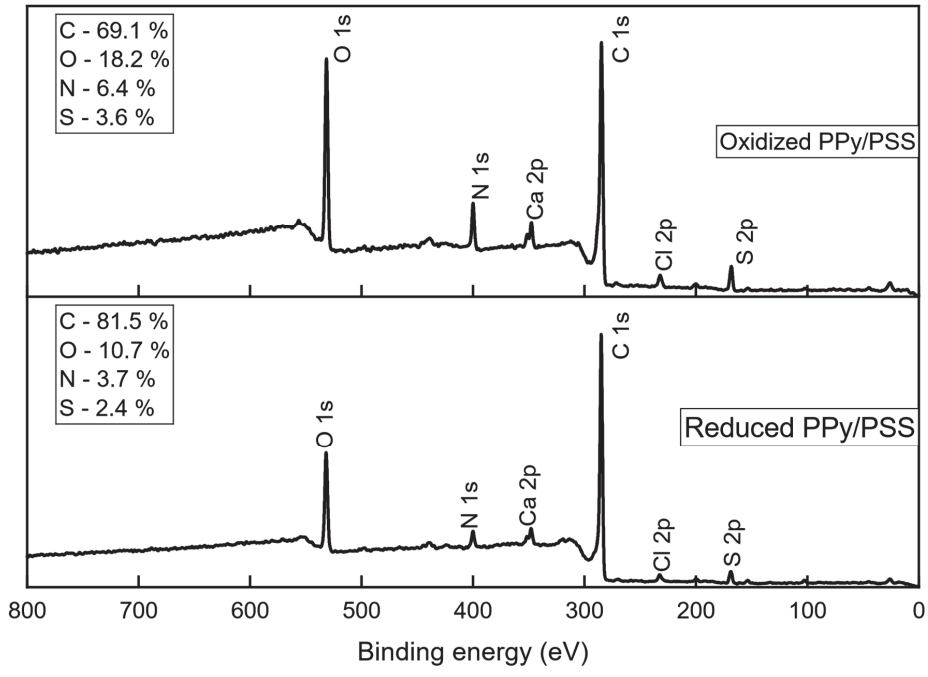

Figure S 5.10: XPS spectra of oxidized and reduced PPy/PSS layer on graphite, cycled in $CaCl_2$ solution.

6 Simultaneous, Monovalent Ion Selectivity with Polyelectrolyte Multilayers and Intercalation Electrodes in Capacitive Deionization

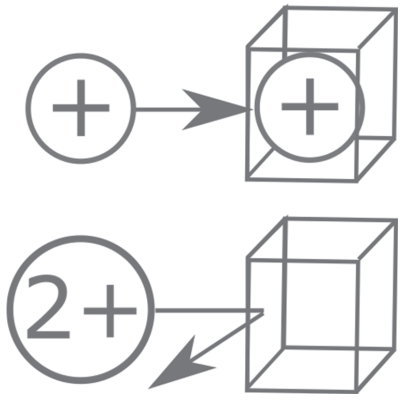

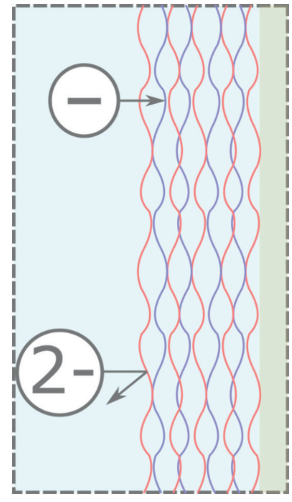

This chapter has been published as:

Singh, K., Sahin, S., Gamaethiralalage, J. G., Zornitta, R. L., & de Smet, L. C. P. M. (**2021**). Simultaneous, Monovalent Ion Selectivity with Polyelectrolyte Multilayers and Intercalation Electrodes in Capacitive Deionization. *Chemical Engineering Journal*, 128329.

Abstract

Selective ion separation via capacitive deionization (CDI) is of relevance because of its environmental and industrial applications in water purification and softening, heavy metal removal, and resource recovery. Conventionally, carbon electrodes and ion-selective membranes have been used for selective removal of anions and cations. In this study, we engineered a CDI cell with two identical NiHCF electrodes, separated by an anion-exchange membrane coated with a polyelectrolyte multilayer (PEM), for simultaneous and selective separation of monovalent over divalent anions and cations. The modified membrane rejects divalent over monovalent anions while the NiHCF electrodes selectively adsorb monovalent over divalent ions. A separation factor (β) of $7 < \beta < 14$ was obtained for Cl^- over SO_4^{2-}, while an average β of ≈ 17 was obtained for Na^+ over Mg^{2+}, reflecting the preference of the modified membrane and the electrodes, respectively. Moreover, this preference was preserved at low concentrations of monovalent ions as well. This tandem use of intercalation electrodes and a PEM membrane provides a new and facile method for simultaneous cation and anion selectivity in CDI, opening new avenues for enhanced and tunable separations from complex ion mixtures.

6.1 Introduction

Capacitive deionization, CDI, is a water desalination technique in which ions are removed from water under the influence of an applied current or a potential difference,[18,20,41] and stored in capacitive electrodes. CDI has been proven to be also applicable in selective ion removal and has been successfully used for cationic as well as anionic separations from aqueous ion mixtures.[3,11,106,234,284] Selective ion removal is necessary for various applications, including water softening,[10] recovery of resources such as lithium[285] or phosphate,[237] and treatment of irrigation water in greenhouses.[117]

Conventionally, due to the limited ion selectivity of the bare porous carbon[73], it has been typically used with either surface modifications[47,286,287] or coupled with ion-exchange membranes in (M)CDI,[288,289] to selectively separate both cations and anions. Alternative pathways to induce ion selectivity in CDI have recently been explored in literature.[3,11,290] On membrane level, special-grade commercial membranes, surface-modified ion-exchange membranes (IEMs), and selective resin coated carbon electrodes have been used for cation and anion selectivity.[34,139,291] Recently, a polyelectrolyte multilayer (PEM) modified cation-exchange membrane was used to obtain selectivity towards monovalent cation in MCDI.[290] This approach of coating PEMs[191,292,293] onto a membrane by a layer-by-layer (LbL) technique[294,295] is a facile and efficient method, and is based on alternating immersions of the membrane into oppositely charged polyelectrolyte solutions. The repeated action results in a thin multilayer whose thickness and composition can be controlled.[296] The final selectivity of a PEM-coated IEM depends on the type of the polyelectrolytes (PEs) used, the terminating layer, and the total number of layers deposited on the membrane surface.[250,297,298] A PEM can function as a selective layer via different mechanisms including electrostatic repulsion, also referred as charge exclusion,[250,299,300] and preferential transport of ions, based on their dehydration energy. [301] Thin films deposited via the LbL technique find use as functional materials and interfaces in various fields, including tissue engineering and capillary electrophoresis,[296] selective ion separation such as heavy metal removal, and anti-fouling applications.[31,302] PEMs have already been used in electro-driven systems, such as electrodialysis, to introduce and tune ion selectivity.[250,298,303] Thus, a PEM-modified membrane is promising for selective ion removal in CDI.

On the electrode level, intercalation materials have been successfully used for selective cation separations in CDI.[3,11,304] Prussian blue analogues (PBAs) are a subclass of intercalation materials[11,54,259] that store only cations in their interstitial lattice sites, unlike graphite, layered oxides, and carbides that can intercalate both cations and anions.[305] The intercalation of ions in PBAs is accompanied by the reduction of a redox-active element in the lattice. [82] These materials have found use in a variety of applications including energy storage,[173] brackish water desalination,[137] and selective ion removal.[11,106] Among all PBAs, nickel hexacyanoferrate, NiHCF, is among the most used intercalation electrode material in CDI[11,54,91] due to its ease of fabrication, non-toxic nature, high charge storage capacity, energy

efficiency,[91] and fast ion-adsorption kinetics.[244] Most importantly, NiHCF shows an inherent size-based selectivity towards monovalent cations[11,54,146] as it has demonstrated ≈ 20 times higher affinity towards Na^+ over Mg^{2+} and Ca^{2+}.[11] However, unlike carbon, NiHCF particles do not store anions in their lattice sites and therefore, their size-based selectivity excludes anions.

In this study, we introduce simultaneous cation and anion selectivity to a symmetric CDI system, assembled according to the rocking chair configuration,[56,109] by implementing measures at both the electrode and the membrane level. This was accomplished by integrating a PE**M**-**c**oated AE**M** (MCM) with two identical NiHCF electrodes in an electrode – membrane – electrode sandwich. Poly(diallyl dimethylammonium chloride) (PDADMAC) and poly(sodium 4-styrenesulfonate) (PSS) were chosen as polycation and polyanion, respectively, to prepare PEMs on an AEM surface via the LbL deposition because they are strong PEs in a wide range of the pH and the concentration of the salt solution. Also, they remain physically (under pressure)[306] and chemically (against oxidants)[307] stable and have been successfully used in ED for anion selectivity.[31] The schematic in **Figure 6.1a** depicts one half of the cell, representing the diluate chamber. The other half of this symmetric cell, depicted elsewhere,[109] undergoes a mirrored operation and produces a concentrated stream. The NiHCF electrodes selectively adsorb cations, based on their size, by storing them in interstitial lattice sites, as demonstrated elsewhere.[11] Simultaneously, the MCM selectively separates anions migrating from the diluate, providing an elegant, one-step configuration for both cation and anion selectivity. Furthermore, we also elucidate the effect of the number of layers coated onto the membrane, and the ionic content of the feed on selective anion separation.

6.2 Experimental Methods

Poly(diallyl dimethylammonium chloride) (PDADMAC, 20 % wt. H_2O), poly(sodium 4-styrenesulfonate) (PSS) sodium chloride (both from Sigma Aldrich) and hydrochloric acid (36.5 - 28.0 %, VWR) were used as received. Standard-grade (Neosepta ASE, Astom) and special-grade monovalent-selective (Neosepta ACS, Astom) AEMs were soaked in Milli-Q water (Milli-Q Integral 3 system, Millipore) for 48 h before use. The multilayer fabrication procedure was adopted from literature with some modifications.[290] Briefly, the standard-grade AEM was dipped in PSS and PDADMAC solutions, by a robotic arm (Dobot), prepared in Milli-Q water, alternately from solutions of 0.05 M polymer in 0.5 M NaCl at pH = 2.3 each for 20 min. After each layer deposition, the membrane was dipped in MQ water for 3 min to remove weakly attached polymers. The process was repeated until the desired number of layers, namely 5, 9, 10, 14, 15, 23, and 31 were reached. When the total number of layers coated onto the membrane surface was odd, a negatively charged PSS was the terminating PE, while the positively charged PDADMAC was the terminating PE when the total number of layers was even. The LbL coating workflow is illustrated in **Figure S 6.1**. Furthermore, the PEMs were coated onto model gold surfaces[290] (1 cm × 1 cm purchased from ECsens) and

characterized with X-ray photoelectron spectroscopy (XPS) and static water contact angle analysis (SWA), an approach similar to those of previous reports.[31,308]

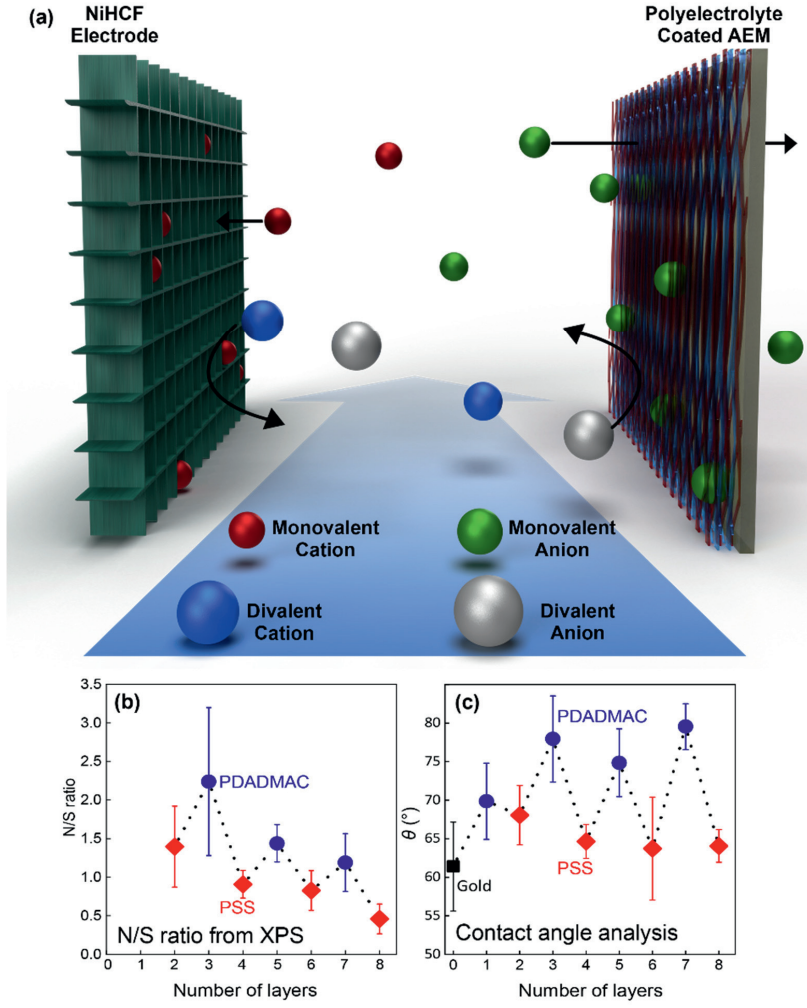

Figure 6.1: (a) Illustration of the cathodic chamber producing the diluate in the symmetric CDI cell, fully illustrated elsewhere,[109] with an NiHCF electrode and a PEM-coated AEM, separated by a flow channel containing a feed with multiple types of ions. Upon applying an electric current or a potential difference to the cell, the cations are driven towards the NiHCF electrode to the left and selectively stored in the lattices.[11] Simultaneously, the anions are selectively allowed to pass through the modified membrane on the right, resulting in a diluted feed in the middle. Surface characterization of the PEM with **(b)** XPS survey scans providing

the N/S ratio and **(c)** static water contact angle (θ) analyses as a function of the number of layers on the membrane surface.

The experimental details are described in the **Section 6 S.1** and **S.2** of the Supporting information, provided after the conclusion of this chapter.

The NiHCF active particles were synthesized via co-precipitation method.[11] Briefly, 24 mM and 12 mM solutions of $NiCl_2 \cdot 6H_2O$ (Alfa Aesar) and $Na_4[Fe(CN)_6] \cdot 10H_2O$ (Sigma-Aldrich), respectively, were added dropwise to the reaction solution (1 % v/v solution of HCl in water) and stirred at 600 rpm for ≈ 12 h. The product was washed three times with Milli-Q water during vacuum filtration and dried at 60 °C under vacuum. The dried powder was milled with conductive carbon black (Cabot) and mixed with polytetrafluoroethylene (PTFE) (Sigma Aldrich) in a weight ratio of 8:1:1, with ethanol as a solvent. The mixture was kneaded into a dough and cold-rolled with a stainless-steel rolling machine (MTI corp.) into 200 μm thick rectangular electrodes with 20 cm^2 area, weighing between 0.35 – 0.45 g. After the cold rolling, the electrodes were dried at 60 °C under vacuum.

Prior to cell assembly, two identical NiHCF electrodes were pre-treated in a three-electrode cell, with a platinum-coated titanium mesh counter, an Ag/AgCl electrode reference, and a 1 M Na_2SO_4 solution as an electrolyte. One electrode was saturated with Na^+, while the other was depleted, by discharging and charging them at 0 and 1 V *vs.* Ag/AgCl, respectively, for 1 h. After the pre-treatment, the electrodes were assembled into a cell, separated by nylon spacer channels (160 μm thick) and an MCM. Two identical 100 mL reservoirs containing feed solutions, whose compositions are provided in **Table 6.1**, fed the cell at a constant flow rate of 10 mL/min. The feed residence time in the cell was 4.3 seconds. The ion-selectivity experiments were performed with two types of feed solutions: one containing a mixture of mono- and divalent anions (**F1** and **F2**) and another containing a mixture of only monovalent anions (**F3** and **F4**), to respectively, provide an insight into the two frequently reported mechanisms of MCM selectivity based on charge exclusion [31] and dehydration energy of anions [34].

The ion-selectivity experiments were performed in a continuous desalination mode[11] during which the CDI cell was operated under constant voltage of ± 1 V via a potentiostat (Ivium n-stat, IVIUM Technologies). One complete desalination cycle consisted of two steps lasting 0.5 h each. During the first step, a voltage of 1 V was applied to the cell. After 0.5 h, 800 μL was taken from both the reservoirs. The anion concentration was analyzed via ion chromatography (Eco IC, Metrohm) while the cation concentration was analyzed via inductively coupled plasma optical emission spectroscopy (PerkinElmer Avio 500 ICP-OES). Next, the electrode polarities were reversed, and the diluate and the concentrate reservoirs were manually switched between the cell chambers, by switching the pipes connecting the reservoirs and the chambers. Following this, a voltage of –1 V was applied for 0.5 h after which, 800 μL was taken from both the reservoirs for concentration analysis. The end of this step concluded one full desalination cycle. The experimental workflow is illustrated in detail

in **Figure S 6.2**. A sample current-voltage profile of one desalination cycle is given in **Figure S 6.3**. The anionic selectivity of the MCM was investigated by varying the number of layers coated onto it and the type of ions in the feed solution. Since the cationic selectivity in symmetric cell with NiHCF electrodes was recently reported,[11] the experiments here focus mainly on the anionic selectivity of the MCM. The experiments were duplicated for reproducibility and the average values of the concentrations were used for selectivity calculations.

Table 6.1: Composition of the feed solutions (10 mM each) in the two chambers of the CDI cell with NiHCF electrodes separated by a MCM for ion selectivity experiments.

Feed number	Na^+ (mM)	NO_3^- (mM)	Cl^- (mM)	SO_4^{2-} (mM)	$H_2PO_4^-$ (mM)	Mg^{2+} (mM)
F1	10	--	10	10	--	10
F2	20	--	10	10	--	--
F3	20	--	10	--	10	--
F4	20	10	10	--	--	--

6.3 Results and Discussion

The chemical composition of the PEM-coated gold substrates was analyzed with XPS. The nitrogen/sulfur (N/S) ratio of the samples, provided in **Figure 6.1b**, shows an alternating trend with the number of polyelectrolyte layers, because nitrogen and sulfur are exclusively present in PDADMAC and PSS, respectively. Therefore, the trend serves as a clear evidence of a successful multilayer build-up on the gold surface, and is in line with literature.[31] Following the XPS, the SWA study of the PEM, results of which are presented in **Figure 6.1c**, shows an odd-even effect, characteristic of an LbL-prepared PEM.[309] This trend can be attributed to the higher hydrophobicity of the PDADMAC-terminated layer than that of the PSS-terminated layer, and gives a clear indication of a successful multilayer deposition on the membrane surface, further verifying the XPS data.

The continuous mode of desalination paired the diluate reservoir with the intercalating electrode, producing deionized water throughout the desalination cycle. Thus, the ion concentration in the diluate decreased continuously with an increasing number of cycles. Due to the symmetric cell operation, the ion concentration increased by a similar amount in the concentrate reservoir. The concentration of both cations and anions as a function of desalination steps, during the treatment of feed **F1**, is shown in **Figure 6.2a** & **b**. The diluate and the concentrate reservoirs are depicted by fading and increasing color gradients, respectively. The trends in the figure confirm the symmetrical operation with respect to cations as well as anions, while they also demonstrate that the proposed cell can successfully distinguish between both cations (Na^+ and Mg^{2+}) and both anions (Cl^- and SO_4^{2-}),

simultaneously. The MCM blocks the divalent SO_4^{2-} and allows the monovalent Cl^- to selectively pass through it, while the NiHCF electrode selectively intercalates monovalent Na^+ over divalent Mg^{2+}. Furthermore, the selective removal of monovalent ions remained highly independent of their concentration over divalent ions in the feed, even after the monovalent ion concentration reduced by over 90 % in the feed. For example, from cycle 3 to 4 in **Figure 6.2a**, the concentration of Cl^- in the diluate went from 12% to 2% while that of SO_4^{2-} went from 93% to 92%. This indicates that even at the ratio of 7:1 SO_4^{2-}: Cl^-, the monovalent Cl^- was preferentially allowed through the MCM. Similar observation was also made during the selective adsorption of Na^+ over Mg^{2+} in the NiHCF electrode, as seen in **Figure 6.2b**.

The effect of the number of layers on the anion selectivity of the membrane was investigated by treating **F2** with a symmetric cell containing a MCM that consisted of 5, 6, 9, 10, 14, 15, 23, or 31 polyelectrolyte layers. **F2** contained only Na^+ to avoid any synergistic effect on the anion selectivity, caused by the presence of two different cations in the feed. Early evidence of such an effect is shown in **Figure S 6.4**, but further investigation is required to reach a conclusion. The resulting concentration of Cl^- and SO_4^{2-} in the diluate for selected 5, 15, and 31 layer PEMs is presented in **Figure 6.2c**. (The full data set for MCM with all other layers, the control experiment with a bare membrane, and with a commercial, monovalent anion-selective membrane is given in **Figure S 6.5.**) It is evident from **Figure 6.2c** that the removal and rejection of Cl^- and SO_4^{2-}, respectively, increases with increasing number of layers from 5 to 15 (**Figure 6.2c** & **S 6.5 a**). For example, the MCM with 5 layers removed ≈15% SO_4^{2-} at 50% Cl^- removal, while the MCM with 15 layers removed only ≈7% SO_4^{2-} at 50% of Cl^- removal. For an odd number of layers on membrane surface, the increase in selectivity follows from an increase in the excess charge density of the MCM. The highest selectivity of the MCM, obtained with 15 layers, towards the monovalent Cl^- over the divalent SO_4^{2-} is attributed to the charge exclusion effect of the outermost, negatively charged PSS layer. The electrostatic repulsion of this outermost layer is larger towards the −2 charge of the SO_4^{2-} than the −1 charge of the Cl^- ion. This charge-based exclusion is driven by the charge of the outermost layer since the MCM preference switched towards SO_4^{2-} when the terminating layer is positively charged, as observed for the even number of PEMs, namely 6, 10, and 14, as shown in **Figure 6.1b**, **c**, and **S 6.5b**. This property of PEMs has also been reported before in ED literature [31,310]. Here, the treatment of feeds **F1** and **F2**, containing a mixture of Cl^- and SO_4^{2-}, provides an insight into the charge-exclusion based selectivity of the MCM. A further increase in the number of layers to 23 (**Figure S 6.5a)** and 31 switches the membrane selectivity towards SO_4^{2-}, resembling the selectivity properties of a bare membrane and MCMs with an even number of PEM, namely 6, 10, and 14, as shown in **Figure S 6.5b** and **c**. The observed switch in preference of the MCM from monovalent towards divalent ions can be related to an overall positive bulk charge that develops on the MCM surface with an increasing number of layers.[311] This phenomenon has been attributed to the charge balance within the PEM which is reported to be a combination of an interlayer attraction between PDADMAC and PSS and extrinsic interactions between PDADMAC/PSS layers and the salt counterion.[311] In short, as the number of layers increase,

the amount of newly adsorbed PSS reduces while the PDADMAC compensates its charge with external counter ions, other than PSS, giving the PEM an overall positive bulk charge. Thus, a switch in selectivity of the MCM, as obtained in this study between 15 and 23 layers, as shown in **Figure 6.2c** and **S3a**, is expected with increasing number of layers.

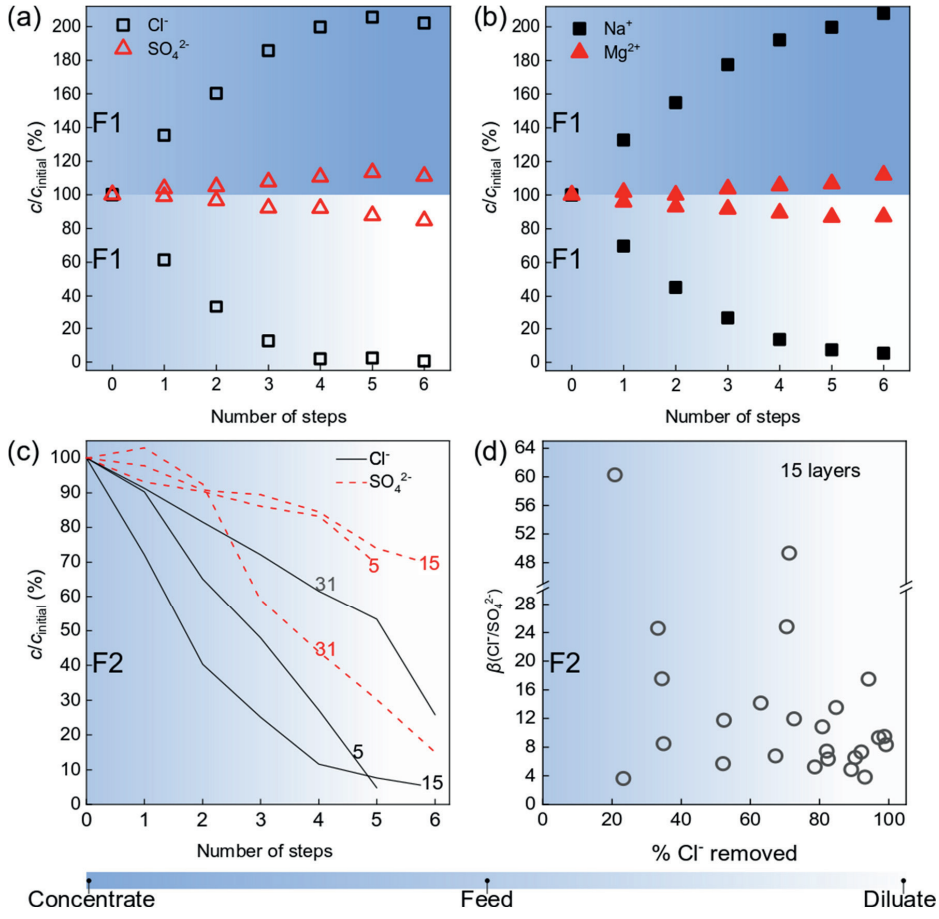

Figure 6.2: (a) Concentration of Cl^- (black hollow squares) and SO_4^{2-} (red hollow triangles) relative to the initial **F1** concentration, in the diluate and the concentrate chambers as a function of the number of steps, treated by the symmetric cell with identical NiHCF electrodes, separated by a MCM with 15 layers. **(b)** Concentration of Na^+ (black squares) and Mg^{2+} (red triangles) relative to the concentration of **F1**, in the diluate and the concentrate chamber as a function of the number of cycles, treated by a symmetric cell with identical NiHCF electrodes, separated by a MCM with 15 layers. **(c)** Concentration of anions in the diluate, during the treatment of **F2**, by MCM with 5, 15, and 31 layers. **(d)** Selectivity, β, of a MCM with 15 layers towards Cl^- over SO_4^{2-} from **F2**, as a function of Cl^- concentration in the diluate, obtained over multiple experiments.

Therefore, a PSS-terminated MCM with ≤ 15 layers prefers the monovalent ions, while divalent ions are preferred by an MCM with ≥ 23 layers, regardless the type of terminating layer. Interestingly, the MCM with ≤ 15 layers can also be made divalent ion-selective when the outermost layer is PDADMAC instead of PSS, as shown in **Figure S 6.5b**.

The preference of MCM towards one anion over the other is quantified as β,[11,47,106,148]

$$\beta = \left(\frac{c_{1,initial} - c_{1,final}}{c_{2,initial} - c_{2,final}}\right)\left(\frac{c_{2,initial}}{c_{1,initial}}\right), \quad (6.1)$$

where 1 and 2 represent the two competing ions and $c_{1,initial}$, $c_{2,initial}$, $c_{1,final}$, and $c_{2,final}$ are the ion concentrations in the beginning and at the end of the adsorption step, respectively. The β for Cl^- over SO_4^{2-}, obtained for 15 layers from multiple experiments is shown in **Figure 6.2d**. Even with the scatter in the data, it can be safely concluded that the selectivity towards Cl^- was maintained even after 90 % of it was removed. The majority of the β values were found to be in the range of $7 < \beta < 14$. The NiHCF electrodes simultaneously removed Na^+ selectively over Mg^{2+} with an average $\beta \approx 17$. The β for Cl^- over SO_4^{2-} fell typically between $3 < \beta < 6$ for 5 layers and $4 < \beta < 9$ for 9 layers, as shown in **Figure S6.6a** and **b**, highlighting the correlation between the anion selectivity and the number of layers. In contrast, the bare membrane from the control experiment showed an affinity towards SO_4^{2-} with $\beta \approx 2$. For further comparison, a $\beta \approx 7$ was obtained towards Cl^- over SO_4^{2-} during the treatment of **F2** with the symmetric CDI cell containing a commercial, monovalent anion-selective membrane (**Figure S 6.5d)**. The β values, obtained here for MCM with 15 layers, are higher than the values reported in electrodialysis[31] and reverse electrodialysis,[308] with membranes coated with poly(allylamine hydrochloride)/PSS and polyethylenimine/PSS PEs, respectively, that resulted in a selectivity of ≈ 2.5. Additionally, the β values presented in **Figure 6.2d** are also comparable to the Cl^-/SO_4^{2-} selectivity of 27, obtained in nanofiltration with PDADMAC/PSS-coated membrane.[312]

To investigate the mechanism of the ion selectivity of the MCM based on dehydration energy of the anions, two additional solutions containing a mixture of only monovalent anions were treated with the symmetric cell containing a MCM with 15 layers. Feeds **F3** and **F4,** as described in **Table 6.1**. contained monovalent phosphate, $H_2PO_4^-$ and nitrate, NO_3^-, respectively, with Cl^-. The concentration of these anions in the diluate, as obtained during the desalination experiment, is given in **Figure 6.3a** & **b**. It is evident from the graph that the PEM does not differentiate much between Cl^- and NO_3^-, as both were removed with only a marginal preference for NO_3^- ions. However, the modified membrane preferred Cl^- over $H_2PO_4^-$, delivering a $\beta \approx 3$ towards Cl ions. This selectivity behavior of the MCM can be ascribed to the dehydration energy of the passing anion, all carrying the same charge. $H_2PO_4^-$ was the second most rejected anion, after SO_4^{2-} which carried a −2 charge. Even though the dehydration energy of SO_4^{2-} is the largest among all the anions here ($\Delta G_{hydration}$ = 1080 kJ/mol),[292] its rejection is better explained by charge-exclusion because, for a bare AEM, SO_4^{2-} was preferentially transported over Cl^-, as shown in **Figure S 6.5c**. Once the membrane surface had a negative charge (*e.g.*, for MCM with 15 layers), the transport of SO_4^{2-} through the MCM was hindered,

hinting that the $\Delta G_{hydration}$ did not play as significant a role as its −2 charge. On the other hand, the reduced degree of rejection of $H_2PO_4^-$ may be attributed to two factors: (a) reduced electrostatic repulsion from the terminating PSS layer because of its −1 charge; (b) smaller dehydration energy ($\Delta G_{hydration}$ = 465 kJ/mol), which can ease the removal of the water solvation shell around the anion, facilitating its passage through the membrane.

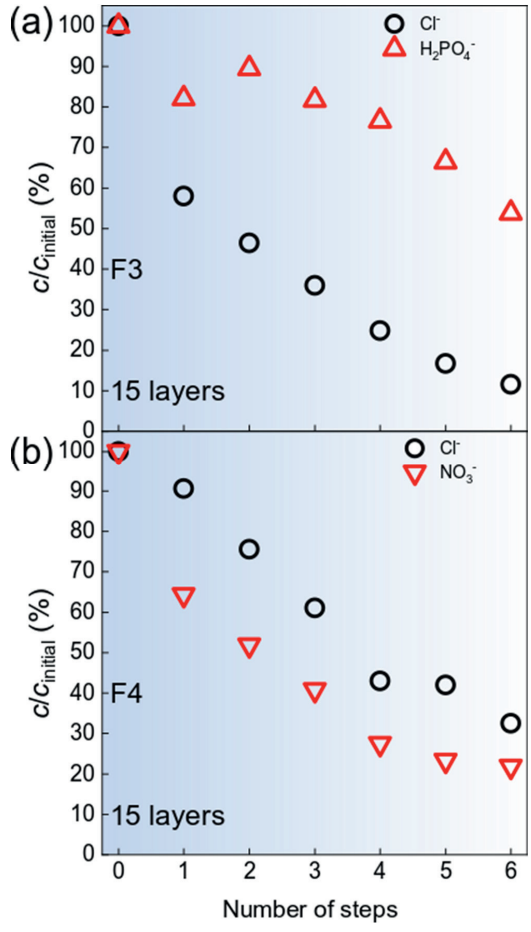

Figure 6.3: Change in concentration of **(a)** monovalent phosphate ($H_2PO_4^-$) and chloride (Cl^-) during treatment of feed **F3** and **(b)** nitrate (NO_3^-) and Cl^- during treatment of feed **F4** by symmetric NiHCF cell containing a MCM with 15 layers.

Finally, NO_3^- was the most preferred anion of all. This high preference may be attributed to its lowest dehydration energy ($\Delta G_{hydration}$ = 300 kJ/mol), which is even smaller than that of Cl^- ($\Delta G_{hydration}$ = 340 kJ/mol). In addition, it retains the advantage of reduced electrostatic repulsion because of its monovalent nature, like Cl^- and $H_2PO_4^-$ ions. Thus, the anion preference of the

MCM, based on the ease of dehydration, can be summarized as: NO_3^- > Cl^- > $H_2PO_4^-$ > SO_4^{2-}. Unlike the size-based exclusion seen towards cations in NiHCF electrodes, the trend observed here does not depend on the hydrated anion size, as NO_3^- is bigger than both Cl^- [253] and $H_2PO_4^-$ [292], and yet it is the easiest to remove. Thus, the size of an anion on its own does not provide complete information about the MCM selectivity.

6.4 Conclusion

A unique combination of PEM-coated anion-exchange membranes with nickel hexacyanoferrate electrodes was successfully used for the first time, to simultaneously and selectively separate both mono- and divalent cations as well as anions. In addition, the selectivity values obtained here for each of them are on par with the current (M)CDI state-of-the-art. Furthermore, the obtained anionic selectivity could also be tuned by changing the number of layers coated onto the membrane, making the system highly adaptable. We also demonstrate the tunability of the membrane with multilayer thickness and the type of terminating layer, by which the ion selectivity can be controlled. Furthermore, the dependence of the selectivity on the charge and the dehydration energy of the ions opens possibilities for enhanced selectivity or rejection towards anions that can change their valence depending on solution conditions like pH (*e.g.*, $H_2PO_4^-$), providing a route to phosphate recovery. The synergistic effects of size-based cation intercalation were also presented in this study. Additional insights into this phenomenon and the effect of feed parameters, such as pH, on selectivity are expected to further optimize the proposed approach for simultaneous cation and anion separation.

Supporting information

6 S.1 Sample preparation for SWA and XPS

Gold substrates (1 cm × 1 cm purchased from ECsens) were sonicated for 5 min in MQ water, dried under argon flow and then plasma cleaned (Brand, model) for 5 min to remove any organic material. After cleaning, the gold substrates were coated by using the same approach for the Standard-grade (Neosepta ASE, Astom) ASE membrane and kept in a vacuum oven at 30 ºC.

XPS spectra were obtained with a JPS-9200 photoelectron spectrometer (JEOL, Japan) under ultra-high vacuum conditions. It was obtained 20 scans per experiment by using a monochromatic Al Kα source at 12 kV and 20 mA. All spectra were processed with CASA XPS software (version 2.3.16) and fitted with Shirley background fitting.

SWA values were measured by using a Krüss drop shape analyzer (DSA 30). It was deposited 3 μL of Milli-Q water drops onto the samples. Contact angles were measured by using a sessile drop method. A charge-couple device camera was used for the analysis. The average values were calculated and reported based on three measurements at different locations on the samples.

6 S.2 Physical properties of PEM

The density of the PDADMAC/PSS multilayers, prepared by a similar procedure, has been reported to be 1.07 g/cm^3.[313] In addition, the dry thickness of 9, 13, and 17 layers of the PEM has been reported to be ≈ 32, 67, and 97 nm, respectively, demonstrating a linear growth in thickness upon the build-up. [314]

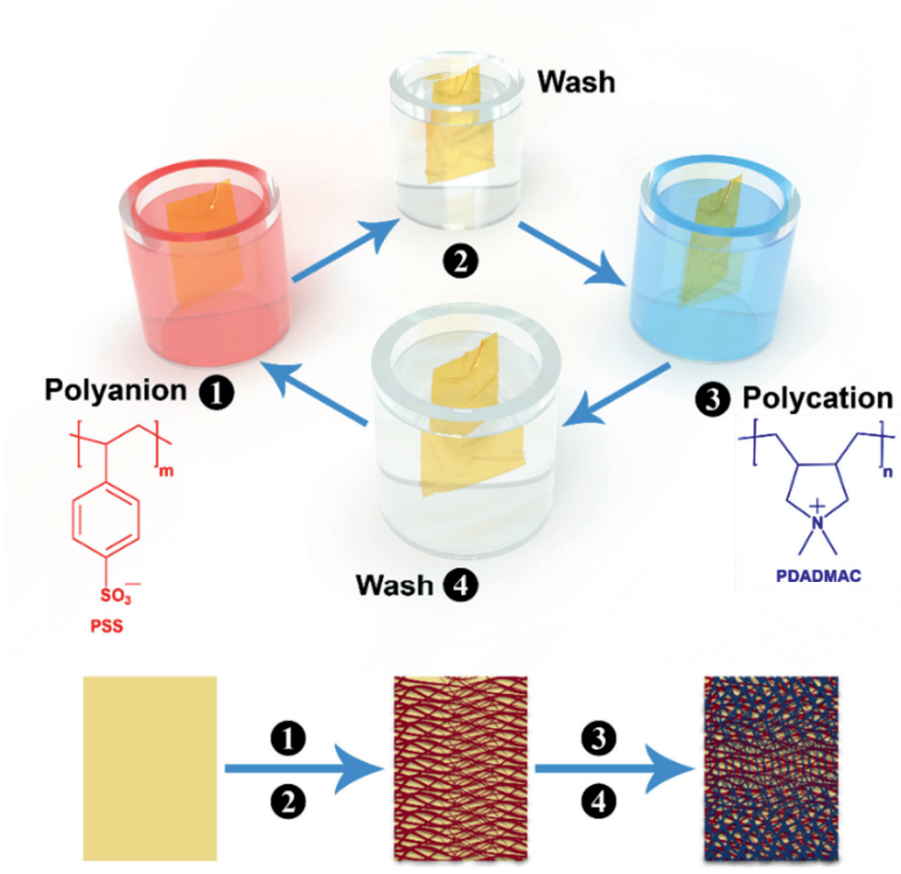

Figure S 6.1: Schematic illustrating the procedure followed for the layer-by-layer deposition of PEM on an AEM surface. A washing step was introduced between the dip coating to get rid of the extra, loosely bound polyelectrolytes.

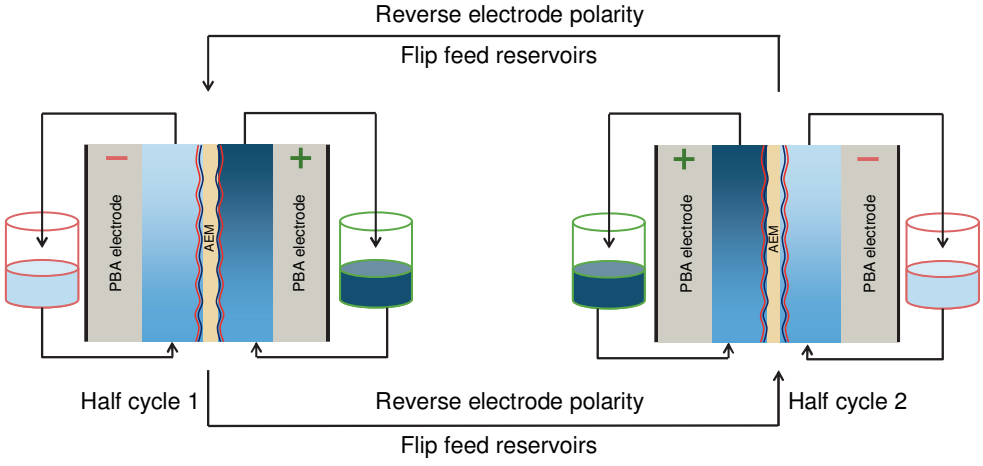

Figure S 6.2: Schematic illustrating the procedure followed during the selectivity experiments. Left figure represents one half of the cycle during which, the left electrode selectively adsorbs cations, the membrane selectively allows anions to pass to the right chamber and the right electrode desorbs the intercalated ions. After 30 min, the electrode polarity and the feed reservoirs are reversed, and the second half of the cycle commences, depicted by the figure on the right, where the right electrode selectively adsorbs cations, the membrane selectively allows anions to pass to the left chamber and the left electrode desorbs the intercalated ions. Only one bilayer of PEs is shown over the membrane for simplicity.

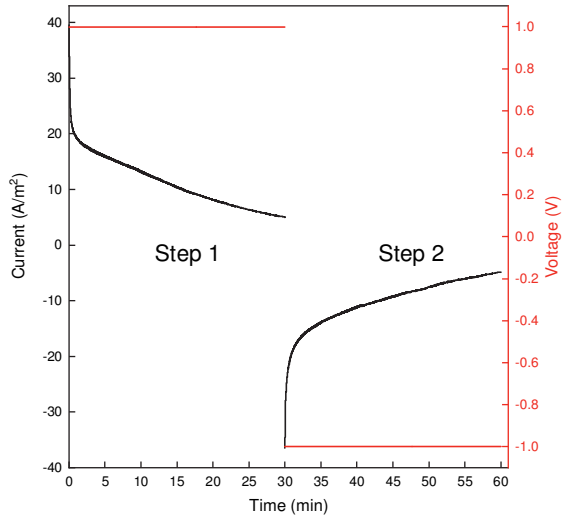

Figure S 6.3: Sample current-voltage (IV) profile obtained during desalination of 10 mM NaCl + Na_2SO_4 feed in constant voltage mode, with symmetric CDI cell containing identical NiHCF electrodes, separated by PEM with 15 layers.

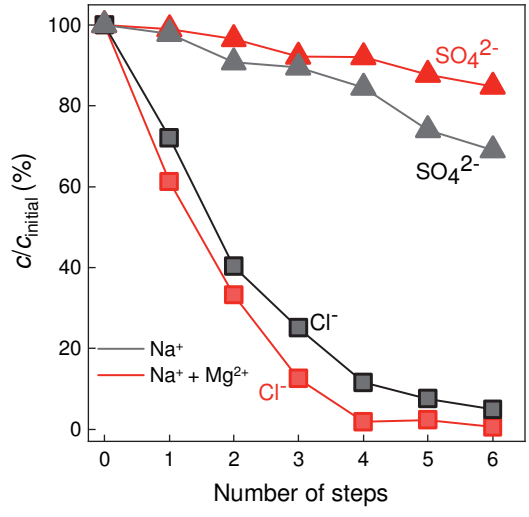

Figure S 6.4: Concentration of anions in the diluate as a function of desalination steps, obtained from the treatment of feeds F1 and F2, containing two cations (Na^+ and Mg^{2+}) and only one cation (Na^+), respectively.

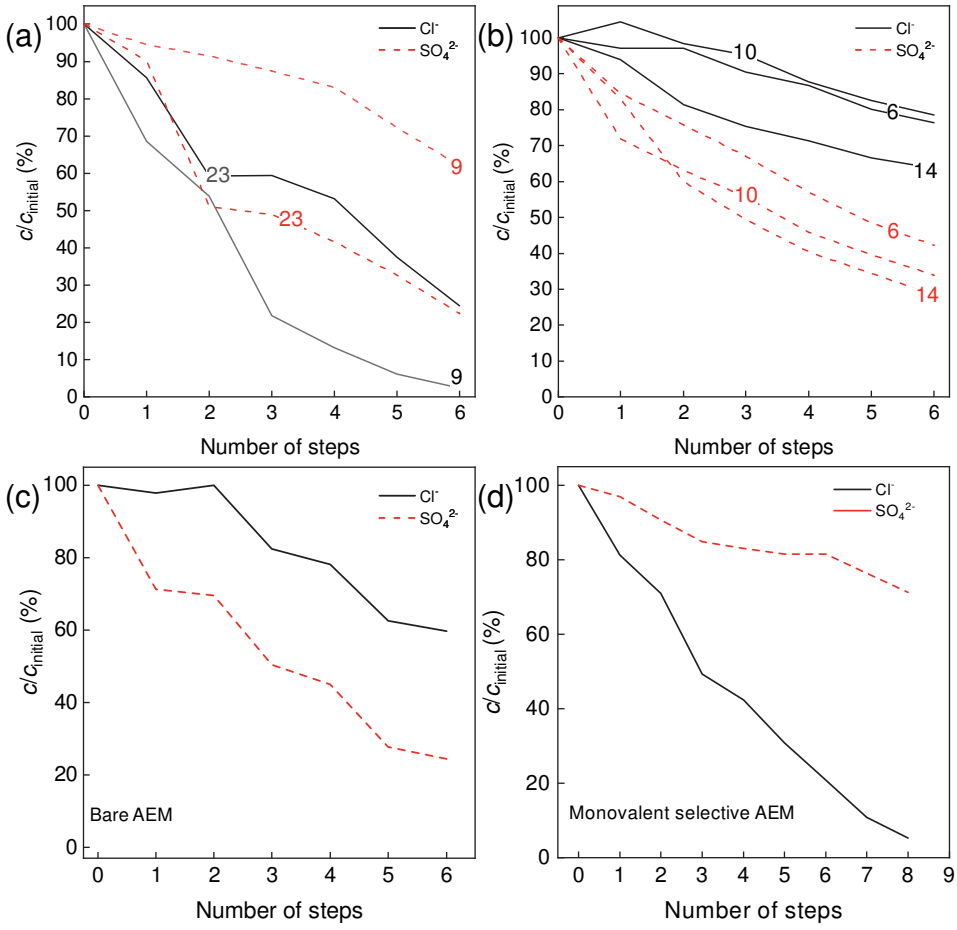

Figure S 6.5: Concentration of anions in the diluate, during the treatment of F2, by MCM with 9 and 23 layers. **(b)** Concentration of anions in the diluate, during the treatment of F2, by MCM with 6, 10, and 14 layers. **(c)** Concentration of anions in the diluate, during the treatment of F2, by bare anion-exchange membrane. **(d)** Concentration of anions in the diluate, during the treatment of F2, by special-grade, monovalent selective anion-exchange membrane.

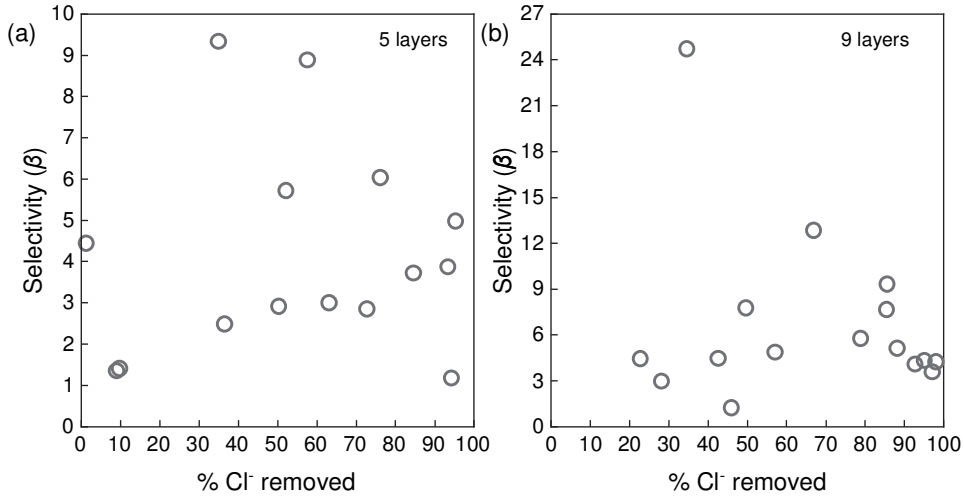

Figure S 6.6: Selectivity, β, of MCM with 5 layers towards Cl^- over SO_4^{2-} from F2, as a function of Cl^- concentration in the diluate, obtained over multiple experiments. (b) Selectivity, β, of MCM with 9 layers towards Cl^- over SO_4^{2-} from F2, as a function of Cl^- concentration in the diluate, obtained over multiple experiments.

7 Theory of Water Desalination with Intercalation Materials

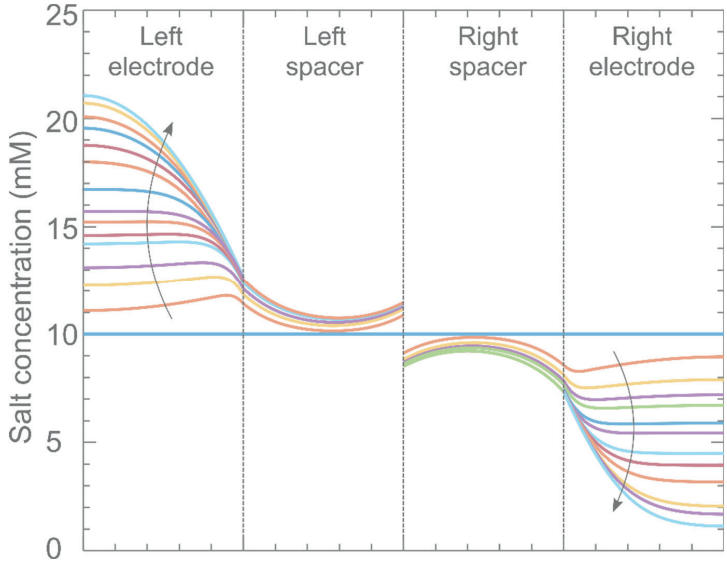

This chapter has been published as:

Singh, K., Bouwmeester, H. J. M., De Smet, L. C. P. M., Bazant, M. Z., & Biesheuvel, P. M. (**2018**). Theory of water desalination with intercalation materials. *Physical review applied*, *9*(6), 064036.

Abstract

We present porous electrode theory for capacitive deionization (CDI) with electrodes made of redox-active nanoparticles. Ionic transport in the aqueous phase is assumed to be the rate-limiting step. The geometry of the setup comprising of an anion-exchange membrane, two spacer channels and two porous electrodes is analysed. This analysis is performed with spacer channels in two configurations: First, with the spacers on the outside sandwiching the electrodes and the membrane; second, with the spacers in between the electrodes and the membrane. We model ion transport in all layers by the Nernst-Planck equation including the ion-exchange membrane that allows passage of anions as well as cations. We only consider a single-salt solution, with unequal diffusion coefficients for the anions and the cations. Similar to the previous works performed for CDI and electrodialysis, we solve the full, dynamic two-dimensional equations, simplified by assuming only advection in the direction parallel to the membrane (axial) and diffusion along with migration in the direction perpendicular to the membrane (orthogonal). Electronic as well as any possible ionic transport limitations are neglected within the redox-active nanoparticles. In these calculations, we demonstrate how the membrane selectivity can be markedly different from the ideal value of unity, and in addition, we show that the configuration with spacer channels in between the electrodes and membrane results in better desalination and energy use, than the configuration with spacer channels located on the outside of the electrodes.

7.1 Introduction

Capacitive deionization (CDI) is a method of water desalination where two porous electrodes adsorb ions from the aqueous phase, and later release the ions again.[18,123,315] Salt removal is achieved by alternatingly charging and discharging the electrodes which are connected through an electrical circuit. The porous electrodes typically contain three phases: water-filled pores for ion transport, a conducting material for electronic current, and a phase where ions are temporarily stored, as shown in **Figure 7.1**. Most work on CDI uses electrodes with ion storage in materials based on carbon (activated carbon, carbon nanotubes, graphene, etc.) where ions are stored in the electrical double layer (EDLs) along the carbon surface.[316]

Another class of materials for ion storage is based on intercalation host compounds, which are examples of redox-active materials that are receiving increased attention because of their potential for higher salt adsorption, lower energy consumption, and tunable ion selectivity. Although our general theory below could be applied to arbitrary intercalation compounds, adsorbing cations or anions, we will focus on the more common case of cation intercalation. Examples of such materials are nickel hexacyanoferrate (NiHCF), which is a Prussian blue analogue,[54,92,137,148,152,317,318] sodium manganese oxide (NMO),[94,95,142,153,319] and iron or titanium phosphates (which are also used in Li-ion batteries).[97,319] In response to an applied voltage, cations intercalate, or are reversibly inserted, into these redox-active host materials. The host crystal structure contains transition metal atoms, such as Fe or Mn which change redox state upon injection of electronic charge. When this material is charged more negatively (redox atoms in the crystal are reduced), to maintain electroneutrality extra cations are incorporated in the pores of the crystal, thus desalinating the water outside the particles. The intercalation materials mentioned above are highly cation selective (not incorporating anions), since the crystal is negatively charged, which provides a background countercharge for the intercalated cations.

To describe desalination by traditional CDI based on double-layer charging, porous electrode theory has been used since the 1970s.[320,321] Johnson and Newman developed the first such theory for CDI and made the assumption that for each electron injected in the EDL of a carbon matrix, one counterion adsorbs.[320] Going beyond this approximation, Bazant, Thornton and Ajdari initiated the microscopic theory of double-layer charging dynamics and salt removal for the model problem of parallel-plate blocking.[322] Since 2010, Biesheuvel and Bazant incorporated this physics into a porous electrode theory for double-layer CDI, applied to carbon-based materials,[57] which allows for incorporation of any quasi-equilibrium, thin or thick EDL structure. This generalized theory can be used for EDL models that consider both counterions and co-ions, ion mixtures of arbitrary valency, presence of chemical surface charge, and Faradaic charge transfer.[323]

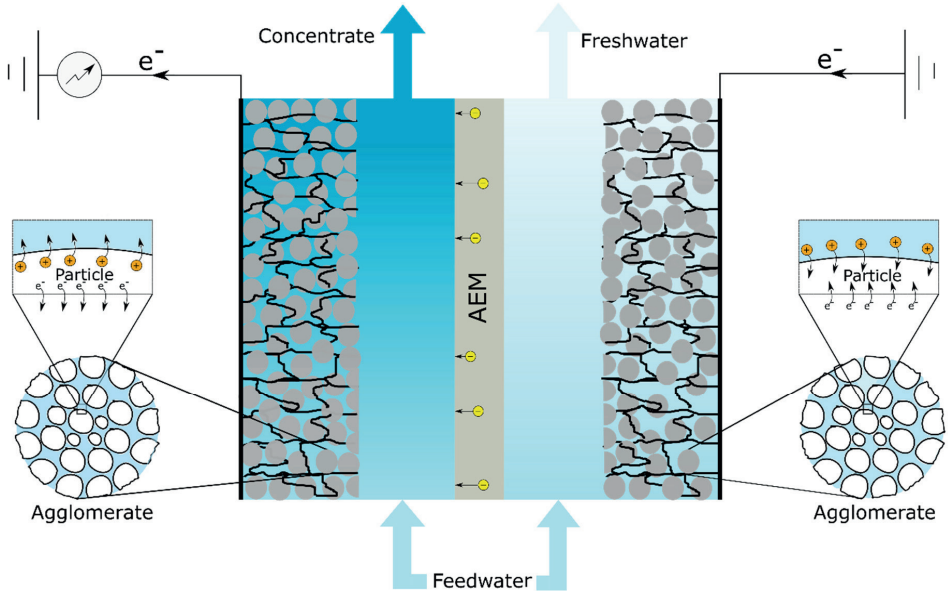

Figure 7.1: Schematic of the CDI cell with porous electrodes containing nanoparticles of redox-active intercalation material. Electronic connections through the electrode (drawn as black lines) allow for injection of charge from an external circuit. Nanoparticles are aggregated in water-filled agglomerates. The electrodes are separated by a pair of spacer channels for water flow, and an anion exchange membrane which preferentially allows transport of anions. The schematic captures the moment when ionic current flows left to right leading to de-intercalation of Na^+ on the left, and intercalation on the right. Depicted in the spacer channels are typical profiles in salt concentration and velocity of the water.

Porous electrode theories have also been developed for intercalation materials, albeit motivated by applications to Li-ion batteries rather than CDI. In 1982, West et al.[194] presented porous electrode theory for energy storage in intercalation, or insertion, materials, where Nernst-Planck theory describes both ion transport across the porous electrode and inside the intercalation material. At the interface of electrolyte intercalation material, the Frumkin intercalation isotherm is used,[324,325] which provides a relation between electrode potential (relative to the electrolyte phase), ion concentration in solution, and intercalation degree (the degree to which the intercalation material is filled with cations). This isotherm is an example of the more general regular solution theory describing the homogeneous Gibbs free energy of mixing of two or more constituents with finite size (*e.g.*, mean field approximation on a crystal lattice), as used in phase-field models of intercalation materials.[326–328] Regular solution models can be used to describe the thermodynamics of host materials containing multiple mobile ionic species and point defects, such as vacancies and interstitials, and form the basis for simulations

of nonlinear diffusion, phase separation, and electrochemical reactions,[326] in both single-crystal nanoparticles and multiphase porous electrodes.[321,329]

In the present work we set up and solve a model for CDI with intercalation materials along the lines of Johnson and Newman[320] and West *et al*.[194] We simplify the model of West *et al.* by neglecting transport limitation within the intercalation material, a common approximation in the modeling of energy storage electrodes consisting of intercalation nanoparticles.[329,330] This is a valid assumption when nanoparticles of intercalation material are very small and accessible on all sides by the ions in the electrolyte (water) with fast insertion reactions.[321] A rigorous criterion is not available for validity of this assumption in all situations, because ion transport in the electrode and adsorption in the particles is not a simple steady-state resistances-in-series process. But a first comparison can be made based on a "critical flux" of Na^+ ions in the two phases, $J_{crit} = cD/L$, with c a typical concentration, D a typical diffusion coefficient and L a typical distance. For the electrolyte we have c=10 mM, D=2.2 × 10^{-10} m^2/s (based on a porosity of 30 % and tortuosity based on the Bruggeman equation), and L=250 μm, while for the nanoparticles, c=2200 mM (at ϑ=0.5 for NiHCF,[54]) D=6.9×10^{-16} m^2/s,[331] and L=5 nm (based on a particle with a size of 30 nm; note that for a sphere, a typical diffusion depth is equal to the volume/area-ratio, which is on sixth of the size of the sphere). These numbers give a critical flux for Na^+ in the nanoparticles that is about 35× that in the electrolyte phase in the electrode, thus underpinning the choice to focus on transport in the electrolyte

Though we simplify the model by West *et al.*,[194] we also extend their approach (which is for a single electrode) by considering a full electrochemical cell consisting of two electrodes, two flow channels, and an anion-exchange membrane (AEM). The geometry is sketched in **Figure 7.1**. This cell design was invented by Smith and Dmello[142] to solve the problem of how to desalinate water using two electrodes made of intercalation materials that both are only capable of adsorbing cations.

An interesting difference of our model with that of Johnson and Newman[320] is that we do not assume a constant capacitance, but instead implement the Frumkin intercalation isotherm (or regular solution model), which for several intercalation materials has been shown to accurately describe chemical equilibrium between electronic structure, intercalation material, and electrolyte.[324–326,329] According to this equation, capacitance is high when the intercalation degree in the material is at an intermediate value $\vartheta = 0.5$), and capacitance drops dramatically when the material either is almost saturated with ions ($\vartheta \rightarrow 1$) or almost empty ($\vartheta \rightarrow 0$). In ref. [325] this equation is referred to as the Frumkin intercalation isotherm.

The electrode model is combined with electro-diffusion of ions in the two flow channels and in the AEM (see geometry depicted in **Figure 7.1**). For ion transport in the pores of the electrode, and in the flow channel, we implement that the ions have a different diffusion coefficient. Besides, we include a full description of the AEM, allowing both passage of cations and anions. Because the membrane has a large concentration of positive fixed charge, the flux of anions is much larger than of cations. We make calculations of complete charge-discharge

cycles and show the development over time of key parameters such as cell voltage, effluent salinity, and the intercalation degree of the electrodes.

Note that our theory considers the intercalation particles to fill up homogeneously, without phase separation inside the solid phase. This phase separation is not occurring for NiHCF in aqueous electrolyte, but does happen for other systems, such as Li-insertion in $FePO_4$ based electrodes in organic solvent, where Li-dense and Li-sparse regions are both found within the $LiFePO_4$ particles. Extensions to porous electrode theory that are required to include phase separation in the solid phase are introduced and reviewed.[321,326,329]

For an electrochemical cell based on porous electrodes containing nanoparticles of redox-active intercalation material, kinetics of ion adsorption depends on various transport processes, and each must be included in a complete theory for the entire device. These processes include:

1. Diffusion and migration of ions through the electrolyte-filled pores of the electrode.
2. Ion insertion (intercalation) into the redox-active material, and transport across these particles.
3. Electronic charge transport across the electrode, from a external current source all the way down into each nanoparticle;
4. Ion transport (advection, diffusion, and migration) in a transport channel located outside the electrode; and
5. Transfer of ions across the ion-exchange membrane.

In the present work, transport by processes 1, 4 and 5 is addressed, while instead of addressing items 2 and 3 in detail, the transport resistance is assumed to be infinitely low. Note that we do not consider rate limitation by the intercalation step of ion transfer between the electrolyte and the intercalation materials. In many situations, the ion-transfer reaction may not be rate-limiting, since the ion does not change solvation degree upon entry into the intercalation material, although there is an activation barrier for de-solvation and electron transfer to the compensating redox-active site in the crystal.[195] Although we assume fast ion transfer here, the intercalation step could be included in future extensions of our model, using various models of electrochemical reaction kinetics.[142,195,326,329]

Similar to Johnson and Newman[320] and West *et al.*,[194] we make use of the Nernst-Planck (NP) equation for ion transport, an equation which is valid for a sufficiently dilute electrolyte, and which describes each ion in the same way. This approach is mathematically different from models developed for (Li-ion) batteries, which incorporate a solution-phase potential as the driving force for transport of cations.[332] This potential combines the electrical potential in solution with a term dependent on Li^+ concentration. Also, thermodynamic non-idealities, beyond the NP-equation, are incorporated in such state-of-the-art battery models. Though these models were also successfully applied for CDI with intercalation materials,[142,159] in the present work we follow refs,[194,320] and make use of porous electrode theory based on the NP

equation. Advantages of the NP approach are that it is mathematically easier to understand and implement, and in a later stage can be readily extended to ionic mixtures. Such modifications are not so straightforward to implement in the available codes for battery models.[329] For a dilute electrolyte, the NP equation is a valid approximation, because thermodynamic non-idealities of the aqueous phase are not very pronounced. Thus, we use the ideal NP equation for migration and diffusion of each ionic species in the different elements in the cell, extended with an advection-term for the flow channel.

In summary, in the present work we aim to develop and present a mathematical model for water desalination by CDI using porous electrodes consisting of nanoparticles of intercalation material. Our approach is to use a theoretical framework which is not excessively complicated while it describes many physical and chemical processes that take place in CDI with intercalation materials. At a later stage, the present model can be extended in a straightforward manner to describe mixtures of salts, by using a generalized Frumkin intercalation isotherm for ionic mixtures.[54,103] Such an extension would be very difficult to make in the classical theoretical framework of modeling Li-ion batteries that use quasi-electrostatic potentials and concentrated solution theory. In our present work we discuss two different modes of operation of the electrochemical cell and the influence thereof on key parameters relevant for understanding cell performance (*e.g.*, salt concentration, intercalation degree, and cell voltage).

7.2 Theory

We make a calculation for a complete CDI desalination cell which consists of two electrodes, two spacer channels, and an anion-exchange membrane (AEM) which is placed in the middle of the cell, as shown in **Figure 7.1**. This arrangement, with the electrodes connected to an external electronic circuit, forms the desalination system that we will describe. The feed streams enter the spacer channels on one side and leave on the other, in a direction longitudinal to membrane and electrode. The spacer channels are in contact with an electrode on one side and the AEM on the other. The channels are not completely open, but contain a porous layer with a certain porosity, ε_s, and tortuosity, τ_s. Feedwater is used with a sufficiently low salt concentration for the assumptions of dilute solution theory to hold (activity coefficient, $\gamma \sim 1$).[321] Ion transport in these channels is described by the NP equation, extended to include advective flow,

$$\boldsymbol{J_i} = c_i v - \frac{\varepsilon_s}{\tau_s} D_i (\nabla c_i - z_i c_i \nabla \phi) \tag{7.1}$$

where J_i is the flux of ion i, v is fluid velocity, and c_i is ion concentration. We relate the tortuosity of the porous material to porosity with the Bruggeman equation, $\tau = 1/\sqrt{\varepsilon}$, like we will also do in the electrode. Furthermore, D_i is the ion diffusion coefficient in free solution, z_i

the valency of the ion, and ϕ is the dimensionless electric potential. Dimensions of this potential can be restored by multiplication with the thermal voltage $V_T = RT/F = k_B T/e$.

Mass conservation describes the change of ion concentration with time at any position in these channels according to

$$\varepsilon_s \frac{\partial c_i}{\partial t} = -\nabla \cdot \boldsymbol{J_i}, \tag{7.2}$$

which can be combined with Eq. (7.1) and further simplified by assuming that:

(a) Water flow in the spacer channels only has a component in the y direction parallel to the membrane and electrode (depicted in **Figure 7.1**); hence $v_x = 0$, and
(b) Diffusion and electro-migration are only considered in the opposite, x, direction (which is perpendicular to the y direction of water flow).

With these assumptions, the balance for each ionic species in the spacer channel becomes[333]

$$\varepsilon_s \frac{\partial c_i}{\partial t} = -v_y \frac{\partial c_i}{\partial y} + \frac{\varepsilon_s}{\tau_s} D_i \left\{ \frac{\partial^2 c_i}{\partial x^2} + z_i \frac{\partial}{\partial x}\left(c_i \frac{\partial \phi}{\partial x} \right) \right\}, \tag{7.3}$$

which is combined with local charge neutrality, $\sum_i z_i c_i = 0$ and solved for each ionic species. For fluid velocity, we assume plug flow, thus v_y is independent of x.

The description of ion transport in the spacer channels acts as the basis for understanding the transport of ions in the porous electrodes, which results in the ion mass balance

$$\varepsilon_e \frac{\partial c_i}{\partial t} = \frac{\varepsilon_e}{\tau_e} D_i \left\{ \frac{\partial^2 c_i}{\partial x^2} + z_i \frac{\partial}{\partial x}\left(c_i \frac{\partial \phi}{\partial x} \right) \right\} - a J_{\text{int},i}, \tag{7.4}$$

where ε_e is electrode porosity (volume fraction of electrode filled with electrolyte), and τ_e is electrode tortuosity. In the electrode the fluid velocity is set to zero. Similar to the spacer channel, electroneutrality is assumed in the electrolyte pore phase in the electrodes. In the model presented here, this corresponds to $[Na^+] = [Cl^-]$. The new addition in Eq. (7.4), $aJ_{\text{int},i}$, is the ion flux from electrolyte into the intercalation material (redox-active nanoparticles), and is defined per unit area a, which is the area of the particles per unit volume of total electrode. For a perfectly cation-selective material, we have for all anions $J_{\text{int},i} = 0$, while for the cations, $J_{\text{int},i}$ follows from a balance over the nanoparticles. Assuming only a single cation to intercalate in the intercalation material, a cation mass balance for the nanoparticles is given by

$$c_{\max} \varepsilon_{\text{im}} \frac{\partial \vartheta}{\partial t} = a J_{\text{int}}, \tag{7.5}$$

where we leave out subscript i, and where $c_{\max}$ is the maximum possible concentration of cations in the intercalation material, ε_{im} is the volume fraction of the intercalation material (as a fraction of the total electrode volume), and ϑ is the average cation intercalation degree (average fraction of active sites in the host particles occupied by a cation).

Finally, local chemical equilibrium is assumed between cations in the intercalation material and in the electrolyte. This chemical equilibrium is described using the Frumkin isotherm for intercalation[54,194,324]

$$\phi_{\mathrm{ecm}} - \phi_{\infty} = \mu^{\dagger} - ln\frac{\vartheta}{1-\vartheta} + ln\frac{c_{+}}{c_{\mathrm{ref}}} - g(\vartheta - \ 1/2), \tag{7.6}$$

re ϕ_{ecm} is the potential of the electron-conducting material (carbon in most cases), and ϕ is the potential in the nearby electrolyte phase, which is the same ϕ as used in Eq. (7.4). Furthermore, c_{+} is the concentration of cations there, c_{ref} is a reference concentration, and $\mu^{\dagger}$ and g are constant factors dependent on the type of cation, where g can be considered as an inter-cation repulsion energy. The Frumkin isotherm fits very well equilibrium data for electrode potential versus charge for electrodes containing the intercalation material NiHCF, a Prussian Blue analogue.[54] As noted above, the Frumkin isotherm is equivalent to the regular solution model for the Gibbs free energy of mixing of intercalated ions and vacancies, which has also been successfully used in phase-field models of Li-ion batteries.[326,328,329]

In the electron-conducting phase in the electrode, the electronic resistance is zero. This implies that the potential here, ϕ_{ecm}, does not vary with position. However, it is different for cathode and anode, and it varies in time. Thus, the voltage as measured between anode and cathode, the cell voltage, is given by $V_{\mathrm{cell}} = V_T \cdot \left(\phi_{\mathrm{ecm},A} - \phi_{\mathrm{ecm},C}\right)$ where A and C refer to anode and cathode.

Finally, ion transport in the AEM separating the two halves of the cell must be described. As in the other regions, transport of ions in the AEM is described by the NP equation (7.1). Ion transport by advection is neglected in the membrane. Like the electrodes and the spacer channels, it is assumed that diffusion and migration occur only in the x direction across the membrane of thickness δ_{m}. Accumulation of mass is neglected in the membrane and therefore, in the membrane the flux of each ion remains invariant with position x. An equal diffusion coefficient D_m, in which the term ε/τ is included, is assumed for all ions in the membrane, and we define a transfer coefficient $k_m = D_m/\delta_m$. The membrane is furthermore defined by the fixed charge density, ωX, which is a positive number for an AEM. A typical value for a commercial membrane is of the order of $X = 4$ M. This is a fixed charge concentration per unit aqueous phase in the membrane. For a binary monovalent electrolyte, charge neutrality in the membrane is given by $c_{+,\mathrm{m}} - c_{-,\mathrm{m}} + \omega X = 0$ and a total ion concentration in the membrane is defined as $c_{\mathrm{T,m}} = c_{+,\mathrm{m}} + c_{-,\mathrm{m}}$. The total ion flux is $J_{\mathrm{ions,m}} = J_{+,\mathrm{m}} + J_{-,\mathrm{m}}$ and the charge flux (ion current density) is $J_{\mathrm{ch,m}} = J_{+,\mathrm{m}} - J_{-,\mathrm{m}}$.

When the fixed charge density in the membrane is much higher than the salinity outside the membrane, the ion concentrations and the electrical potential, ϕ, can be assumed to be varying linearly with position inside the membrane.[334] As a consequence, the fluxes $J_{\mathrm{ions},m}$ and $J_{\mathrm{ch},m}$ become

$$\begin{aligned} J_{\mathrm{ions,m}} &= -k_{\mathrm{m}}\left(\Delta c_{\mathrm{T,m}} - \omega X \Delta\phi_{\mathrm{m}}\right) \\ J_{\mathrm{ch,m}} &= -k_{\mathrm{m}}\langle c_{\mathrm{T,m}}\rangle \Delta\phi_{\mathrm{m}}, \end{aligned} \tag{7.7}$$

where ⍰..⟩ is an average between values at the extreme ends of the membrane, and Δ refers to a difference between these positions (with fluxes defined from left to right, Δ is defined as **right** minus **left**). The total ion concentration on each side of the membrane is related to the salt concentration just outside (*i.e.*, in the spacer channel, at a position right next to the membrane), c^*, as

$$c_{\mathrm{T,m}} = \sqrt{X^2 + (2c^*)^2}, \tag{7.8}$$

while the Donnan potential (change in electrical potential) across each membrane edge is given by

$$\Delta\phi_D = \sinh^{-1}(\omega X/2c^*). \tag{7.9}$$

7.3 Results and Discussion

The calculations for the CDI cell are set up for an electrolyte with a single cation, Na^+, that can intercalate into the redox-active nanoparticles under the influence of an applied electrical current. As a specific geometrical example of an electrochemical desalination cell, we consider CDI with porous electrodes containing intercalation particles where the electrode has the spacer channel on one side and the "current collector" on the other side. Here, electronic current is injected in the electrode. The spacer channels are positioned next to the AEM which is in the middle of the cell, as shown in **Figure 7.1**. The electrolyte, a NaCl solution, flows through the spacer channel and both ions diffuse in and out of the electrodes, while Cl^- ions (and some Na^+ ions) also diffuse through the membrane. Note that also other designs are possible: in ref. [142] a cell design was theoretically analyzed with the water flowing through the electrodes, and in ref.[54] the spacer channel was located on the other side of the electrodes (on the outsides of the cell).

7.3.1 Numerical aspects

The CDI cell model for our geometry is solved numerically, based on the conservation equations (7.3) – (7.5). These equations are used for both ions, for spacer and electrode, along with the Frumkin isotherm (7.6) and the equations for the membrane. In x direction (left-right direction in **Figure 7.1**), discretization of the partial differential equations in each domain is done using a large number of nodes (>20 in each domain), but in y direction we use only use a single node and an implicit Euler scheme (backward Euler). Because of this choice it is as if in the flow direction each flow line is one (very thin) "stirred tank", an approach successfully applied for CDI in ref. [75] and for electrodialysis in [335]. For the low desalination degrees as obtained in the present work, discretization in the y direction into more nodes, will not significantly change the results of the calculations. Note that in case of "one node in y direction," the geometry of how inlets and outlets of the two cell compartments are oriented

relative to one another (*e.g.*, co-current vs counter-current) does not matter; this only starts to influence the calculation outcome with a higher discretization in y direction. Another numerical aspect of our model is as follows: with more than one node in y direction, constant current operation, where a certain current I is made to flow from anode to cathode, requires solving all equations on each node in y direction simultaneously, because current I will not be evenly distributed over all y coordinates. However, when a boundary condition of constant cell voltage is used, then it is possible to solve each y node "sequentially", *i.e.*, one after the other. Especially for steady-state operation in electrodialysis, this is particularly useful. Finally, note that because we have neglected diffusion and migration in y direction, we do not have to deal with various numerical complications at the inlet and outlet of the cell, such as ionic currents straying outside the cell, or the choice of correct boundary conditions in advection-diffusion problems, where the concentration decay in y direction can propagate upward into feed tubes.[336]

For our calculations, parameters are based on experiments in ref.,[54] resulting in: $c_{\mathrm{salt,inflow}} = 10$ mM, $\varepsilon_s = 1.00$, $\varepsilon_e = 0.30$, $\varepsilon_{IM} = 0.50$, $c_{\mathrm{max}} = 4.4$ M, cell area A=36 cm^2, electrode thickness δ_e =m, spacer thickness δ_s =m, and water flow rate per channel $\Phi_v = 5.0$ mL/min, which results in a residence time of (water in) each spacer channel of $A\delta_s/\Phi_v = 30$ s. Diffusion coefficients of Na^+ and Cl^- are 1.33×10^{-9} m^2/s and 2.00×10^{-9} m^2/s, respectively. For the membrane, the transfer coefficient is set to the value $k_m = 0.55$ μm/s (based on taking the average of D_{Na^+} and D_{Cl^-}, reducing that by a factor of 20, and implementing a membrane thickness of δ_m =m). Membrane charge density is X = 4.0 M ($\omega = +1$ for an AEM). Operation is always with constant current at a value of $I = \pm 10$ mA. With this current running for one hour, this implies that the average intercalation degree in a certain electrode then changes by about $\Delta\vartheta = 0.20$, because $A\delta_e F\varepsilon_{\mathrm{im}} c_{\mathrm{max}}\Delta\vartheta = I\Delta t$ where Δt is the duration of charging. The Temkin parameter of relevance is the inter-cation repulsion g, for which we use g = 3.50 (dimensionally, 90 mV). The factor μ^+ does not influence any calculation output and neither does the choice of c_{ref}.

7.3.2 Initial charging and discharge

In all cases we start the calculation with both electrodes charged half-way, *i.e.*, $\vartheta = 0.5$, without gradients in ϑ across the electrode. Then we charge one electrode relative to the other for a period of 1 h, resulting in one electrode reaching an average ϑ_{avg}=0.30 and the other ϑ_{avg}=0.70. Then we discharge (*i.e.*, reverse the direction of current) for the same duration of 1 hr, after which each electrode is back to ϑ_{avg}=0.5.

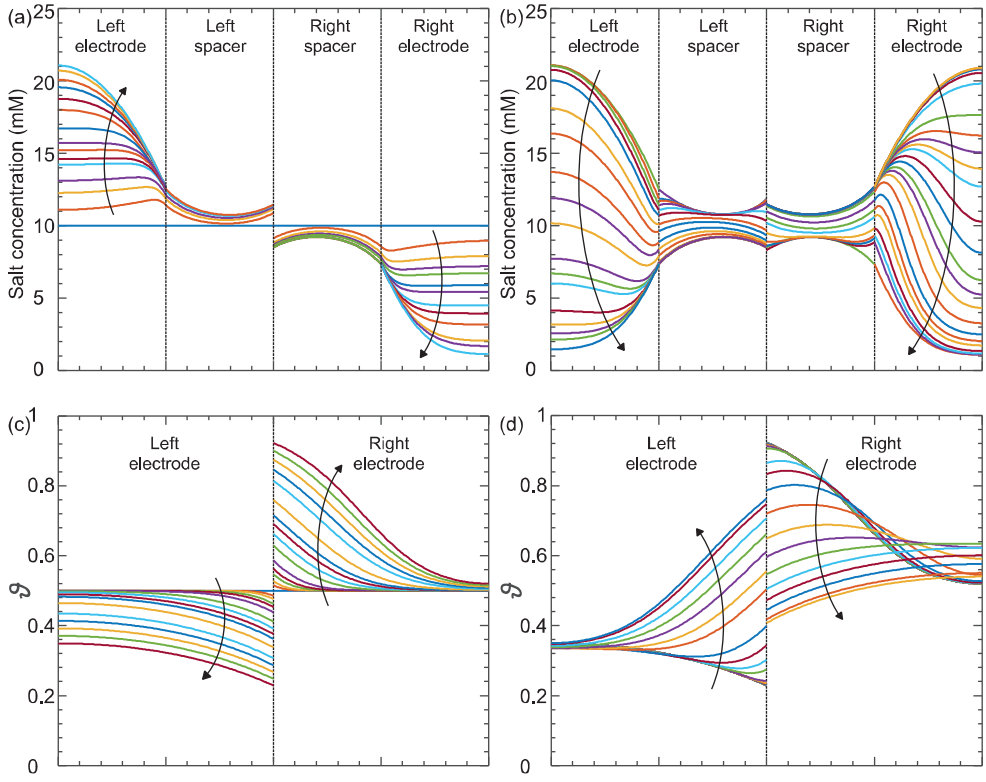

Figure 7.2: Time-dependent profiles of salt concentration and intercalation degree during water desalination with intercalation electrodes. **a,b)** Salt concentration in electrodes and spacers; **c,d)** Intercalation degree in the two electrodes, ϑ. These profiles are given as a function of position in the cell during **a,b**) first charging step, and **c,d**) first discharge step. Arrows depict the progression of time.

These are average values of ϑ, with the profiles in ϑ across each electrode as presented in **Figure 7.2c** for different moments during the first hour of charging, and in **Figure 7.2d** for various times during discharge. The salt concentration profiles during these periods are presented in **Figure 7.2a** and **2b**. This initial cycle of charge and discharge is also shown as the first 2 hr in **Figure 7.3**, as well as the first 2 hr in **Figure 7.4**.

7.3.3 Two modes of operation of charge/discharge cycles

After that time (from t=2 h onward), two distinct operational modes are considered. In Mode 1, at t=2 hr we again reverse the current direction and go back to the situation we had at t=1 hr, at least in terms of ϑ_{avg}. This cycle is then repeated with the current reversed every hour. Mode 1 is depicted in **Figure 7.3a,c** and in **Figure 7.4**. Instead, in Mode 2, at t=2 hr, nothing is changed, and the current continues such that after another hour, at t=3 hr, we reach a situation

that the values of ϑ_{avg} are now reversed compared to the situation at t=1 hr, *i.e.*, the electrode that had ϑ_{avg}=0.70 at t=1 hr, now, at t=3 hr, has ϑ_{avg}=0.30 (and vice versa).

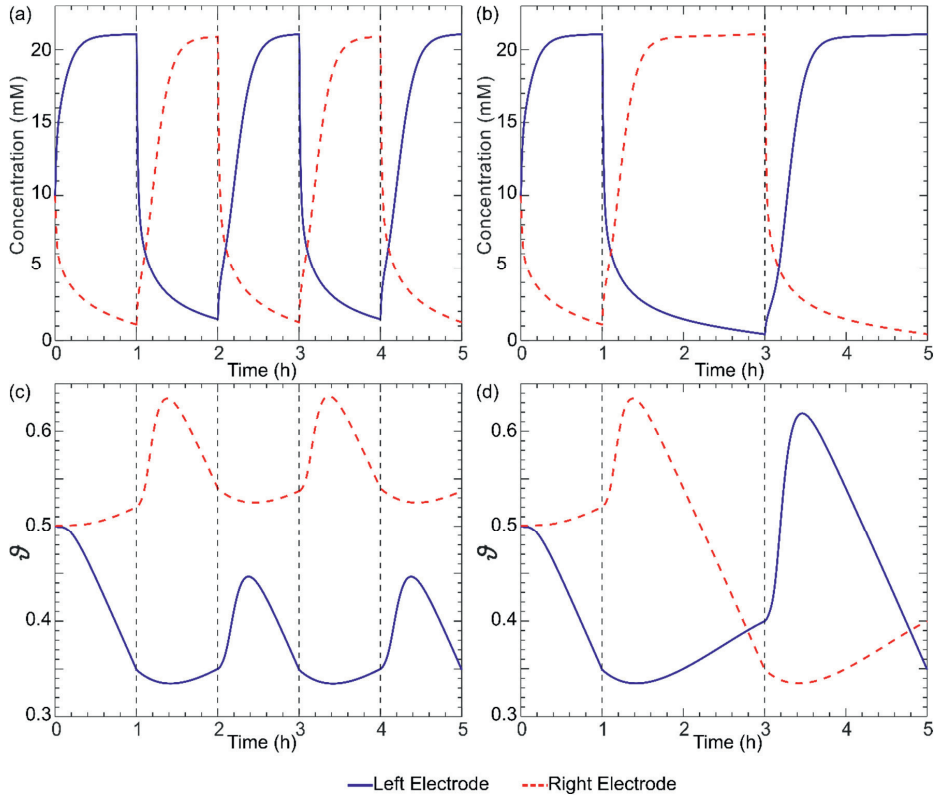

Figure 7.3: Salt concentration and intercalation degree ϑ versus time for **a**,**c**) operation in Mode 1, and **b**,**d**) operation in Mode 2. In all cases calculation results are presented for the positions deepest in the electrode, thus furthest from the flow channel, for **a**,**b**) salt concentration, and **c**,**d**) intercalation degree.

Only now, at time t=3 hr, is the current reversed, and a period of charging starts that in 2 hr will bring us back to the other end of the cycle (so that in terms of ϑ_{avg}, the cell is the same at t=5 hr as at t=1 hr). The main advantage of Mode 2 operation is that (when the limit cycle is reached, and for a perfectly symmetric system) operation goes from a cell voltage of $+V$ at one end of the cycle, to a voltage of $-V$ at the other end, see **Figure 7.4**. This symmetry is not found for operation according to Mode 1. Thus Mode 2-operation is very easily established experimentally by setting a value of $\pm V$ at which the cell reverses the direction of current. Interestingly, each "half-cycle" in Mode 2 is then the same as that in the next half-cycle, with the only difference being that what happens in electrode 1 during a certain half-cycle, now happens in electrode 2 in the next. This can be observed in **Figure 7.3d**, where the red dashed line during period 1-3 hr, is almost the same as the blue solid line in the period 3-5 hr, and the

same for the blue line in the period 1-3 hr which can be compared with the red dashed line in the period 3--5 hr. In **Figure 7.3**, the behavior is not yet exactly the same because the limit cycle or "dynamic steady state" was not yet reached after 1 hr. Note that for operation in Mode 2, it is impossible to find an objective criterion about which half of the cycle is to be called "charge" and which "discharge" because both halves of the cycle are exactly identical in terms of desalination performance, energy consumption, etc. Note that this exact symmetry only occurs when for both halves of the cell all operational setting are the same such as water flow rate and electrode mass. Interestingly, it is not necessary for both electrodes to have the same initial ϑ at time zero.

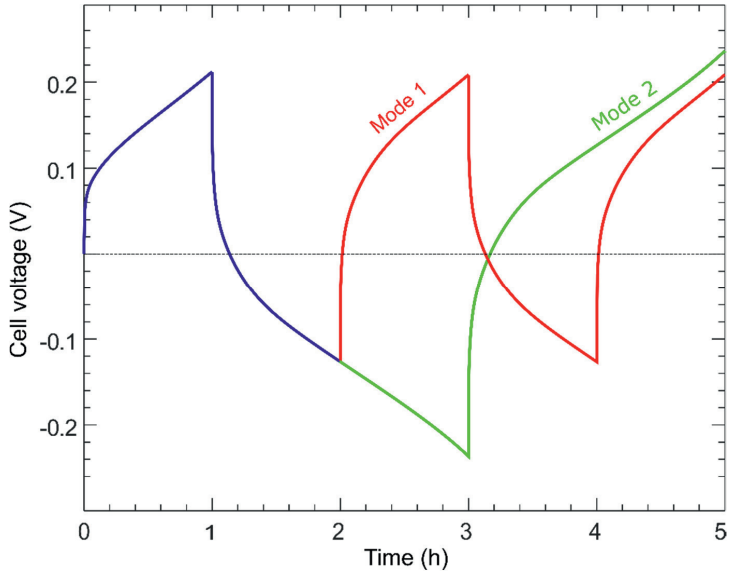

Figure 7.4: Cell voltage for Mode 1 and Mode 2 of operation. Cell voltage changes suddenly when current changes direction. The blue curve shows the first cycle, while red and green refer to operation in Mode 1 and Mode 2.

Finally we show in **Figure 7.4** calculation results for the development in time of cell voltage for the two modes of operation. These voltage (V)--time (t) plots are important as they fully describe the electrical energy input in the process: for a constant current of $\pm I$, the electrical energy input is proportional to the area under the V--t curve (and delineated by the line $V_{\text{cell}} = 0$). As **Figure 7.4** shows, after reversal of the current direction, a small "area" is found which corresponds to energy "output" (*e.g.*, from 1 to 1.15 hr), *i.e.*, where energy recovery is in theory possible,[40] after which a much longer period follows where energy must be invested to run the cell (from 1.15 to 3 hr for mode 2).

7.4 Conclusion

In this work we combined porous electrode theory for electrodes with redox-active intercalation materials with a description of spacer channels and a membrane, to describe an electrochemical system for capacitive deionization (CDI) with two intercalation electrodes that are chemically the same. The CDI cell design has an intrinsic symmetry as it is composed of two identical porous electrodes, both interfacing a spacer channel, separated by one anion exchange membrane. We considered a single salt solution, and calculated transport of ions by diffusion, migration, and advection in two dimensions. Transport of ions in the pores of the electrodes was modeled based on the Nernst-Planck equation. Thermodynamics of cation adsorption from electrolyte into the intercalation material was described by the Frumkin isotherm (regular solution theory), which factors in the lattice occupancy, inter-cation repulsion, electrolyte salinity and electrode potential. Homogeneous adsorption of ions was assumed, *i.e.*, without phase separation within the nanoparticles. Including of this effect may be of importance for certain material chemistries. The required model extensions can be based on approaches discussed elsewhere.[321,326,329]

In our model, a limitation in transport of ions within the intercalation material is neglected, just as is a resistance for flow of electronic current across the electrode. The model describes the development in time of salt concentration, intercalation degree, and cell voltage, parameters important for the description of performance of a CDI desalination cell. This work intends to provide a platform upon which future models can be constructed for more realistic water sources with ionic mixtures and for other geometries of desalination systems involving porous electrodes with redox-active intercalation materials.

“ लेने से ताजो-तख़्त मिलता है

मांगे से भीख भी नहीं मिलती “

–फ़िराक़ गोरखपुरी

8 Discussion & Future perspectives

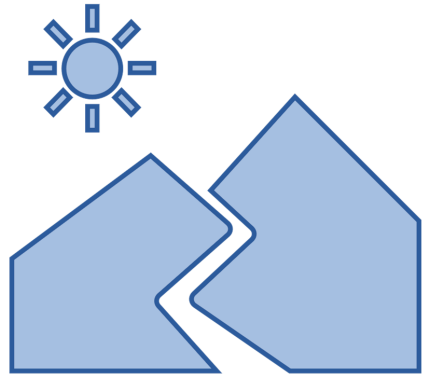

Parts of this chapter have been published as:

Gamaethiralalage, J.G., Singh, K., Sahin, S., Yoon, J., Elimelech, M., Suss, M.E., Liang, P., Biesheuvel, P.M., Zornitta, R.L. and de Smet, L.C.P.M., (**2021**). Recent advances in ion selectivity with capacitive deioni zation. *Energy & Environmental Science*, *14*(3), pp.1095-1120.

Following the research presented in this thesis and the inferences drawn from them, a perspective looking towards the future of the CDI state-of-the-art constitutes the logical next step. To that end, the sections below elaborate upon the questions that need to be answered to contribute to this rapidly developing field. These questions focus on both, the indiscriminate water deionization desirable for water desalination, as well as the selective ion removal, desirable for water softening and resource recovery-type applications. The answers to these questions are, in part, informed by the observations derived from the investigations presented in the previous chapters. The answers to these questions will also contribute to the bigger picture of global sustainable development, embodied in the 17 sustainable development goals (SDGs) adopted by the UN. The 6th goal concerning clean water, as introduced in **Chapter 1**, falls under the purview of this work. Consequently, the results and outcome of this thesis contribute towards this goal and are highlighted below.

8.1.1 The quest for new electrode materials in CDI

Even as new applications and research directions keep coming up, the most popular pursuit within the field of CDI remains the search for new electrode materials with more advanced properties. This ceaseless quest to find new electrode materials is in parts propelled by the following prerequisites:

- High ion adsorption capacity,
- High rate of ion adsorption/desorption,
- Inherent ion selectivity, ideally not only including size-based exclusions, and
- Stable long-term operation.

This relentless pursuit for new and better electrode material is aimed at fulfilling the requirements mentioned above. Research into new materials, as documented in **Chapter 2,** has resulted in the use of several new electrode materials including oxides of Mn, V and Ru, carbides of Ti, also referred to as MXenes, crystalline and redox-active phosphates of Ti and V, PB and its numerous analogues, sulphides of Ti and Mo and covalent organic frameworks (COFs) among others.[337] The last category, COFs, are highly versatile and nanoporous (1.8 – 3.2 nm in diameter)[338] materials constituted by organic building blocks linked with a (dynamic) covalent bond to form, depending on the geometry of the building blocks, 3D networks or 2D sheets.[339–343] These 2D polymeric sheets can stack on top of each other to form a framework, which is usually obtained as a powder. Dynamic covalent bonds employed in COF synthesis include boronated esters,[344] imines,[345] azines,[346] among others.[347–349] The variety of building blocks, and the possibility to post-functionalize COFs, has resulted in their application in several fields including photocatalysis,[350] catalysis,[351] gas[352] and energy storage.[353] Very recently, a redox-active β-ketoenamine (a condensation product of special aldehydes (ortho-hydroxy benzaldehydes) with primary amines)-linked COF electrode was successfully used in HCDI.[205] Reversible and stable operation was obtained for 5000 cycles but no selectivity was investigated. In our own group, we prepared an imine-linked COF, that

was also tested as an electrode. A preliminary characterization result from a cyclic voltammetry experiment performed in 1M solution of NaCl, KCl, and $CaCl_2$ is given in **Figure 8.2**. From the peaks obtained during the oxidation and reduction scans, it becomes apparent that the COF electrodes underwent reversible redox reactions between 0.25 – 0.5 V (*vs.* Ag/AgCl) for both monovalent as well as divalent ions. It is also apparent that the electrode responds differently to Na and K ions, despite them both being monovalent ions, as shown in **Figure 8.2 a** & **b**. Furthermore, the voltammograms for divalent Ca ions are different than that to either of the monovalent ions. These two observations give an early indication that the COF electrodes may be able to differentiate between ions of similar as well as different valences.

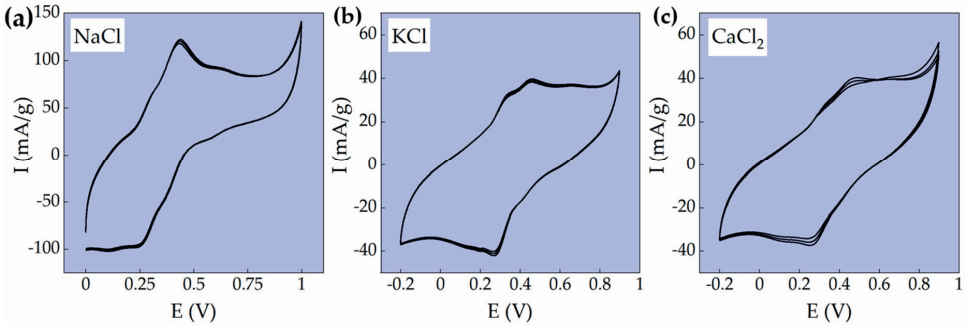

Figure 8.2: Cyclic voltammograms obtained by cycling COF electrodes in a 1M solution of (a) NaCl, (b) KCl, and (c) $CaCl_2$ at 1 mV/s.

These CVs are an indicator of an unexplored potential of COFs that can be utilised as (selective) electrodes in CDI. Considering the customizability of the COFs, exciting opportunities may lie in fabricating a redox-active COF to intentionally discriminate between ions.

While the prospect of new electrodes with bespoke chemistries is endlessly fascinating and intellectually stimulating, a cautious optimism must be exercised about their feasibility as an electrode in CDI. Development of these new materials for an electrode should also focus on benchmarking them with the state-of-the-art by subjecting them to a set of standardized performance metrics, like those described earlier on in **Chapter 1**. A lack of such benchmark tests mostly results in SACs and energy consumption values obtained under non-standard conditions, making the study difficult to compare with the others. Furthermore, reliance on only one metric to judge the feasibility of an electrode may not give a complete picture. For example, while the (equilibrium) SAC, one of the most cited metrics in CDI literature, is indeed a relevant parameter and its high value is desirable, it is often obtained under conditions that do not represent real-life conditions. Therefore, a high (equilibrium) SAC value does not necessarily imply a high salt rejection and rate of salt adsorption. Besides, a high (equilibrium) SAC value differs with differing feed concentration or the rate of charge/discharge. Hence, enthusiasm based solely on SAC should be restrained as it disregards important metrics and conditions useful for application of CDI in real-life applications.

In addition to the electrode material, another crucial stage of electrode development is **cell design**. The potential of an electrode can only be utilised by a well-designed cell. This would also help gauge the feasibility of the new electrode materials. Consequently, the applicability of a new CDI system to enhance the current water desalination and harvesting infrastructure, as aimed in the SDG on clean water, will depend on it. The process of cell design can be thought along the following lines:

- Optimized electrode deployment: Electrodes can either be free standing or coated onto the current collector. In either case, preparation of electrodes should be such that the diffusion of ions to and inside these electrodes is facilitated. A high electrode porosity would be advantageous here. In a free-standing electrode this can be achieved by adding ammonium bicarbonate in the slurry, a measure developed in the field of energy storage.[354] Interestingly, the above-mentioned class of COF materials are inherently highly porous. When used in the fabrication of electrodes via non-carbonization approaches, leaving the COF structure, and consequently, its porosity intact, can become useful in CDI as well,
- Optimized placement of electrodes, in relation to each other, to minimize distance between them and reduce cell resistance.

Finally, the prediction of CDI performance is also a part of the electrode-cell development process. **Chapters 2** and **7** in this thesis make use of and explain an ion transport model developed using Nernst-Planck equation coupled with a Frumkin adsorption isotherm. A high degree of agreement was obtained between the experimental observations and model predictions at low to moderate applied currents. A lack of agreement at higher currents points towards an incomplete understanding of all the resistances in the cell. Therefore, more work is required to understand how and where the resistances lie in a cell and how does the cell geometry affect them. Use of visualization and simulation software such as COMSOL[355,356] might aid in understanding the fluid dynamics inside a cell and highlight the transport resistances that may develop inside the cell due to irregular flow patterns resulting in channeling and dead volumes. Such insights will be valuable in guiding the design of a cell. More insight on the future of modeling in CDI is provided in the conclusions section of **Chapter 2**.

8.1.2 The quest for electrode stability in CDI

Another aspect of electrode development, as essential as the discovery of new electrode materials and chemistries, is the assessment of their stability for the simple reason – if the electrode is not able to withstand repeated adsorption and desorption of ions, it will be of limited utility in real-life applications and would add little value to the desalination and harvesting infrastructure. Therefore, a stability assessment should form a fundamental step in electrode and CDI cell production processes. There are at least two benefits of such an exercise:

- A thorough assessment of the stability will indicate how long the electrodes shall last under realistic conditions of use,
- Once stability is assessed, appropriate steps can be taken to mitigate electrode degradation and enhance lifetime. This is currently being done by either modifying the electrode or the environment and will be elaborated upon later in the section.

The introduction of stability assessment among the sequence of steps in the electrode fabrication procedure can be highly valuable, provided the assessment is done objectively under a standard set of operation parameters. Hawks et al.[357] introduced a set of operation and separation conditions along with well-defined performance metrics, detailed in **Chapter 1**, that can be used to objectively assess and compare any two different CDI cells. This difference may arise either from the use of a different electrode material or different cell configurations, shown in **Figure 1.2.** The stability assessment of an electrode may take a similar route in which:

The separation conditions – water recovery and Δc can be fixed for a given flowrate (through each channel of the cell) for the duration of the test,

- The deionization is performed in a constant current operation with a pre-decided half cycle time and cell voltage cut-offs. The current is chosen according to the separation conditions (a minimum current must be applied to achieve the desired Δc at the given feed flowrate),
- The total duration of the test is fixed. This can be anywhere between a day to a week to a month. The increase in testing period will depend on the success of the tests in the previous smaller duration tests.

This approach of testing electrode stability is illustrated as a flowchart in **Figure 8.3**.

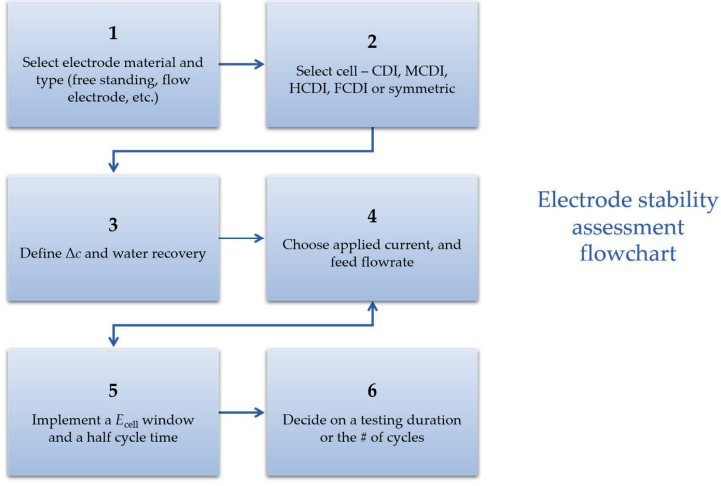

Figure 8.3: Illustration depicting the flowchart of the proposed electrode stability testing procedure.

As shown, the stability testing workflow starts with the selection of electrode materials, cell design, and the separation conditions (steps 1 – 3) under which the testing is required. This selection fixes the applied current density and the flowrate (step 4) as these parameters have direct consequence on the separation conditions. Once the cell voltage (E_{cell}) window and the half cycle time has been fixed (step 5), the duration of the test can be chosen (step 6). It must be pointed out that steps 4 and 5 may require multiple iterations, as depicted by a circular arrow between the two steps in **Figure 8.3**, before a satisfactory set of current, flowrate, E_{cell}, and half cycle time values is found to achieve the separation conditions imposed on the cell. This multi-step approach to has various advantages, such as:

- Easy to judge the cell response to the imposed operation conditions,
- Easy to compare with other studies, following similar approach and reporting performance via similar metrics,
- Easy to identify the set of operation conditions that cause the least damage to the electrode while fulfilling the separation conditions. For instance, high cell voltages or complete charging/discharging might accelerate electrode degradation via parasitic side reactions or internal structure changes, respectively. A set of current, flowrate, E_{cell}, half cycle time can help avoid these high voltages or complete charging/discharging of electrodes during operation, thus enhancing electrode stability.

In addition to the standardisation of electrode testing and optimisation of operation parameters, electrodes can also be reinforced against degradation. An example of this is found in a recent report in literature where a set of PBA electrodes were coated with Nafion, a copolymer bearing sulfonate moieties, to essentially cut their contact with the feed solution and enhance stability of the electrodes for 100 cycles.[55] This solution may economically prohibitive for practical application. A similar rational was used in **Chapter 5**, when the VHCF electrodes were coated with PPy/PSS, although the goal was different. This approach holds promise as an inspiration for an efficient ion-conductive coating can be obtained by the highly developed field of membranes.

In the same spirit as coating electrodes with polymers, ion-exchange membranes can be used to isolate the electrodes from the feed compartment. These isolated chambers provide much room for exploration and can be filled with an electrolyte, which usually happens to be a high salinity salt solution.[358,359] In case of PBA electrodes, the isolated electrode chambers can also be filled with high concentration salt solution that matches the feed in terms of ion type, potentially eliminating any concentration related ion-transport limitations. While the membranes potentially open numerous lines of investigation, they can have an adverse consequence on the inherent selectivity of those electrodes who possess it, such as PBAs. If not, an ion-conductive coating (or a membrane) can provide an opportunity to induce ion selectivity in an electrode while at the same time, enhancing its stability.

While coating electrodes is a measure that is adopted after its fabrication, some measures can also be taken during electrode fabrication. For example, in the case of PBA electrode, it has

been reported that NiHCF electrodes are more capable of retaining their ion-storage capacity during repeated cycling when compared to other PBAs.[144,360] Therefore, the presence of Ni in PBA lattice appears to help in stabilizing it against degradation during repeated cycling. However, since the properties of PBAs change with the transition metal that replaces the N-coordinated Fe, it is conceivable that the transition metals, other than Ni, might be required for a specific application (CuHCF can better differentiate between NH_4^+ and Na^+ in comparison to NiHCF[106]). Keeping this in mind, new PBA electrodes can be fabricated in which a fraction of the N-coordinated Fe sites present in the original PB can be replaced by Ni and the rest by another transition metal necessary for a specific application. The resulting blended electrode may have an enhanced stability. An early study reported on this blending of transition metals to tune cation intercalation potentials for energy storage application.[241] In case of another redox-active intercalation material, MnO_2,[168] that uses cations to stabilise its tunnel structure, various combination of metal cations can be explored to see their effect on the stability of the resulting electrode.

8.1.3 The quest for ion selectivity in CDI

It is evident from the research presented in this thesis and the state-of-the-art, described **Chapter 2** and in literature reviews,[3,361,362] that the interest in ion-selective CDI is growing swiftly. This has led to significant advances, especially in the use of different electrode materials and membrane modifications for cation as well as anion selectivity in CDI. Furthermore, the theory of ion selectivity has been developed and validated with experiments. These developments have a direct impact on the global resource harvesting efforts from water which are crucial towards a more sustainable and circular economy, as highlighted in the SDGs. However, due to diverse methods, techniques, and materials employed in achieving selectivity, a direct comparison of these studies is proving to be difficult. Furthermore, ion-selectivity studies carried out in single-salt solutions, comparing individual electrosorption rates to calculate selectivity, provide little information on electrosorption behaviour in competitive environments that resemble real-life conditions. While it is challenging to introduce a standardized procedure to report ion selectivity due to countless different ion combinations, it may be sensible to provide a selectivity coefficient for one ion in a mixture over the others, an approach commonly used in sensor studies.[363,364]

Going forward, research into new electrode materials and chemistries, modification and optimization of existing materials, investigation of parameters for selectivity, and modelling of selectivity at the system and molecular level will be vital for fully realizing the potential of ion-selectivity via CDI. These research lines will be briefly addressed now.

New alternatives to carbon such as PBAs, TiS_2, NMO and layered oxides show remarkable inherent selectivity towards certain cations. This thesis already presented two PBAs as being capable of differentiating among monovalent and divalent ions and between them as well. A better understanding of the preference of these materials, like the presence of different

intercalation sites in PBAs[279] or the complexation of ions with transition metal at the adsorption site of a double layered hydroxide,[365] would help to further tune – or even switch – the preference of the materials, leading to a higher adaptability of selective CDI systems. Inspiration for the development of new electrode materials for CDI can be drawn from the more developed field of energy storage. As an example, manganese hexacyanoferrate (MnHCF), another PBA, previously explored for energy storage,[366–368] also shows promise when used as an active material in an electrode for selective CDI. When used to treat a feed containing multiple cations, both monovalent and divalent ones, MnHCF behaves like NiHCF, as made clear from the concentration profiles provided in **Figure 8.4**. These effluent concentrations were measured for an experiment performed with a symmetric CDI cell containing two identical MnHCF electrodes, along the lines of the work presented in **Chapter 4**. As expected, the selectivity of MnHCF electrodes follows a trend based on the hydration energy of the intercalation cations, as reported for other PBAs in literature as well.[135] This can be easily inferred from **Figure 8.4a**. There is a sharp increase in the amount of Na ions adsorbed over K and more prominently, Rb ions. This demonstrates the dependence of the preferential adsorption on the size/hydration energy of the intercalating cations. Surprisingly, such a trend is not observed between Na and Ca ions when a binary feed containing these ions is deionized by the MnHCF symmetric cell. (**Figure 8.4b)**.

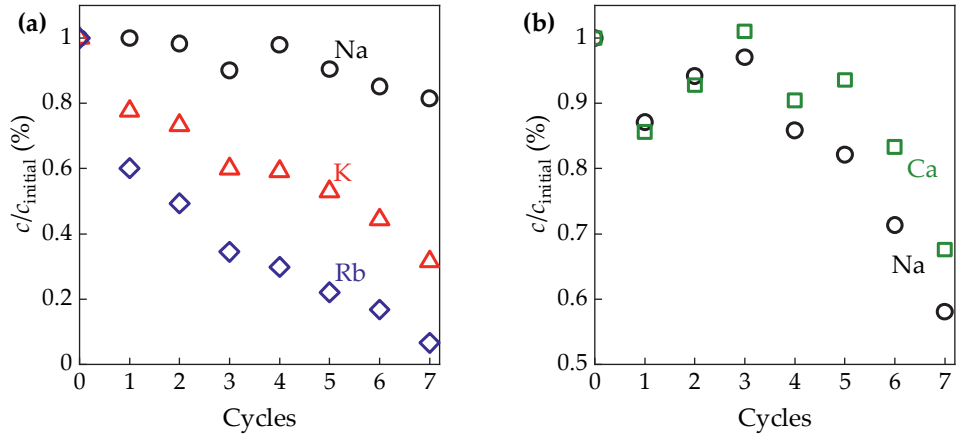

Figure 8.4: Concentration of Na and Ca ions in the effluent streams out of the symmetrical MnHCF cell after deionization performed on **(a)** equimolar mixture of Na, K, and Rb ions and **(b)** an equimolar solution of Na and Ca ions.

This observation contrasts with the high selectivity obtained between Na and Ca ions with NiHCF electrodes, as detailed in **Chapter 4** and is closer to the observations made in **Chapter 5** using VHCF electrodes, as the relative preference for Na ions reduces and more Ca is adsorbed by MnHCF, resembling the VHCF electrodes. The placement of Mn in the PBA lattice, and the following change in the ion selectivity of the resulting MnHCF confirms the hypothesis laid down in **Chapter 5** that the preference towards ions demonstrated by PBA electrodes is significantly affected by the transition metal chosen to replace the nitrogen-bound Fe in the

original PB lattice. This knowledge opens numerous opportunities for exploring the use of various transition metals (and their mixtures) for tuning the selectivity of ion-selective electrodes and contributing to the resource harvesting efforts.

Moving from electrodes that have inherent capability to differentiate between ions to the ones that do not, electrode modifications will be the key for inducing selectivity. Since the modifications can be controlled and fine-tuned, this line of investigation can lead to application-specific CDI systems. The modification of the electrode may be as simple as changing the activation conditions of a carbon electrode to obtain very narrow micropores,[357,369] by adding functional groups or resins with affinity towards specific species,[26,287] or by modifying carbon electrodes with redox active-organometallic polymers to remove organic ions.[370] In MCDI cells, selectivity is derived from the ion-exchange membranes (IEMs) separating the carbon electrodes from the feed. These IEMs can be further modified *e.g.*, by adding polyelectrolyte multilayers, to introduce monovalent selectivity.[260]

Once a CDI cell has an ion-selective element, be it an electrode or a membrane, the dependence of this selectivity on operation parameters such as applied current, cell voltage, ion concentration, and pH among others must be systematically studied to find optimum conditions. Intercalation electrodes such as TiS_2 show switchable preference depending on the potential of the electrode, as shown recently.[100] In another instance, selective adsorption of NH_4^+ over Na^+ reduced when the voltage of a symmetric CDI cell, containing two identical copper hexacyanoferrate (CuHCF) PBA electrodes, was increased.[106] Such observations and insights will be useful in realizing the full potential of existing (and the search for new) electrode materials. A standard set of operational parameters, like those proposed to objectively assess CDI systems,[40] would further enable a better comparison between results in ion-selective literature. For example, it would be beneficial to provide at least one set of experiments using single-pass mode under constant current, with the values of feed and outlet concentration of each ion clearly defined. Since the constant current mode of operation enables continuous transport of ions to the electrodes or the membranes, selectivity of the system can be easily evaluated. Furthermore, this will also closely resemble real-life cases encountered during system scale-up.

Finally, an ability to predict ion-selectivity will help to streamline the efforts being made in this field of CDI, enhancing the strength of the technology to remove ions selectively. A physical model put forward by our groups at Wetsus and Wageningen University takes a step in this direction by putting forward a theory, at the system level, for the prediction of ion-selectivity for a class of intercalation electrodes.[3] A logical next step is the investigation of the molecular origins for the preference of electrode materials towards different ions. Further insight into the mechanism of preferential electrosorption of ions can help to tune the selectivity-inducing properties of the electrode material. Molecular dynamics (MD) and DFT simulations may further prove to be useful in fabricating materials with inherent selectivity towards desired ions. Hawks et al.[357] carried out MD simulations to elucidate the selective

adsorption of NO_3^- over Cl^- and SO_4^{2-} in carbon electrodes. This simulation assisted in understanding how hydration of the ions influenced the anion selectivity in very narrow micropores. For intercalation materials such as PBA, DFT simulations, as performed by Jiang *et al.*,[279] are useful to understand the preference of the electrode for a certain ion. In this study, binding energy, and volume of a CuHCF lattice was calculated after intercalation of Li^+, Na^+, and K^+. The results showed that cations, based on their size, preferred intercalating at different sites within the lattice. The preference of the lattice towards a cation was reflected by the reduced binding energy upon intercalation of that ion into the intercalation electrode. In addition, the calculated change in the volume was also found to be the smallest for the most preferred cation, K^+ in this case, which has been confirmed experimentally as well.[279] Such modelling exercises can help in fabrication of new intercalation materials with properties that suit selective removal of a desired ion. A glimpse into such an exercise can be found in **Chapter 5**, where DFT simulations predicted an easier intercalation of Ca ions into the lattice of VHCF electrodes than that of Na ions. This prediction was later confirmed by experiments in which VHCF electrodes were found to be selective towards Ca over Na ions, thus demonstrating the increasing utility of modelling at the molecular level.

Summary

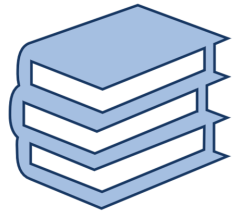

"Don't adventures ever have an end?

I suppose not. Someone else always has to carry on the story"

LOTR

Any long journey remains incomplete without a reflective throwback, summarizing its highlights and the lessons learned. To that end, the text below summarizes the outcomes of the research presented in the chapters above and highlights their key discoveries and insights.

The work described in this thesis aims to further enhance the CDI state-of-the-art by exploring new, advanced materials to fabricate capacitive electrodes, the very heart of a CDI cell. The motives behind this pursuit, that include the inadequate ability of the existing materials to store ions, consume less energy while storing ions, and differentiate between the different ions, are elaborated in **Chapter 1**. This description forms a segue to the **aim** of the research: to study **new** electrode materials to be used in a **new** cell design to boost (**selective**) CDI performance. In addition, **Chapter 1** also recaps the performance metrics that should be understood to objectively evaluate the performance of any CDI cell, regardless of its make.

Towards this aim, **Chapter 2** begins by systematically recounting the application of intercalation materials in CDI. This exercise results in three central contributions to the field:

a) It paints a precise picture of what has been done before and where the field of CDI stands, in terms of the use of alternative electrode materials,
b) It highlights the research gaps and areas that required attention,
c) It explores the most promising avenues for the development of the CDI state-of-the-art.

Following the exercise of **Chapter 2**, a study comparing the desalination performance of the conventional carbon electrodes, in an MCDI cell, to that of nickel hexacyanoferrate (NiHCF) electrodes, in a symmetric/rocking chair cell, was performed. **Chapter 3** reports on the findings of this study. The elements of the hardware, including the current collectors, spacers, and membranes were kept identical between the carbon and NiHCF based cells to maintain uniformity between them. Furthermore, the comparison was kept as objective as possible by running both cells under identical experimental conditions to assess their CDI performance. As a result, it was found in this study that the symmetric CDI cells with NiHCF electrodes were more energy efficient than carbon-based MCDI cells by typically obtaining a 2.5-fold reduced energy consumption for identical separation conditions. In addition, the average salt adsorption rate (ASAR) of the NiHCF cell was typically 2-fold higher than that of the carbon cell. This finding is crucial to the development and application of intercalation material-based CDI cells and has direct implications for the development of desalination systems, in line with the sustainable development goals adopted by the UN regarding clean water. Finally, this study also used a Nernst-Planck transport model, including a Frumkin adsorption isotherm, to accurately predict the salt adsorption by the NiHCF cell. In addition, it also provided a qualitative description of the energy input, *via* the cell voltage prediction, to the NiHCF cell. This is the first use of a physics-based predictive model to understand cell performance in CDI with intercalation materials and can be used in future to test various cell designs (including electrode material-based parameters) and operation conditions to check

their suitability for water desalination. This approach can significantly enhance the current CDI state-of-the-art.

While the study reported in **Chapter 3** focuses on a symmetric NiHCF cell that adsorbed cations indiscriminately, **Chapter 4** describes the behaviour of the same cell when faced with a feed solution that contains both monovalent Na and divalent Ca and Mg ions. It was found that the average selectivity, indicated by the parameter β, varied between 15 and 25 towards Na over Ca and Mg ions, respectively, when the NiHCF symmetric cell was used to desalinate an equimolar mixture of all three ions. The presence of such high inherent selectivity was attributed to the difference between the hydration energies of the monovalent Na and divalent Ca and Mg ions. Since they all must intercalate into the fixed NiHCF lattices, they must shed the water shell around them. This neatly demonstrates the inherent ability of lattice type intercalation materials to differentiate between the adsorbing cations. In addition to the high selectivity, it was also found that the preference towards Na did not decrease with its decreasing concentration in the diluate. This implies that the NiHCF electrodes can be used to selectively remove monovalent cations over the divalent ones over a wide range of their relative concentrations in feed solutions.

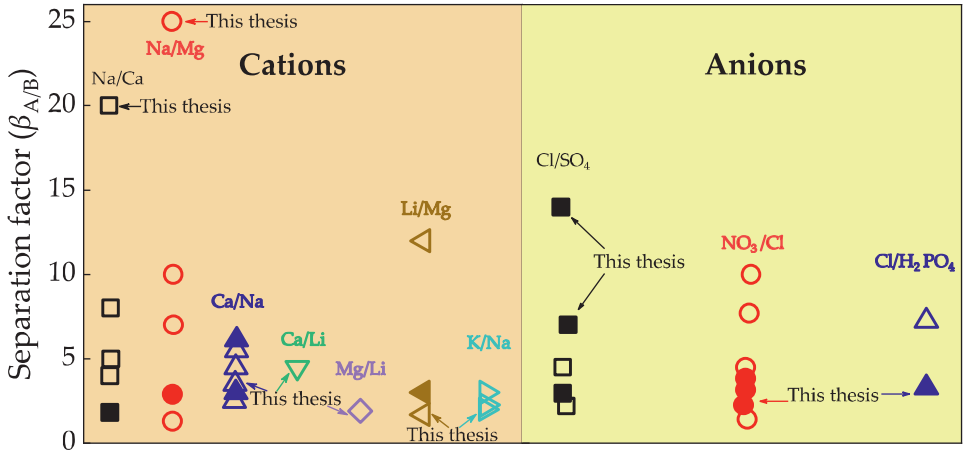

Figure 8.1: The selectivity values reported in this thesis in comparison to the CDI state of the art. The open symbols indicate the selectivity values obtained via an electrode while the closed symbols indicate the selectivity values obtained via a membrane in a CDI cell. The closed symbols (*e.g.*, ▪) indicate electrode-based selectivity while the open symbols (*e.g.*, ▫) indicate membrane-based selectivity. The β values for electrode-based cation separation were adopted from references[54,56,136,165,173,232,286,371] whereas those for membrane-based cation separation were adopted from references.[139,234,280,290,372] Similarly, the β values obtained by electrode-based anion selectivity were adopted from references[47,141,222,357,367,373–375] while those obtained using a membrane were adopted from references.[287,376,377]

This finding will be instrumental in building resource recovery and harvesting systems in the future, contributing directly to the sustainable development goal (SDG) of clean water adopted

by the UN. Furthermore, even after 200 cycles of complete (de)intercalation, the electrodes retained a significant part of their original selectivity towards Na, as the β delivered by the electrodes after 200 cycles varied between the 7 and 15. Therefore, the observations reported here enhance the efforts of fabricating durable CDI cells with size and charge-based ion selectivity.

A comparison with literature puts these values in context, as depicted graphically in **Figure 8.1**. To make this comparison, the β values were adopted from studies that used either an electrode or a membrane to achieve ion selectivity in a CDI cell from an ion mixture. The $\beta_{Na/Ca}$ and $\beta_{Na/Mg}$ values found in **Chapter 4** remain the highest reported in CDI literature so far, for electrode-based cation selectivity. The β values for K over Na, also found during experiments with NiHCF were comparable with those in literature while the competitive advantage in Li over Mg removal was lost with NiHCF. Interestingly, this comparison also highlights that electrode in general delivered higher β values than membranes for cations. This observation does not always hold for anions, thus showing the different successful approaches, based on either electrodes or membranes, taken in the CDI state-of-the-art to achieve ion selectivity for cations and anions.

Building on the use of PBAs to fabricate ion-selective CDI cells, as described in **Chapter 4**, **Chapter 5** introduces vanadium hexacyanoferrate (VHCF) as a divalent cation selective electrode in CDI. It was found that the substitution of nickel with vanadium in the lattice of a PBA switches its preference in CDI experiments from monovalent ions toward divalent ions. The discovery of divalent ion selectivity in a PBA is significant for at least two reasons:

1. PBA electrodes can also be employed in applications that require divalent ion selectivity, such as reduction of hardness from water.
2. The properties of PBAs can be altered significantly by altering its chemistry at a lattice level. Therefore, the selectivity of a PBA electrode can be tuned or tailored according to the application requirements.

This study was also the first to use VHCF as an electrode for CDI, and the first to intercalate monovalent ions such as Li and divalent ions such as Ca and Mg into the VHCF lattice. The flip in selectivity towards divalent ions from the commonly observed monovalent ions was also supported by density functional theory (DFT) simulations. The results of these simulations showed that the energy of VHCF lattices reduces upon intercalation of a cation. This reduction in energy is larger when a divalent Ca cation intercalates into the lattice as compared to when a monovalent Na cation intercalates into the lattice. These simulations show the ease with which quantum-chemical calculations can be used to predict properties of intercalation electrodes in CDI. As for the divalent-selective nature of the electrode, it was hypothesized that the presence of vanadium in the lattice as V=O may be behind it. The extra oxygen present in the lattice together with vanadium may have an electrostatic attraction towards the intercalating cation. This attraction will be higher for Ca than Na, resulting in an overall selectivity of the electrode towards Ca. Finally, the study also reported the use of a

polymeric coating to protect the treated water from contamination caused by the electrode degradation. This coating successfully prevented the contamination of the diluate stream as the electrode degraded over time. The discovery of divalent ion intercalation and selectivity in a VHCF electrode, together with the development of a polymeric coating, are two new additions to the field of CDI. Comparison with the β values reported in literature for $\beta_{Ca/Na}$, $\beta_{Mg/Na}$, and $\beta_{Ca/Li}$ shows that the values found in **Chapter 5**, in the range of $2 < \beta < 5$, remain comparable with the values reported in state-of-the-art, as depicted in **Figure 8.1**.

The selectivity narrative presented until **Chapter 5** focuses solely on the differentiation among cations by a PBA electrode. This is a direct consequence of the inability of PBA to intercalate and store anions. As a result, to remove anions from water, researchers resort to using either a hybrid CDI cell with a different anode capable of storing anions or a symmetric CDI cell with two identical electrodes separated by a membrane, capable of displacing anions from one compartment to another. Due to the limited number of anode materials that can be used to fabricate a feasible CDI cell with inherent anion selectivity, the symmetric cell provides a new and yet familiar alternative. This concept is described in **Chapter 6** where a unique combination of modified anion-exchange membrane (AEM) and NiHCF electrodes is successfully used for the first time, to simultaneously and selectively separate both mono- and divalent cations and anions. The selectivity between mono- and divalent cations was made possible by the identical NiHCF electrodes, while the selectivity between mono- and divalent anions was made possible by the AEM separating the two NiHCF electrode compartments. The ion-selective nature was imparted to the membrane by layers of positively and negatively charged polymers, also called polyelectrolytes. These polyelectrolytes were assembled on top of an AEM to form polyelectrolyte multilayers (PEMs), enabling differentiation among monovalent ions, divalent ions, and between monovalent and divalent ions. The preference of the layers towards an anion is dictated by either its hydration energy or the charge carried by it. This mechanism resulted in the selectivity values in the range of $7 < \beta < 14$ between monovalent Cl and divalent SO_4 anions. These values were higher than the ones achieved with commercially available monovalent anion-selective membranes ($\beta \approx 7$). Also, a β of 3 was obtained from a feed containing monovalent Cl and H_2PO_4 anions, highlighting the ability of the PEMs to differentiate ions carrying identical charge. Comparison with literature, as done for anions in **Figure 8.1**, shows that the values of $\beta_{Cl/SO4}$ were highest among all reported so far in CDI, irrespective of whether the selectivity element was an electrode or a membrane. However, higher values of $\beta_{Cl/NO3}$ and $\beta_{Cl/H2PO4}$ have been reported in CDI literature. Nevertheless, the values obtained here remain competitive. In conjunction with the PEM-coated AEMs, the NiHCF electrodes exhibited a high inherent selectivity towards monovalent ions over divalent ions, delivering a $\beta \approx 17$ towards monovalent Na over the divalent Mg ions. This clearly showed that the use of a PEM-modified membrane had no adverse effect on the inherent ion selectivity of the NiHCF electrodes. This tandem use of intercalation electrodes and a PEM-coated membrane provides a new and facile method for simultaneous cation and

anion selectivity in CDI from complex ion mixtures and will help to catalyze the development of the resource recovery and harvesting infrastructure.

Chapters 3 – 6 describe knowledge acquired predominantly via experiments. However, a complete description of a system also demands a theoretical understanding. These theoretical endeavors were hinted in **Chapters 3** and **5**. While a quantum-chemical modeling was performed in **Chapter 5** to simulate adsorption of cations at the lattice level and make predictions on the relative ease of cation intercalation, the model used in **Chapter 3** has a larger scope and considers a complete CDI cell. Therefore, this physics-based model of the cell accounts for the ion transport across the cell components and their adsorption into the capacitive electrodes. The intercalation of cations in this model is accounted by the Frumkin isotherm. While **Chapter 3** makes use of this model to predict cell performance that is later verified with experimental data, **Chapter 7** describes this physics-based model in detail for a cell containing two identical intercalation electrodes, separated by an AEM. It shows how the transport and adsorption of ions can be modeled with a Nernst-Planck equation and a Frumkin isotherm, respectively, to predict effluent concentration, cation mole fraction inside the electrode, and cell voltage. The model made use of the symmetric cell design to predict the mirrored operation in the two electrode chambers. One of the strengths of this model is that it is not predominantly dictated by the type of intercalation material. Therefore, if the adsorption of cations in the electrode can be reasonably described by a chosen isotherm, this model can provide reasonably accurate predictions, as evidenced by the results described in **Chapter 3**. The intention behind this model is to provide a platform upon which future models can be conceived for more realistic water sources with ionic mixtures, as was done in a later article from our group (Gamaethiralalage *et. al*, 2021[3]) that gave a theory on the selective adsorption of one cation over another from a binary feed solution into an intercalation-based electrode, and for other geometries of desalination systems involving porous electrodes with redox-active intercalation materials.

References

[1] N. Ghaffour, T. M. Missimer, G. L. Amy, *Desalination* **2013**, *309*, 197.

[2] R. Damania, S. Desbureaux, M. Hyland, A. Islam, S. Moore, A.-S. Rodella, J. Russ, E. Zaveri, *Uncharted Waters: The New Economics of Water Scarcity and Variability*, World Bank, Washington, DC, **2017**.

[3] J. G. Gamaethiralalage, K. Singh, S. Sahin, J. Yoon, M. Elimelech, M. E. Suss, P. Liang, P. M. Biesheuvel, R. L. Zornitta, L. C. P. M. de Smet, *Energy Environ. Sci.* **2021**, *14*, 1095.

[4] M. Elimelech, W. A. Phillip, *Science (80-.).* **2011**, *333*, 712.

[5] E. Jones, M. Qadir, M. T. H. van Vliet, V. Smakhtin, S. mu Kang, *Sci. Total Environ.* **2019**, *657*, 1343.

[6] N. C. Darre, G. S. Toor, *Desalination of Water: a Review*, Vol. 4, Springer, **2018**, pp. 104–111.

[7] V. G. Gude, *Desalination and water reuse to address global water scarcity*, Vol. 16, Springer Netherlands, **2017**, pp. 591–609.

[8] F. S. Pinto, R. C. Marques, *Desalination projects economic feasibility: A standardization of cost determinants*, Vol. 78, Elsevier Ltd, **2017**, pp. 904–915.

[9] R. Chen, T. Sheehan, J. L. Ng, M. Brucks, X. Su, *Capacitive deionization and electrosorption for heavy metal removal*, Vol. 6, Royal Society of Chemistry, **2020**, pp. 258–282.

[10] S. J. Seo, H. Jeon, J. K. Lee, G. Y. Kim, D. Park, H. Nojima, J. Lee, S. H. Moon, *Water Res.* **2010**, *44*, 2267.

[11] K. Singh, Z. Qian, P. M. Biesheuvel, H. Zuilhof, S. Porada, L. C. P. M. de Smet, *Desalination* **2020**, *481*, 114346.

[12] Y. Yang, X. Meng, H. Cao, X. Lin, C. Liu, Y. Sun, Y. Zhang, Z. Sun, *Green Chem.* **2018**, *20*, 3121.

[13] I. Korolev, P. Altınkaya, P. Halli, P. M. Hannula, K. Yliniemi, M. Lundström, *J. Clean. Prod.* **2018**, *186*, 840.

[14] Y. Lei, B. Song, M. Saakes, R. D. van der Weijden, C. J. N. Buisman, *Water Res.* **2018**, *142*, 10.

[15] E. Bakker, M. Telting-Diaz, *Electrochemical sensors*, Vol. 74, American Chemical Society , **2002**, pp. 2781–2800.

[16] M. Al-Sahali, H. Ettouney, *Desalination* **2007**, *214*, 227.

[17] Chapter 1 Overview of ion-exchange membrane processes, In *Membrane Science and Technology*, Elsevier, **2004**, pp. 1–22.

[18] M. E. Suss, S. Porada, X. Sun, P. M. Biesheuvel, J. Yoon, V. Presser, *Energy Environ. Sci.*

2015, *8*, 2296.

[19] A. Subramani, J. G. Jacangelo, *Water Res.* **2015**, *75*, 164.

[20] S. Porada, R. Zhao, A. Van Der Wal, V. Presser, P. M. Biesheuvel, *Prog. Mater. Sci.* **2013**, *58*, 1388.

[21] F. A. AlMarzooqi, A. A. Al Ghaferi, I. Saadat, N. Hilal, *Desalination* **2014**, *342*, 3.

[22] I. G. Wenten, Khoiruddin, *Desalination* **2016**, *391*, 112.

[23] C. Fritzmann, J. Löwenberg, T. Wintgens, T. Melin, *Desalination* **2007**, *216*, 1.

[24] S. Porada, L. Zhang, J. E. Dykstra, *Desalination* **2020**, *488*, 114383.

[25] Y. Dreizin, A. Tenne, D. Hoffman, *Desalination* **2008**, *220*, 132.

[26] R. Epsztein, R. M. DuChanois, C. L. Ritt, A. Noy, M. Elimelech, *Nat. Nanotechnol.* **2020**, *15*, 426.

[27] X. Zhou, Z. Wang, R. Epsztein, C. Zhan, W. Li, J. D. Fortner, T. A. Pham, J. H. Kim, M. Elimelech, *Sci. Adv.* **2020**, *6*, 1.

[28] G. M. Geise, M. A. Hickner, B. E. Logan, *ACS Appl. Mater. Interfaces* **2013**, *5*, 10294.

[29] H. Strathmann, A. Grabowski, G. Eigenberger, *Ion-exchange membranes in the chemical process industry*, Vol. 52, American Chemical Society, **2013**, pp. 10364–10379.

[30] L. Ouyang, R. Malaisamy, M. L. Bruening, *J. Memb. Sci.* **2008**, *310*, 76.

[31] S. Mulyati, R. Takagi, A. Fujii, Y. Ohmukai, H. Matsuyama, *J. Memb. Sci.* **2013**, *431*, 113.

[32] T. Sata, Y. Mizutani, *J. Polym. Sci. Polym. Chem. Ed.* **2003**, *17*, 1199.

[33] T. Sata, T. Sata, W. Yang, *J. Memb. Sci.* **2002**, *206*, 31.

[34] T. Mubita, S. Porada, P. Aerts, A. van der Wal, *J. Memb. Sci.* **2020**, *607*, 118000.

[35] B. Van Der Bruggen, A. Koninckx, C. Vandecasteele, *Water Res.* **2004**, *38*, 1347.

[36] N. Kabay, Ö. Ipek, H. Kahveci, M. Yüksel, *Desalination* **2006**, *198*, 84.

[37] S. Al-Amshawee, M. Y. B. M. Yunus, A. A. M. Azoddein, D. G. Hassell, I. H. Dakhil, H. A. Hasan, *Chem. Eng. J.* **2020**, *380*.

[38] M. A. Anderson, A. L. Cudero, J. Palma, *Capacitive deionization as an electrochemical means of saving energy and delivering clean water. Comparison to present desalination practices: Will it compete?*, Vol. 55, **2010**, pp. 3845–3856.

[39] A. Alabi, A. AlHajaj, L. Cseri, G. Szekely, P. Budd, L. Zou, *npj Clean Water* **2018**, *1*.

[40] S. A. Hawks, A. Ramachandran, S. Porada, P. G. Campbell, M. E. Suss, P. M. Biesheuvel, J. G. Santiago, M. Stadermann, *Water Res.* **2018**, *152*, 126.

[41] K. Singh, S. Porada, H. D. de Gier, P. M. Biesheuvel, L. C. P. M. de Smet, *Desalination* **2019**, *455*, 115.

[42] P. M. Biesheuvel, J. E. Dykstra, *Physics of Electrochemical Processes*, **2020**.

[43] J. Dykstra, *J. Membr. Sci.* **2016**, *356*, 256.

[44] J. Kang, T. Kim, H. Shin, J. Lee, J. I. Ha, J. Yoon, *Desalination* **2016**, *398*, 144.

[45] S. J. Seo, H. Jeon, J. K. Lee, G. Y. Kim, D. Park, H. Nojima, J. Lee, S. H. Moon, *Water Res.* **2010**, *44*, 2267.

[46] X. Su, T. A. Hatton, *Adv. Colloid Interface Sci.* **2017**, *244*, 6.

[47] D. I. Oyarzun, A. Hemmatifar, J. W. Palko, M. Stadermann, J. G. Santiago, *Water Res. X* **2018**, *1*, 100008.

[48] R. Zhao, S. Porada, P. M. Biesheuvel, A. Van Der Wal, *Desalination* **2013**, *330*, 35.

[49] D. A. Vermaas, S. Bajracharya, B. B. Sales, M. Saakes, B. Hamelers, K. Nijmeijer, *Energy Environ. Sci.* **2013**, *6*, 643.

[50] S. Porada, L. Weinstein, R. Dash, A. Van Der Wal, M. Bryjak, Y. Gogotsi, P. M. Biesheuvel, *ACS Appl. Mater. Interfaces* **2012**.

[51] Z.-H. Huang, Z. Yang, F. Kang, M. Inagaki, *J. Mater. Chem. A* **2017**, *5*, 470.

[52] S. Il Jeon, H. R. Park, J. G. Yeo, S. Yang, C. H. Cho, M. H. Han, D. K. Kim, *Energy Environ. Sci.* **2013**, *6*, 1471.

[53] S. Porada, D. Weingarth, H. V. M. Hamelers, M. Bryjak, V. Presser, P. M. Biesheuvel, *J. Mater. Chem. A* **2014**, *2*, 9313.

[54] S. Porada, A. Shrivastava, P. Bukowska, P. M. Biesheuvel, K. C. Smith, *Electrochim. Acta* **2017**, *255*, 369.

[55] J. Ahn, S. Kim, S. il Jeon, C. Lee, J. Lee, J. Yoon, *Desalination* **2021**, *500*, 114778.

[56] J. Lee, S. Kim, J. Yoon, *ACS Omega* **2017**, *2*, 1653.

[57] P. M. Biesheuvel, M. Z. Bazant, *Phys. Rev. E - Stat. Nonlinear, Soft Matter Phys.* **2010**, *81*, 031502.

[58] P. M. Biesheuvel, S. Porada, M. Levi, M. Z. Bazant, *J. Solid State Electrochem.* **2014**, *18*, 1365.

[59] P. M. Biesheuvel, Y. Fu, M. Z. Bazant, *Phys. Rev. E - Stat. Nonlinear, Soft Matter Phys.* **2011**, *83*, 061507.

[60] R. L. Zornitta, P. Srimuk, J. Lee, B. Krüner, M. Aslan, L. A. M. Ruotolo, V. Presser, *ChemSusChem* **2018**, *11*, 2101.

[61] A. Banerjee, R. Gokhale, S. Bhatnagar, J. Jog, M. Bhardwaj, B. Lefez, B. Hannoyer, S. Ogale, *J. Mater. Chem.* **2012**, *22*, 19694.

[62] E. R. Reale, A. Shrivastava, K. C. Smith, *Water Res.* **2019**, *165*, 114995.

[63] M. Aslan, M. Zeiger, N. Jäckel, I. Grobelsek, D. Weingarth, V. Presser, *J. Phys. Condens. Matter* **2016**, *28*.

[64] R. L. Zornitta, K. M. Barcelos, F. G. E. Nogueira, L. A. M. Ruotolo, *Carbon N. Y.* **2020**,

156, 346.

[65] E. Frackowiak, F. Béguin, *Carbon materials for the electrochemical storage of energy in capacitors*, Vol. 39, Elsevier Ltd, **2001**, pp. 937–950.

[66] P. Liang, L. Yuan, X. Yang, S. Zhou, X. Huang, *Water Res.* **2013**, *47*, 2523.

[67] C.-C. Huang, Y.-J. Su, *J. Hazard. Mater.* **2010**, *175*, 477.

[68] D. I. Oyarzun, A. Hemmatifar, J. W. Palko, M. Stadermann, J. G. Santiago, *Sep. Purif. Technol.* **2018**, *194*, 410.

[69] J. Lee, K. Jo, J. Lee, S. P. Hong, S. Kim, J. Yoon, *ACS Sustain. Chem. Eng.* **2018**, *6*, 10815.

[70] S. Porada, F. Schipper, M. Aslan, M. Antonietti, V. Presser, T.-P. Fellinger, *ChemSusChem* **2015**, *8*, 1867.

[71] J. Ma, J. Ma, C. Zhang, J. Song, W. Dong, T. D. Waite, *Water Res.* **2020**, *168*, 115186.

[72] A. Omosebi, X. Gao, J. Landon, K. Liu, *ACS Appl. Mater. Interfaces* **2014**, *6*, 12640.

[73] M. E. Suss, *J. Electrochem. Soc.* **2017**, *164*, E270.

[74] A. C. Arulrajan, J. E. Dykstra, A. van der Wal, S. Porada, *Environ. Sci. Technol.* **2021**, *55*, 14165−14172.

[75] J. E. Dykstra, K. J. Keesman, P. M. Biesheuvel, A. van der Wal, *Water Res.* **2017**, *119*, 178.

[76] Y. Cheng, Z. Hao, C. Hao, Y. Deng, X. Li, K. Li, Y. Zhao, *RSC Adv.* **2019**, *9*, 24401.

[77] A. L. Lipson, S. D. Han, S. Kim, B. Pan, N. Sa, C. Liao, T. T. Fister, A. K. Burrell, J. T. Vaughey, B. J. Ingram, *J. Power Sources* **2016**, *325*, 646.

[78] S. Il Park, I. Gocheva, S. Okada, J. Yamaki, *J. Electrochem. Soc.* **2011**, *158*, A1067.

[79] Y. Lu, L. Wang, J. Cheng, J. B. Goodenough, *Chem. Commun.* **2012**, *48*, 6544.

[80] R. Y. Wang, B. Shyam, K. H. Stone, J. N. Weker, M. Pasta, H. W. Lee, M. F. Toney, Y. Cui, *Adv. Energy Mater.* **2015**, *5*, 1.

[81] Q. Li, Y. Zheng, D. Xiao, T. Or, R. Gao, Z. Li, M. Feng, L. Shui, G. Zhou, X. Wang, Z. Chen, **2020**, *2002213*.

[82] A. A. Karyakin, *Electroanalysis* **2001**, 813.

[83] Y. Liu, Y. Qiao, W. Zhang, Z. Li, X. Ji, L. Miao, L. Yuan, X. Hu, Y. Huang, *Nano Energy* **2015**, *12*, 386.

[84] J. Qian, C. Wu, Y. Cao, Z. Ma, Y. Huang, X. Ai, H. Yang, *Prussian Blue Cathode Materials for Sodium-Ion Batteries and Other Ion Batteries*, Vol. 8, Wiley-VCH Verlag, **2018**.

[85] B. Paulitsch, J. Yun, A. S. Bandarenka, *ACS Appl. Mater. Interfaces* **2017**, *9*, 8107.

[86] K. Hurlbutt, S. Wheeler, I. Capone, M. Pasta, *Joule* **2018**, *2*, 1950.

[87] M. R. Lukatskaya, O. Mashtalir, C. E. Ren, Y. Dall'Agnese, P. Rozier, P. L. Taberna, M.

Naguib, P. Simon, M. W. Barsoum, Y. Gogotsi, *Science (80-.).* **2013**, *341*, 1502.

[88] Z. Lin, P. Rozier, B. Duployer, P.-L. Taberna, B. Anasori, Y. Gogotsi, P. Simon, *Electrochem. commun.* **2016**, *72*, 50.

[89] P. Srimuk, F. Kaasik, B. Kruner, A. Tolosa, S. Fleischmann, N. Jackel, M. C. Tekeli, M. Aslan, M. E. Suss, V. Presser, *J. Mater. Chem. A* **2016**, *4*, 18265.

[90] S. Porada, P. Bukowska, A. Shrivastava, P. M. Biesheuvel, K. C. Smith, *arXiv Prepr. arXiv1612.08293v1* **2016**.

[91] K. Singh, L. Zhang, H. Zuilhof, L. C. P. M. de Smet, *Desalination* **2020**, *496*, 114647.

[92] F. Ma, Q. Li, T. Wang, H. Zhang, G. Wu, *Sci. Bull.* **2017**, *62*, 358.

[93] S. Kjeldgaard, I. Dugulan, A. Mamakhel, M. Wagemaker, B. B. Iversen, A. Bentien, *R. Soc. Open Sci.* **2021**, *8*, 201779.

[94] T. Wu, G. Wang, S. Wang, F. Zhan, Y. Fu, H. Qiao, J. Qiu, *Environ. Sci. Technol. Lett.* **2018**, *5*, 98.

[95] J. Lee, S. Kim, C. Kim, J. Yoon, *Energy Environ. Sci.* **2014**, *7*, 3683.

[96] W. Shi, X. Zhou, J. Li, E. R. Meshot, A. D. Taylor, S. Hu, J.-H. Kim, M. Elimelech, D. L. Plata, *Environ. Sci. Technol. Lett.* **2018**, acs. estlett.8b00397.

[97] S. Kim, J. Lee, C. Kim, J. Yoon, *Electrochim. Acta* **2016**, *203*, 265.

[98] X. Y. Wu, M. Y. Sun, Y. F. Shen, J. F. Qian, Y. L. Cao, X. P. Ai, H. X. Yang, *ChemSusChem* **2014**, *7*, 407.

[99] F. Xing, T. Li, J. Li, H. Zhu, N. Wang, X. Cao, *Nano Energy* **2017**, *31*, 590.

[100] P. Srimuk, J. Lee, S. Fleischmann, M. Aslan, C. Kim, V. Presser, *ChemSusChem* **2018**, *11*, 2091.

[101] M. E. Suss, V. Presser, *Joule* **2018**, *2*, 25.

[102] V. D. Neff, *J. Electrochem. Soc.* **1978**, *125*, 886.

[103] C. Erinmwingbovo, M. S. Palagonia, D. Brogioli, F. La Mantia, *ChemPhysChem* **2017**, *18*, 917.

[104] J. H. Lee, G. Ali, D. H. Kim, K. Y. Chung, *Adv. Energy Mater.* **2017**, *7*.

[105] A. Paolella, C. Faure, V. Timoshevskii, S. Marras, G. Bertoni, A. Guerfi, A. Vijh, M. Armand, K. Zaghib, *A review on hexacyanoferrate-based materials for energy storage and smart windows: Challenges and perspectives*, Vol. 5, **2017**, pp. 18919–18932.

[106] T. Kim, C. A. Gorski, B. E. Logan, *Environ. Sci. Technol. Lett.* **2018**, *5*, 578.

[107] K. Singh, G. Li, J. Lee, H. Zuilhof, B. L. Mehdi, R. L. Zornitta, L. C. P. M. de Smet, *Adv. Funct. Mater.* **2021**, 2105203.

[108] P. Marzak, J. Yun, A. Dorsel, A. Kriele, R. Gilles, O. Schneider, A. S. Bandarenka, *J. Phys. Chem. C* **2018**, *122*, 8760.

[109] K. Singh, H. J. M. Bouwmeester, L. de Smet, M. Z. Bazant, P. M. Biesheuvel, *Phys. Rev. Appl.* **2018**, *9*, 64036.

[110] J. E. Dykstra, S. Porada, A. van der Wal, P. M. Biesheuvel, *Water Res.* **2018**, *143*, 367.

[111] W. Blair John, W. Murphy George, In *Saline Water Conversion*, **1960**, pp. 206–223.

[112] P. Długołecki, A. Van Der Wal, *Environ. Sci. Technol.* **2013**, *47*, 4904.

[113] J. Lee, P. Srimuk, S. Fleischmann, X. Su, T. A. Hatton, V. Presser, *Redox-electrolytes for non-flow electrochemical energy storage: A critical review and best practice*, Vol. 101, Elsevier Ltd, **2019**, pp. 46–89.

[114] J. Ahn, J. Lee, S. Kim, C. Kim, J. Lee, P. M. Biesheuvel, J. Yoon, *Desalination* **2020**, *476*, 114216.

[115] Y. Liu, X. Gao, K. Wang, X. Dou, H. Zhu, X. Yuan, L. Pan, *J. Mater. Chem. A* **2020**, *8*, 8476.

[116] E. N. Guyes, A. N. Shocron, Y. Chen, C. E. Diesendruck, M. E. Suss, *npj Clean Water* **2021**, *4*, 1.

[117] Z. Qian, H. Miedema, L. C. P. M. de Smet, E. J. R. Sudhòlter, *Chem. Eng. Res. Des.* **2018**, *134*, 154.

[118] M. Kolasinska, R. Krastev, T. Gutberlet, P. Warszynski, *Langmuir* **2009**, *25*, 1224.

[119] R. Zhao, O. Satpradit, H. H. M. Rijnaarts, P. M. Biesheuvel, A. van der Wal, *Water Res.* **2013**, *47*, 1941.

[120] P. M. Biesheuvel, B. van Limpt, A. van der Wal, *J. Phys. Chem. C* **2009**, *113*, 5636.

[121] S. Porada, L. Zhang, J. E. Dykstra, *Desalination* **2020**, *488*, 114383.

[122] X. Liu, S. Shanbhag, T. V. Bartholomew, J. F. Whitacre, M. S. Mauter, *ACS ES&T Eng.* **2021**, *1*, 261.

[123] P. M. Biesheuvel, M. Z. Bazant, R. D. Cusick, T. A. Hatton, K. B. Hatzell, M. C. Hatzell, P. Liang, S. Lin, S. Porada, J. G. Santiago, *arXiv Prepr. arXiv1709.05925* **2017**.

[124] M. Li, H. G. Park, *ACS Appl. Mater. Interfaces* **2018**, *10*, 2442.

[125] C. Kim, P. Srimuk, J. Lee, S. Fleischmann, M. Aslan, V. Presser, *Carbon N. Y.* **2017**, *122*, 329.

[126] Y. Liu, C. Nie, X. Liu, X. Xu, Z. Sun, L. Pan, *Rsc Adv.* **2015**, *5*, 15205.

[127] S. Y. Pan, S. W. Snyder, Y. J. Lin, P. C. Chiang, *Environ. Sci. Water Res. Technol.* **2018**, *4*, 613.

[128] J. F. Whitacre, A. Tevar, S. Sharma, *Electrochem. commun.* **2010**, *12*, 463.

[129] H. Kim, R. a. Shakoor, C. Park, S. Y. Lim, J.-S. Kim, Y. N. Jo, W. Cho, K. Miyasaka, R. Kahraman, Y. Jung, J. W. Choi, *Adv. Funct. Mater.* **2012**, *23*, 1147.

[130] G. W. Murphy, D. D. Caudle, *Electrochim. Acta* **1967**, *12*, 1655.

[131] P. M. Biesheuvel, R. Zhao, S. Porada, A. van der Wal, *J. Colloid Interface Sci.* **2011**, *360*, 239.

[132] P. M. Biesheuvel, A. van der Wal, *J. Memb. Sci.* **2010**, *346*, 256.

[133] Y.-J. Kim, J.-H. Choi, *Water Res.* **2009**, *44*, 990.

[134] T. Wu, G. Wang, F. Zhan, Q. Dong, Q. Ren, J. Wang, J. Qiu, *Water Res.* **2016**, *93*, 30.

[135] T. Ikeshoji, *J. Electrochem. Soc.* **1986**, *133*, 2108.

[136] R. Zhao, M. Van Soestbergen, H. H. M. Rijnaarts, A. Van der Wal, M. Z. Bazant, P. M. Biesheuvel, *J. Colloid Interface Sci.* **2012**, *384*, 38.

[137] T. Kim, C. A. Gorski, B. E. Logan, *Environ. Sci. Technol. Lett.* **2017**, *4*, 444.

[138] J. E. Dykstra, J. Dijkstra, A. Van der Wal, H. V. M. Hamelers, S. Porada, *Desalination* **2016**, *390*, 47.

[139] J. Choi, H. Lee, S. Hong, *Desalination* **2016**, *400*, 38.

[140] P. G. Campbell, S. A. Hawks, M. R. Cerón, T. A. Pham, P. Shea, B. C. Wood, M. Stadermann, In *Meeting Abstracts*, The Electrochemical Society, **2018**, p. 1284.

[141] K. Zuo, J. Kim, A. Jain, T. Wang, R. Verduzco, M. Long, Q. Li, *Environ. Sci. Technol.* **2018**, *52*, 9486.

[142] K. C. Smith, R. Dmello, *J. Electrochem. Soc.* **2016**, *163*, A530.

[143] L. F. Schneemeyer, S. E. Spengler, D. W. Murphy, *Inorg. Chem.* **1985**, *24*, 3044.

[144] C. D. Wessells, S. V. Peddada, M. T. McDowell, R. A. Huggins, Y. Cui, *J. Electrochem. Soc.* **2012**, *159*, A98.

[145] M. Naguib, V. N. Mochalin, M. W. Barsoum, Y. Gogotsi, *Adv. Mater.* **2014**, *26*, 992.

[146] A. B. Bocarsly, S. Sinha, *J. Electroanal. Chem.* **1982**, *140*, 167.

[147] M. a. A. Lilga, R. J. J. Orth, J. P. H. P. H. Sukamto, S. M. M. Haight, D. T. T. Schwartz, *Sep. Purif. Technol.* **1997**, *11*, 147.

[148] S. D. Rassat, J. H. Sukamto, R. J. Orth, M. A. Lilga, R. T. Hallen, *Sep. Purif. Technol.* **1999**, *15*, 207.

[149] J. Yang, L. Zou, H. Song, Z. Hao, *Desalination* **2011**, *276*, 199.

[150] C. Z. Yuan, B. Gao, L. H. Su, X. G. Zhang, *J. Colloid Interface Sci.* **2008**, *322*, 545.

[151] S. Il Park, I. Gocheva, S. Okada, J. Yamaki, *J. Electrochem. Soc.* **2011**, *158*, A1067.

[152] C. D. Wessells, S. V. Peddada, R. A. Huggins, Y. Cui, *Nano Lett.* **2011**, *11*, 5421.

[153] M. Pasta, C. D. Wessells, Y. Cui, F. La Mantia, *Nano Lett.* **2012**, *12*, 839.

[154] B. Sun, X.-G. Hao, Z.-D. Wang, G.-Q. Guan, Z.-L. Zhang, Y.-B. Li, S.-B. Liu, *J. Hazard. Mater.* **2012**, *233–234*, 177.

[155] R. Chen, H. Tanaka, T. Kawamoto, M. Asai, C. Fukushima, H. Na, M. Kurihara, M.

Watanabe, M. Arisaka, T. Nankawa, *Electrochim. Acta* **2013**, *87*, 119.

[156] C. Weidlich, K. M. Mangold, K. Jüttner, *Electrochim. Acta* **2005**, *50*, 5247.

[157] R. Chen, H. Tanaka, T. Kawamoto, J. Wang, Y. Zhang, *Sep. Purif. Technol.* **2017**, *173*, 44.

[158] B. Chen, Y. Wang, Z. Chang, X. Wang, M. Li, X. Liu, L. Zhang, Y. Wu, *RSC Adv.* **2016**, *6*, 6730.

[159] K. C. Smith, *Electrochim. Acta* **2017**, *230*, 333.

[160] M. Acerce, D. Voiry, M. Chhowalla, *Nat. Nanotechnol.* **2015**, *10*, 313.

[161] S. Porada, P. Bukowska, A. Shrivastava, P. M. Biesheuvel, K. C. Smith, *arXiv Prepr. arXiv1612.08293* **2016**, *255*, 1.

[162] D.-H. Nam, K.-S. Choi, *J. Am. Chem. Soc.* **2017**, *139*, 11055.

[163] F. Chen, Y. Huang, L. Guo, M. Ding, H. Y. Yang, *Nanoscale* **2017**, *9*, 10101.

[164] P. Srimuk, J. Lee, S. Fleischmann, S. Choudhury, N. Jäckel, M. Zeiger, C. Kim, M. Aslan, V. Presser, *J. Mater. Chem. A* **2017**, *5*, 15640.

[165] S. Kim, H. Yoon, D. Shin, J. Lee, J. Yoon, *J. Colloid Interface Sci.* **2017**, *506*, 644.

[166] L. Guo, R. Mo, W. Shi, Y. Huang, Z. Y. Leong, M. Ding, F. Chen, H. Y. Yang, *Nanoscale* **2017**, *9*, 13305.

[167] H. Yoon, J. Lee, S. Kim, J. Yoon, *Hydrometallurgy* **2018**, *175*, 354.

[168] B. W. Byles, D. A. Cullen, K. L. More, E. Pomerantseva, *Nano Energy* **2018**, *44*, 476.

[169] J. Lee, P. Srimuk, K. Aristizabal, C. Kim, S. Choudhury, Y.-C. Nah, F. Mücklich, V. Presser, *ChemSusChem* **2017**, *10*, 3611.

[170] P. Srimuk, J. Lee, A. Tolosa, C. Kim, M. Aslan, V. Presser, *Chem. Mater.* **2017**, *29*, 9964.

[171] W. Bao, X. Tang, X. Guo, S. Choi, C. Wang, Y. Gogotsi, G. Wang, *Joule* **2018**, *2*, 778.

[172] S. Liu, K. C. Smith, *Electrochim. Acta* **2018**, *271*, 652.

[173] S. Choi, B. Chang, S. Kim, J. Lee, J. Yoon, J. W. Choi, *Adv. Funct. Mater.* **2018**, *28*, 1.

[174] X. Ma, Y.-A. Chen, K. Zhou, P.-C. Wu, C.-H. Hou, *Electrochim. Acta* **2019**, *295*, 769.

[175] B. W. Byles, B. Hayes-Oberst, E. Pomerantseva, *ACS Appl. Mater. Interfaces* **2018**, *10*, 32313.

[176] W. Shi, X. Zhou, J. Li, E. R. Meshot, A. D. Taylor, S. Hu, J.-H. Kim, M. Elimelech, D. L. Plata, *Environ. Sci. Technol. Lett.* **2018**.

[177] W. Zhao, L. Guo, M. Ding, Y. Huang, H. Y. Yang, *ACS Appl. Mater. Interfaces* **2018**, *10*, 40540.

[178] L. Agartan, B. Hayes-Oberst, B. W. Byles, B. Akuzum, E. Pomerantseva, E. C. Kumbur, *Desalination* **2019**, *452*, 1.

[179] P. Srimuk, J. Halim, J. Lee, Q. Tao, J. Rosen, V. Presser, *ACS Sustain. Chem. Eng.* **2018**,

6, 3739.

[180] J. E. Dykstra, R. Zhao, P. M. Biesheuvel, A. Van der Wal, *Water Res.* **2016**, *88*, 358.

[181] A. Hemmatifar, M. Stadermann, J. G. Santiago, *J. Phys. Chem. C* **2015**, *119*, 24681.

[182] J. Kang, T. Kim, K. Jo, J. Yoon, *Desalination* **2014**, *352*, 52.

[183] J. Lee, P. Srimuk, S. Carpier, J. Choi, R. L. Zornitta, C. Kim, M. Aslan, V. Presser, *ChemSusChem* **2018**, *11*, 1.

[184] M. Gautam, K. Poudel, C. S. Yong, J. O. Kim, *Int. J. Pharm.* **2018**, *549*, 712.

[185] M. H. Han, E. Gonzalo, G. Singh, T. Rojo, *Energy Environ. Sci.* **2015**, *8*, 81.

[186] B. Anasori, M. R. Lukatskaya, Y. Gogotsi, *Nat. Rev. Mater.* **2017**, *2*, 16098.

[187] M. Acerce, D. Voiry, M. Chhowalla, *Nat. Nanotechnol.* **2015**, *10*, 313.

[188] Y. Liu, C. Nie, X. Liu, X. Xu, Z. Sun, L. Pan, *RSC Adv.* **2015**, *5*, 15205.

[189] M. S. Gaikwad, C. Balomajumder, *Electrochem. Energy Technol.* **2016**, *2*.

[190] D. J. Miller, D. R. Dreyer, C. W. Bielawski, D. R. Paul, B. D. Freeman, *Angew. Chemie - Int. Ed.* **2017**, *56*, 4662.

[191] C. Cheng, A. Yaroshchuk, M. L. Bruening, *Langmuir* **2013**, *29*, 1885.

[192] J. B. Schlenoff, *Zwitteration: Coating surfaces with zwitterionic functionality to reduce nonspecific adsorption*, Vol. 30, **2014**, pp. 9625–9636.

[193] L. Li, G. Zhou, Z. Weng, X.-Y. Shan, F. Li, H.-M. Cheng, *Carbon N. Y.* **2014**, *67*, 500.

[194] K. West, T. Jacobsen, S. Atlung., *J. Electrochem. Soc.* **1982**, *129*, 1480.

[195] P. Bai, M. Z. Bazant, *Nat. Commun.* **2014**, *5*, 3585.

[196] W. Weppner, *J. Electrochem. Soc.* **1977**, *124*, 1569.

[197] A. Shrivastava, K. C. Smith, *J. Electrochem. Soc.* **2018**, *165*, A1777.

[198] J. Lee, P. Srimuk, R. Zwingelstein, R. L. Zornitta, J. Choi, C. Kim, V. Presser, *J. Mater. Chem. A* **2019**, *7*, 4175.

[199] D. Sriramulu, H. Y. Yang, *Nanoscale* **2019**, *11*, 5896.

[200] H. Younes, F. Ravaux, N. El Hadri, L. Zou, *Electrochim. Acta* **2019**, *306*, 1.

[201] J. Lee, P. Srimuk, R. L. Zornitta, M. Aslan, B. L. Mehdi, V. Presser, *ACS Sustain. Chem. Eng.* **2019**, *7*, 10132.

[202] Z. Yue, Y. Ma, J. Zhang, H. Li, *J. Mater. Chem. A* **2019**, *7*, 16892.

[203] Y. Li, Z. Ding, J. Li, J. Li, T. Lu, L. Pan, *Desalination* **2019**, *469*, 114098.

[204] N. Kim, S. P. Hong, J. Lee, C. Kim, J. Yoon, *ACS Sustain. Chem. Eng.* **2019**, *7*, 16182.

[205] Y. Li, Z. Ding, X. Zhang, J. Li, X. Liu, T. Lu, Y. Yao, L. Pan, *J. Mater. Chem. A* **2019**, *7*, 25305.

[206] X. Wen, M. Zhao, M. Zhang, X. Fan, D. Zhang, *ACS Sustain. Chem. Eng.* **2020**, *8*, 1268.

[207] G. Tan, S. Lu, N. Xu, D. Gao, X. Zhu, *Environ. Sci. Technol.* **2020**, *54*, 5843.

[208] F. He, A. Hemmatifar, M. Z. Bazant, T. A. Hatton, *Water Res.* **2020**, *182*.

[209] E. Sebti, M. M. Besli, M. Metzger, S. Hellstrom, M. J. Schultz-Neu, J. Alvarado, J. Christensen, M. Doeff, S. Kuppan, C. V. Subban, *Desalination* **2020**, *487*.

[210] F. Chen, J. Wang, C. Feng, J. Ma, T. David Waite, *Chem. Eng. J.* **2020**, *401*, 126111.

[211] Y. Pan, L. Yao, D. Wu, A. Bentalib, J. Li, Z. Peng, *Desalination* **2020**, *496*, 114762.

[212] L. Guo, M. Ding, D. Yan, M. E. Pam, S. Vafakhah, C. Gu, W. Zhang, P. Valdivia y Alvarado, Y. Shi, H. Y. Yang, *Desalination* **2020**, *496*, 114750.

[213] X. Liu, S. Zhang, G. Feng, Z. G. Wu, D. Wang, M. D. Albaqami, B. Zhong, Y. Chen, X. Guo, X. Xu, Y. Yamauchi, *Chem. Mater.* **2021**, *33*, 1657.

[214] W. Si, H. Li, *Adv. Mater. Interfaces* **2021**, *8*, 1.

[215] L. Wang, J. E. Dykstra, S. Lin, *Environ. Sci. Technol.* **2019**, *53*, 3366.

[216] S. Porada, M. Bryjak, A. Van Der Wal, P. M. Biesheuvel, *Electrochim. Acta* **2012**, *75*, 148.

[217] R. L. Zornitta, J. J. Lado, M. A. Anderson, L. A. M. Ruotolo, *Sep. Purif. Technol.* **2016**, *158*, 39.

[218] R. L. Zornitta, F. J. García-Mateos, J. J. Lado, J. Rodríguez-Mirasol, T. Cordero, P. Hammer, L. A. M. Ruotolo, *Carbon N. Y.* **2017**, *123*, 318.

[219] P. Ratajczak, M. E. Suss, F. Kaasik, F. Béguin, *Carbon electrodes for capacitive technologies*, Vol. 16, Elsevier B.V., **2019**, pp. 126–145.

[220] R. Zhao, O. Satpradit, H. H. M. Rijnaarts, P. M. Biesheuvel, A. van der Wal, *Water Res.* **2013**, *47*, 1941.

[221] L. Han, K. G. Karthikeyan, M. A. Anderson, K. B. Gregory, *J. Colloid Interface Sci.* **2014**, *430*, 93.

[222] Y. Li, C. Zhang, Y. Jiang, T. J. Wang, H. Wang, *Desalination* **2016**, *399*, 171.

[223] R. Wang, S. Lin, *J. Colloid Interface Sci.* **2020**, *574*, 152.

[224] M. Qin, A. Deshmukh, R. Epsztein, S. K. Patel, O. M. Owoseni, W. S. Walker, M. Elimelech, *Desalination* **2019**, *455*, 100.

[225] S. K. Patel, M. Qin, W. S. Walker, M. Elimelech, *Environ. Sci. Technol.* **2020**, *54*, 3663.

[226] M. Aslan, M. Zeiger, N. Jäckel, I. Grobelsek, D. Weingarth, V. Presser, *J. Phys. Condens. Matter* **2016**, *28*, 114003.

[227] P. M. Biesheuvel, H. V. M. Hamelers, M. E. Suss, *Colloids Interface Sci. Commun.* **2015**, *9*, 1.

[228] R. Zhao, P. M. Biesheuvel, A. Van Der Wal, *Energy Environ. Sci.* **2012**, *5*, 9520.

[229] N. Kim, J. Lee, S. P. Hong, C. Lee, C. Kim, J. Yoon, *Desalination* **2020**, *479*, 114315.

[230] M. Metzger, M. M. Besli, S. Kuppan, S. Hellstrom, S. Kim, E. Sebti, C. V. Subban, J. Christensen, *Energy Environ. Sci.* **2020**, *13*, 1544.

[231] S. Porada, L. Borchardt, M. Oschatz, M. Bryjak, J. S. Atchison, K. J. Keesman, S. Kaskel, P. M. Biesheuvel, V. Presser, *Energy Environ. Sci.* **2013**, *6*, 3700.

[232] H. Yoon, J. Lee, S. R. Kim, J. Kang, S. Kim, C. Kim, J. Yoon, *Desalination* **2016**, *392*, 46.

[233] P. Nativ, O. Lahav, Y. Gendel, *Desalination* **2018**, *425*, 123.

[234] L. Wang, S. Lin, *Environ. Sci. Technol.* **2019**, acs. est.9b00655.

[235] W. Chen, X. H. Xia, *Adv. Funct. Mater.* **2007**, *17*, 2943.

[236] D. H. Lee, T. Ryu, J. Shin, J. C. Ryu, K. S. Chung, Y. H. Kim, *Hydrometallurgy* **2017**, *173*, 283.

[237] C. J. Gabelich, T. D. Tran, I. H. Suffet, *Environ. Sci. Technol.* **2002**, *36*, 3010.

[238] D. L. Suarez, J. D. Wood, S. M. Lesch, *Agric. Water Manag.* **2006**, *86*, 150.

[239] J. L. Zhang, T. J. Flowers, S. M. Wang, *Plant Soil* **2010**, *326*, 45.

[240] A. Läuchli, S. R. Grattan, In *Advances in Molecular Breeding Toward Drought and Salt Tolerant Crops*, **2007**, pp. 1–32.

[241] C. D. Wessells, M. T. McDowell, S. V. Peddada, M. Pasta, R. A. Huggins, Y. Cui, *ACS Nano* **2012**, *6*, 1688.

[242] Y. Mizuno, M. Okubo, E. Hosono, T. Kudo, H. Zhou, K. Oh-Ishi, *J. Phys. Chem. C* **2013**, *117*, 10877.

[243] M. Asai, A. Takahashi, K. Tajima, H. Tanaka, M. Ishizaki, M. Kurihara, T. Kawamoto, *RSC Adv.* **2018**, *8*, 37356.

[244] R. Y. Wang, C. D. Wessells, R. A. Huggins, Y. Cui, *Nano Lett.* **2013**, *13*, 5748.

[245] F. Scholz, A. Dostal, *Angew. Chemie Int. Ed. English* **2004**, *34*, 2685.

[246] J. J. García-Jareño, D. Giménez-Romero, F. Vicente, C. Gabrielli, M. Keddam, H. Perrot, *J. Phys. Chem. B* **2003**, *107*, 11321.

[247] A. Shrivastava, S. Liu, K. C. Smith, *Phys. Chem. Chem. Phys.* **2019**, *21*, 20177.

[248] C.-H. Hou, C.-Y. Huang, *Desalination* **2013**, *314*, 124.

[249] F. Radmanesh, T. Rijnaarts, A. Moheb, M. Sadeghi, W. M. de Vos, *J. Colloid Interface Sci.* **2019**, *533*, 658.

[250] T. Rijnaarts, D. M. Reurink, F. Radmanesh, W. M. de Vos, K. Nijmeijer, *J. Memb. Sci.* **2019**, *570*, 513.

[251] S. Shanbhag, Y. Bootwala, J. F. Whitacre, M. S. Mauter, *Langmuir* **2017**.

[252] M. Peschke, A. T. Blades, P. Kebarle, *J. Phys. Chem. A* **2002**, *102*, 9978.

[253] E. R. Nightingale, Jr., *J. Phys. Chem.* **1959**, *63*, 1381.

[254] A. Omosebi, X. Gao, J. Landon, K. Liu, *ACS Appl. Mater. Interfaces* **2014**.

[255] R. L. Zornitta, L. A. M. Ruotolo, *Chem. Eng. J.* **2018**, *332*, 33.

[256] M. Jayalakshmi, F. Scholz, *J. Power Sources* **2000**, *91*, 217.

[257] Y. Moritomo, S. Urase, T. Shibata, *Electrochim. Acta* **2016**, *210*, 963.

[258] V. Pothanamkandathil, J. Fortunato, C. A. Gorski, *Environ. Sci. Technol.* **2020**.

[259] S. Choi, B. Chang, S. Kim, J. Lee, J. Yoon, J. W. Choi, *Adv. Funct. Mater.* **2018**, *28*, 1.

[260] K. Singh, S. Sahin, J. G. Gamaethiralalage, R. L. Zornitta, L. C. P. M. de Smet, *Chem. Eng. J.* **2021**, 128329.

[261] G. Kresse, J. Furthmüller, *Phys. Rev. B - Condens. Matter Mater. Phys.* **1996**, *54*, 11169.

[262] X. Gao, S. Porada, A. Omosebi, K. L. Liu, P. M. Biesheuvel, J. Landon, *Water Res.* **2016**, *92*, 275.

[263] G. Kresse, D. Joubert, *Phys. Rev. B* **1999**, *59*, 1758.

[264] J. P. Perdew, K. Burke, M. Ernzerhof, *Phys. Rev. Lett.* **1996**, *77*, 3865.

[265] P. E. Blöchl, *Phys. Rev. B* **1994**, *50*, 17953.

[266] B. Stahl, T. Bredow, *J. Comput. Chem.* **2020**, *41*, 258.

[267] S. Grimme, S. Ehrlich, L. Goerigk, *J. Comput. Chem.* **2011**, *32*, 1456.

[268] Y. Xu, H. Zhou, G. Wang, Y. Zhang, H. Zhang, H. Zhao, *ACS Appl. Mater. Interfaces* **2020**, *12*, 41437.

[269] M. A. Lumley, D. H. Nam, K. S. Choi, *ACS Appl. Mater. Interfaces* **2020**, *12*, 36014.

[270] M. K. Carpenter, R. S. Conell, S. J. Simko, *Inorg. Chem.* **1990**, *29*, 845.

[271] C. G. Tsiafoulis, P. N. Trikalitis, M. I. Prodromidis, *Electrochem. commun.* **2005**, *7*, 1398.

[272] N. Imanishi, T. Morikawa, J. Kondo, R. Yamane, Y. Takeda, O. Yamamoto, H. Sakaebe, M. Tabuchi, *J. Power Sources* **1999**, *81–82*, 530.

[273] X. Sun, V. Duffort, L. F. Nazar, *Adv. Sci.* **2016**, *3*, 1.

[274] F. A. Miller, C. H. Wilkins, *Anal. Chem.* **1952**, *24*, 1253.

[275] S. N. Ghosh, *J. Inorg. Nucl. Chem.* **1974**, *36*, 2465.

[276] Y. Xu, M. Chang, C. Fang, Y. Liu, Y. Qiu, M. Ou, J. Peng, P. Wei, Z. Deng, S. Sun, X. Sun, Q. Li, J. Han, Y. Huang, *ACS Appl. Mater. Interfaces* **2019**, *11*, 29985.

[277] X. Peng, H. Guo, W. Ren, Z. Su, C. Zhao, *Chem. Commun.* **2020**, *56*, 11803.

[278] C. D. Wessells, R. A. Huggins, Y. Cui, *Nat. Commun.* **2011**, *2*, 2.

[279] P. Jiang, H. Shao, L. Chen, J. Feng, Z. Liu, *J. Mater. Chem. A* **2017**, *5*, 16740.

[280] C. He, J. Ma, C. Zhang, J. Song, T. D. Waite, *Environ. Sci. Technol.* **2018**, *52*, 9350.

[281] Y. Marcus, *A simple empirical model describing the thermodynamics of hydration of ions of widely varying charges, sizes, and shapes*, Vol. 51, Elsevier, **1994**, pp. 111–127.

[282] M. I. Redondo, C. B. Breslin, *Corros. Sci.* **2007**, *49*, 1765.

[283] C. R. Susana, P. J. Jorge, H. Pablo, M. L. M. Luis, M. Paul, *Langmuir* **2010**, *26*, 1271.

[284] M. R. Cerón, F. Aydin, S. A. Hawks, D. I. Oyarzun, C. K. Loeb, A. Deinhart, C. Zhan, T. A. Pham, M. Stadermann, P. G. Campbell, *ACS Appl. Mater. Interfaces* **2020**, *12*, 42644.

[285] H. Joo, S. Kim, S. Kim, M. Choi, S. H. Kim, J. Yoon, *Environ. Sci. Water Res. Technol.* **2020**, *6*, 290.

[286] J. Kim, A. Jain, K. Zuo, R. Verduzco, S. Walker, M. Elimelech, Z. Zhang, X. Zhang, Q. Li, *Water Res.* **2019**, *160*, 445.

[287] Y.-J. Kim, J.-H. Choi, *Water Res.* **2012**, *46*, 6033.

[288] W. Shi, X. Liu, C. Ye, X. Cao, C. Gao, J. Shen, *Sep. Purif. Technol.* **2019**, *210*, 885.

[289] W. Tang, D. He, C. Zhang, T. D. Waite, *Water Res.* **2017**, *121*, 302.

[290] S. Sahin, J. E. Dykstra, H. Zuilhof, R. Linzmeyer Zornitta, L. C. P. . de Smet, *ACS Appl. Mater. Interfaces* **2020**.

[291] J. H. Yeo, J. H. Choi, *Desalination* **2013**, *320*, 10.

[292] Z. Cao, P. I. Gordiichuk, K. Loos, E. J. R. Sudhölter, L. C. P. M. de Smet, *Soft Matter* **2016**, *12*, 1496.

[293] L. Paltrinieri, K. Remmen, B. Müller, L. Chu, J. Köser, T. Wintgens, M. Wessling, L. C. P. M. de Smet, E. J. R. Sudhölter, *J. Memb. Sci.* **2019**, *587*, 117162.

[294] G. Decher, J. -D Hong, *Makromol. Chemie. Macromol. Symp.* **1991**, *46*, 321.

[295] G. Decher, *Science (80-.).* **1997**, *277*, 1232.

[296] J. J. Richardson, J. Cui, M. Björnmalm, J. A. Braunger, H. Ejima, F. Caruso, *Innovation in Layer-by-Layer Assembly*, Vol. 116, American Chemical Society, **2016**, pp. 14828–14867.

[297] Y. Zhu, M. Ahmad, L. Yang, M. Misovich, A. Yaroshchuk, M. L. Bruening, *J. Memb. Sci.* **2017**, *537*, 177.

[298] S. Abdu, M. C. Martí-Calatayud, J. E. Wong, M. García-Gabaldón, M. Wessling, *ACS Appl. Mater. Interfaces* **2014**, *6*, 1843.

[299] B. W. Stanton, J. J. Harris, M. D. Miller, M. L. Bruening, *Langmuir* **2003**, *19*, 7038.

[300] B. Tansel, *Sep. Purif. Technol.* **2012**, *86*, 119.

[301] W. Cheng, C. Liu, T. Tong, R. Epsztein, M. Sun, R. Verduzco, J. Ma, M. Elimelech, *J. Memb. Sci.* **2018**, *559*, 98.

[302] T. Luo, S. Abdu, M. Wessling, *J. Memb. Sci.* **2018**, *555*, 429.

[303] C. Cheng, N. White, H. Shi, M. Robson, M. L. Bruening, *Polymer (Guildf).* **2014**, *55*, 1397.

[304] S. Kim, H. Yoon, D. Shin, J. Lee, J. Yoon, *J. Colloid Interface Sci.* **2017**, *506*, 644.

[305] E. Pomerantseva, F. Bonaccorso, X. Feng, Y. Cui, Y. Gogotsi, *Science (80-.).* **2019**, *366*.

[306] E. N. Durmaz, M. I. Baig, J. D. Willott, W. M. de Vos, *ACS Appl. Polym. Mater.* **2020**.

[307] J. de Grooth, B. Haakmeester, C. Wever, J. Potreck, W. M. de Vos, K. Nijmeijer, *J. Memb. Sci.* **2015**, *489*, 153.

[308] H. Gao, B. Zhang, X. Tong, Y. Chen, *J. Memb. Sci.* **2018**, *567*, 68.

[309] J. de Grooth, R. Oborný, J. Potreck, K. Nijmeijer, W. M. de Vos, *J. Memb. Sci.* **2015**, *475*, 311.

[310] N. White, *ProQuest Diss. Theses Glob.* **2015**.

[311] H. Riegler, F. Essler, *Langmuir* **2002**, *18*, 6694.

[312] R. Malaisamy, M. L. Bruening, *Langmuir* **2005**, *21*, 10587.

[313] R. Köhler, I. Dönch, P. Ott, A. Laschewsky, A. Fery, R. Krastev, *Langmuir* **2009**, *25*, 11576.

[314] D. M. Reurink, J. P. Haven, I. Achterhuis, S. Lindhoud, (Erik) H D W Roesink, W. M. de Vos, *Adv. Mater. Interfaces* **2018**, *5*.

[315] F. He, P. M. Biesheuvel, M. Z. Bazant, T. A. Hatton, *Water Res.* **2018**, *132*, 282.

[316] Z.-H. Huang, Z. Yang, F. Kang, M. Inagaki, *J. Mater. Chem. A* **2017**, *5*, 470.

[317] K. Itaya, I. Uchida, V. D. Neff, *Acc. Chem. Res.* **2002**, *19*, 162.

[318] J. W. McCargar, V. D. Neff, *J. Phys. Chem.* **2002**, *92*, 3598.

[319] S. Shanbhag, Y. Bootwala, J. F. Whitacre, M. S. Mauter, *Langmuir* **2017**, *33*, 12580.

[320] A. M. Johnson, J. Newman, *J. Electrochem. Soc.* **1971**, *118*, 510.

[321] T. R. Ferguson, M. Z. Bazant, *J. Electrochem. Soc.* **2012**, *159*, A1967.

[322] M. Z. Bazant, K. Thornton, A. Ajdari, *Phys. Rev. E* **2004**, *70*, 021506.

[323] P. M. Biesheuvel, Y. Fu, M. Z. Bazant, *Russ. J. Electrochem.* **2012**, *48*, 580.

[324] B. E. Conway, E. Gileadi, *Trans. Faraday Soc.* **1962**, *58*, 2493.

[325] M. D. Levi, D. Aurbach, *Electrochim. Acta* **1999**, *45*, 167.

[326] M. Z. Bazant, *Acc. Chem. Res.* **2013**, *46*, 1144.

[327] E. B. Nauman, D. Q. He, *Chem. Eng. Sci.* **2001**, *56*, 1999.

[328] W. Lai, F. Ciucci, *Electrochim. Acta* **2010**, *56*, 531.

[329] R. B. Smith, M. Z. Bazant, *J. Electrochem. Soc.* **2017**, *164*, E3291.

[330] T. R. Ferguson, M. Z. Bazant, *Electrochim. Acta* **2014**, *146*, 89.

[331] Y. You, X.-L. Wu, Y.-X. Yin, Y.-G. Guo, *J. Mater. Chem. A* **2013**, *1*, 14061.

[332] M. Doyle, T. F. Fuller, J. Newman, *J. Electrochem. Soc.* **1993**, *140*, 1526.

[333] A. A. Sonin, R. F. Probstein, *Desalination* **1968**, *5*, 293.

[334] T. M. Mubita, S. Porada, P. M. Biesheuvel, A. van der Wal, J. E. Dykstra, *Electrochim. Acta* **2018**, *270*, 165.

[335] M. Tedesco, H. V. M. Hamelers, P. M. Biesheuvel, *J. Memb. Sci.* **2017**, *531*, 172.

[336] E. N. Guyes, A. N. Shocron, A. Simanovski, P. M. Biesheuvel, M. E. Suss, *Desalination* **2017**, *415*, 8.

[337] Y. Xu, S. Xiang, H. Zhou, G. Wang, H. Zhang, H. Zhao, *ACS Appl. Mater. Interfaces* **2021**, *13*, 38886.

[338] S. Y. Ding, J. Gao, Q. Wang, Y. Zhang, W. G. Song, C. Y. Su, W. Wang, *J. Am. Chem. Soc.* **2011**, *133*, 19816.

[339] A. P. Côté, A. I. Benin, N. W. Ockwig, M. O'Keeffe, A. J. Matzger, O. M. Yaghi, *Science (80-.).* **2005**, *310*, 1166.

[340] H. M. El-Kaderi, J. R. Hunt, J. L. Mendoza-Cortés, A. P. Côté, R. E. Taylor, M. O'Keeffe, O. M. Yaghi, *Science (80-.).* **2007**, *316*, 268.

[341] Z. Wang, S. Zhang, Y. Chen, Z. Zhang, S. Ma, *Chem. Soc. Rev.* **2020**, *49*, 708.

[342] S. J. Rowan, S. J. Cantrill, G. R. L. Cousins, J. K. M. Sanders, J. F. Stoddart, *Angew. Chemie Int. Ed.* **2002**, *41*, 898.

[343] J. L. Segura, M. J. Mancheño, F. Zamora, *Covalent organic frameworks based on Schiff-base chemistry: Synthesis, properties and potential applications*, Vol. 45, The Royal Society of Chemistry, **2016**, pp. 5635–5671.

[344] A. P. Côté, H. M. El-Kaderi, H. Furukawa, J. R. Hunt, O. M. Yaghi, *J. Am. Chem. Soc.* **2007**, *129*, 12914.

[345] B. J. Smith, A. C. Overholts, N. Hwang, W. R. Dichtel, *Chem. Commun.* **2016**, *52*, 3690.

[346] S. Dalapati, S. Jin, J. Gao, Y. Xu, A. Nagai, D. Jiang, *J. Am. Chem. Soc.* **2013**, *135*, 17310.

[347] F. J. Uribe-Romo, C. J. Doonan, H. Furukawa, K. Oisaki, O. M. Yaghi, *J. Am. Chem. Soc.* **2011**, *133*, 11478.

[348] S. Kandambeth, K. Dey, R. Banerjee, *Covalent Organic Frameworks: Chemistry beyond the Structure*, Vol. 141, American Chemical Society, **2019**, pp. 1807–1822.

[349] J. Hu, S. K. Gupta, J. Ozdemir, M. H. Beyzavi, *ACS Appl. Nano Mater.* **2020**, *3*, 6239.

[350] H. Wang, H. Wang, Z. Wang, L. Tang, G. Zeng, P. Xu, M. Chen, T. Xiong, C. Zhou, X. Li, D. Huang, Y. Zhu, Z. Wang, J. Tang, *Chem. Soc. Rev.* **2020**, *49*, 4135.

[351] J. Guo, D. Jiang, *ACS Cent. Sci.* **2020**, *6*, 869.

[352] S. Y. Ding, W. Wang, *Chem. Soc. Rev.* **2013**, *42*, 548.

[353] R. Van Der Jagt, A. Vasileiadis, H. Veldhuizen, P. Shao, X. Feng, S. Ganapathy, N. C. Habisreutinger, M. A. Van Der Veen, C. Wang, M. Wagemaker, S. Van Der Zwaag, A. Nagai, *Chem. Mater.* **2021**, *33*, 818.

[354] D. P. Singh, F. M. Mulder, M. Wagemaker, *Electrochem. commun.* **2013**, *35*, 124.

[355] J. J. Lado, V. Cartolano, E. García-Quismondo, G. García, I. Almonacid, V. Senatore, V. Naddeo, J. Palma, M. A. Anderson, *Desalination* **2021**, *501*, 114912.

[356] S. Rubin, M. E. Suss, P. M. Biesheuvel, M. Bercovici, **2016**.

[357] S. A. Hawks, M. R. Ceróncerón, D. I. Oyarzun, T. A. Pham, C. Zhan, C. K. Loeb, D. Mew, A. Deinhart, B. C. Wood, J. G. Santiago, M. Stadermann, P. G. Campbell, M. R. Cerón, D. I. Oyarzun, T. A. Pham, C. Zhan, C. K. Loeb, D. Mew, A. Deinhart, B. C. Wood, J. G. Santiago, M. Stadermann, P. G. Campbell, *Environ. Sci. Technol.* **2019**, *53*, 10863.

[358] J. Lee, J. Lee, J. Ahn, K. Jo, S. P. Hong, C. Kim, C. Lee, J. Yoon, *ACS Appl. Mater. Interfaces* **2019**, *11*, 36580.

[359] J. Lee, J. Lee, S. W. Hong, C. Kim, J. Yoon, *Desalination* **2021**, *515*.

[360] V. Pothanamkandathil, J. Fortunato, C. A. Gorski, *Environ. Sci. Technol.* **2020**, *54*, 3653.

[361] X. Zhang, K. Zuo, X. Zhang, C. Zhang, P. Liang, *Selective ion separation by capacitive deionization (CDI) based technologies: A state-of-the-art review*, Vol. 6, The Royal Society of Chemistry, **2020**, pp. 243–257.

[362] R. Chen, T. Sheehan, J. L. Ng, M. Brucks, X. Su, *Capacitive deionization and electrosorption for heavy metal removal*, Vol. 6, The Royal Society of Chemistry, **2020**, pp. 258–282.

[363] E. Bakker, E. Pretsch, P. Bühlmann, *Selectivity of potentiometric ion sensors*, Vol. 72, American Chemical Society, **2000**, pp. 1127–1133.

[364] W. J. Peveler, M. Yazdani, V. M. Rotello, *ACS Sensors* **2016**, *1*, 1282.

[365] S. P. Hong, H. Yoon, J. Lee, C. Kim, S. Kim, J. Lee, C. Lee, J. Yoon, *J. Colloid Interface Sci.* **2020**, *564*, 1.

[366] L. Wang, Y. Lu, J. Liu, M. Xu, J. Cheng, D. Zhang, J. B. Goodenough, *Angew. Chemie - Int. Ed.* **2013**, *52*, 1964.

[367] A. Mullaliu, G. Aquilanti, P. Conti, M. Giorgetti, S. Passerini, *ChemSusChem* **2020**, *13*, 608.

[368] Y. Tang, W. Li, P. Feng, M. Zhou, K. Wang, Y. Wang, K. Zaghib, K. Jiang, *Adv. Funct. Mater.* **2020**, *30*, 1.

[369] L. Eliad, G. Salitra, A. Soffer, D. Aurbach, *J. Phys. Chem. B* **2001**, *105*, 6880.

[370] X. Su, H. J. Kulik, T. F. Jamison, T. A. Hatton, *Adv. Funct. Mater.* **2016**, *26*, 3394.

[371] S. Kim, J. Lee, J. S. Kang, K. Jo, S. Kim, Y.-E. Sung, J. Yoon, *Chemosphere* **2015**, *125*, 50.

[372] W. Shi, X. Liu, C. Ye, X. Cao, C. Gao, J. Shen, *Sep. Purif. Technol.* **2019**, *210*, 885.

[373] J. Chang, Y. Li, F. Duan, C. Su, Y. Li, H. Cao, *Sep. Purif. Technol.* **2020**, *240*, 116600.

[374] S. P. Hong, H. Yoon, J. Lee, C. Kim, S. Kim, J. Lee, C. Lee, J. Yoon, *J. Colloid Interface Sci.* **2020**, *564*, 1.

[375] T. M. Mubita, J. E. Dykstra, P. M. Biesheuvel, A. van der Wal, S. Porada, *Water Res.* **2019**, *164*, 114885.

[376] J. H. Yeo, J. H. Choi, *Desalination* **2013**, *320*, 10.

[377] S. Mao, L. Chen, Y. Zhang, Z. Li, Z. Ni, Z. Sun, R. Zhao, *J. Colloid Interface Sci.* **2019**, *544*, 321.

Acknowledgements

Dankbetuigingen

आभार

"To get the full value of joy, you must have someone to divide it with"

Mark Twain

The discoveries and insights described in the chapters of this thesis represent the scientific side of my PhD. This description, however elaborate, remains incomplete without the description of people who made it possible for me to write about the scientific part to begin with. Also, it would be a folly to assume that a PhD is for and by a single individual because as always, it takes an entire orchestra to perform a symphony. Therefore, the following section is about that orchestra in which I played a part for the last 4 years and is thus, a befitting end of this work.

My **thesis committee**

Thank you for spending your precious time and effort in critically examining my work and imparting an extra layer of scientific rigor to my PhD.

My promotors **Louis de Smet** and **Han Zuilhof**

Louis – I shall be forever grateful to you for hiring me and having the confidence in me to bring this work to a successful conclusion. Also, I am grateful that you supported me, and provided me with every conceivable opportunity and freedom to perform experiments and publish. It inculcated in me a habit to think independently, responsibly, and shrewdly. In addition, it imparted essential and invaluable scientific and professional skills in me. Thank you for precisely defining the goal and not the road to it. I became a better researcher because of it, and by extension, you. In addition to learning how to manage my PhD, I also learnt scientific writing from you. Therefore, it would be a gross neglect to not acknowledge your far-reaching contribution to my career.

Han – My PhD work would have been unimaginably more difficult without you. Thank you for supporting me through the lows, that are usual in any PhD, and facilitating a hastened move to Wageningen, a feature unusual for a PhD. Furthermore, the conclusion sections of my papers are, and will be, incalculably better and more informative because of you. Thank you for the efforts in keeping the labs going during COVID-19.

My supervisors at Wetsus – **Maarten Biesheuvel** and **Slawomir Porada**

Maarten – Thank you for introducing me to what became my main research area and fascination. A big part of my education in CDI started with you and I could not have asked for anything better. I shall always remain grateful for your contribution in building a theoretical framework of my research, constructive feedback, and rigorous examination of my scientific understanding, writing, and illustrations. It improved my science and enhanced my critical thinking, a skill of immeasurable value in today's world of excess.

Slawomir – It would not be putting too heavy a burden on a sentence if I were to frame it in this manner – My experimental education in CDI began with you. I learnt to do experiments in CDI from you, right from the second week of my PhD. Thank you for the knowledge as I shall be relying heavily on them in my career ahead.

Wetsus – The driven and enthusiasm-infused atmosphere at Wetsus, created by the exemplary efforts of **Cees**, **Bert** (thank you for your kind and encouraging feedback on my presentations. It was a pleasure to speak to you about science and academia), and **Johannes**, is an incredibly fertile place to give shape to any research idea. Thank you for giving me the opportunity to be a part of this stimulating environment.

Staying with Wetsus,

The **members** of the CDI/AWT theme – Thank you for your continued encouragement. My fellow PhD in the theme – **Antony** and **Ettore** – Thank you for the support and motivation. With you in the audience, I never found myself nervous while presenting. **Tania** – Special acknowledgements for being a continuous support and a dear friend to me.

Michel – Your enthusiasm towards science and engineering is unparalleled and I have enjoyed every conversation with you. I hope you keep inspiring students in the future. **Roel** – Thank you for hosting me (although on paper) in your house for two months while I was in India. It truly showed me the value of cooperation, professed at Wetsus. **Doekle** – We could not continue the project we conceived together after I moved but nevertheless, I learnt a lot from our conversations. And they were great fun!

The people holding the fort at Wetsus –

The analytical team – **Janneke**, **Jelmer**, **Jan Willem**, **Marianne**, **Lisette** – Thank you for the hassle-free analysis. It made the difficulties in experiments bearable. Special acknowledgement to **Mieke** for conducting sample analysis for me during COVID-19.

Thanks to the technical team – **Harm**, **Jan**, **Wim, Jan-Jurjen** – for their support with my experimental setup. Special thanks to **Ernst** for making endless adjustments to my cells.

Further acknowledgments and regards to people behind the curtain, keeping Wetsus running smoothly everyday – **Nynke**, **Gerrit**, **Linda**, **Willy**, **Janny**, **Anke**, **Trienke**, **Roely**, **Lucy**, **Hester**, **Jan**, **Rienk**, **Wiebe**. Thank you for your time and unflinching support. **Gerben** , **Catharina**, and **Riet** – Thank you for the sandwiches and keeping the canteen running!

Residents of **office 1.10C** – **Prashant**, **Hector**, **Mariana**, **Emanuel**, **Rebeca**, **Emad**, and **Bárbara** – I consider myself fortunate for having made your acquaintance and I shall forever cherish our time together. **Diego** (can't thank you enough for helping me move), **Rose**, and **Gosia** – I thoroughly appreciated our afternoon conversations over coffee. I felt very much at home with you!

Fellow PhDs **outside** office 1.10C – **Chris, Mariana, Suyash, Nimmy, Caspar, Swarupa** – Thank you for your company. I thoroughly enjoyed doing courses with you. **Steffen, Shuyana** – We interviewed for our PhD positions together and we managed to even live near each other. My memories of Wetsus will be terribly incomplete without you lovely people. I hope we meet again soon! **Casper** – It was always a pleasure and a source of

motivation to talk to you about problems in lab. Also, thank you for helping me move. I could not have done it without you. **Zexin** – We went from being neighbors, to friends, to collaborators, and finally co-authors together and I am very glad for it. It was tremendous fun working with you. **Natascha** – I am happy we shared a part of our PhD journey together. I greatly enjoyed our afternoon coffees and conversations, and hope we get to do it again soon. **Deepika** – I am happy that we started at Wetsus together and became friends almost immediately. Your energy and enthusiasm are tremendously inspiring, and I hope I get a chance to work with you in the future.

My student **Newton** – I thoroughly enjoyed learning by doing experiments with you together. I wish you all the best in your future endeavors.

Onwards to the **Laboratory of Organic chemistry** (**ORC**) at WUR –

Bauke, **Floris**, **Teris**, **Maarten**, **Hans-Gerd**, **Michel**, **Gert, Fedor**, and **Simone** – It was a singular privilege to present my work to you in department seminars. Thank you for your feedback. **Guanna** – Thank you for a fruitful collaboration. Your contribution elevated our work which has now become one of the most thorough papers I have written. **Maurice**, **Hendra**, **Anne-Marie**, **Carel**, **Tjerk**, **Judith**, **Dieuwertje** – I was fortunate to give practical with you, especially considering how often I was clueless about everything. You kept me going! Thank you. **Sidhu** – It was great to learn different analytical techniques from you. Your work ethic and dedication to science is admirable and I have learnt a lot from it. **Barend** – Thank you for countless XRD and XPS analyses and being the go-to person for nearly everything in lab**.** **Hans** – Thank you for kind and continuous support with the IC.

The inimitable PhD's at ORC – **Pepijn**, **Jorick**, **Jordi** (I will cherish our conversations that mostly involved venting about respective researches), **Ian**, **Esther**, **Annemieke** (friend and confidant and my go-to person to speak uninhibited with), **Alyssa**, **Sybren**, **Andrii**, and **Michel** (helpful neighbor and less-than-lucky roommate in another country) – I am glad to have had shared my PhD journey with you that includes sharing a dance floor in the middle of a desert in Israel, and me being alarmingly fastidious about a certain door and whether it was locked or not. **Ellen** – Thank you for tolerating and being kind to me in lab. **Daniele** – It was great giving practical with you. Your high-spirited nature and Spotify playlists kept me energized! **Lucas** – Thank you for preventing me from flooding the lab on an embarrassingly high number of occasions. It was great fun to attend the presentation course with you. I wish you all the best with your PhD. **Alice** – It was great to walk with you halfway to Ede. Your energy is contagious and please never change! **Ariadni** – Thank you for all the dinners and conversations that started with high promise and purpose before invariably descending into a mutual ridicule contest. I enjoyed every second of it and am glad to have made your acquaintance. **Sevil** – Thank you for always being kind and there to help and support me. I thoroughly enjoyed our fruitful collaboration and I wish you all the best in your career ahead. **Jay** – It would have been very difficult for me to resettle in ORC without **Sevil** and you. I have enjoyed talking to you about everything there has ever been to talk about. Furthermore, I

admire your depth of knowledge and it was a privilege to work with you over the widest range of experiments! I wish you all the best in finishing your PhD. To the relatively new (mostly because you good people started after me) PhDs – **Julian**, **Natassa**, **Tunan**, **Si** (welcome back!), **Simon**, **Yuri**, **Jasper**, **Canan** – It was a pleasure to interact with you and I wish you all the best with your PhD ahead.

My office mates – **Jacob**, **Albert, Fridolin** – It was a pleasure to share office and conversations with you that ranged from molecular simulations to football and Formula 1. **Ai** – Thank you for the brownies! They shall remain unrivalled, and I am going to miss them. **Rafael** – We started as office mates and rapidly grew into close collaborators and dear friend. You were a mentor, a sounding board, a curiosity-experiment accomplice, a tremendous co-author, a first contact for far-flung ideas. I am glad we met, and I hope we get to work together again! **Stijn** – It is a pity you joined us just when my time at ORC was coming to an end. Still, it surprises me how quickly we became friends. Thank you for all the afternoon coffees, conversations and bearing the sub-par Indian food with me. I wish you all the luck with your PhD and hope you make exciting new discoveries. I do not doubt that we shall remain friends in the coming years.

My time at ORC ran smoothly because of **Elly**, **Aleida**, **Henny**, and **Esther** – thank you for your support. You keep the department running!

Outside WUR and Wetsus, it would be a mistake to fail in acknowledging the following people:

Armin Michel – Thank you for enthusiastically encouraging my research. I became confident in my approach towards research because of it.

Juhan Lee – I had only heard about you being a highly accomplished scientist before we started our collaboration. After that, I also discovered that you were among the most knowledgeable, curious, driven, and helpful researchers in the field. I learnt a lot from you, and it was an absolute delight to collaborate with you!

Clemens Bechinger – You were the last straw that tipped the balance towards a PhD for me. I learnt how to be curious, to never give up, and to pursue a research line from you. Thank you for being a true role model.

My friends and family who inspired, soothed, uplifted, and motivated me throughout my PhD. **Saurabh** – We have been friends since bachelors. We changed cities and countries together. It is safe to say that it is difficult for us to get rid of each other and I hope it remains that way. My uncles – **Siddharth** and **Richev**, cousins – **Deepshikha**, **Prashant**, **Avanish,** and niece **Vidushi** – Thank you for being categorically encouraging. I hope to be the person you already think I am. Special acknowledgements to: **Nishant** – My idea of a scientist developed and evolved by observing you and you have been a constant influence on me and my scientific outlook. I am blessed to have your support; **Anisha** – Thanking you would be a disservice to

everything you mean to me and have done for me. So, allow me to just appreciate your love and affection for me. You will always be my elder sister.

Melissa – I feel I have known you forever. And yet, at the same time, I regret not meeting you sooner as my life is unimaginably richer now with you in it. Your positive outlook, calm demeanor, and a magnetic sense of humor reassured me during the difficult times of self-doubt and imposter syndrome. Doubtlessly, I am a better person, one who is kinder and more considerate, because of you as you are all these and much more. Thank you for all the love, affection, support, laughing at my jokes that don't always land, and making me want to be better. I know we will remain happy and in love, forever.

Finally, and fittingly, it must end where it all began – with my **Mum** and **Dad**. I will not separately write about you two since you belong together, out in the world and here in my thesis. All that I am, or hope to be, is because of you. Whatever I have achieved is a culmination of your efforts, goodwill, prayers, and actions. It is neither easy nor possible to describe the efforts you put in raising me. Not all times were easy. But you did it, with unwavering resolve and profound love. You have always been there for me, unconditionally. Perhaps that is why even after being 7000 kms away, I feel deeply loved and supported. You both have been my biggest supporter, true teachers, and unbiased mentors. It was not always easy to be my parents, but it has been effortless being your son. I want you to know that none of this would have been possible without you. I love you and hope that we stay together, for each other and by each other, for all times to come.

Kaustub Singh

February 2022

About the Author

Kaustub Singh was born on December 24, 1993, in Jaunpur, Uttar Pradesh, India. In 2015, Kaustub obtained a Bachelor's degree in Chemical Engineering from Birla Institute of Technology and Science, located in the coastal province of Goa, India. Following that, Kaustub moved to Delft to pursue a Master's degree in Chemical Engineering from TU Delft, which he obtained in 2017.

Following his Master's, Kaustub joined the Laboratory of Organic Chemistry at Wageningen University and Wetsus, Leeuwarden in October of 2017 as a PhD candidate. The doctoral research was carried out at Wetsus (1 year 4 months) as well as Wageningen University (2 year and 8 months) and was concluded in October of 2021. The results obtained during the research period are described in this thesis.

As of November 2021, Kaustub started as a post-doctoral fellow in the Department of Chemical Engineering at TU Delft and an R&D engineer at AquaBattery B.V., Leiden.

List of Publications

1. Singh, K., Bouwmeester, H.J.M., de Smet, L.C.P.M., Bazant, M.Z. and Biesheuvel, P.M., 2018. Theory of water desalination with intercalation materials. *Physical review applied*, *9*(6), p.064036.
2. Singh, K., Porada, S., de Gier, H.D., Biesheuvel, P.M. and de Smet, L.C.P.M., 2019. Timeline on the application of intercalation materials in Capacitive Deionization. *Desalination*, *455*, pp.115-134.
3. Singh, K., Qian, Z., Biesheuvel, P.M., Zuilhof, H., Porada, S. and de Smet, L.C.P.M., 2020. Nickel hexacyanoferrate electrodes for high mono/divalent ion-selectivity in capacitive deionization. *Desalination*, *481*, p.114346.
4. Singh, K., Zhang, L., Zuilhof, H. and de Smet, L.C.P.M., 2020. Water desalination with nickel hexacyanoferrate electrodes in capacitive deionization: Experiment, model, and comparison with carbon. *Desalination*, *496*, p.114647.
5. Gamaethiralalage, J.G., Singh, K., Sahin, S., Yoon, J., Elimelech, M., Suss, M.E., Liang, P., Biesheuvel, P.M., Zornitta, R.L. and de Smet, L.C.P.M., 2021. Recent advances in ion selectivity with capacitive deionization. *Energy & Environmental Science*, *14*(3), pp.1095-1120.
6. Singh, K., Sahin, S., Gamaethiralalage, J.G., Zornitta, R.L. and de Smet, L.C.P.M., 2021. Simultaneous, monovalent ion selectivity with polyelectrolyte multilayers and intercalation electrodes in capacitive deionization. *Chemical Engineering Journal*, p.128329.
7. Singh, K., Li, G., Lee, J., Zuilhof, H., Mehdi, B.L., Zornitta, R.L. and de Smet, L.C.P.M., 2021. Divalent ion selectivity in capacitive deionization with vanadium hexacyanoferrate: experiments and quantum-chemical computations. *Advanced Functional Materials*, *31*(41), p.2105203.

Overview of Completed Training Activities

Discipline-specific activities	Organizer	Year
Han-Sur-less winter school on Physical chemistry	PCC/ORC	2018
8th European summer school on Electrochemistry	University of Toulouse	2018
Advanced Organic chemistry	ORC	2018 – 2022
Conference on CDI- Electrosorption & Electrodialysis	CDI working group	2021
Wageningen Molecular Life Sciences Seminars	WUR	2017 – 2020
Course - COMSOL Multiphysics Training - online	COMSOL	2020
Environmental Technology for Impact (ETEi) 2020	ETE	2020
Computational methods in water technology	WIMEK/SENSE	2021
12th European Symposium on Electrochemical Engineering	WETSUS	2021

General Courses		
Introduction to R	VLAG	2018
VLAG PhD week	VLAG	2018
Starting day	WETSUS	2018
Communication styles	WETSUS	2018
Presentation course	WETSUS	2018
Supervision course	WETSUS	2018
Scientific Writing	WGS	2019
Presenting with Impact	WGS	2019
Career Orientation	WGS	2020
Introduction to Python and Linux	VLAG/WIMEK	2021

Other Activities

Research proposal	ORC	2017
PhD study trip	ORC	2019
CDI theme meeting	WETSUS	2017 – 2021
Lunch presentations	WETSUS	2017 - 2021

The research described in this thesis has received funding from the European Research Council (ERC) under the European Union's Horizon 2020 research and innovation program (ERC Consolidator Grant to Dr. Louis C.P.M. de Smet, Grant agreement No. 682444) and was performed in collaboration with Wetsus, European Centre of Excellence for Sustainable Water Technology. Wetsus is co-funded by the Dutch Ministry of Economic Affairs and Climate Policy, the Northern Netherlands Provinces, and the Province of Fryslân.

Financial support from Wageningen University and Wetsus for printing this thesis is gratefully acknowledged.

Cover design by J. G. Gamaethiralalage and K. Singh

Printed by ProefschriftMaken